University of Salerno

Department of Chemistry

and Biology

PhD Thesis in Chemistry

XXXVIII Cycle

Recyclable and bio-based polyesters and polycarbonates enabled by biocompatible metal catalysts

Tutors **PhD Student**

Prof. Marina Lamberti

Prof. Mina Mazzeo Federica Tufano

Coordinator

Prof. Alessandra Lattanzi

Academic Year 2024-2025

INDEX

LIST OF ABBREVIATIONS

2-Me-THF 2-Methyltetrahydrofuran

1-Me-TMC 1-Methyltrimethylene Carbonate

AMM Activated Monomer Mechanism

APCs Aliphatic Polycarbonates

BDM Benzendimethanol

BnOH Benzyl Alcohol

BPA Bisphenol A

CCs Cyclic Carbonates

CHO Cyclohexene Oxide

ε-CL Caprolactone

CO_2 Carbon Dioxide

Đ Dispersity

DBU 1,8-Diazabicyclo(5.4.0)undec-7-ene

DCM Dichloromethane

DMAP 4-(N,N-Dimethylamino)pyridine

DFT Density Functional Theory

DOSY Diffusion-ordered Spectroscopy

DSC Differential Scanning Calorimetry

DTC Dimethyltrimethylene Carbonate

Et-La Ethylactate

GA Glycolide

GLO Globalide

GPC Gel Permeation Chromatography

^{i}PrOH Isopropyl Alcohol

KH Potassium Hydride

LA Lactide

MALDI-FT-ICR Matrix assisted laser desorption/ionization-Time of Flight

Me-La Methylactate

M_n Number Average molecular weight

$MgCl_2$ Magnesium Dichloride

$Mg[N(TMS)_2]_2$ Magnesium Bis(hexamethyldisilazide)

NaH Sodium Hydride

NaI Sodium Iodide

NHCs N-Heterocyclic Carbenes

NMR Nuclear Magnetic Resonance

PA Phthalic Anydride

PCL Polycaprolactone

PDL Pentadecalactone

PEG Polyethyleneglycol

PHB Polyhydroxybutyrate

PLA Polylactide

PPNCl Bis(triphenylphosphoranylidene) Ammonium Chloride

PTMC Polytrimethylene Carbonate

P_r Probability of heterotactic enchainment

P_s Probability of syndiotactic enchainment

rac- βBL *rac*-Butyrrolactone

ROCOP Ring-Opening Copolymerisation

ROP Ring-Opening Polymerisation

RT Room Temperature

$Sn(Oct)_2$ Sn (2-ethylhexanoate)$_2$

$S_{R\text{-}La}$ Selectivity of alkyl-lactate

TBAB Tetrabutylammonium Bromide

TBD 1,5,7-Triazabicyclo[4.4.0]dec-5-ene

T_g Glass Transition Temperature

TGA Thermogravimetric Analysis

THF Tetrahydrofuran

T_m Melting Temperature

TMC Trimethylene Carbonate

TMEDA N,N,N′,N′-Tetramethylethylenediamine

TMS Tetramethylsilane

TMSS Tris(trimethylsilyl)silane

TOF Turnover Frequency

X_{Int} Conversion of PLA degraded

X_{Reg} Percentage of Head Tail bond

$Y_{R\text{-}La}$ Yield of alkyl-lactate

$ZnCl_2$ Zinc Dichloride

$ZnEt_2$ Diethylzinc

$Zn[N(TMS)_2]_2$ Zinc Bis[bis(trimethylsilyl)amide]

$Zn(OAc)_2$ Zinc Acetate

Abstract

Plastic has become irreplaceable in our daily lives thanks to its multiple advantages. On the other hand, problems related both to the employment of non-renewable raw materials and to the disposal of the final products at the end of their life cycle, have arisen a growing interest in the development of more sustainable alternative polymers. Among them, aliphatic polyesters and polycarbonates have attracted significant attention as they can be derived from renewable resources and are biodegradable. Currently, the industrial production of these polymers relies largely on toxic tin-based catalysts. To preserve the greenness of the productive process, research is shifting toward the development of catalytic systems based on abundant non-toxic and abundant metals. In this context, the aim of this doctoral thesis was to develop new complexes based on biocompatible metals, such as zinc and magnesium, able to promote the synthesis of the targeted polymers, employing diverse classes of ancillary ligands to modulate the reactivity of the metal centre.

The study initially focused on a N-heterocyclic carbene zinc complex, with *syn*- phenyl groups on the backbone and N-tolyl groups, applied in the polymerization of trimethylene carbonate (TMC) and its alkyl derivatives, synthesized via sustainable procedures starting from CO_2 and 1,3-diols. The zinc complex, in combination with an alcohol as the initiator, demonstrated a high level of control of the polymerization process, which was subsequently exploited for the synthesis of PTMC block copolymers with polylactide (PLA) and polyethylene glycol (PEG) through two different synthetic strategies. Subsequently, the research was extended to zinc and magnesium complexes, using NHC ligands with *syn- or anti*-phenyl groups on the backbone. All catalysts proved active in both the polymerization of various cyclic esters and cyclic carbonates and the methanolysis of PLLA. Interestingly, the activity of the complexes is strongly influenced by the nature of the metal and of the monomer.

In a second phase of the project, attention shifted to novel heteroleptic zinc and magnesium complexes supported by tridentate naphthoxy-imino-pyridine ligands. These new complexes were applied in the homopolymerization of various bioderived cyclic monomers (both esters and carbonates), where the zinc complex demonstrated a significantly higher catalytic activity and, simultaneously, better control than magnesium analogue. Finally, the performance of the zinc complex was also evaluated in the depolymerization of PTMC and its copolymers, utilizing microwaves as a more sustainable alternative to conventional heating methods.

The final part of the doctoral project focused on the development of polynuclear catalytic systems using multinucleating ligands, designed to position metal centers at optimal interatomic distances. First, sulfur-functionalized salen ligands were synthesized to prepare mono- and bimetallic zinc complexes. Although their effectiveness in the ROCOP Ring-Opening COPolymerization (ROCOP) of CO_2 with epoxide was already known, this work evaluated their performance in the ring-opening polymerization of cyclic esters and the ring-opening copolymerization of epoxides and anhydrides. Subsequently, we introduced a new variant of hexadentate salen ligands, functionalized with amino pendants *ortho* to phenol to create a coordination pocket for a second metal. The synthetic strategy and preliminary studies on the corresponding homo- and heterodinuclear complexes in ROCOP reactions are described. To further explore heterometallic cooperativity, the study was extended to include heterotrimetallic complexes based on zinc and alkali metals, supported by apentadentate ProPhenol ligand. We presented the application of these systems to the polymerization of cyclic carbonates and macrolactones, representing, to our knowledge, the first evaluation of such complexes with these specific classes of monomers.

Chapter One

General Introduction

Plastics have become an essential element of modern society: thanks to significant advantages, such as low cost, lightweight, and high versatility, they have seen steady growth since their introduction in the first half of the last century. According to recent data, global production reached 430.9 million tonnes, of which 54.6 million tones were produced in Europe.[1] These materials are used in key market sectors, with a clear predominance in packaging (39%), followed by building and construction (3%), and the automotive sector (8%).[2] On the other hand, growing production has given rise to several concerns, like the continued use of limited petroleum resources for their synthesis. This dependence is especially alarming because their use is inexorably linked to serious environmental issues, such as global pollution and climate change.[3]

An equally critical issue concerns end-of-life management: currently, the disposal of plastic packaging waste exhibits serious inefficiencies. Globally, approximately 79% of waste ends up in landfills, 12% is incinerated for energy recovery and only 9% is actually recycled (**Figure 1.1**).[4] Most alarmingly, the remainder escapes collection systems, leaking into the environment, tending to accumulate, especially in marine environments and fragmenting into persistent microplastics.[5]

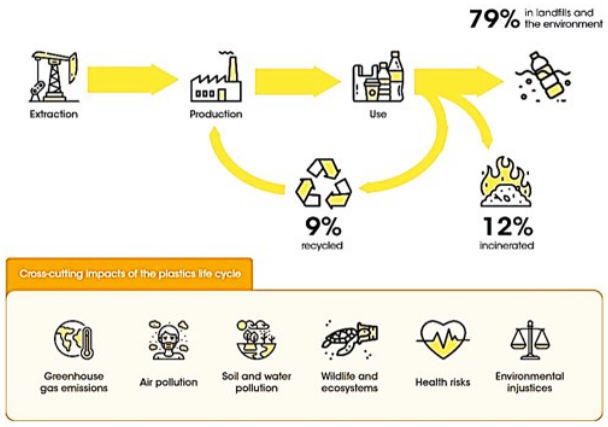

Figure 1.1: The plastics life cycle and its impact on people and the environment.[4]

In light of these drawbacks, a radical change is needed to combat plastic pollution. Among the various options, in recent years research has focused on developing recovery strategies for traditional plastics and, at the same time, on the transition to alternative materials. The latter aims to replace current plastics by offering not only biodegradability and biorenewability, but also competitive mechanical and thermal performance.

1. 1 Sustainable Polymers

Sustainable polymers represent the most promising technological solution to mitigate the environmental impact of the plastics industry. Unlike conventional materials, these innovative alternatives address both the dependence on petrochemical resources and the critical issues of end-of-life management. They can be divided into bio-based polymers and biodegradable polymers (**Figure 1.2**): the former are produced entirely or partially from renewable biological raw materials such as biomass, while the latter are capable of undergoing microbial degradation under specific environmental conditions.

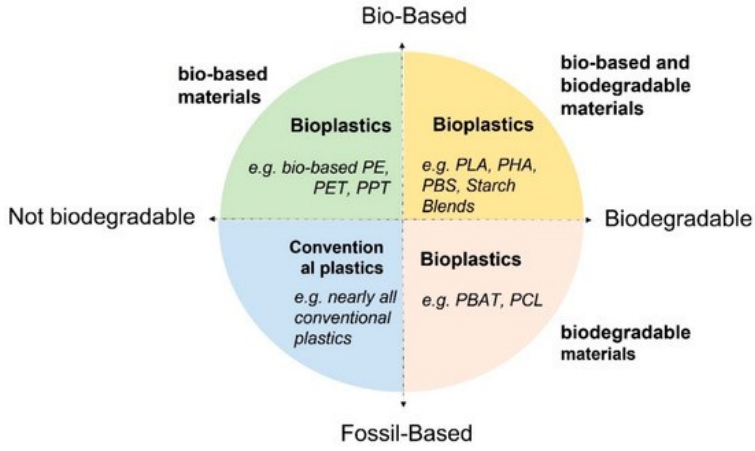

Figure 1.2: Classification of bio-based and biodegradable polymers.[6]

It is important to note that bio-based does not necessarily imply biodegradability, just as biodegradable polymers do not always come from renewable sources.[7] Among these materials, aliphatic polyesters and aliphatic polycarbonates have emerged as ideal

candidates as alternatives to conventional polymers, thanks to potential for renewable sourcing, and end-of-life biodegradability, together with their tunable physical properties.

1.1.1 Aliphatic Polyesters

Aliphatic polyesters have attracted growing interest among sustainable polymers due to their combination of mechanical performance, processability, and biodegradability. Structurally, polyesters consist of ester bonds [–C(=O)–O–] within the backbone chain. Unlike aromatic polyesters, which contain rigid benzene rings, aliphatic polyesters consist of flexible aliphatic segments that make the ester bonds more accessible to hydrolysis and enzymatic attack under appropriate environmental conditions. The versatility of polyesters stems from the wide variety of monomers that can be used in their synthesis, including both renewable and petroleum-derived precursors. This allows for the modulation of physical, mechanical, and thermal properties through careful control of the molecular architecture.

Representative examples include:

- Polylactic acid (PLA), produced from lactic acid derived from the fermentation of renewable carbohydrates, is the most widely used bio-based thermoplastic and is industrially compostable under controlled conditions;
- Polycaprolactone (PCL), although traditionally synthesized from petroleum-derived ε-caprolactone, can also be obtained from biological sources and it is valued for its high flexibility, low melting point, and biocompatibility, making it suitable for biomedical applications such as drug delivery and tissue engineering.
- Polyhydroxybutyrate (PHB), belonging to the group of polyhydroxyalkanoates (PHAs), polyesters biosynthesized by microorganisms. Classified as a highly crystalline thermoplastic polymer, it can be produced directly from renewable resources via bacterial fermentation and degrades completely into carbon dioxide and water under aerobic conditions.

1.1.1.1 Polylactic Acid

Polylactic acid (PLA) stands out as one of the most promising aliphatic polyesters: a thermoplastic polymer, with chemical and physical properties that make it suitable for a wide range of applications, such as 3D printing filaments, disposable products, and agricultural applications.[8] The gradual degradation of PLA into non-toxic products and the possibility of modifying its surface properties make it a promising option for the creation of biocompatible devices, such as prosthetics and controlled drug release systems.[9] Finally, it can be recycled both mechanically through reprocessing and re-extrusion and chemically through solvolysis or depolymerisation (**Figure 1.3**).

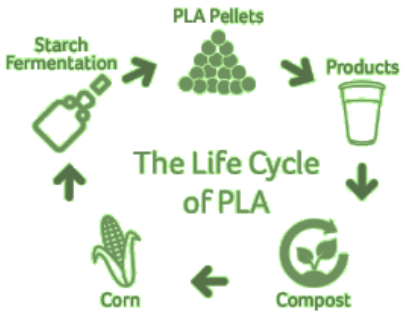

Figure 1.3: Life cycle of Polylactic acid.

The most widely used strategy for the synthesis of this material is the ring-opening polymerization of lactide, a cyclic dimer of lactic acid obtained from the microbial fermentation of carbohydrates. This cyclic monomer has two stereogenic centers and exists in the form of three different stereoisomers: L-lactide (where the chiral centers are *S,S*), D-lactide (where the chiral centers are *R,R*), and *meso*-lactide (where the chiral centers are *R,S*). Commercially, it is available as L-lactide or, alternatively, as a racemic mixture in a 1:1 ratio of L-LA and D-LA. Following the polymerization of the different stereoisomers, polymers with different microstructures with specific chemical, physical, and mechanical properties can be obtained (**Figure 1.4**). They are:

- Atactic: an amorphous material composed of a random arrangement of stereogenic centers.
- Isotactic: a semi-crystalline material with the same configuration for all stereogenic centers. Two types of isotactic PLA can be distinguished: PLLA and PDLA with only S stereogenic centers or only R stereogenic centers, respectively. These polymers are synthesized by ROP of pure L- and D-lactide or by stereoselective polymerization of the racemic mixture.
- Syndiotactic: a semi-crystalline material with an alternating stereochemical configuration, for example -*SR*; this polymer is obtained from *meso* lactide.
- Heterotactic: A polymeric material with regularly alternating pairs of stereocenters with the same configuration, e.g., *SSRR*; this can be achieved by both *rac*-lactide and *meso* lactide.

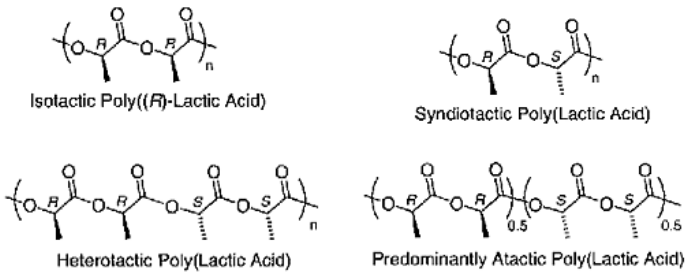

Figure 1.4: Possible microstructures of PLA.

1.1.1.2 Polycaprolactone

Polycaprolactone (PCL) (**Figure 1.5**) has gained considerable attention in the sustainable polymer landscape, particularly in biomedical applications, due to its biocompatibility and high permeability. It is a semicrystalline polyester with a melting point (T_m) of approximately 58–60°C and relatively high solubility in common organic solvents at room temperature. Its degradation in the environment occurs through the hydrolytic cleavage

of ester bonds, followed by microbial uptake under both aerobic and anaerobic conditions.

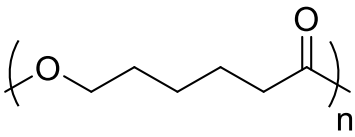

Figure 1.5: Chemical Structure of PCL.

PCL can be synthesized through two main routes: the polycondensation of ω-hydroxycarboxylic acids or the ring-opening polymerization of ε-caprolactone, the more widely used method. Traditionally, ε-caprolactone is obtained from cyclohexanone or cyclohexanol, products of fossil origin, but recent advances in green chemistry and biotechnological synthesis have enabled the production of bioderived ε-caprolactone. These pathways include the fermentation of sugars to 6-hydroxyhexanoic acid, which can then be cyclized to ε-caprolactone, as well as the chemical conversion of bioderived cyclohexanol from vegetable oils.[10]

1.1.1.3 Poly(3-hydroxybutyrate)

Another aliphatic polyester that has attracted interest is poly(3-hydroxybutyrate) (PHB), which can be naturally produced by numerous bacteria through the fermentation of carbohydrates.[11] It has an isotactic microstructure, which gives it high crystallinity and biodegradability, characterized by considerable rigidity and brittleness. A limitation to its processability lies in its high melting temperature (T_m ≈ 175 °C), close to the thermal degradation point, combined with bacterial synthesis, which are cost-effective compared to conventional petrochemical processes.

A valid alternative is the ring-opening polymerization of racemic β-butyrolactone (*rac*-βBL), mediated by metal complexes. In this context, stereochemical control during polymerization is crucial, as it directly determines the thermal, mechanical, and degradability properties of the polymer (**Figure 1.6**).

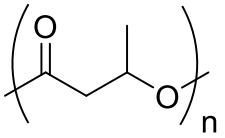

Figure 1.6: Chemical Structure of PBL.

1.1.2 Aliphatic Polycarbonates (APCs)

Aliphatic polycarbonates (aPCs) are polymers characterized by the presence of carbonate bonds [–O–(C=O)–O–] along the backbone. First synthesized in the 1930s,[12] they initially attracted limited interest compared to their aromatic counterparts due to their reduced thermal stability and greater susceptibility to hydrolytic degradation. Since the 1990s, however, this class of materials has seen renewed attention: in fact, they can be obtained from renewable and bio-based monomers, unlike conventional aromatic polycarbonates, which are synthesized from potentially toxic or carcinogenic compounds such as bisphenol A (BPA) and phosgene.[13] Furthermore, they are materials with great elasticity and flexibility, as well as having the potential to be biodegradable and biocompatible.

1.1.2.1 Polytrimethylene Carbonate

The largest exponent of this category of polymers is poly(trimethylene carbonate) (PTMC). Typically synthesized via the ring-opening polymerization of trimethylene carbonate (TMC), a 6-membered cyclic carbonate, this commercially available aPC is hydrophobic, amorphous, and has a glass transition temperature (T_g) of approximately −20 °C **(Figure 1.7)**.[14]

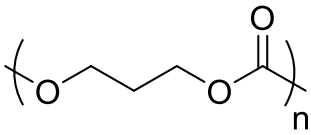

Figure 1.7: Chemical Structure of PTMC.

These properties make PTMC suitable as a soft material for applications such as scaffolds for soft tissue regeneration and as a hydrophobic block in amphiphilic copolymers for drug delivery. In particular, in biomedical applications, a key advantage is that, unlike polyesters, this material does not release acidic products, but rather neutral ones, with weak inflammatory potential.[14] Furthermore, its degradation rate is generally lower than that of polyesters, making it suitable for applications requiring long-term durability, such as medical implants and coatings.[15] Finally, although its thermomechanical properties have limited its use as thermoplastics, in recent years it has found significant industrial utility as a low molecular weight macromonomer.[16]

1.1.2.2 Cyclic Carbonate-Derived Aliphatic Polycarbonates.

A key advantage of aliphatic polycarbonates (aPCs) lies in their structural versatility, enabling the specific tuning of properties to suit desired applications. This is possible through the ring-opening polymerization of functionalized cyclic carbonates, which affords for precise control over the polymer structure.

For example, the incorporation of pendant polar groups or branched aliphatic chains can improve water absorption and hydrolytic susceptibility, while the introduction of rigid segments or aromatic groups can improve mechanical and thermal resistance, without compromising overall biocompatibility.

The introduction of these substituents onto the main chain can occur through the use of substituted cyclic carbonates: specifically, the functional groups on these monomers can be protected, requiring post-polymerization deprotection, or directly unmasked, when compatible with the polymerization conditions. These monomers, analogous to TMC,

are particularly attractive because they are highly stable compounds under ambient conditions, easy to manipulate, and, more importantly, to modify.

While the synthesis of cyclic carbonates still largely relies on the use of phosgene or its derivatives, such as triphosgene, di-tert-butyl decarbonate and 1,1'-carbonyldiimidazole,[16] research has focused on the development of synthetic strategies, seeking to employ alternative and safe primary sources: one of these is based on the direct carbonylation of diols with CO_2. This approach is attractive from a sustainability perspective, as many differently substituted diols can be obtained from the fermentation of sugars, while CO_2 serves as a safe, economical, and renewable C1 element.[17]

The first to report this approach was Zhang, who synthesized the unsubstituted cyclic carbonate by coupling 3-chloro-1-propanol with CO_2 under mild conditions (40°C, 1 atm) using Cs_2CO_3, achieving 95% yield (**Figure 1.8**).[18] This work highlighted a dual activation strategy, involving the activation of the hydroxyl group by CO_2 and the simultaneous generation of an effective leaving group (a halide) to facilitate ring closure.

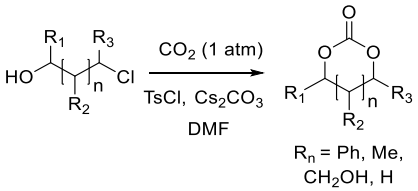

Figure 1.8: Zhang's synthesis of CCs

Inspired by these results, Buchard and colleagues developed an alternative two-step procedure for the synthesis of six-membered cyclic carbonates from 1,3-diols (**Figure 1.9**). The first step involves the selective DBU-mediated monoinsertion (DBU) of CO_2 into a hydroxyl group. The second step uses tosyl chloride and triethylamine to facilitate rapid cyclization. This method, usable at ambient temperature and pressure, has been applied to a wide range of diols, including sterically hindered sugar derivatives, producing cyclic carbonates in 40–70% yield and providing a versatile platform for the synthesis of these monomers.[19,20]

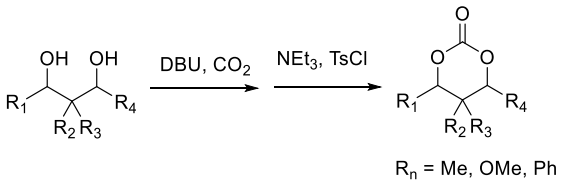

Figure 1.9: Buchard's two-step CO_2 insertion and cyclization pathway.

1.1.3 Polyesters/Polycarbonates Copolymers

Copolymerization represents a powerful synthetic strategy: depending on the nature of the initial monomers and their combination, it is possible to produce materials with easily adjustable chemical, physical, and mechanical properties, completely different from those of individual homopolymers. A good example of this category is polyester/polycarbonate copolymers, which can overcome the limitations of their respective homopolymers in various fields, without compromising the biodegradability.

For example, in biomedical applications, the copolymerization strategy can mitigate tissue inflammation caused by the release of acidic byproducts through polyester hydrolysis. Indeed, the presence of polycarbonates buffers these products, preventing severe inflammation.[14] Conversely, in engineering, the insertion of polycarbonate segments substantially alters the thermomechanical properties by affecting the glass transition temperature, conferring greater elasticity and toughness to otherwise brittle matrices.[21]

Copolymerization can be performed by simultaneous or sequential addition of monomers: the former can lead to the synthesis of random or gradient copolymers, depending on the relative reactivity ratios of the comonomers. From the point of view of final properties, microstructural disorder prevents crystallization, resulting in amorphous materials. Sequential addition leads to the synthesis of well-defined multiblock architectures, allowing the formation of materials with crystalline domains in an amorphous matrix, resulting in high durability and resistance.[22]

1.2 Synthetic Strategies for Aliphatic Polyesters and Polycarbonates

Over the years, various synthetic strategies have been developed to obtain aliphatic polyesters and aliphatic polycarbonates. These include:

- Polycondensation between aliphatic diols with diacids or dialkylcarbonates.
- Ring-opening copolymerization (ROCOP) between epoxides with anhydrides or carbon dioxide.
- Ring-opening polymerization (ROP) of cyclic esters or cyclic carbonates.

1.2.1 Polycondensation

Considered the most widely used industrial method today, this process involves the condensation of diols with diacids for the synthesis of aliphatic polyesters and with dialkylcarbonates for the synthesis of aliphatic polycarbonates (**Figure 1.10**).

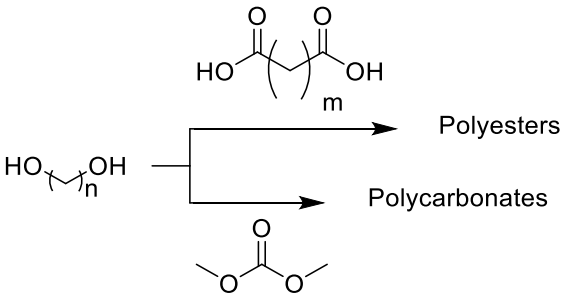

Figure 1.10: Polycondensation for the synthesis of polyesters and polycarbonates.

One of the advantages of this approach lies in the wide availability of monomers, often of renewable origin, with which it is possible to modify the structure and consequently the properties of the final polymers. For example, the presence of bulky groups produces polymers with high glass transition temperatures, while varying chain lengths can influence crystallinity and the rate of biodegradation.[23]

A critical challenge for this strategy is the difficult control of molecular weight, which depends on precise stoichiometric equivalence between the functional groups: any deviation can lead to premature chain termination, resulting in a drop in molecular mass. Furthermore, achieving high conversions requires high temperatures and high vacuum to remove condensation byproducts, such as water and alcohol. However, as the viscosity of the polymer melt increases, the high and prolonged conditions can trigger side reactions, such as thermal degradation, complicating the synthesis of high molecular weight polymers. Consequently, although relevant, polycondensation remains limited in its ability to produce aliphatic polymers with high molecular weights and precise architectural control.

1.2.2 Ring-Opening Copolymerization

Ring-opening copolymerization (ROCOP) of epoxides with cyclic anhydrides or CO_2 represents an alternative strategy for the synthesis of polyesters and aliphatic polycarbonates, respectively. Notably, the ROCOP with anhydrides yields either aliphatic or semi-aromatic polyesters, dictated by the nature of the cyclic anhydride employed.

This approach allows the production of polymers under mild, controlled conditions, avoiding high temperatures and high vacuum for byproduct removal, as is the case with traditional polycondensation. Furthermore, thanks to the wide availability of monomers, both synthetic and renewable,[24] and their structural versatility, it is possible to obtain materials with highly tunable chemical and physical properties, ranging from rigid plastics to elastomers (**Figure 1.11**). More recently, new monomers with unsaturated groups have been employed in this copolymerization to ensure post-polymerization modification and crosslinking, significantly expanding the range of accessible architectures.[25,26] Finally, in the context of sustainability, the synthesis of polycarbonates by this approach enables the valorisation of a non-toxic, abundant, and renewable waste gas such as carbon dioxide (CO_2), which constitutes up to 30–50% of the polymer mass.[27]

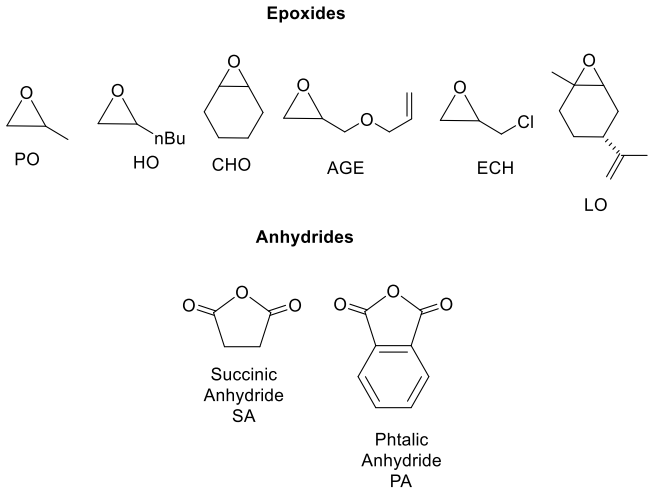

Figure 1.11: Examples of epoxide and cyclic anhydride monomers used in ROCOP.

The copolymerization proceeds through an insertion and coordination mechanism and is catalysed by an LMX-type metal complex, where L is an auxiliary ligand, M is the metal center, and X is the initiator group. The mechanism begins with the coordination of the metal center to the epoxide (**Figure 1.12**),[28] followed by a nucleophilic attack by the initiator group X to generate a metal-alkoxide species.

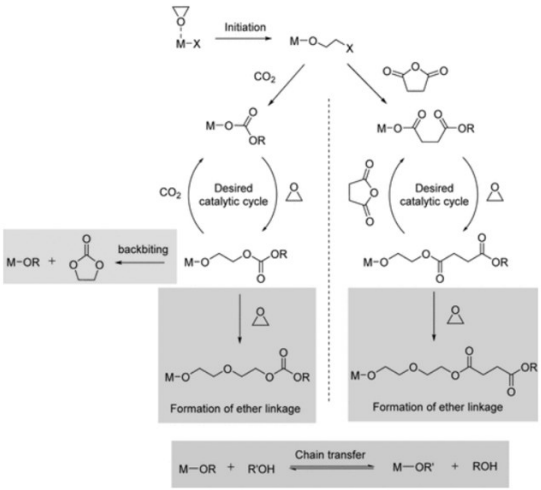

Figure 1.12: Proposed Mechanism for the ROCOP of Epoxides with CO_2 or Cyclic Anhydride.

The CO_2 or the anhydride then reacts with this species, inserting into the metal-oxygen bond and forming a new metal-carbonate/carboxylate intermediate. Chain propagation then occurs through the alternating insertion of CO_2/cyclic anhydride and the epoxide, resulting in the formation of polycarbonates or polyesters.

During the copolymerization of epoxides with carbon dioxide, one of the main competing reactions is intramolecular cyclization, which leads to the formation of thermodynamically stable five-membered cyclic carbonates (5CC).[29] Traditionally, the generation of 5CC has been considered an undesirable secondary pathway due to its irreversible nature and the resulting loss of yield. However, recent research has demonstrated that these compounds can represent valuable platform molecules, finding applications as solvents, electrolytes in lithium-ion batteries, or precursors for non-isocyanate polyurethanes. The outcome of the reaction is influenced by the selectivity of the catalyst, as well as the structure of the epoxide and the temperature and CO_2 pressure conditions: for example, lower temperatures and higher CO_2 pressures tend to favor chain propagation over cyclization, promoting polymer formation.[27]

Although advances in catalyst design have mitigated many of these side reactions, ROCOP technology has several limitations: the first is the restriction to obtain only polymers with C2-C3 chain lengths, making longer chain architectures inaccessible.[30] Furthermore, this mechanism is susceptible to several side reactions that can compromise the final properties of the polymer: one of these is the formation of polyether bonds within the chain (**Figure 1.12**), due to the insertion of two consecutive epoxide molecules or to decarboxylation phenomena. A second side reaction is due to chain transfer phenomena, caused by alcohols that can be formed during the copolymerization reaction, which cause a decrease in molecular weight and an increase in dispersity of the obtained polymers.

1.2.3 Ring-opening Polymerization (ROP)

Ring-opening polymerization of cyclic monomers is an efficient method for producing both aliphatic polyesters and aliphatic polycarbonates. Unlike traditional polycondensation, it does not require harsh conditions that can compromise control over molecular mass and dispersity. Unlike ROCOP, it uses a single type of monomer, which already contains the relevant functionality, simplifying the reaction kinetics.

Polymerization occurs thanks to the thermodynamic profile of the monomers, which is strongly influenced by the ring size and its degree of substitution. Specifically, for small and medium-sized monomers (<8 members), polymerization is driven by enthalpy, due to ring strain, while larger rings undergo entropy-driven ring opening, due to greater conformational freedom.

The mechanism of ROP consists of an active site reacting with a cyclic monomer, causing its opening and subsequent addition as a linear unit, with the regeneration of the active species. Depending on the electronic nature of the active site, ROP can be classified as cationic, anionic, activated monomer, and coordination-insertion. Specific features and reaction schemes of each mechanism will be discussed in the section **2.3.1**.

As with other approaches, side reactions may occur. In the case of polycarbonates, decarboxylation can occur, resulting in the insertion of ether defects in the main chain,

typically initiated by a chain end of a nucleophilic alkoxide or an alkoxide from a separate chain (**Figure 1.13**).[31]

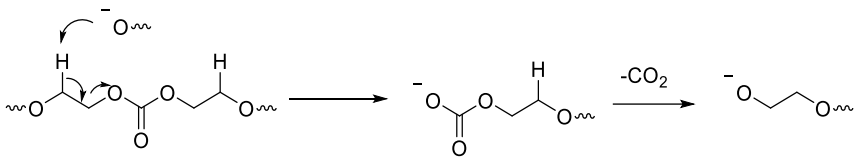

Figure 1.13: Decarboxylation phenomena for polycarbonates.

In the case of polyesters, intermolecular transesterification can occur, leading to chain scrambling, or intramolecular transesterification (backbiting) (**Figure 1.14**). The latter involves the attack of the terminal alkoxide on the ester carbonyl within the chain itself, leading to the formation of cyclic oligomers. Both phenomena lead to an increase in the dispersity of the molecular masses. Furthermore, backbiting causes a decrease in the active chain ends, thus limiting the achievable molecular weight.

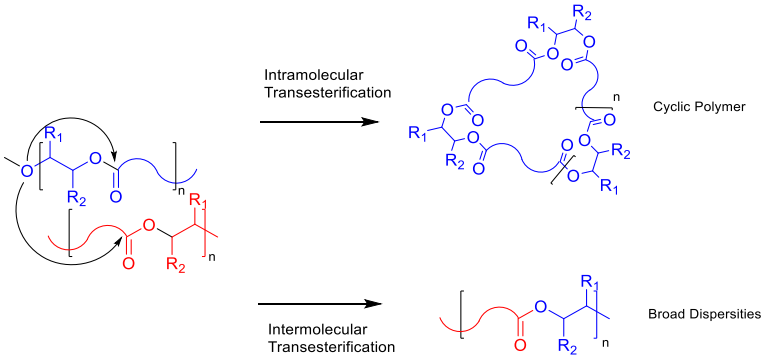

Figure 1.14: Side reaction during polymerisation of cyclic esters.

1.2.3.1 ROP Pathways

Anionic ROP is driven by the nucleophilic attack of the active species on the electrophilic carbonyl carbon of the monomer. The process begins with initiation, where an external nucleophile attacks the carbonyl group, resulting in the cleavage of the acyl-oxygen bond and the formation of an anionic active center**.** Subsequently, in the propagation step, this newly formed alkoxide anion acts as the nucleophile, attacking another monomer molecule to extend the polymer chain (**Figure 1.15a**).[32] Unfortunately, the strong nucleophilic and basic character of anionic species often leads to undesirable side reactions, including transesterification. Consequently, their instability and high reactivity limit their industrial utility.

Cyclic esters and cyclic carbonates can also undergo cationic ROP (**Figure 1.15b**), driven by electrophilic activation of the carbonyl or ether group of the monomer, which acts as a Lewis base. In this case, the active center is a cation generated by interaction with a strong acid or alkylating agent. The propagation step occurs through the nucleophilic attack of the oxygen of the incoming monomer on the cationic center located at the end of the growing chain; this attack induces the cleavage of the carbon-heteroatom bond of the active ring and the consequent transfer of the positive charge to the newly inserted terminal unit. As with anionic ROP, its application presents severe limitations due to the poorly controllable nature of the active center, which triggers frequent transesterification reactions.

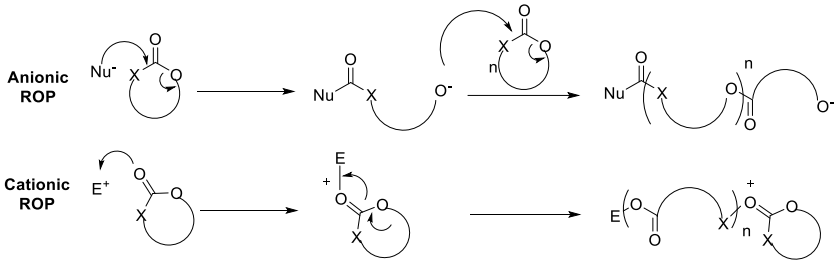

Figure 1.15: Mechanism for anionic and cationic ROP.

The most effective synthetic methods exploit the "insertion-coordination" mechanism, or the Activated Monomer Mechanism (AMM). For the activation mechanism (AMM), the metal center functions exclusively as a Lewis acid, coordinating the carbonyl oxygen of the monomer. This coordination activates the carbonyl carbon for intermolecular nucleophilic attack by an exogenous initiator. Ring opening then generates a polymer chain with a terminal hydroxyl group and regenerates the metal catalyst (**Figure 1.16a**). Crucially, in this mechanism, the metal is not covalently bound to the propagating chain at any stage; instead, it plays a dual role: electrophilic activation of the monomer and simultaneous activation of the ROH group towards nucleophilic attack via coordination.[33]

For the coordination-insertion mechanism, a metal complex featuring by a nucleophilic ligand (e.g., an alkoxide) and a Lewis acidic metal center is used. The process begins when the carbonyl oxygen of the monomer coordinates to the Lewis acidic metal center. This interaction polarizes the carbonyl carbon, increasing its electrophilicity and facilitating nucleophilic attack. Subsequent intramolecular nucleophilic attack by the metal-bound alkoxide opens the ring through cleavage of the oxygen-acyl bond (O–C(O)), inserting the monomer into the metal-alkoxide bond. This step regenerates the metal-alkoxide site, which now has an extended polymer chain (M–O polymer), allowing continued propagation (**Figure 1.16b**).[34]

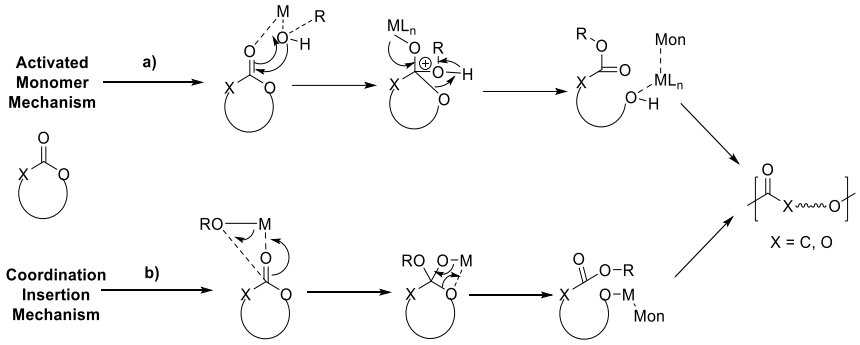

Figure 1.16: Differences between Coordination-Insertion Mechanism and Activated Monomer Mechanism.

The distinction between these mechanisms is crucial: the coordination-insertion mechanism involves the metal as a component covalently bonded to the active end of the chain, while the activation mechanism uses the metal as a regenerable Lewis acid catalyst that remains outside the chain.

1.2.3.2 Living and Immortal Polymerisation

The ring-opening polymerisation can proceed through two distinct regimes: “living” and/or “immortal” polymerization. Reactions promoted by organometallic complexes proceed "live," when termination and chain transfer reactions are absent. The result is that as many growing macromolecules as there are active sites available on the catalyst are formed (**Figure 1.17a**).[35] These reactions tipically give rise to chains of equal length, with molecular masses dependent on the monomer/initiator ratio and very low dispersity. Living polymerization is desirable because it offers precision and control in macromolecular synthesis.

On the other hand, immortal ROP (iROP) offers an efficient alternative to classical ROP. This process involves a two-component system consisting of a catalyst and an external nucleophile, which acts simultaneously as an initiator and a chain transfer agent. The number of growing polymer chains exceeds the number of catalyst molecules used and is equal to the initial amount of transfer agent introduced. Consequently, this polymerization can lead to polymers with narrow molecular mass distributions and molecular mass values inversely proportional to the amount of transfer agent introduced (**Figure 1.17b**). In the general context of green and sustainable chemistry, iROP is a very interesting strategy, especially when performed in the absence of solvents.[35]

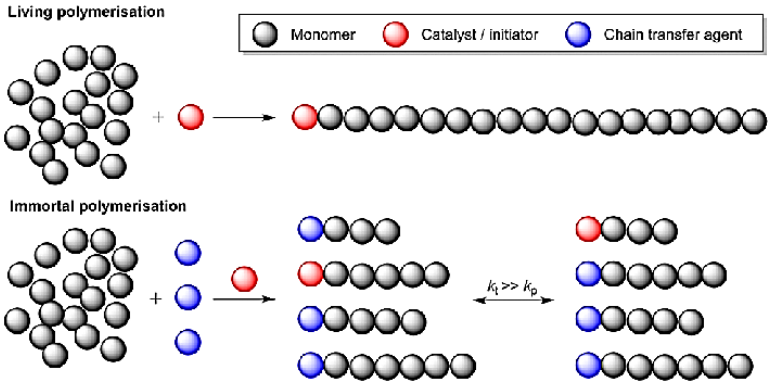

Figure 1.17: Differences between Living and Immortal Polymerisation.

1.3 Metal Catalysts Reported in Literature

As mentioned in the previous sections, choosing an appropriate catalyst is crucial in the polymerization process, in fact, by influencing the reaction mechanism it determines the control of parameters such as molecular mass and dispersity. Furthermore, it can ensure the mitigation of side reactions that negatively impact the final polymer properties or the polymer yield.

Historically, tin octoate ($Sn(Oct)_2$) is the most widely used catalyst in industry, due to its high activity on a wide range of substrates and widespread commercial availability.[36,37] However, the toxicity of tin residues has raised a number of concerns, especially for biomedicine and food packaging applications, where even trace amounts of heavy metals are unacceptable. For these reasons, in recent years, research has focused on the development of catalysts based on non-toxic or biocompatible metals, such as magnesium, zinc, calcium, and aluminum.[38–40]

Among the various classes of catalysts investigated, organometallic complexes with the general formula LMX have emerged as the most efficient and versatile systems. These species consist of a metal center (M), an initiating group (X), and one or more ancillary ligands (L): the latter play the crucial role of defining the chemical environment of the active site. Catalytic performance depends critically on the coordination sphere of the metal: through targeted ligand design, it is possible to finely tune the Lewis acidity and steric hindrance, thereby governing monomer activation, propagation kinetics, and stereochemical control of the resulting polymer. From this perspective, the following sections will focus on several classes of ligands capable of combining stability and reactivity, such as N-heterocyclic carbenes (NHCs), phenoxy-imine and -amine ligands with an additional nitrogen donor, and multinucleating penta- and hexa-dentate ligands.

1.3.1 N-Heterocyclic Carbenes

The use of N-heterocyclic carbenes (NHCs) as ligands stems from a combination of key properties: as exceptional σ-donors, they promote strong coordination to a wide range of metal centers, conferring stability to the resulting metal complexes. Furthermore, they exhibit weak π-accepting character, which increases the electron density at the metal center, modulating their catalytic reactivity.[41] Finally, their properties are easily tunable through simple structural modifications, allowing precise control of metal-ligand interactions. These characteristics make NHCs attractive tools for the design of tailored catalysts.

The development of NHC-metal catalysts for the ROP of cyclic esters has seen substantial progress over the years. Tolman and colleagues reported the first zinc complex with a Zn-alkoxide bearing an unsatured NHC ligand (**Figure 1.18**) with alkylated phenyls on the nitrogen atoms capable of polymerizing 130 equivalents of *rac*-lactide in 75 minutes at 25°C, demonstrating good control thanks to the production of heterotactic polymers with molecular weights close to theoretical values and a turnover frequency (TOF) of 104 h^{-1}.[42]

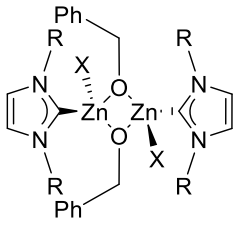

1 X = OCH_2Ph
R = 2,4,6-trimethylphenyl

Figure 1.18: Tolman's Complexes.

Subsequent work by the same group revealed that NHC-metal dissociation could occur after the addition of initiator, suggesting that polymerization may proceed either via a metal-centric or carbene-free pathway.[43] This ambiguity prompted the study of

strategies to strengthen the metal-NHC bond, enhancing metal-carbene backdonation, for example, using ring-expanded NHCs.[44] As illustrated in **Figure 1.19**, these complexes showed high activity in the ROP of *rac*-lactide, converting 100 equivalents of monomer at room temperature with a conversion >90% within 2 hours to produce isotactic-enriched PLA. These systems maintained excellent control, producing polymers with low dispersities ($Đ \approx 1.0$) and experimental molecular weights matching theoretical values.

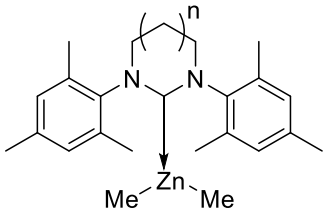

2 n=1
3 n=2

Figure 1.19: NHC Zinc Complexes with expanded ring

Subsequently, Dagorne and colleagues explored NHC-zinc complexes with additional donors as nitrogenous substituents (**Figure 1.20**), which showed activity in the ROP of cyclic esters and carbonates. The complex **4** catalysed the ROP of β-BL at 90 °C in toluene, producing well-defined PBL with narrow molecular weight distributions ($Đ$ = 1.17–1.22). Additionally, the complex promotes the polymerisation of L-LA at room temperature with moderate activity (TOF = 5 h^{-1}) and good control over molecular weights.[45] This class of complexes also showed moderate control over the ROP of TMC, producing polycarbonates with M_n = 16.8 kDaand dispersity $Đ$ = 1.57. Furthermore, the complex proved efficient in the sequential copolymerization of TMC and *rac*-LA, exceeding 90% conversion for both monomers in less than 6 h.[46]

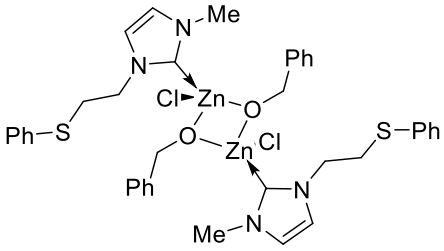

4

Figure 1.20: Dagorne's Zinc Complexes.

As for other cyclic lactones, saturated NHC-metal complexes (**Figure 1.21**) were also employed as initiators in the ROP of ε-caprolactone (ε -CL) at 70 °C, producing PCL with molecular masses (M_n) of 2–20 kDa and dispersities of 1.20–1.7.[47] The zinc complex (**5**) showed an induction period before the onset of rapid polymerization, while a dimeric precursor (**6**) required thermal activation at 130 °C to provide 100% yield within 15 minutes, highlighting the critical role of temperature in catalyst dissociation and initiation. By changing the nature of the metal center, these complexes demonstrated high yields in significantly shorter times: among them, the Mg complex (**7**) proved to be the most active, an efficiency directly related to its Lewis acidity, with quantitative ε-CL conversion in less than five minutes at 130 °C.

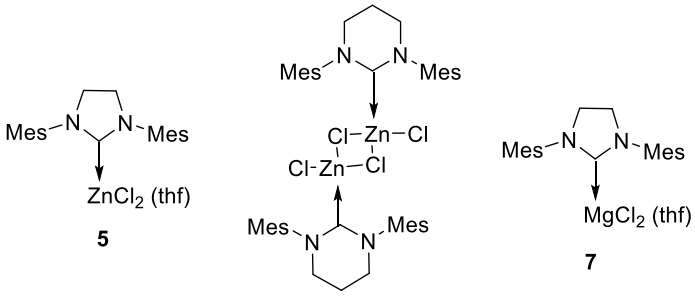

Figure 1.21: Buchmeiser's Zinc and Magnesium Complexes

Tooze and co-workers reported alcohol-functionalized saturated NHC systems for Zn and Mg, which were active for ROP of *rac*-LA at room temperature in THF (**Figure 1.22**).[48] The binuclear complex **8** gave the best results, producing PLA with M_n = 27.5 kDa and $Đ$ = 1.30. The polymerizations were more controlled than with Mg analogue **9**, although the reaction rates were higher for the Mg complex. This difference in polymerization rates was attributed to the difference in electronegativity between Mg and Zn, which results in different insertion mechanisms.

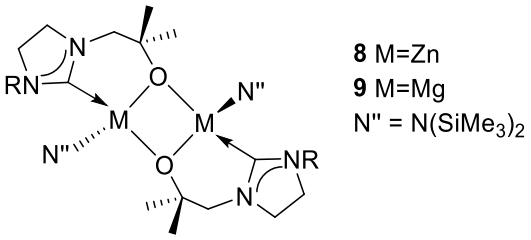

Figure 1.22: Tooze's Zinc and Magnesium Complexes

Further developments included Zn and Mg complexes with NHC-phenoxyimine ligands (**Figure 1.23**), developed by Mazzeo, Costabile, and colleagues, employed in the ROP of *rac*-LA at 25°C in dichloromethane, which produced PLA with molecular weights (M_n) of 4-68 kDa. Although the ligand is chiral, the resulting PLA was atactic. It was also observed that, in the absence of an initiator, the Mg complex formed exclusively cyclic PLA, while the Zn complexes produced linear PLA.[49]

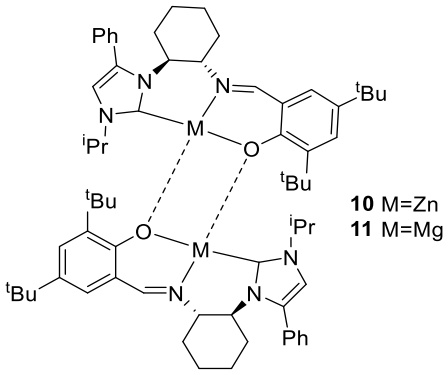

Figure 1.23: Mazzeo's Zinc and Magnesium Complexes.

Recently, my own research group developed catalytic systems based on zinc complexes supported by saturated NHC ligands with N-*ortho*-tolyl substituents and *syn* and *anti*-phenyl groups on the saturated backbone (**Figure 1.24**).[50] Both complexes were active in the synthesis of aliphatic polyesters. In particular, the *syn* isomer showed superior activity and control, polymerizing 100 equivalents of *rac*-lactide in 90 minutes at 25 °C (TOF = 67 h^{-1}). Mechanistic studies of our systems suggested that the ROP mechanism varies depending on the conditions: in the absence of a cocatalyst, a coordination-insertion mechanism was claimed, while with the addition of alcohol, a dual mechanism was hypothesized in which the metal species acts as a Lewis acid and the carbene as a nucleophile or a base. The greater activity of the *syn* isomer was attributed to the higher σ-donor character of the corresponding NHC ligand.

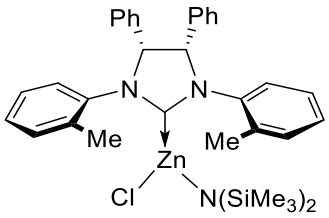

12

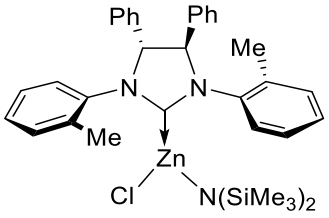

13

Figure. 1.24: Lamberti's NHC Zinc Complex.

1.3.2 Tridentate Phenoxy-Imine and Amine Ligands

Phenoxy-imine and phenoxy-amine represent some of the most versatile classes of ancillary ligands used in catalysis, thanks to their ease of synthesis and structural tunability. Within this broad family, specific attention is focused to tridentate systems, equipped with an additional donor atom via a pendant arm.[51]

Tolman *et al*. reported zinc complexes with phenoxy-type tridentate ligands bearing two neutral amino-type donors (**Figure 1.25**).[52] The alkoxide derivate **15,** obtained through the addition of ethanol to the zinc ethyl complex **14**, showed high activity for the ROP of *rac*-LA, conducted in dichloromethane at 25°C (96% conversion of 650 equiv. in 5 min), whereas the mononuclear analogue **14**, without an alkoxide group, was inactive toward *rac*-LA polymerization, demonstrating that the alkyl group is not a good nucleophile. The complex **15** displayed good control of the molecular weights for lactide polymerization even with catalyst loadings <0.1%.

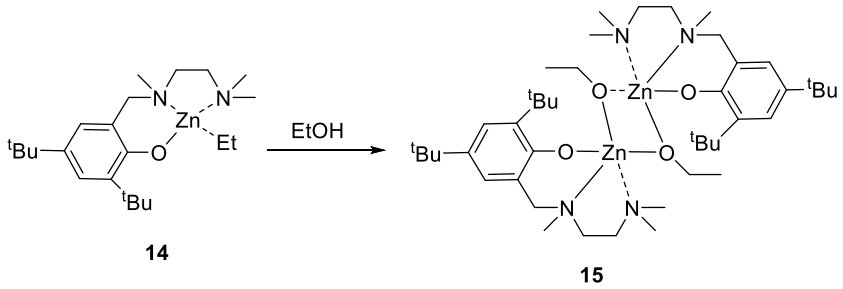

Figure 1.25 Tolman's complexes.

Jones *et al.* reported Mg and Zn-Schiff base complexes, beating a simple ethyleneamine moieties, for the ROP of lactide under industrially relevant conditions (**Figure 1.26**).[53] Incredibly high activities were achieved with the Zn complex **16a** using low catalyst loading and high temperatures (180°C), reaching TOF values of 180000 h^{-1}. Keeping the substituents on the phenoxy portion unchanged, the use of a tertiary amine as an additional donor group, complex **16b** was found to be three times less active then complex **16a**, keeping the substituents on the phenoxy portion unchanged. The Mg complex **17a** showed lower activity than zinc analogue **16a** under the same reaction conditions, with TOF = 14000 h^{-1}. However, reasonable molecular weight control was maintained and MALDI-FT-ICR analysis of these polymers confirmed the terminal benzyl alcohol groups, derived from the initiator BnOH.

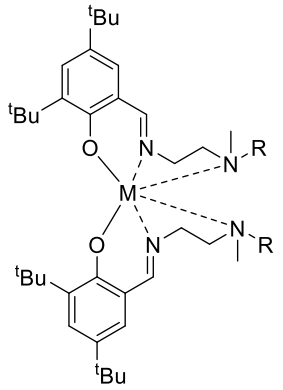

16a M=Zn R=H **17a** M=Mg
16b M=Zn R=Me

Figure 1.26 Jones' complexes

Some of us have developed a family of highly active catalysts for the synthesis of polylactide (PLA) that are structurally analogous to the systems reported by Jones, but feature a key modification: the replacement of the aliphatic amine donor with a pyridine nitrogen (**Figure 1.27**). This seemingly small modification yielded significant improvements. Tested under demanding conditions with 5000 equivalents of monomer and 50 equivalents of initiator, the lead catalyst **18** demonstrated superior performance with a TOF of 49200 h^{-1}, outperforming the Jones catalysts. This increased activity is likely attributable to the stronger electron-donating character of the sp^2 pyridine nitrogen compared to the sp^3 amine nitrogen, as well as potential steric differences arising from the distinct substituents of the phenoxy ring or the reduced steric profile of the pyridine arm. Under milder conditions (400:1 monomer: initiator ratio at room temperature), catalyst **18** maintained high activity with a TOF of approximately 28000 h^{-1}.[54] A subsequent study on the structure-activity relationship examined complexes **19-22** with variable substituents on the phenolic ring. These catalysts were evaluated in the ROP of L-lactide (working with 100:1 monomer:initiator ratio in CH_2Cl_2 at room temperature), revealing a clear electronic dependence: electron-donating groups increased reactivity, while electron-withdrawing groups decreased it compared to the original unsubstituted complex. It is important to note that all catalysts in this series

produced polymers with expected molecular weights and low dispersities, confirming excellent control over the polymerization process.[55]

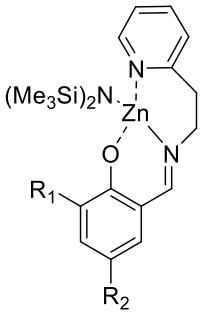

18 R_1=R_2=H
19 R_1=H; R_2=OMe
20 R_1=H; R_2=Me
21 R_1=H; R_2=^{t}Bu
22 R_1=R_2=Cl

Figure 1.27: Mazzeo's zinc complexes.

Building on this work, the study was extended to heteroleptic complexes of zinc and magnesium, supported by the same family of ligands (**Figure 1.28**). This comparative study revealed pronounced metal-dependent activity, with zinc complexes significantly outperforming their magnesium counterparts in the ROP of lactide. For example, zinc complex **23** achieved a TOF of 1700 h^{-1}, approximately three orders of magnitude higher than magnesium complex **24**. NMR spectroscopic investigations clarified this disparity: zinc complexes formed well-defined, discrete active species, while magnesium complexes existed as a mixture of species in dynamic equilibrium, leading to an uncontrolled polymerization process.[56]

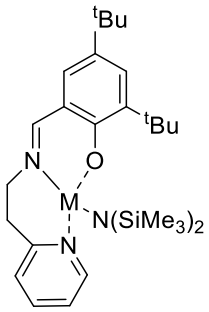

23 M=Zn
24 M=Mg

Figure 1.28: Homoleptic and heteroleptic complexes of zinc and magnesium.

In the context of cyclic carbonate polymerization, Darensbourg *et al.* reported calcium and zinc complexes supported by phenoxy-imine ligands with an additional amine donor. The calcium complex **25a** was shown to be more active than its zinc analogue **25a'** in the ROP of lactide, exhibiting first-order kinetics in both the monomer and catalyst. When applied to TMC polymerization, the calcium complex demonstrated an even higher conversion rate than lactide and was successfully used to synthesize random and block copolymers of TMC and lactide.[57]

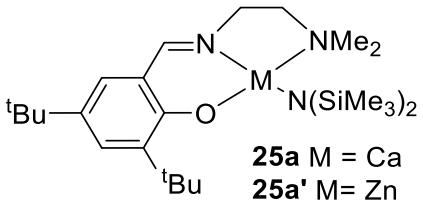

Figure. 1.29: Darensbourg's tridentate Schiff base complexes of calcium and zinc**.**

In a separate study using salen based complexes of zinc, magnesium and calcium (**Figure 1.30**), with different tetrabutyl ammonium salts used as cocatalysts, under solvent-free conditions, the activity profile was clearly established as Ca (TOF ~1300 h^{-1}) > Mg (TOF

~540 h^{-1}) > Zn (TOF ~250 h^{-1}), with the calcium complex converting 300 equivalents of TMC in 15 min.[58]

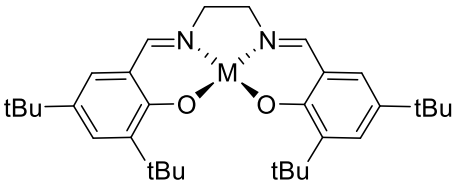

26 M=Zn **27** M=Mg **28** M=Ca

Figure 1.30: General structure of metal salen complexes utilized as catalysts for the polymerization of TMC.

Finally, Ma and colleagues tested Mg and Zn complexes bearing a phenoxyimine with an additional amine donor ligand (**Figure 1.31**), in the ROP of methyl-TMC. The magnesium complex was significantly more active (94% conversion in 5 min, TOF ~2300 h^{-1}) than the zinc complex (84% conversion in 1 h, TOF ~168 h^{-1}). However, the zinc complex, although less active, showed significantly higher regioselectivity (X_{reg} up to 0.98) than the magnesium analogue (X_{reg} = 0.78).[59]

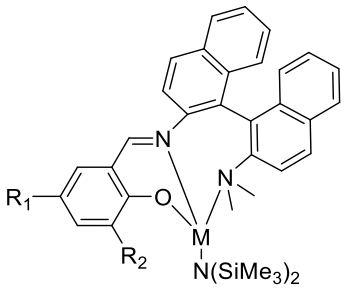

29a M= Mg; R_1=R_2=Cumyl
29b M= Zn; R_1=R_2=Cumyl

Figure 1.31: Ma's Mg and Zn complexes.

1.3.3 Phenoxy-Based Multinucleating Ligands

Phenoxy-based multinucleating ligands have assumed a central role in modern coordination chemistry. Thanks to their ability to simultaneously coordinate multiple metal ions, they allow the metal centers to be positioned at such an intermetallic distance that intramolecular cooperativity phenomena are possible. It is this precise and optimal spatial preorganization, guaranteed by the ligand, that makes the synthesis and efficiency of multinuclear complexes possible.

The di(amino)phenolate zinc monoalkoxide **30** proposed by Hillmayer and Tolman (**Figure 1.32**) was highly active for the ROP of *rac*-LA, polymerizing 90% of 300 equiv. of monomer, at 1 M concentration, in dichloromethane at room temperature, but unfortunately it was not stereoselective.[60]

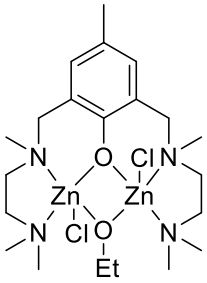

30

Figure 1.32: Hillmayer's and Tolman's binuclear complexes.

In case of polymerization of TMC, Williams *et al.* studied complex **31**, supported by a Robson-type macrocyclic ligand: this specie features phenyl groups, that react rapidly with alcohols to form the initiator in situ (**Figure 1.33**). Polymerization control was characterized by a linear increase of molar mass with monomer conversion, whilst maintaining narrow molar mass distributions (dispersity, $Đ$<1.3). PTMC with high M_n of 167 kDa ($Đ$=1.34) were accessed by conducting polymerizations in THF at room temperature using low catalyst loadings (0.03 mol %, TOF≈3000 h^{-1}). Polymerizations were also successful in the melt (130 °C) reaching high conversions in <10 mins at 4000

equivalents of TMC to catalyst.[61] The same group tested the heterobimetallic Zn and Mg complex **32** in ROCOP polymerisation: this species, likely operating via a chain-shuttling mechanism, had a TOF = 188 h^{-1}, at 1 mol% catalyst loading in neat epoxide, with a catalyst:PA:CHO molar ratio of 1:100:800 at 100 °C. Its activity was 40 times higher than the 1:1 LMg_2Br_2:LZn_2Br_2 mixture. The complex also showed excellent selectivity for polyester formation (>99%) and good polymerisation control with M_n values up to 11 kDa (bimodal $Đ$ = 1.04, 1.09).[62]

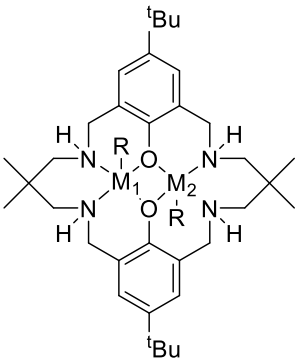

31 $M_1 = M_2$ = Zn R=Ph
32 M_1 = Zn M_2 = Mg R=Br

Figure 1.33: Williams' homo and hetero binuclear complexes

Recently, Williams' group synthesized a bimetallic Zn and Mg acetate complex **33-34**, based on a salen ligand derived from the aforementioned *ortho*-vanillin (**Figure 1.34**). Both systems were active for the copolymerisation, achieving complete conversion of 100 equiv. of PA in neat epoxide, at 100°C, at 1 mol % as catalyst loading, which gave high selectivity for esters bonds (>99%). Also in this case, the zinc complex showed higher activity (TOF = 149 h^{-1}).[63] They also prepared a series of heterobimetallic complexes of zinc by monovalent and divalent metals **35-37**, tested as catalysts in the ROCOP of phthalic anhydride and cyclohexene oxide (**Figure 1.34**). Polymerizations were conducted using a catalyst:PA:CHO molar ratio of 1:100:1000, at a temperature of 100°C. The results showed that all heterobimetallic complexes were active in the ROCOP of PA/CHO, with turnover frequencies ranging from 29 to 67 h^{-1}. In all cases, high selectivity for ester bonds (>99%) and relatively narrow molecular mass distributions ($Đ$

= 1.08–1.23) were observed. Interestingly, none of the tested heterobimetallic complexes showed higher activity than that of the homobimetallic zinc complex (TOF = 149 h^{-1}). This result suggests that simply combining two different metals in a bimetallic complex is not sufficient to achieve catalytic synergy, but it may be necessary to use salen ligands with more electron-donating substituents, or to explore different metal combinations.[64]

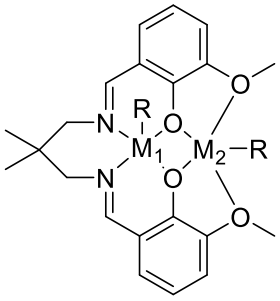

33 M_1=M_2=Zn R= OAc
34 M_1=M_2= Mg R= OAc
35 M_1=M_2=Zn R= I
36 M_1=Zn M_2=Na R=I
37 M_1=Zn M_2= Ca R=I

Figure 1.34: Williams' bimetallic Zn Complex**.**

Exceptionally active heterotrimetallic Na/Zn_2 and K/Zn_2 complexes supported by a ProPhenol ligand have been reported for the ROP of cyclic esters (**Figure 1.35**). The ProPhenol scaffold is a chiral ligand originally developed by Trost,[65] consisting of two pyrrolidine units linked to a central phenolic core, via methylene bridges. In the presence of two equivalents of co-initiator BnOH, the complex K/Zn_2 **38b** polymerized 60 equivalents of *rac*-LA in only 20 s in THF at 25 °C, five times faster than the Na/Zn_2 complex **38a**. Both complexes outperformed the homobimetallic analogue, by combining the high activity of the alkali metals with the superior polymerization control of the zinc framework. The scope of these systems was also extended to ε-caprolactone (ε-CL); notably Na/Zn_2 converting 760 equiv. in 4 minutes at 25°C in THF.[66]

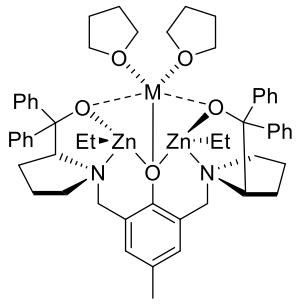

38a M=Na
38b M=K

Figure 1.35: Garden's heterometallic complexes.

1.4 End of Life Options: Chemical Recycling

The growing accumulation of plastic waste in terrestrial and marine ecosystems has made the development of efficient and sustainable recycling strategies a global necessity. Among various end-of-life management options, chemical recycling has emerged as a solution due to its ability to convert waste into high-purity monomers for direct repolymerization, as well as essential raw materials and chemical intermediates for the synthesis of new materials. To maximize the efficiency of these processes, the use of catalysts capable of promoting targeted bond cleavage under mild operating conditions is essential.

This strategy encompasses several approaches, most notably depolymerization and solvolysis (**Figure 1.36**). The former aims to recover the original monomers by thermodynamically reversing the synthesis process. Furthermore, the recovered monomers can be repolymerized, regenerating a virgin material that preserves the mechanical and optical properties of the native polymer intact.[67]

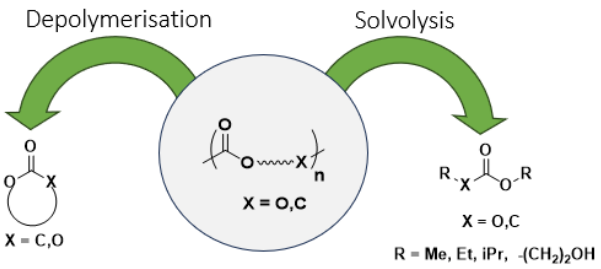

Figure 1.36: Chemical Recycling for Sustainable Polymers.

In solvolysis processes, the degradation of the polymer chain is mediated by chemical interaction with a solvent, which acts as a nucleophile towards the labile bonds in the chain.[68] Depending on the solvent used, the reaction is called hydrolysis, ammonolysis (with ammonia or amines), or alcoholysis (with methanol or ethylene glycol). This approach has attracted particular interest because it allows for the selective production

of high-value products, which can be reintroduced into the production cycle to regenerate the polymer or used for the synthesis of fine chemicals, resins, or plasticizers.

1.4.1 Alcoholysis of Polylactide

Polyester alcoholysis, particularly polylactic acid (PLA), represents a widely investigated valorisation strategy for converting post-consumer waste into alkyl lactates of high industrial interest (**Figure 1.37**). These derivatives have physical and chemical characteristics that allow them to be used as environmentally friendly solvents,[69] diluents for polymer resins,[70] or emulsifying agents in pharmaceutical formulations.[71] Of particular strategic importance are methyl lactate (Me-La) and ethyl lactate (Et-La): these compounds can also be purified and reconverted into lactide, then reused in the polymerization process. This approach allows for the closure of the material's life cycle, regenerating PLA of a quality indistinguishable from virgin material.

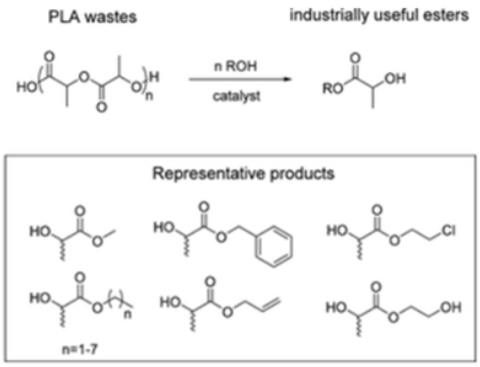

Figure 1.37: Alcoholysis of PLA into lactate esters

The depolymerization process involves the nucleophilic attack of the alcohol on the carbonyl carbon, activated by zinc, which acts as a Lewis acid. In some cases, the attack occurs randomly within the polymer chain, initially producing intermediate oligomers, which are then progressively converted to alkyl lactates (**Figure 1.38a**). Alternatively, the process can proceed through a progressive erosion of the chain ends, leading to the direct and continuous formation of alkyl lactate monomers (**Figure 1.38b**).

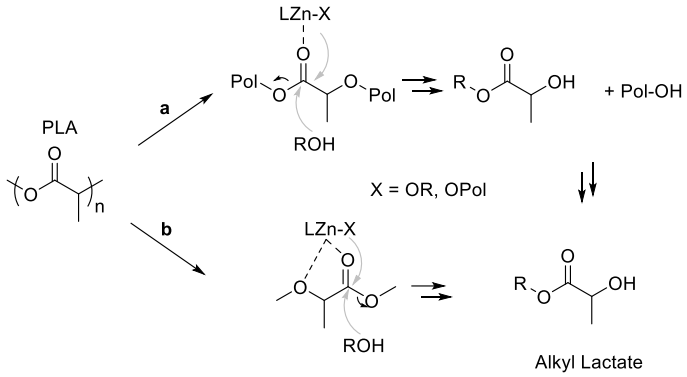

Figure 1.38: Alcoholysis of PLA via random scission of the chains (**a**) or by chain-end cutting (**b**).

Many metal-based and organic catalysts have been implemented in this process, including discrete metal complexes: for instance, complexes of zinc and magnesium, presented by Jones (**Figure 1.39**), were found to be active for the methanolysis of PLA under mild conditions, achieving up to 85% Me-LA yield within 30 min at 50 °C in THF, at 1 mol% as catalyst loading.[72]

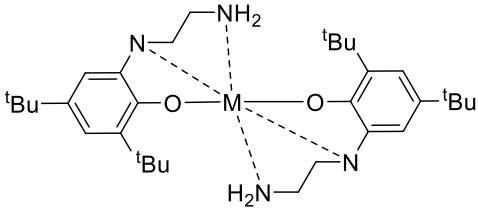

39 M=Zn
40 M=Mg

Figure 1.39: Jones' Zn complex**.**

Fliedel *et al*. reported the first example of a zinc-carbene (NHC) alkoxide complexes for the controlled degradation of PLA (**Figure 1.40**) [45] After quenching the PLA polymerization with methanol, ^{1}H NMR spectrum of the sample contained signals

corresponding to PLA along with the traces of Me-La and associated oligomers. This observation was confirmed by GPC analyses of MeOH quenched sample in which two peaks at lower molecular weight was observed, corresponding to smaller oligomers and methyl lactate. Based on these preliminary results, the authors managed a controlled degradation of a commercial PLLA (M_n = 18410 Da). In presence of methanol, only oligomeric PLA (M_n = 2000 Da) and Me-La (30%) were present in the solution after 24 h at room temperature.

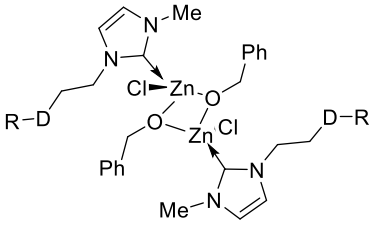

41 D=S; R=Ph
42 D=O; R=Me

Figure 1.40: Fliedel's complexes**.**

Part of our research group has reported heteroleptic complexes of zinc and magnesium supported by tridentate phenoxy-imine-pyridine ligands (section **1.3.2**, see **18-23-24**), active in both lactide polymerization and PLA alcoholysis, demonstrating a direct correlation between polymerization activity and depolymerization efficiency. Using simple alcohols (methanol or ethanol), the most active ROP catalysts achieved PLA conversion above 90% within 1–2 hours at room temperature, without solvent, and with excellent selectivity toward monomeric products.[54,56]

Subsequently, homoleptic zinc complexes with variable electron-donating or electron-withdrawing substituents on the phenolic ring were tested (**Figure 1.41**). Under clean conditions, these same catalyst systems enabled quantitative degradation of PLA in less than 30 minutes at 80°C, maintaining catalytic activity for multiple cycles. The study highlighted how the electronic effects due to electron-donating substituents on the phenoxy group are decisive in increasing the activity.[73]

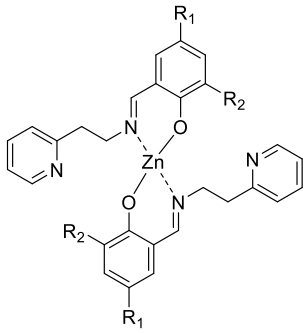

43 R_1 = H R_2 = H
44 R_1 = H R_2 = CH_3
45 R_1 = OCH_3 R_2 = H
46 R_1 = H R_2 = OCH_3
47 R_1 = H R_2 = NO_2
48 R_1 = ^{t}Bu R_2 = ^{t}Bu

Figure 1.41: Mazzeo's complexes**.**

Recently, the same research group extended their investigation to the alcoholysis of PLA, this time assisted by microwave heating. This study revealed that the implementation of alternative dielectric heating significantly improves both the efficiency and selectivity of the alcoholysis process compared to conventional thermal methods. The recycling reactions were conducted in methanol or ethanol, using 5 mol% of catalysts at temperatures ranging from 80 to 100 °C. Under microwave irradiation, quantitative conversion of PLA (>99%) was achieved within 10–20 minutes, while comparable degradation with conventional heating required up to 120 minutes. Among the systems tested, zinc-based catalysts showed the greatest activity and selectivity, producing methyl or ethyl lactate as the predominant products, while magnesium analogues showed slightly slower kinetics but similar product distributions. The remarkable rate enhancement observed under microwave conditions was attributed to more efficient energy transfer, uniform volumetric heating, and rapid activation of the metal-alkoxide intermediates, which collectively facilitate ester bond cleavage along the polymer backbone.[74]

1.4.2 Depolymerisation of APCs

The chemical recycling of aliphatic polycarbonates is governed by the intrinsic susceptibility of carbonate bonds to nucleophilic attack.[75] However, the mechanism and efficiency of depolymerization vary dramatically depending on the polymer's origin.

Specifically, ROCOP-derived polymers undergo a selective "back-biting" mechanism, in which a terminal alkoxide, activated by a catalyst, intramolecularly attacks the adjacent carbonate carbonyl, leading to the formation of a five-membered cyclic carbonate molecule. The high selectivity for the cyclic carbonate rather than the epoxide depends on the more favourable ring strain in the five-membered cyclic carbonate product. (**Figure 1.42, blue arrows**)

In contrast, polycarbonates obtained via ring-opening polymerization of trimethylene carbonate and analogues are governed by a delicate thermodynamic equilibrium between polymer and monomer. In this case, the reverse driving force is the release of ring strain, which is significant in six-membered monomers such as TMC (**Figure 1.42, green arrows**). However, because these rings exhibit lower strain than three- or four-membered rings, the enthalpy of polymerization is less exothermic. This means that when attempting thermal depolymerization, an equilibrium is often reached that favours a mixture of monomers, oligomers, and polymer, making quantitative recovery of the original monomer difficult.[76]

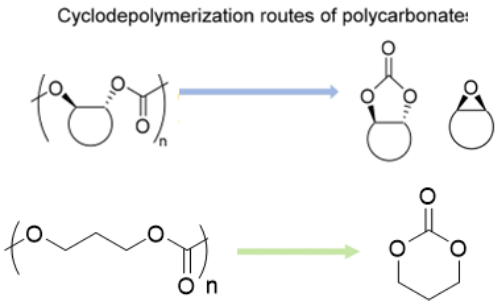

Figure 1.42 Depolymerization for Polycarbonates.

Consequently, the main challenge for synthesized polycarbonates is shifting the equilibrium to achieve quantitative monomer recovery, using suitable and efficient catalytic systems. Among the various approaches explored for chemical recycling of poly(trimethylene carbonate), the organocatalytic systems have demonstrated the highest levels of activity and selectivity under mild conditions. In particular, the strong bifunctional base 1,5,7-Triazabicyclo[4.4.0]dec-5-ene (TBD) has been identified as the reference catalyst for the methanolysis of PTMC, promoting rapid and quantitative depolymerization at room temperature and atmospheric pressure[61,77]

1.5 Aim of the Thesis

The massive use of plastics in modern society, due to their versatility and low production costs, has inevitably led to two critical issues: the depletion of non-renewable raw materials and the growing accumulation of waste. These challenges have spurred considerable interest in the design of sustainable and degradable polymer alternatives, such as aliphatic polyesters and aliphatic polycarbonates. They can be synthesized from renewable resources and offer intrinsic biodegradability, maintaining mechanical properties suitable for applications ranging from biomedical devices to packaging. Since the industrial production of these polymers still largely relies on toxic tin-based catalysts, research is decidedly shifting toward the development of catalytic systems based on abundant, economically viable, and biocompatible metals, eliminating the need to remove residual traces from final products. In this context, the aim of this doctoral thesis was to develop new catalytic systems based on biocompatible metals, such as zinc and magnesium, naturally present in human metabolism, able to promote the synthesis of the targeted polymers, ensuring the safety of the final product. To achieve this goal, some of the most versatile classes of ancillary ligands were employed, exploiting their steric and electronic properties to modulate the reactivity of the metal center. Furthermore, these ligands are characterized by low toxicity, making them ideal candidates for the biomedical applications.

Initially, the study focused on the use of N-heterocyclic carbene (NHC) ligands as ancillary ligands, selected for their unique stereoelectronic properties and high modularity, essential for finely controlling the reactivity of metal centers. Previously, our research group developed zinc complexes supported by a saturated NHC ligand, functionalized on the saturated backbone with *syn*- or *anti*-phenyl groups, in combination with N-tolyl substituents, and used for the ROP of lactide.[50] Taking advantage of the known similarities between esters and cyclic carbonates, the application of one of the systems was extended to the polymerization of trimethylene carbonate and its alkyl-substituted derivatives, monomers specifically synthesized via CO_2 fixation on 1,3-diols. The characterization of the polycarbonates and the study of the polymerization process

demonstrated a high level of control exerted by the employed catalytic systems, subsequently exploited for the synthesis of block copolymers of PTMC with both polylactide (PLA) and polyethylene glycol (PEG) through two different synthetic strategies. Subsequently, the research was extended to the development of new zinc and magnesium complexes, using the two distinct ancillary ligands with different backbone configurations. This precise molecular design generates a specific steric pocket around the metal center, capable of finely modulating its activity and selectivity. In this perspective, the interest in the synthesis of aliphatic polyesters and aliphatic polycarbonates has been extended to the complexes obtained, describing polymerization experiments aimed at making a direct and systematic comparison of the catalytic performances.

In a second phase of the project, attention shifted to tridentate phenoxyimino-based: these represent one of the most versatile platforms, thanks to their ease of synthesis, high structural tunability, and the ability to offer mixed donor atoms capable of forming stable complexes. Here, we proposed new heteroleptic complexes of zinc and magnesium supported by a tridentate naphthoxy-imino-pyridine ligand: the choice of this structure is related to previous studies of our research's group. These studies highlighted how analogous phenoxy-imino-pyridine systems played a decisive role in modulating the catalyst's performance, by changing the nature of the substituents on the phenolic moiety plays.[56] Based on this evidence, it was decided to evolve the design toward the naphthyl moiety. Therefore, we applied these new complexes in homo- and copolymerization of various bio-derived cyclic monomers (both esters and carbonates). Finally, confirming the versatility of the system, the performance of the zinc complex was also evaluated in the depolymerization of PTMC and its copolymers, exploiting microwaves as a more energetically sustainable alternative to conventional heating methods.

The final part of the doctoral project aimed to develop binuclear catalytic systems using multinucleating ligands: their ability to simultaneously coordinate multiple ions allows the metal centers to be positioned at optimal interatomic distances to ensure intramolecular cooperativity, thus surpassing the activity and selectivity of mononuclear

counterparts. For this purpose, salen-type ligands suitably modified to make them capable of coordinating more than one metal centre were used. First, sulfur-functionalized salen ligands were synthesized for the preparation of bimetallic zinc complexes. These systems, already known to be effective in the synthesis of polycarbonates,[78] by ROCOP of epoxides and CO_2 were evaluated here as catalysts in the synthesis of polyesters through ROP and in the alternating copolymerization of epoxides and anhydrides. Subsequently, research focused on a new variant of hexadentate salen ligands, functionalized with amino pendants *ortho* to the phenoxy groups, designed to create a coordination pocket for accommodating a second metal. We described the synthetic strategy adopted for this new class of ligands and initial efforts to isolate the corresponding homo- and heterodinuclear complexes, presenting preliminary studies of their performance in the ROCOP of anhydrides and epoxides.

In the last part of my PhD, I spent a research period abroad at the University of Edinburgh in Dr. Jennifer Garden's research group, where I continued to work on multimetallic complexes, also having the opportunity to explore the potential of heterometallic cooperativity. During this period, my research focused on the synthesis of heterotrimetallic complexes based on zinc and alkali metals, supported by chiral pentadentate ProPhenol ligands, featuring N_2O_3 donors, designed to stabilize the multimetallic core. These catalysts, known in the literature for the polymerization of cyclic esters, exploit a unique synergy between the metal centers: the zinc center hosts the propagating polymer chain, while the alkali metal coordinates and activates the monomer. This cooperative arrangement significantly accelerates reaction kinetics. Here, we present a novel application of these systems, extended to the polymerization of cyclic carbonates and several macrolactones: to our knowledge, this represents the first study aimed at evaluating such complexes with these specific classes of monomers, opening new perspectives for the controlled synthesis of advanced polymeric materials.

1.6 References

(1) *Plastics the Fast Facts 2025 • Plastics Europe*. Plastics Europe. https://plasticseurope.org/knowledge-hub/plastics-the-fast-facts-2025/ (accessed 2025-11-22).

(2) *Plastics – the fast Facts 2023 • Plastics Europe*. Plastics Europe. https://plasticseurope.org/knowledge-hub/plastics-the-fast-facts-2023/ (accessed 2025-11-22).

(3) Shafiee, S.; Topal, E. When Will Fossil Fuel Reserves Be Diminished? *Energy Policy* **2009**, *37* (1), 181–189. https://doi.org/10.1016/j.enpol.2008.08.016.

(4) GEN_Plastics_Dialogues_Outcomes_2021.Pdf. https://www.genevaenvironmentnetwork.org/wp-content/uploads/2022/05/GEN_Plastics_Dialogues_Outcomes_2021.pdf (accessed 2025-11-10).

(5) Bonanno, G.; Orlando-Bonaca, M. Ten Inconvenient Questions about Plastics in the Sea. *Environmental Science & Policy* **2018**, *85*, 146–154. https://doi.org/10.1016/j.envsci.2018.04.005.

(6) Visco, A.; Scolaro, C.; Facchin, M.; Brahimi, S.; Belhamdi, H.; Gatto, V.; Beghetto, V. Agri-Food Wastes for Bioplastics: European Prospective on Possible Applications in Their Second Life for a Circular Economy. *Polymers* **2022**, *14* (13), 2752. https://doi.org/10.3390/polym14132752.

(7) Okolie, O.; Kumar, A.; Edwards, C.; Lawton, L. A.; Oke, A.; McDonald, S.; Thakur, V. K.; Njuguna, J. Bio-Based Sustainable Polymers and Materials: From Processing to Biodegradation. *J. Compos. Sci.* **2023**, *7* (6), 213. https://doi.org/10.3390/jcs7060213.

(8) Singhvi, M. S.; Zinjarde, S. S.; Gokhale, D. V. Polylactic Acid: Synthesis and Biomedical Applications. *Journal of Applied Microbiology* **2019**, *127* (6), 1612–1626. https://doi.org/10.1111/jam.14290.

(9) Madhavan Nampoothiri, K.; Nair, N. R.; John, R. P. An Overview of the Recent Developments in Polylactide (PLA) Research. *Bioresource Technology* **2010**, *101* (22), 8493–8501. https://doi.org/10.1016/j.biortech.2010.05.092.

(10) Pyo, S.-H.; Park, J. H.; Srebny, V.; Hatti-Kaul, R. A Sustainable Synthetic Route for Biobased 6-Hydroxyhexanoic Acid, Adipic Acid and ε-Caprolactone by Integrating Bio- and Chemical Catalysis. *Green Chem.* **2020**, *22* (14), 4450–4455. https://doi.org/10.1039/D0GC01454K.

(11) Choi, S. Y.; Rhie, M. N.; Kim, H. T.; Joo, J. C.; Cho, I. J.; Son, J.; Jo, S. Y.; Sohn, Y. J.; Baritugo, K.-A.; Pyo, J.; Lee, Y.; Lee, S. Y.; Park, S. J. Metabolic Engineering for the Synthesis of Polyesters: A 100-Year Journey from Polyhydroxyalkanoates to Non-Natural Microbial Polyesters. *Metabolic Engineering* **2020**, *58*, 47–81. https://doi.org/10.1016/j.ymben.2019.05.009.

(12) Thomas, S.; Visakh, P. M. *Handbook of Engineering and Specialty Thermoplastics, Volume 3: Polyethers and Polyesters*; John Wiley & Sons, 2011; Vol. 3.

(13) Shelnutt, S.; Kind, J.; Allaben, W. Bisphenol A: Update on Newly Developed Data and How They Address NTP's 2008 Finding of "Some Concern." *Food and Chemical Toxicology* **2013**, *57*, 284–295. https://doi.org/10.1016/j.fct.2013.03.027.

(14) Brannigan, R. P.; Dove, A. P. Synthesis, Properties and Biomedical Applications of Hydrolytically Degradable Materials Based on Aliphatic Polyesters and Polycarbonates. *Biomater. Sci.* **2017**, *5* (1), 9–21. https://doi.org/10.1039/C6BM00584E.

(15) Suriano, F.; Coulembier, O.; Hedrick, J. L.; Dubois, P. Functionalized Cyclic Carbonates: From Synthesis and Metal-Free Catalyzed Ring-Opening Polymerization to Applications. *Polym. Chem.* **2011**, *2* (3), 528–533. https://doi.org/10.1039/C0PY00211A.

(16) Xu, J.; Feng, E.; Song, J. Renaissance of Aliphatic Polycarbonates: New Techniques and Biomedical Applications. *Journal of Applied Polymer Science* **2014**, *131* (5). https://doi.org/10.1002/app.39822.

(17) *Update and Challenges in Carbon Dioxide-Based Polycarbonate Synthesis*. https://chemistry-

europe.onlinelibrary.wiley.com/doi/epdf/10.1002/cssc.201902719 (accessed 2025-10-18).

(18) Reithofer, M. R.; Sum, Y. N.; Zhang, Y. Synthesis of Cyclic Carbonates with Carbon Dioxide and Cesium Carbonate. *Green Chem.* **2013**, *15* (8), 2086. https://doi.org/10.1039/c3gc40790j.

(19) McGuire, T. M.; López-Vidal, E. M.; Gregory, G. L.; Buchard, A. Synthesis of 5- to 8-Membered Cyclic Carbonates from Diols and CO_2: A One-Step, Atmospheric Pressure and Ambient Temperature Procedure. *Journal of CO_2 Utilization* **2018**, *27*, 283–288. https://doi.org/10.1016/j.jcou.2018.08.009.

(20) Gregory, G. L.; Jenisch, L. M.; Charles, B.; Kociok-Köhn, G.; Buchard, A. Polymers from Sugars and CO_2 : Synthesis and Polymerization of a D -Mannose-Based Cyclic Carbonate. *Macromolecules* **2016**, *49* (19), 7165–7169. https://doi.org/10.1021/acs.macromol.6b01492.

(21) Han, Y.; Fan, Z.; Lu, Z.; Zhang, Y.; Li, S. In Vitro Degradation of Poly[(L-Lactide)-Co-(Trimethylene Carbonate)] Copolymers and a Composite with Poly[(L-Lactide)-Co-Glycolide] Fibers as Cardiovascular Stent Material. *Macromolecular Materials and Engineering* **2012**, *297* (2), 128–135. https://doi.org/10.1002/mame.201100113.

(22) Widjaja, L. K.; Kong, J. F.; Chattopadhyay, S.; Lipik, V. T.; Liow, S. S.; Abadie, M. J. M.; Venkatraman, S. S. Triblock Copolymers of ε-Caprolactone, L-Lactide, and Trimethylene Carbonate: Biodegradability and Elastomeric Behavior. *Journal of Biomedical Materials Research Part A* **2011**, *99A* (1), 38–46. https://doi.org/10.1002/jbm.a.33161.

(23) Zhang, J.; Zhu, W.; Li, C.; Zhang, D.; Xiao, Y.; Guan, G.; Zheng, L. Effect of the Biobased Linear Long-Chain Monomer on Crystallization and Biodegradation Behaviors of Poly(Butylene Carbonate)-Based Copolycarbonates. *RSC Adv.* **2015**, *5* (3), 2213–2222. https://doi.org/10.1039/C4RA10466H.

(24) Byrne, C. M.; Allen, S. D.; Lobkovsky, E. B.; Coates, G. W. Alternating Copolymerization of Limonene Oxide and Carbon Dioxide. *J. Am. Chem. Soc.* **2004**, *126* (37), 11404–11405. https://doi.org/10.1021/ja0472580.

(25) Yang, G.-W.; Zhang, Y.-Y.; Wang, Y.; Wu, G.-P.; Xu, Z.-K.; Darensbourg, D. J. Construction of Autonomic Self-Healing CO_2 -Based Polycarbonates via One-Pot Tandem Synthetic Strategy. *Macromolecules* **2018**, *51* (4), 1308–1313. https://doi.org/10.1021/acs.macromol.7b02715.

(26) Bhat, G. A.; Rashad, A. Z.; Folsom, T. M.; Darensbourg, D. J. Placing Single-Metal Complexes into the Backbone of CO_2 -Based Polycarbonate Chains, Construction of Nanostructures for Prospective Micellar Catalysis. *Organometallics* **2020**, *39* (9), 1612–1618. https://doi.org/10.1021/acs.organomet.9b00704.

(27) Taherimehr, M.; Pescarmona, P. P. Green Polycarbonates Prepared by the Copolymerization of CO_2 with Epoxides. *Journal of Applied Polymer Science* **2014**, *131* (21). https://doi.org/10.1002/app.41141.

(28) Coates, G. W.; Moore, D. R. Discrete Metal-Based Catalysts for the Copolymerization of CO_2 and Epoxides: Discovery, Reactivity, Optimization, and Mechanism. *Angewandte Chemie International Edition* **2004**, *43* (48), 6618–6639. https://doi.org/10.1002/anie.200460442.

(29) Trott, G.; Saini, P. K.; Williams, C. K. Catalysts for CO_2 /Epoxide Ring-Opening Copolymerization. *Phil. Trans. R. Soc. A.* **2016**, *374* (2061), 20150085. https://doi.org/10.1098/rsta.2015.0085.

(30) Darensbourg, D. J.; Moncada, A. I. Tuning the Selectivity of the Oxetane and CO_2 Coupling Process Catalyzed by (Salen)CrCl/ *n* -Bu_4 NX: Cyclic Carbonate Formation vs Aliphatic Polycarbonate Production. *Macromolecules* **2010**, *43* (14), 5996–6003. https://doi.org/10.1021/ma100896x.

(31) Yu, W.; Maynard, E.; Chiaradia, V.; Arno, M. C.; Dove, A. P. Aliphatic Polycarbonates from Cyclic Carbonate Monomers and Their Application as Biomaterials. *Chem. Rev.* **2021**, *121* (18), 10865–10907. https://doi.org/10.1021/acs.chemrev.0c00883.

(32) Keul, H. Polycarbonates. In *Handbook of Ring-Opening Polymerization*; John Wiley & Sons, Ltd, 2009; pp 307–327. https://doi.org/10.1002/9783527628407.ch12.

(33) Mankaev, B. N.; Karlov, S. S. Metal Complexes in the Synthesis of Biodegradable Polymers: Achievements and Prospects. *Materials* **2023**, *16* (20), 6682. https://doi.org/10.3390/ma16206682.

(34) Nifant'ev, I.; Ivchenko, P. Coordination Ring-Opening Polymerization of Cyclic Esters: A Critical Overview of DFT Modeling and Visualization of the Reaction Mechanisms. *Molecules* **2019**, *24* (22), 4117. https://doi.org/10.3390/molecules24224117.

(35) Bridging the Gap in Catalysis via Multidisciplinary Approaches. *Dalton Trans.* **2010**, *39* (36), 8354. https://doi.org/10.1039/c0dt90044c.

(36) Dechy-Cabaret, O.; Martin-Vaca, B.; Bourissou, D. Controlled Ring-Opening Polymerization of Lactide and Glycolide. *Chem. Rev.* **2004**, *104* (12), 6147–6176. https://doi.org/10.1021/cr040002s.

(37) Kricheldorf, H. R.; Kreiser-Saunders, I.; Jürgens, C.; Wolter, D. Polylactides - Synthesis, Characterization and Medical Application. *Macromolecular Symposia* **1996**, *103* (1), 85–102. https://doi.org/10.1002/masy.19961030110.

(38) Fazekas, E.; Lowy, P. A.; Abdul Rahman, M.; Lykkeberg, A.; Zhou, Y.; Chambenahalli, R.; Garden, J. A. Main Group Metal Polymerisation Catalysts. *Chem. Soc. Rev.* **2022**, *51* (21), 8793–8814. https://doi.org/10.1039/D2CS00048B.

(39) Kremer, A. B.; Mehrkhodavandi, P. Dinuclear Catalysts for the Ring Opening Polymerization of Lactide. *Coordination Chemistry Reviews* **2019**, *380*, 35–57. https://doi.org/10.1016/j.ccr.2018.09.008.

(40) Santoro, O.; Zhang, X.; Redshaw, C. Synthesis of Biodegradable Polymers: A Review on the Use of Schiff-Base Metal Complexes as Catalysts for the Ring Opening Polymerization (ROP) of Cyclic Esters. *Catalysts* **2020**, *10* (7), 800. https://doi.org/10.3390/catal10070800.

(41) Bourissou, D.; Guerret, O.; Gabbaï, F. P.; Bertrand, G. Stable Carbenes. *Chem. Rev.* **2000**, *100* (1), 39–92. https://doi.org/10.1021/cr940472u.

(42) Jensen, T. R.; Schaller, C. P.; Hillmyer, M. A.; Tolman, W. B. Zinc N-Heterocyclic Carbene Complexes and Their Polymerization of d,l-Lactide. *Journal of*

Organometallic Chemistry **2005**, *690* (24–25), 5881–5891. https://doi.org/10.1016/j.jorganchem.2005.07.070.

(43) Jensen, T. R.; Breyfogle, L. E.; Hillmyer, M. A.; Tolman, W. B. Stereoelective Polymerization of d,l-Lactide Using N-Heterocyclic Carbene Based Compounds. *Chem. Commun.* **2004**, No. 21, 2504. https://doi.org/10.1039/b405362a.

(44) Collins, L. R.; Moffat, L. A.; Mahon, M. F.; Jones, M. D.; Whittlesey, M. K. Lactide Polymerisation by Ring-Expanded NHC Complexes of Zinc. *Polyhedron* **2016**, *103*, 121–125. https://doi.org/10.1016/j.poly.2015.09.022.

(45) Fliedel, C.; Vila-Viçosa, D.; Calhorda, M. J.; Dagorne, S.; Avilés, T. Dinuclear Zinc–N-Heterocyclic Carbene Complexes for Either the Controlled Ring-Opening Polymerization of Lactide or the Controlled Degradation of Polylactide Under Mild Conditions. *ChemCatChem* **2014**, *6* (5), 1357–1367. https://doi.org/10.1002/cctc.201301015.

(46) Fliedel, C.; Mameri, S.; Dagorne, S.; Avilés, T. Controlled Ring-Opening Polymerization of Trimethylene Carbonate and Access to PTMC-PLA Block Copolymers Mediated by Well-Defined N-Heterocyclic Carbene Zinc Alkoxides. *Applied Organometallic Chemistry* **2014**, *28* (7), 504–511. https://doi.org/10.1002/aoc.3154.

(47) Naumann, S.; Schmidt, F. G.; Frey, W.; Buchmeiser, M. R. Protected N-Heterocyclic Carbenes as Latent Pre-Catalysts for the Polymerization of ε-Caprolactone. *Polym. Chem.* **2013**, *4* (15), 4172. https://doi.org/10.1039/c3py00548h.

(48) Arnold, P. L.; Casely, I. J.; Turner, Z. R.; Bellabarba, R.; Tooze, R. B. Magnesium and Zinc Complexes of Functionalised, Saturated N-Heterocyclic Carbene Ligands: Carbene Lability and Functionalisation, and Lactide Polymerisation Catalysis. *Dalton Trans.* **2009**, No. 35, 7236. https://doi.org/10.1039/b907034f.

(49) Ferrentino, N.; Franco, F.; Grisi, F.; Pragliola, S.; Mazzeo, M.; Costabile, C. Ring Opening Polymerization of Lactide Promoted by Zinc and Magnesium Complexes with a N-Heterocyclic Carbene-Phenoxy-Imine Hybrid Non-Innocent

Ligand. *Molecular Catalysis* **2022**, *533*, 112799. https://doi.org/10.1016/j.mcat.2022.112799.

(50) Tufano, F.; Santulli, F.; Grisi, F.; Lamberti, M. N-Heterocyclic Carbene-Based Zinc Complexes: Same Precursors for Different Lactide Ring-Opening Polymerization Mechanisms. *ChemCatChem* **2022**, *14* (20), e202200962. https://doi.org/10.1002/cctc.202200962.

(51) Cozzi, P. G. Metal–Salen Schiff Base Complexes in Catalysis: Practical Aspects. *Chem. Soc. Rev.* **2004**, *33* (7), 410–421. https://doi.org/10.1039/B307853C.

(52) Williams, C. K.; Breyfogle, L. E.; Choi, S. K.; Nam, W.; Young, V. G.; Hillmyer, M. A.; Tolman, W. B. A Highly Active Zinc Catalyst for the Controlled Polymerization of Lactide. *J. Am. Chem. Soc.* **2003**, *125* (37), 11350–11359. https://doi.org/10.1021/ja0359512.

(53) McKeown, P.; McCormick, S. N.; Mahon, M. F.; Jones, M. D. Highly Active Mg(II) and Zn(II) Complexes for the Ring Opening Polymerisation of Lactide. *Polym. Chem.* **2018**, *9* (44), 5339–5347. https://doi.org/10.1039/C8PY01369A.

(54) Santulli, F.; Lamberti, M.; Mazzeo, M. A Single Catalyst for Promoting Reverse Processes: Synthesis and Chemical Degradation of Polylactide. *ChemSusChem* **2021**, *14* (24), 5470–5475. https://doi.org/10.1002/cssc.202101518.

(55) Santulli, F.; Pappalardo, D.; Lamberti, M.; Amendola, A.; Barba, C.; Sessa, A.; Tepedino, G.; Mazzeo, M. Simple and Efficient Zinc Catalysts for Synthesis and Chemical Degradation of Polyesters. *ACS Sustainable Chem. Eng.* **2023**, *11* (43), 15699–15709. https://doi.org/10.1021/acssuschemeng.3c04927.

(56) Santulli, F.; Gravina, G.; Lamberti, M.; Tedesco, C.; Mazzeo, M. Zinc and Magnesium Catalysts for the Synthesis for PLA and Its Degradation: Clues for Catalyst Design. *Molecular Catalysis* **2022**, *528*, 112480. https://doi.org/10.1016/j.mcat.2022.112480.

(57) Darensbourg, D. J.; Choi, W.; Richers, C. P. Ring-Opening Polymerization of Cyclic Monomers by Biocompatible Metal Complexes. Production of Poly(Lactide), Polycarbonates, and Their Copolymers. *Macromolecules* **2007**, *40* (10), 3521–3523. https://doi.org/10.1021/ma062780n.

(58) Darensbourg, D. J.; Choi, W.; Ganguly, P.; Richers, C. P. Biometal Derivatives as Catalysts for the Ring-Opening Polymerization of Trimethylene Carbonate. Optimization of the Ca(II) Salen Catalyst System. *Macromolecules* **2006**, *39* (13), 4374–4379. https://doi.org/10.1021/ma0603433.

(59) Huang, M.; Pan, C.; Ma, H. Ring-Opening Polymerization of Rac-Lactide and α-Methyltrimethylene Carbonate Catalyzed by Magnesium and Zinc Complexes Derived from Binaphthyl-Based Iminophenolate Ligands. *Dalton Trans.* **2015**, *44* (27), 12420–12431. https://doi.org/10.1039/C5DT00158G.

(60) Williams, C. K.; Brooks, N. R.; Hillmyer, M. A.; Tolman, W. B. Metalloenzyme Inspired Dizinc Catalyst for the Polymerization of Lactide. *Chem. Commun.* **2002**, No. 18, 2132–2133. https://doi.org/10.1039/b206437e.

(61) Gregory, G. L.; Sulley, G. S.; Kimpel, J.; Łagodzińska, M.; Häfele, L.; Carrodeguas, L. P.; Williams, C. K. Block Poly(Carbonate-Ester) Ionomers as High-Performance and Recyclable Thermoplastic Elastomers. *Angewandte Chemie International Edition* **2022**, *61* (47), e202210748. https://doi.org/10.1002/anie.202210748.

(62) Garden, J. A.; Saini, P. K.; Williams, C. K. Greater than the Sum of Its Parts: A Heterodinuclear Polymerization Catalyst. *J. Am. Chem. Soc.* **2015**, *137* (48), 15078–15081. https://doi.org/10.1021/jacs.5b09913.

(63) Thevenon, A.; Garden, J. A.; White, A. J. P.; Williams, C. K. Dinuclear Zinc Salen Catalysts for the Ring Opening Copolymerization of Epoxides and Carbon Dioxide or Anhydrides. *Inorg. Chem.* **2015**, *54* (24), 11906–11915. https://doi.org/10.1021/acs.inorgchem.5b02233.

(64) Deacy, A. C.; Durr, C. B.; Kerr, R. W. F.; Williams, C. K. Heterodinuclear Catalysts Zn(Ⅱ)/M and Mg(Ⅱ)/M, Where M = Na(Ⅰ), Ca(Ⅱ) or Cd(Ⅱ), for Phthalic Anhydride/Cyclohexene Oxide Ring Opening Copolymerisation. *Catal. Sci. Technol.* **2021**, *11* (9), 3109–3118. https://doi.org/10.1039/D1CY00238D.

(65) Trost, B. M.; Bartlett, M. J. ProPhenol-Catalyzed Asymmetric Additions by Spontaneously Assembled Dinuclear Main Group Metal Complexes. *Acc. Chem. Res.* **2015**, *48* (3), 688–701. https://doi.org/10.1021/ar500374r.

(66) Gruszka, W.; Lykkeberg, A.; Nichol, G. S.; Shaver, M. P.; Buchard, A.; Garden, J. A. Combining Alkali Metals and Zinc to Harness Heterometallic Cooperativity in Cyclic Ester Ring-Opening Polymerisation. *Chem. Sci.* **2020**, *11* (43), 11785–11790. https://doi.org/10.1039/D0SC04705H.

(67) Payne, J.; Jones, M. D. The Chemical Recycling of Polyesters for a Circular Plastics Economy: Challenges and Emerging Opportunities. *ChemSusChem* **2021**, *14* (19), 4041–4070. https://doi.org/10.1002/cssc.202100400.

(68) Hong, M.; Chen, E. Y.-X. Chemically Recyclable Polymers: A Circular Economy Approach to Sustainability. *Green Chem.* **2017**, *19* (16), 3692–3706. https://doi.org/10.1039/C7GC01496A.

(69) Pereira, C. S. M.; Silva, V. M. T. M.; Rodrigues, A. E. Ethyl Lactate as a Solvent: Properties, Applications and Production Processes – a Review. *Green Chem.* **2011**, *13* (10), 2658. https://doi.org/10.1039/c1gc15523g.

(70) Bakker, H. R.; Kranz, M. T. C. Paint Composition Based on a Chemical Cross Linking System and/or Oxidative Drying, with Lactates as Solvent and Thinner. *EP1023405 A1* **1999**.

(71) Muse, J.; Colvin, H. A. (73) Assignee: Ther Panel Midland Company,.

(72) Payne, J. M.; Kociok-Köhn, G.; Emanuelsson, E. A. C.; Jones, M. D. Zn(II)- and Mg(II)-Complexes of a Tridentate {ONN} Ligand: Application to Poly(Lactic Acid) Production and Chemical Upcycling of Polyesters. *Macromolecules* **2021**, *54* (18), 8453–8469. https://doi.org/10.1021/acs.macromol.1c01207.

(73) D'Aniello, S.; Laviéville, S.; Santulli, F.; Simon, M.; Sellitto, M.; Tedesco, C.; Thomas, C. M.; Mazzeo, M. Homoleptic Phenoxy-Imine Pyridine Zinc Complexes: Efficient Catalysts for Solvent Free Synthesis and Chemical Degradation of Polyesters. *Catal. Sci. Technol.* **2022**, *12* (20), 6142–6154. https://doi.org/10.1039/D2CY01092E.

(74) Santulli, F.; Ferrandino, M. P.; Cioffi, C.; Acocella, M. R.; Lamberti, M.; Mazzeo, M. Chemical Recycling of Polylactide by Microwave-Assisted Processes. *Faraday Discuss.* **2025**, 10.1039.D5FD00078E. https://doi.org/10.1039/D5FD00078E.

(75) Jehanno, C.; Alty, J. W.; Roosen, M.; De Meester, S.; Dove, A. P.; Chen, E. Y.-X.; Leibfarth, F. A.; Sardon, H. Critical Advances and Future Opportunities in Upcycling Commodity Polymers. *Nature* **2022**, *603* (7903), 803–814. https://doi.org/10.1038/s41586-021-04350-0.

(76) Saxon, D. J.; Gormong, E. A.; Shah, V. M.; Reineke, T. M. Rapid Synthesis of Chemically Recyclable Polycarbonates from Renewable Feedstocks. *ACS Macro Lett.* **2021**, *10* (1), 98–103. https://doi.org/10.1021/acsmacrolett.0c00747.

(77) Fukushima, K.; Watanabe, Y.; Ueda, T.; Nakai, S.; Kato, T. Organocatalytic Depolymerization of Poly(Trimethylene Carbonate). *Journal of Polymer Science* **2022**, *60* (24), 3489–3500. https://doi.org/10.1002/pol.20220551.

(78) Cozzolino, M.; Melchionno, F.; Santulli, F.; Mazzeo, M.; Lamberti, M. Aldimine-Thioether-Phenolate Based Mono- and Bimetallic Zinc Complexes as Catalysts for the Reaction of CO_2 with Cyclohexene Oxide. *European Journal of Inorganic Chemistry* **2020**, *2020* (17), 1645–1653. https://doi.org/10.1002/ejic.202000119.

Chapter Two

NHC-Zinc Complex as Efficient Catalysts for Ring-Opening Polymerization of CO_2-based Cyclic Carbonates

The results described in this *Chapter* have been published in:

Tufano F., Napolitano C., Mazzeo M., Grisi F., and Lamberti M., CO_2-Based Polycarbonates through Ring-Opening Polymerization of Cyclic Carbonates Promoted by a NHC-Based Zinc Complex *Biomacromolecules* **2024** *25* (7), 4523-4534

2.1 Introduction

Aliphatic polycarbonates (APCs) represent an emerging class of sustainable polymers that has attracted growing interest in recent years for a variety of applications.[1] Among the various synthetic strategies, ring-opening polymerization (ROP) of cyclic carbonates plays a key role.[2,3] These monomers can be obtained through environmentally sustainable processes starting from CO_2, an abundant, renewable, and inexpensive resource—and diols, derived from the fermentation of carbohydrates.[4,5] To ensure that the sustainability criteria are respected throughout the entire life cycle of the polymer, the use of high-performance ROP catalysts is required. ROP of cyclic carbonates by metal complexes has been conventionally performed using tin based catalysts,[6] while a valid alternative is the use of biometal-based complexes. This approach eliminates the risk associated with the difficulty of removing trace amounts of metal residues from the produced polycarbonates. In this context, zinc is particularly interesting: as an active participant in human metabolism, trace amounts of zinc are well tolerated in the final product. Our group has previously developed zinc complexes supported by saturated N-heterocyclic carbene (NHC) as active catalysts in the ROP of lactides.[7] Given the similarities between the ROP of lactides and of cyclic carbonates, these catalysts offer a promising platform for the synthesis of APCs. This chapter describes the application of one of the previously developed NHC-zinc complexes in the ROP of TMC and of alkyl-substituted derivatives, specifically synthesized from CO_2 and 1,3-diols. The characterization of the polycarbonates and the study of the polymerization process demonstrated a high level of control exerted by the employed catalytic systems, subsequently exploited for the synthesis of block copolymers of PTMC with both polylactide (PLA) and polyethylene glycol (PEG) through two different synthetic strategies.

2.2 Results and Discussions

The zinc complex employed in this study (**Scheme 2.1**) was synthesized following a previously reported procedure, via the amine elimination reaction between the corresponding NHC carbene salt and one equivalent of $Zn[N(SiMe_3)_2]_2$.[7]

The resulting complex was isolated with high purity and fully characterized by NMR spectroscopy **(Figures 2.11 and 2.12**), confirming the formation of the predicted species. Given the excellent results in terms of control of polymerisation for lactide, we decided to extend our study to polymerisation of TMC and CO_2-based cyclic carbonates.

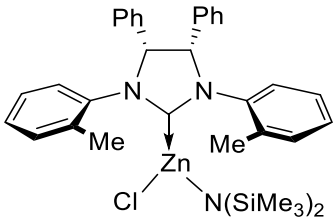

Scheme 2.1. Zinc Complex **1a** Studied in This Chapter.

2.2.1 Ring Opening Polymerisation of TMC

Our research began by evaluating the catalytic performance of the zinc complex in the ROP of trimethylene carbonate (TMC). Polymerizations were conducted at 20 °C using various initiators and solvents, and reaction progress was monitored by ^{1}H NMR spectroscopy through the integration of the PTMC (4.23 ppm) and TMC (4.45 ppm) resonances (**Table 2.1**).

Table 2.1. Ring-opening polymerization of TMC by the NHC zinc complex.

Entry [a]	Comp.: TMC: cocat	Cocat	Solv.	Time	Conv.[b] (%)	M_n^{th} [c]	M_n^{exp} [d]	$Đ$[d]
1	1:30:0	BnOH	DCM	30 min 5.50 h	15 78	2.4	29.5	2.0
2	1:30:1	BnOH	DCM	30 min 5.50 h	40 81	2.5	2.1 **2.8**	1.2
3	1:100:1	BnOH	DCM	30 min 1.5 h	57 91	9.3	9.4	1.2
4	1:100:3	BnOH	DCM	30 min 3 h	30 78	2.8	2.7 **3.3**	1.2
5	1:100:1	BnOH	THF	30 min 1.5 h	36 88	8.6	8.2	1.2
6	1:100:1	BnOH	Me-THF	30 min 6.5 h	21 55	5.6	4.9	1.3
7	1:100:1	BnOH	toluene	30 min 16 h	9 85	8.7	9.5	1.3

8	1:30:1	^{i}PrOH	DCM	30 min 3 h	48 84	2.4	**3.5**	
9	1:30:0.5	BDM	DCM	30 min 3 h	24 60	3.7	**3.3**	

[a] $[Zn]_0$ = 1.0 mM (8.0 µmol in 0.8 mL of solvent). [b] Conversion determined by ^{1}H NMR ($CDCl_3$) integrals of TMC (δ = 4.45 ppm) and PTMC (δ = 4.23 ppm). [c] Theoretical M_n based on starting monomer to initiator ratio, TMC conversion and MM_{TMC} = 102.1 Da . [d] $M_{n,}^{exp}$: $M_{n,}^{GPC}$ and $Đ$ (= M_w/M_n) determined by GPC (RI detector vs PS standards), with M_n^{GPC} corrected using the factors: 0.57 for M_n < 5000, 0.73 for 5000 < M_n < 10000, 0.88 for M_n > 10000,[36] in bold M_n determined by MALDI-FT-ICR spectrometry.

Initial screening experiments in dichloromethane (DCM) showed that, in the absence of an initiator, the polymerization proceeded slowly and exhibited poor molecular-weight control. In contrast, the addition of one equivalent of benzyl alcohol (BnOH) markedly enhanced catalytic activity, affording polymers with molecular weights determined by GPC and MALDI-FT-ICR in close agreement with theoretical values. The influence of solvent was explored by performing polymerizations in tetrahydrofuran (THF), 2-methyltetrahydrofuran (2-MeTHF), and toluene. Comparing the conversion after 30 min, the following activity trend was established: DCM > THF > 2-MeTHF > toluene. This correlation with solvent polarity suggests a beneficial effect of more polar media: the reduced activity in toluene may also be attributed to the lower solubility of the monomer. Although 2-MeTHF resulted in slower kinetics, its status as an environmentally friendly biomass-derived solvent improves the overall sustainability of the process.

We subsequently evaluated the efficiency of several initiators, including isopropyl alcohol and the bifunctional initiator 1,4-benzene dimethanol. Under identical conditions (see Entries 2, 8, and 9), all initiators produced active catalytic systems, although BnOH allowed for the fastest polymerization. Notably, the initiator variation provides a direct method for installing specific end groups, a feature explored in detail

below. As mentioned previously, the resulting polymers were comprehensively characterized by NMR, MALDI-FT-ICR, and GPC. ^{1}H NMR spectra consistently showed a triplet at 4.23 ppm and a quintet at 2.04 ppm in an intensity ratio of 2:1, confirming the polycarbonate structure.

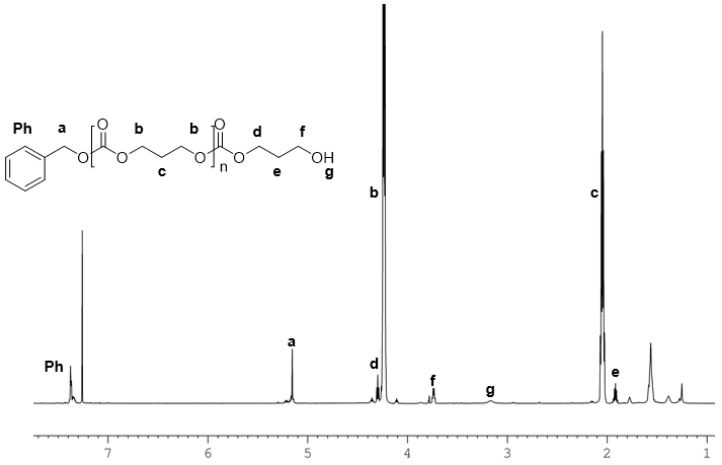

Figure 2.1: ^{1}H NMR spectrum of sample of poly(TMC) with benzyloxy and hydroxylic terminal groups (Entry 2 in **Table 2.1**, $CDCl_3$, 600 MHz, 20°C).

It is crucial to note that the absence of resonances at 1.8 and 3.4 ppm indicates the absence of detectable polyoxetane formation, ruling out decarboxylation. For PTMCs synthesized with BnOH, minor resonances corresponding to end groups were observed: signals at 1.92, 3.73, and 4.30 ppm were assigned to the terminal methylenes of the ω chain, while signals at 5.15 and 7.38 ppm were attributed to the α-terminus of the benzyloxy α chain (**Figure 2.1**). ^{13}C NMR spectra, consistent with this structure (**Figure 2.13**), support a mechanism involving initiation by BnOH and termination by hydrolysis. This end-group fidelity was maintained with other initiators (Entries 8, 9; **Figures 2.14-2.15**), enabling the synthesis of telechelic polymers with hydroxyl end groups for subsequent functionalization.

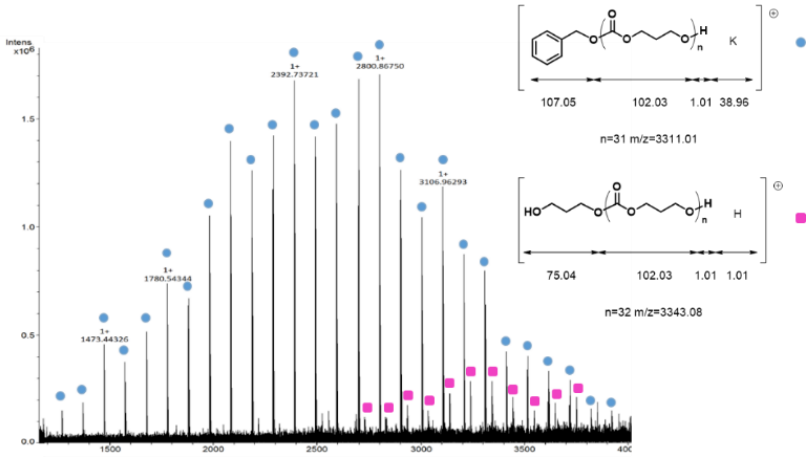

Figure 2.2: MALDI-FT-ICR spectrum of the PMTC obtained in Entry 2 of **Table 2.1**.

MALDI-FT-ICR analysis corroborated the NMR results. The spectrum of the polymer from Entry 2 (**Figure 2.2**) showed a primary series of peaks spaced at intervals of ~102 Da, corresponding to PTMC chains without decarboxylation. The peak at 2800.87 was assigned to the potassium adduct of a 26-mer with a benzyloxy terminal group and a hydroxyl terminal group ($[M + K]^+$ calcd. 2800.85 Da). The absence of cyclic oligomer peaks indicates that intramolecular transesterification was negligible, confirming the high degree of control. A minor distribution was also observed, attributed to dihydroxyl-terminated chains resulting from hydrolysis. The use of different initiators produced MALDI-FT-ICR spectra consistent with the predicted α-chain terminal: isopropoxy groups from isopropyl alcohol **(Figure 2.16**) and hydroxyl-terminated telechelic chains from BDM **(Figure 2.17).** The controlled nature of the polymerization was further highlighted by the close agreement between theoretical and experimental molecular weights (GPC, MALDI-FT-ICR) and the linear increase in M_n with conversion, while maintaining low dispersity ($Đ \leq 1.2$). Kinetic studies revealed a first-order dependence on monomer concentration in all solvents (**Figure 2.3**), with observed rate constants (k_{obs}) that mirrored the solvent activity trend.

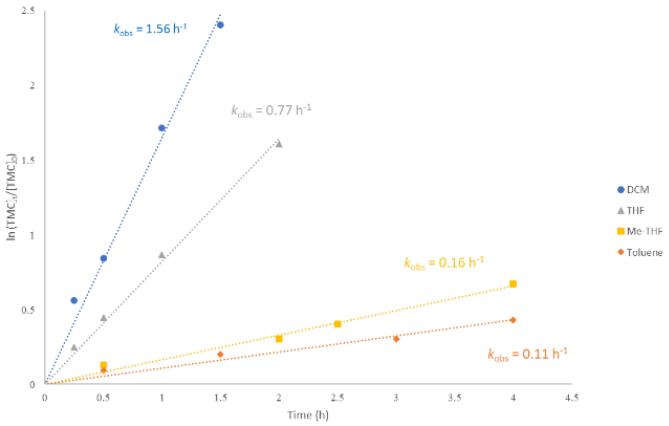

Figure 2.3: First-order kinetic plots for the consumption of TMC by complex **1a** in different solvents (see Entries 3 and 5-7 of **Table 2.1**) in combination with BnOH, at 25°C. Conditions: [**1a**]:[BnOH]:[TMC]$_0$ = 1:1:100

To determine the reaction order for the catalyst, polymerizations were carried out in CD_2Cl_2 at different concentrations of complex Zn (**Figure 2.18**). A plot of ln k_{obs} versus ln [**1a**] yielded a slope of 1.1 (**Figure 2.4**), establishing a first-order dependence. Consequently, the overall rate law for the TMC polymerization catalysed by complex Zn/BnOH is: d[TMC]/dt = k_p[**1a**][TMC].

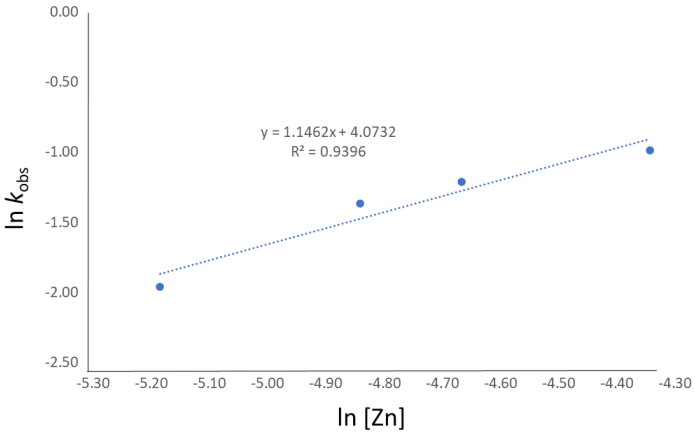

Figure 2.4: Plot of ln k_{obs} versus ln [**1a**] for the polymerization of TMC with the zinc complex 0.56, 0.79, 0.94 and 1.30 mM) and BnOH (one equivalent) (CD_2Cl_2, 25 °C, $[TMC]_0$ = 0.47 M).

2.2.2 Mechanistic Investigations

To clarify the polymerization mechanism, we conducted a series of NMR spectroscopic studies. The stoichiometric reaction of the Zn complex with benzyl alcohol in C_6D_6 at room temperature led to the formation of the alcohol adduct L1HOBn (**Scheme 2.2**).

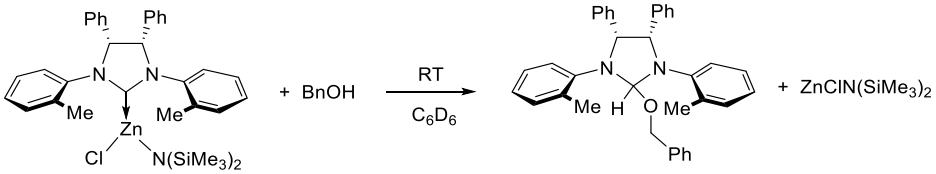

Scheme 2.2: Synthesis of the alcohol adduct L1HOBn from complex **1a.**

The formation of this species is indicated by the appearance of characteristic signals at 2.50 ppm and 6.50 ppm in the ^{1}H NMR spectrum, assigned to the methylene protons of the benzyloxy group and the C*-H proton of the NHC backbone, respectively. The remaining signals are consistent with the proposed structure (**Figure 2.5**), confirming

the formation of the adduct. A smaller signal at 4.28 ppm, attributable to excess benzyl alcohol, further demonstrates the stability of the L1HOBn adduct under these conditions. The spectral symmetry suggests a well-defined and symmetrical species in solution.

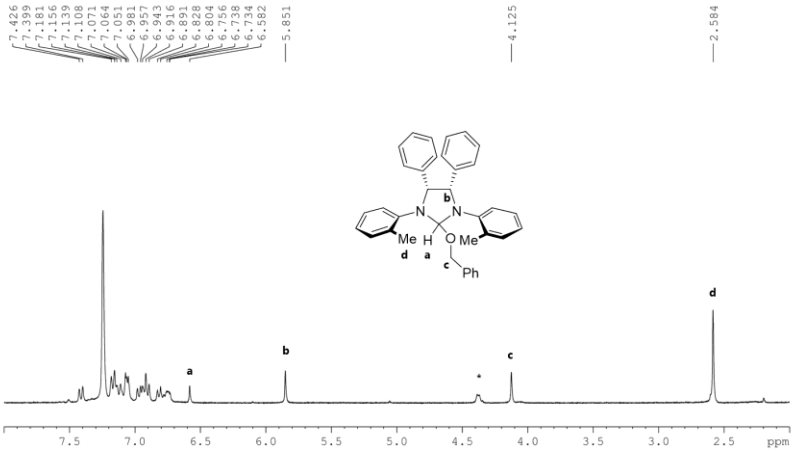

Figure 2.5: ^{1}H-NMR spectrum of the alcohol adduct L1HOBn (solvent: C_6D_6, 400 MHz, 25 °C). * benzyl alcohol.

Subsequently, addition of 15 equivalents of TMC to the L1HOBn adduct and monitoring by ^{1}H NMR spectroscopy revealed TMC consumption and PTMC formation over time. Simultaneously, the alcohol adduct was converted to a novel species, identified as the propagating alcohol intermediate (**Figure 2.6**).

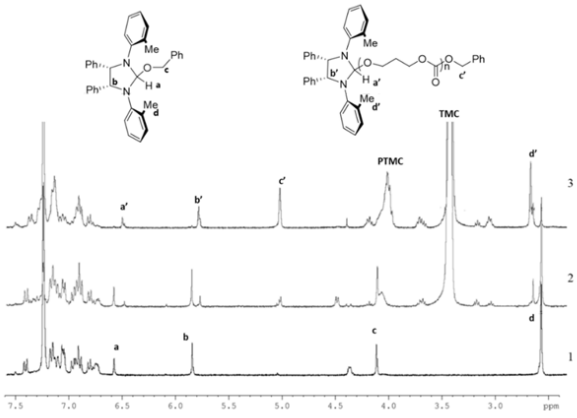

Figure 2.6: Comparison between alcohol adduct L1HOBn (1), with the addition of 15 equiv. of TMC after 15 minutes (2) and after 5 hours (3) (solvent: C_6D_6, 400 MHz, 25 °C). * benzyl alcohol.

This behaviour is consistent with our previous observations for the lactide polymerization catalysed by the Zn complex and isopropyl alcohol.[7] By reaction between the zinc complex and benzyl alcohol, the carbene alcohol adduct is generated, which is a masked form of the NHC. The free carbene, supposed to be the active species of the polymerization, may react with the metal-activated monomer either by the formation of an acylazolium intermediate (pathway a in **Scheme 2.3**) or by the activation of the OH moiety of the alcohol (pathway b in **Scheme 2.3**).

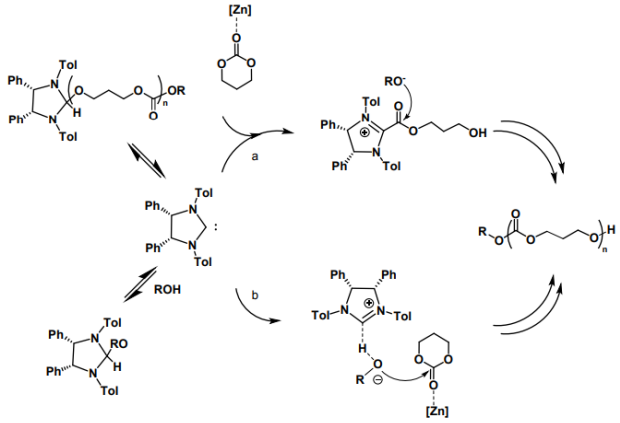

Scheme 2.3: Hypothesized mechanism for the polymerization of trimethylene carbonate promoted by complex Zn and alcohol, used as cocatalyst (R= ^{i}Pr, Bn).

2.2.3 Synthesis and Ring-Opening Polymerization of Alkyl Substituted Trimethylene Carbonates

Alkyl-substituted TMCs offer a route to materials with altered properties, yet their ROP has been less explored.[7,] To investigate this, we evaluated the efficacy of our catalytic system with these monomers. Commercial TMC was used for this study, although it is noteworthy that it can be sustainably synthesized from CO_2 and 1,3-propanediol at room temperature and 1 atm CO_2 pressure.[10] Emulating this green approach, we synthesized 1-Methyl Trimethylene carbonate (1-MeTMC) and 2,2-Dimethyl Trimethylene carbonate (DTC) from CO_2 and the corresponding biorenewable diol. The zinc complex, combined with one equivalent of BnOH, was then tested for the ROP of 1-MeTMC and DTC under solvent-free (bulk) conditions (**Table 2.2**).

Table 2.2. Polymerization of trimethylene carbonate, 1-Methyl Trimethylene carbonate and 2,2-Dimethyl Trimethylene carbonate by complex **1a**.

Entry[a]	**Monomer (equiv)**	**Temp (°C)**	**Time**	**Conv**[b] **(%)**	M_n^{th} [c]	M_n^{exp} [d]	$Đ$ [d]
10	1-MeTMC (50)	20	4 h	64	3.7	5.6 **5.8**	1.5
11	1-MeTMC (50)	70	1 h	75	3.8	6.2 **5.9**	1.3
12	DTC (50)	160	1 h	79	5.1	**4.6**	
13	TMC (50)	70	1 h	96	4.9	**3.6**	
14	TMC (500)	70	0.5 h	63	6.7	6.7	1.7
15	TMC (500)	70	1 h	80	8.2	11.2	1.7
16	1-MeTMC (500)	70	1 h	90	10.4	-	-
17	DTC (500)	160	1 h	71	9.2	7.0	1.8

18[e]	TMC (50)	20	6 h	70	3.6	**4.1**	
19[e]	DTC (50)	20	1.5 h	86	5.6	**6.0**	
20[e]	1-MeTMC (50)	20	32 h	76	4.4	**4.3**	

[a] General conditions: complex: 8 μmol; initiator: BnOH, 1 equivalent (with respect to the complex) for the experiments with 50 equiv of monomer, 5 equivalents for polymerizations with 500 equiv of monomer. [b] Conversion determined by ^{1}H NMR ($CDCl_3$) integrals of 1-MeTMC (δ = 4.65 ppm) and P(MeTMC) (δ = 4.90 ppm), DTC (δ = 4.10 ppm) and P(DTC) (δ = 4.01 ppm). [c] Theoretical M_n based on starting monomer to initiator ratio, monomer conversion and $MM_{1\text{-MeTMC}}$ = 116.1 Da , MM_{DTC} = 130.1 Da . [d] $M_{n,}^{exp}$: $M_{n,}^{GPC}$ and $Đ$ determined by GPC (RI detector vs PS standards). $Đ = M_w/M_n$, in bold M_n determined by MALDI-FT-ICR spectrometry [e]Polymerization experiments carried out in 0.8 mL of toluene.

For comparison, TMC polymerizations were also performed under identical bulk conditions. The data confirm that the Zn complex is highly active for the ROP of all three monomers, even in the absence of solvent. Structural characterization of the resulting poly(1-MeTMC) by ^{1}H NMR spectroscopy (**Figure 2.7**) confirmed the polymer structure, revealing mainchain proton resonances at 2.00, 4.19, and 4.88 ppm and a methyl proton signal at 1.32 ppm.

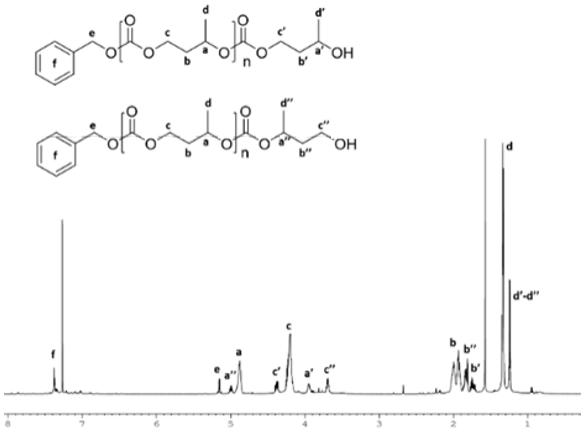

Figure 2.7. ^{1}H NMR spectrum of a sample of poly(Me-TMC) terminated by BnOH (Entry 10 in **Table 2.2**, $CDCl_3$, 600 MHz, 20°C).

The spectrum also clearly showed end-group signals: aromatic protons (7.36–7.37 ppm) and a benzyl methylene signal (5.25 ppm), consistent with initiation by BnOH and termination by hydrolysis. Furthermore, the analysis indicated the formation of two distinct chain ends from hydrolysis of the metal-oxygen bond: a primary alcohol (~60%) and a secondary alcohol (~40%), resulting from cleavage at the less and more hindered positions of the asymmetric monomer, respectively (**Figure 2.7, inset**). The ROP of an asymmetric monomer such as 1-MeTMC can give rise to three microstructures: head-to-head (HH), head-to-tail (HT), and tail-to-tail (TT) (**Scheme 2.4**).

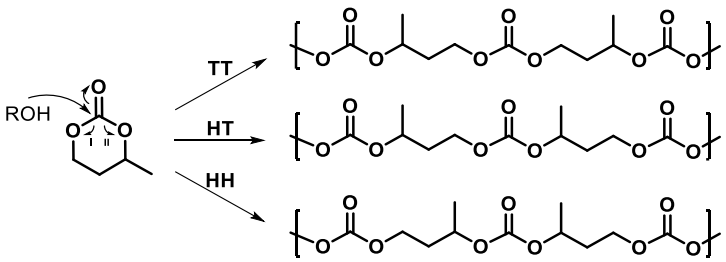

Scheme 2.4. Possible ring-opening sites of 1-Methyl Trimethylene Carbonate and the corresponding polymer microstructures.

Regioregularity, defined as the percentage of HT bonds (X_{reg} = HT/(HT+HH+TT)), was determined from the carbonyl region of the ^{13}C NMR spectrum (**Figure 2.8,** inset).[9]

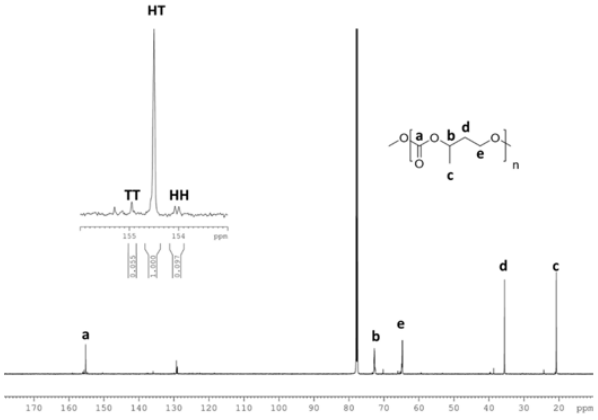

Figure 2.8. ^{13}C NMR spectrum of a poly(Me-TMC) sample (Entry 11 of **Table 2.2**, $CDCl_3$, 100.6 MHz, 20°C).

A perfectly regioregular HT polymer has an X_{reg} of 1.0, while a statistical distribution yields 0.5. Our catalyst demonstrated high regioselectivity, with X_{reg} values of 0.92 and 0.87 at 20 °C and 70 °C, respectively (Entries 10, 11). The minimal temperature dependence suggests a robust and selective propagation mechanism. Given the high regioregularity (~90%) and the nearly 1:1 ratio of chain-end isomers, we propose that

the propagation step is highly regioselective, with regiochemistry determined by the last inserted unit, while the initiation step is not. MALDI-FT-ICR analysis further corroborated the polymer structure.

The spectrum **(Figure 2.23)** showed a primary distribution with a peak spacing of 116 m/z, corresponding to the mass of the 1-MeTMC repeating unit. The main peak at 5819 m/z was assigned to the sodium adduct of a 49-mer initiated by BnOH. Polymerization of the more sterically hindered DTC monomer required a high temperature (160 °C) due to its high melting point. Under these conditions, 79% conversion to poly(DTC) was achieved within an hour (Entry 12).

Subsequent NMR and MALDI-FT-ICR analyses **(Figures 2.23, 2.24)** confirmed a well-defined polymer structure, consistent with the proposed mechanism. Notably, high conversions were maintained even under "immortal" polymerization conditions, using 500 equivalents of monomer and 5 equivalents of BnOH (Entries 14–17), highlighting the efficiency and robustness of the catalyst. To directly compare monomer reactivity, polymerizations were conducted in toluene under standardized conditions (50 equivalents of monomer, 1 equivalent of BnOH, 20 °C; Entries 18–20). Catalyst activity varied significantly, with approximately 70% conversion achieved in 30 minutes for DTC, 6 hours for TMC, and 32 hours for 1-MeTMC. This trend underscores the substantial influence of monomer substitution on reactivity. In all cases, excellent agreement was observed between theoretical molecular masses and those determined by MALDI-FT-ICR, confirming the controlled nature of the polymerizations.

2.2.4 Synthesis of Block Copolymers

The excellent biocompatibility and tunable degradability of aliphatic polycarbonates (APCs) make them ideal as soft, hydrophobic segments in block copolymers for applications ranging from drug delivery to membrane synthesis to thermoplastic elastomers.[1] Notable examples include AB or ABA block copolymers containing poly(ethylene glycol) (PEG) as the hydrophilic segment and PTMC as the hydrophobic block, used for polymeric micelles and flexible clinical scaffolds. [13] Similarly, PTMC and poly(L-lactide) (PLLA) blocks have been combined to improve the ductility and reduce

the processing temperature of PLLA, mitigating thermal degradation, while PLLA-PTMC-PLLA triblock structures have been explored as biodegradable thermoplastic elastomers.[14] We exploited the controlled nature of complex Zn-catalysed polymerizations to synthesize PTMC-PEG and PTMC-PLLA block copolymers using these two methods, sequential addition, and in the presence of a macroinitiator.[15]

First, dihydroxyl-terminated PEG (M_n = 3000 Da) was used as the macroinitiator. It was mixed with two equivalents of the Zn complex (one per chain end) in dichloromethane, followed by the addition of variable equivalents of TMC (Entries 21, 22, **Table 2.3**; **Scheme 2.5**).

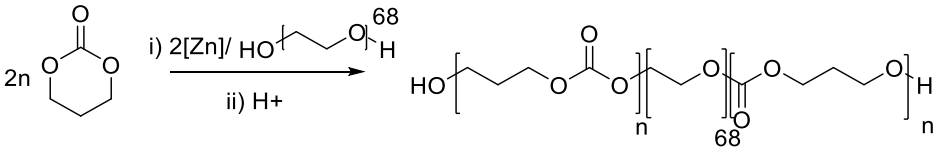

Scheme 2.5. Synthesis of Triblock Copolymers by Polymerization of TMC Promoted by Complex **1a** and HO-PEG-OH as a Macroinitiator.

Table 2.3. Synthesis of di- and tri-block copolymers of PTMC with PEG or PLLA.

Entry [a] (Copolymer)	**TMC (equiv)**	**L-LA (equiv)**	**Alcohol (equiv)**	**Time (h)**	**Conv. TMC [b] (%)**	**Conv. L-LA [b] (%)**
21 PTMC-PEG-PTMC	60	-	PEG3000 (0.5)	6	66	-
22 PTMC-PEG-PTMC	100	-	PEG3000 (0.5)	3	90	-

23 PTMC-PLLA	30	30	BnOH (1)	6	90	81
24 PTMC-PLLA	100	100	BnOH (1)	25	90	86
25 PLLA-PTMC-PLLA	100	100	BDM (1)	25	92	86

[a] [Zn] = 8.0 µmol Solvent: DCM. [b] Conversion determined by ^{1}H NMR ($CDCl_3$) of the reaction mixture.

The resulting polymers were thoroughly characterized. ^{1}H NMR spectroscopy confirmed the presence of both blocks, showing signals for the PTMC end groups (**Figure 2.27**). DOSY NMR experiments provided definitive evidence of the block structure, revealing a single diffusion coefficient for the PEG and PTMC segments (**Figure 2.9**).

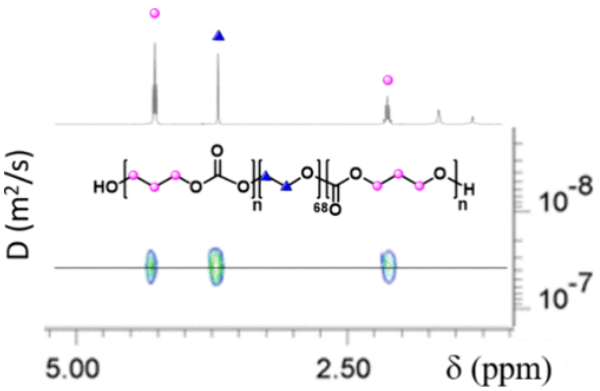

Figure 2.9 Structure and DOSY NMR spectrum (600 MHz, $CDCl_3$) of the PTMC/PGA triblock copolymer (Entry 22 in **Table 2.3**).

GPC analysis showed unimodal molecular weight distributions with experimental values in good agreement with theoretical predictions (**Table 2.4**).

Table 2.4. Characterization of di- and tri-block copolymers of PTMC with PEG or PLLA.

Entry **(Copolymer)**	M_n^{th} [a] **(**KDa**)**	M_n^{exp} [b] **(**KDa**)**	$Đ$ [b]	T_g **(°C)**	T_m **(°C)**	T_d **(°C)**
21 PTMC-PEG-PTMC	11.2	15.6	1.6	-21	37	229 383
22 PTMC-PEG-PTMC	21.4	10.7	1.4	-26	-	262 390
23 PTMC-PLLA	6.3	10.1	1.2	-23 53	145	230 276
24 PTMC-PLLA	21.6	23.0	1.2	-21 47	158	237 259
25 PLLA-PTMC-PLLA	22.5	20.7	1.2	-19 50	148	273 290

[a] Theoretical M_n based on starting monomer(s) to initiator ratio, conversion(s) and molecular weights of the single monomeric units. [b] M_n^{GPC} and $Đ$ determined by GPC (RI detector vs PS standards). $Đ = M_w/M_n$.

Differential scanning calorimetry (DSC) of the copolymer with a lower PTMC content (Entry 21) showed a glass transition (T_g) for the PTMC block and a melting point (T_m) for

the crystalline PEG block (**Figure 2.28**). As expected, increasing PTMC content suppressed the T_m of PEG (Entry 22), consistent with literature findings on phase separation.[16] Thermogravimetric analysis (TGA) further confirmed the blocky structure, revealing two distinct maximum decomposition temperatures (T_{max}) around 230 °C and 380 °C, corresponding to the degradation of the PTMC and PEG blocks, respectively **(Figure 2.29**, **Table 2.4**).

We then synthesized PTMC-*b*-PLLA diblock copolymers by sequentially adding monomers to the catalyst system (Zn/BnOH complex) in DCM at 20 °C (Entries 23, 24, **Table 2.3**; **Scheme 2.6**).

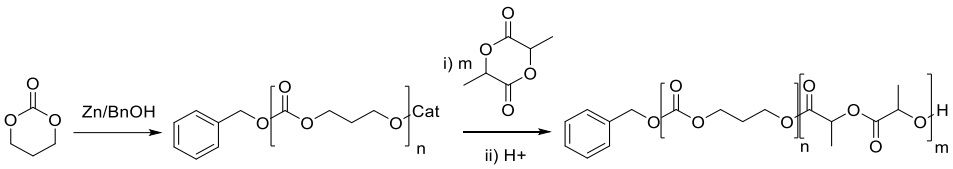

Scheme 2.6. Synthesis of Diblock Copolymers by Sequential Polymerization of TMC and LLA Promoted by Complex Zn **1a** and BnOH.

After TMC consumption, L-lactide was added to the reaction mixture to extend the chain. NMR analysis of the ^{1}H and ^{13}C end groups confirmed the correct formation of the diblock structure; the absence of ω-hydroxyl chain ends from the PTMC block and the presence of new lactidyl end groups were particularly suggestive (**Figures 2.30–2.32**). DOSY NMR again showed a single diffusion coefficient for both blocks. GPC analysis of a representative copolymer (TMC:LA composition 43:57) revealed a molecular weight of 10 kDa with a narrow dispersity ($Đ$ = 1.2), underscoring the living nature of the polymerization. DSC thermograms showed thermal events characteristic of both blocks: a T_g below −20 °C for PTMC, a T_g around 50 °C for PLLA, and a Tm between 145 and 157.9 °C for the crystalline domains of PLLA (**Table 2.4**, **Figure 2.33**), consistent with reported values. TGA profiles showed the expected T_{max} values for the PTMC (~230 °C) and PLLA (~276 °C) blocks (**Figure 2.34**).

Finally, to demonstrate the versatility of our system, we synthesized a PLLA-PTMC-PLLA triblock thermoplastic elastomer. This was achieved by first preparing a dihydroxyl-terminated telechelic PTMC block, followed by the addition of L-LA to both ends (Entry 25, **Table 2.3**). The correct formation of the three-block architecture was verified by NMR spectroscopy and GPC. The DOSY NMR spectrum showed a unified diffusion coefficient for all blocks (**Figure 2.10**, bottom), and GPC analysis of aliquots taken after the formation of the PTMC macroinitiator and the final copolymer showed a clear increase in molar mass with narrow monomodal distributions ($Đ$ < 1.22) throughout the process (**Figure 2.10**, top).

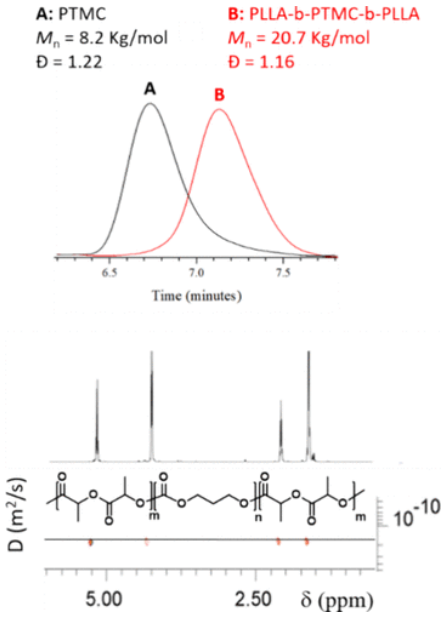

Figure 2.10. Top: Overlaid GPC analyses were performed for isolated PTMC (A: before L-LA addition) and PLLA-PTMC-PLLA samples (B). Bottom: DOSY NMR spectrum of the triblock copolymer PLLA-PTMC-PLLA.

2.3 Conclusions

This chapter describes the use of a zinc complex, supported by an N-heterocyclic carbene (NHC) ligand, for the synthesis of biodegradable aliphatic polycarbonates (APCs) and their copolymers. The catalyst system demonstrated activity in the ring-opening polymerization (ROP) of these monomers, even under green and industrially relevant conditions. Turn Over Frequency (TOF) up to 760 h^{-1} for melt polymerization carried out at 70°C was registered. Polymerizations were well controlled, yielding polymers with predictable molecular weights, low dispersities, and precisely defined end groups. Furthermore, the catalyst showed excellent control of regioselectivity in the polymerization of the asymmetric monomer 1-methyltrimethylene carbonate. Kinetic studies revealed an overall second-order rate law, first-order with respect to both monomer and catalyst concentration. Subsequent mechanistic investigations via NMR spectroscopy delineated a reaction pathway that involves the initial formation of an alcohol adduct, followed by the generation of free carbene and metal species; the latter coordinated to the monomer, facilitating subsequent nucleophilic attack. Finally, the living nature of this system was successfully exploited in sequential one-pot copolymerizations, allowing the isolation of well-defined PTMC-PLLA diblock and triblock copolymers (PTMC-PEG-PTMC and PLLA-PTMC-PLLA). This highlights the ability of our catalytic system to synthesize copolymers with tailored properties and degradation behaviour.

2.4 Experimental Part

All the operations of synthesis and handling of air-sensitive chemicals were performed in an inert atmosphere, using Schlenk techniques and/or a glove-box in nitrogen atmosphere. The used glassware was dried in an oven at 120 °C and subsequently subjected to vacuum-nitrogen cycles. Solvents used for polymerization experiments and for the synthesis of substances instable toward air and moisture, were distilled prior to use on the opportune drying agent. In particular, THF, toluene, and benzene were dried by refluxing over sodium and benzophenone and stored under nitrogen.

Dichloromethane was dried over calcium hydride and distilled prior to use. Benzyl alcohol and isopropanol were dried by refluxing over sodium. Deuterated solvents were purchased from Sigma–Aldrich and dried over activated 3-Å molecular sieves prior to use. All the reagents used for the synthesis of the complexes were purchased from Sigma Aldrich, while trimethylene carbonate was purchased from TCI. TMC was purified twice by recrystallization from dry THF and stored in a glovebox before use. The NMR spectra were recorded with BRUKER AVANCE instruments operating at 600, 400 and 300 MHz for ^{1}H. Molecular masses (M_n and M_w) and their dispersities (M_w/M_n) were measured by GPC, using THF as the eluent (1.0 mL min^{-1}) and narrow polystyrene standards as the reference. MALDI mass spectra were recorded using a Bruker solariX XR Fourier transform ion cyclotron resonance (FT-ICR) mass spectrometer (Bruker Daltonik GmbH,Bremen, Germany) equipped with a 7 T refrigerated actively shielded superconducting magnet (Bruker Biospin, Wissembourg, France). The samples were prepared at the concentration of 1.0 mg mL^{-1} in THF, while the matrix (DCTB) was mixed at a concentration of 10.0 mg mL^{-1}. Thermogravimetric analysis (TGA) measurements were carried out by using a TGA Q500 apparatus manufactured by TA Instruments (Waters/TA instruments, New Castle, DE, USA) in flowing N2 (100 cm^3 /min). Polymer samples was placed into platinum crucibles and heated at 10 °C/min from 20° to 800 °C. Thermal analysis was carried out by using a TA-DSC Q2000 apparatus manufactured by Waters/TA instruments (Waters, New Castle, DE, USA) in flowing N2. Polymer samples was placed into aluminium crucibles and heated/cooled runs were carried out in the range -40 ÷ 180 °C at 10 °C/min

2.4.1 Synthesis of the Zn complex

Zinc-based complex was synthesized, according to the synthetic procedure reported in the literature,[7] using zinc bis [bis (trimethylsilyl) amide] $Zn[N(SiMe_3)_2]_2$ as the metal precursor: the zinc complex was then characterized by NMR spectroscopy. The reaction was carried out in a glove box: in a vial, 0.200 g (4.545 x 10^{-4} mol) of the NHC precursor ligand[17] was weighed, dissolved in 8 mL of anhydrous benzene and transferred into a 20

mL vial, equipped with a magnetic stirrer. In another vial, 0.176 g (4.545 x 10^{-4} mol) of $Zn[N(SiMe_3)_2]_2$ was weighed and dissolved in 8 mL of anhydrous benzene. The solution of the metal precursor was transferred to the solution of the salt and the mixture was left stirring for one hour at room temperature. The solvent was subsequently removed under reduced pressure and the complex obtained was a white powdery solid (Yield = 80%).

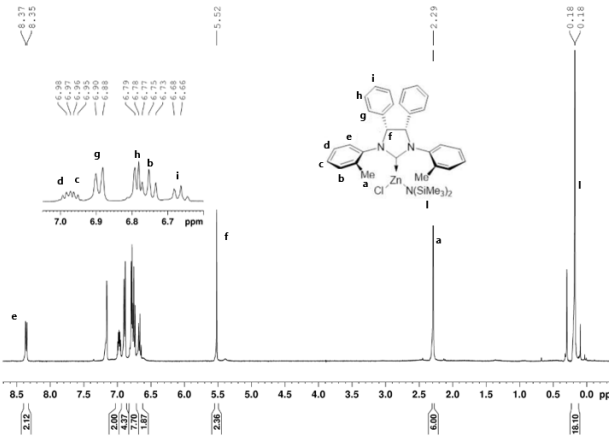

Figure 2.11: ^{1}H-NMR spectrum of L1-ZnN$(SiMe_3)_2$ complex (solvent: C_6D_6, 400 MHz, 25 °C).

^{1}H NMR (400 MHz, C_6D_6, 25 °C): δ 0.18 (s, 18H, $Si(CH_3)_3$), 2.29 (s, 6H, CH_3), 5.52 (s, 2H, CH), 6.66 (t, 2H, Ar-H), 6.75 (t, 2H, Ar-H), 6.79 (d, 2H, Ar-H), 6.89 (d, 2H, Ar-H), 6.96 (t, 2H, Ar-H), 6.98 (t, 2H, Ar-H), 8.36 (d, 2H, Ar-H).

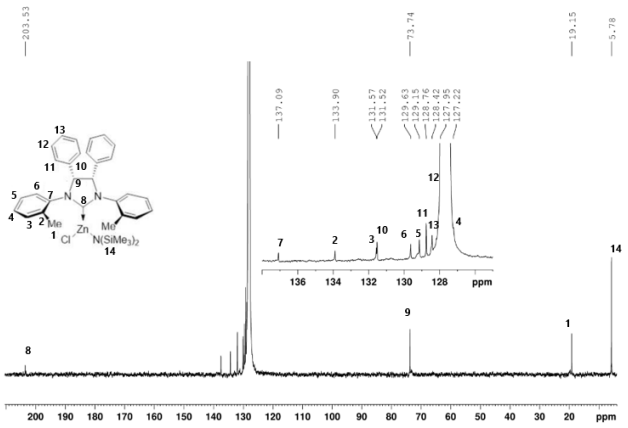

Figure 2.12: ^{13}C-NMR spectrum of L1-ZnN(SiMe$_3$)$_2$ complex. (Solvent: C_6D_6 100.6 MHz, 25 °C).

^{13}C NMR (400 MHz, C_6D_6, 25 °C): δ 5.78 (Si(CH_3)$_3$), 19.15 (2 CH_3), 73.74 (2 CH), 127.22 (2 CH) 127.95 (2 CH), 128.42 (2 CH) 128.76 (2 CH), 129.15 (2 CH), 129.63 (2 CH), 131.52 (2 Cq), 131.57 (2 CH), 133.90 (2 Cq), 137.09 (2 Cq), 203.53 (C Carbenic).

2.4.2 Ring-Opening Polymerization (ROP) of trimethylene carbonate

Polymerization in solution

The polymerization experiments were carried out in a glovebox. In a typical procedure, the complex (8.0 x 10^{-6} mol) and the monomer were weighed into two different 4 mL vials, fitted with magnetic stirrers. Both monomer and complex were dissolved in the desired solvent. Subsequently, the solution of the initiator in the same solvent used to dissolve monomer and complex, was added to the solution of the complex and left to stir for a few minutes: finally, the monomer solution was added to the reaction mixture. All the used vials were washed with solvent to recover the whole amount of each weighed compound; the total amount of solvent was 0.8 mL.

Polymerization in bulk

In a typical procedure, the zinc complex (8.0 x 10^{-6} mol) was weighed into a vessel: subsequently, the initiator was added to the complex and left to stir for a few minutes, then the monomer, weighed into a 4 mL vial, was added to the reaction mixture. For the polymerization experiments conducted at higher temperature, the same procedure was followed and after the addition, the vial was closed, pulled out of the glove box and immersed in a thermostated oil bath at the desired temperature.

All the polymerization experiments were stopped using wet dichloromethane, after taking the vial out of the glovebox. The solvent was removed under reduced pressure and the polymer was washed in methanol, dried and characterized by NMR spectroscopy, MALDI mass spectrometry and/or GPC analysis.

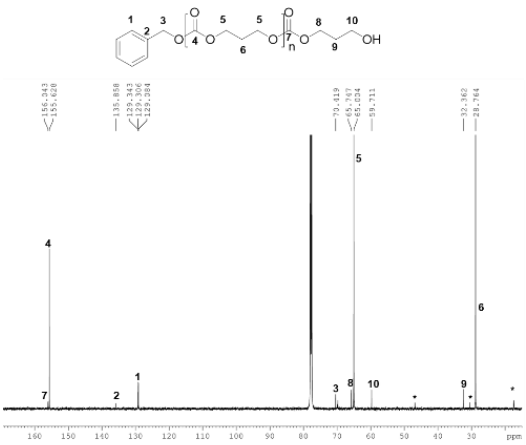

Figure 2.13: ^{13}C-NMR spectrum of a polytrimethylenecarbonate (solvent: $CDCl_3$, 100.6 MHz, 25 °C, Entry 4 of **Table 2.1**). *hexane

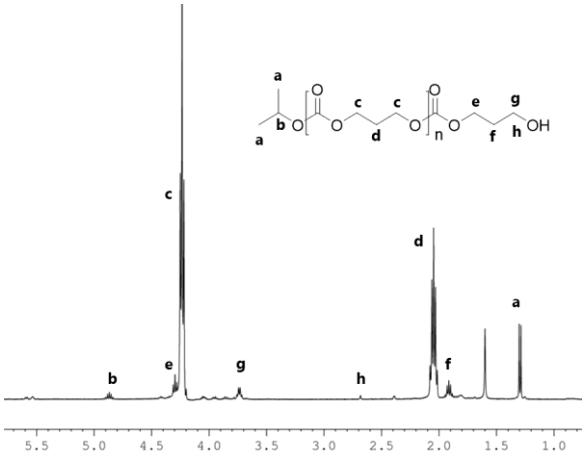

Figure 2.14: ^{1}H-NMR spectrum of the polytrimethylenecarbonate, obtained by using isopropyl alcohol as initiator (solvent: $CDCl_3$, 400 MHz, 25 °C , Entry 8 of **Table 2.1**).

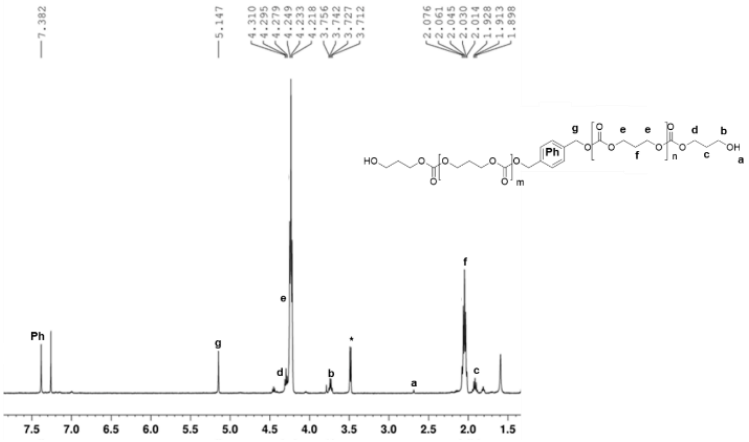

Figure 2.15: ^{1}H-NMR spectrum of the polytrimethylenecarbonate, obtained with 1,4 benzendimethanol as initiator (solvent: $CDCl_3$,400 MHz, 25 °C , Entry 9 in **Table 2.1**).

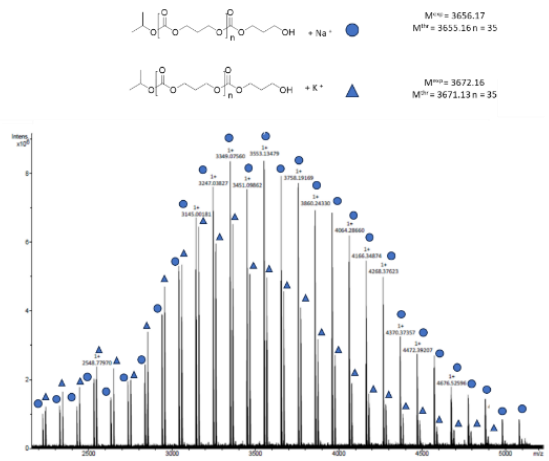

Figure 2.16: MALDI-FT-ICR mass spectrum (matrix: DCTB) of the polymer isolated from trimethylene carbonate polymerization (Entry 8 of **Table 2.1**). Polymerization conditions: $[TMC]_0$:$[^{i}PrOH]_0$:[**1a**] = 30:1:1, temperature: 25 °C, solvent: DCM.

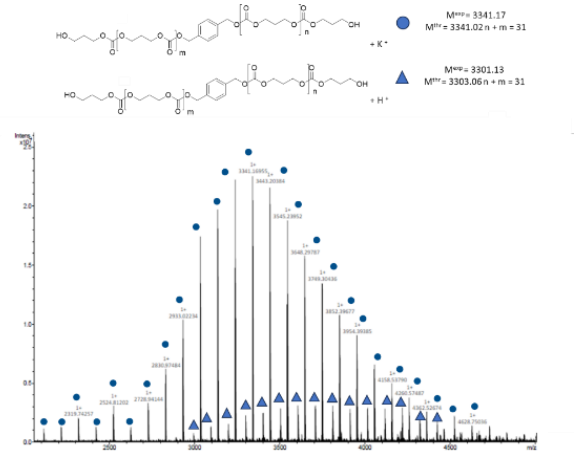

Figure 2.17: MALDI-FT-ICR mass spectrum (matrix: DCTB) of the polymer isolated from trimethylene carbonate polymerization (Entry 9 of Table 2.1). Polymerization conditions: [TMC]0:[BDM]0 :[1] = 30:0.5:1, temperature: 25 °C, solvent: DCM.

2.4.3 Mechanistic investigations

A deuterated benzene solution (0.5 mL) of BnOH (1.63 mg, 1.51 x 10^{-5} mol) was added to a deuterated benzene solution (0.3 mL) of complex **1a** (10.0 mg, 1.51 x 10^{-5} mol). Once the addition was complete, the reaction mixture was left to stir for a few minutes and transferred to the J-Young tube at room temperature. The formation of the corresponding alcohol adduct was observed. Subsequently, a deuterated benzene solution (0.5 mL) of TMC (23.0 mg, 2.25 x 10^{-4} mol) was added to the reaction mixture was left to stir for a few hours. The reaction was monitored by ^{1}H-NMR spectroscopy.

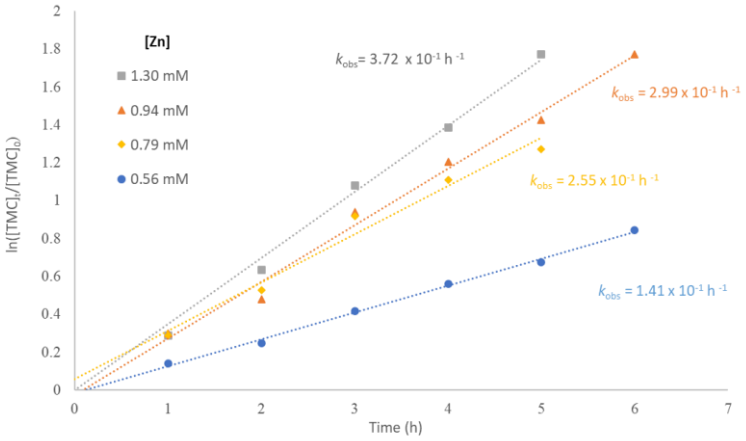

Figure 2.18: First-order kinetic plots for the consumption of TMC by complex **1a** at different concentrations (0.56, 0.79, 0.94 and 1.30 mM) in combination with BnOH, in CD_2Cl_2 at 25°C.

2.4.4 Synthesis of Alkyl Substituted Trimethylene Carbonates

Following literature procedures,[10] 1-Methyl-Trimethylene Carbonate (1-Me-TMC) and Dimethyl-Trimethylene Carbonate (DTC) were prepared from CO_2 and respectively from 1,3-butanediol and 2,2-dimethyl-1,3 propanediol.

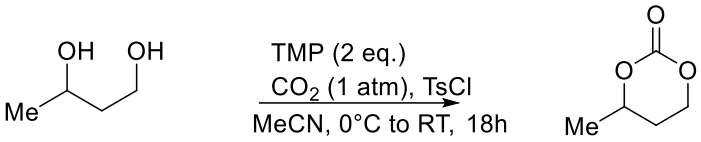

Scheme 2.7: Synthesis of Methyl-Trimethylene Carbonate (Me-TMC).

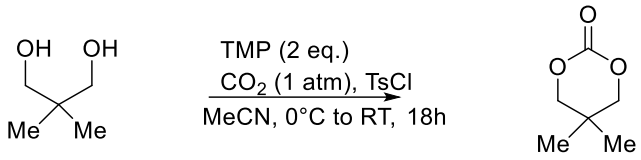

Scheme 2.8: Synthesis of 2,2 Dimethyl-Trimethylene Carbonate (DTC).

A 0.40 mol L^{-1} solution of the opportune diol (1.70 mmol) and tosylchloride (325 mg, 1.7 mmol, 1 equiv.) in anhydrous acetonitrile (4.3 mL) was prepared in a flask. The atmosphere of the flask is exchanged for CO_2 and the solution saturated with CO_2. Under a continuous feed of gas, 2,2,6,6 – Tetramethylpiperidine (575 µL, 3.40 mmol, 2 equiv.) was added dropwise at 0 °C, then the reaction was left to reach room temperature under stirring. After approximately 20 minutes, a bright white precipitate formed and CO_2 stopped being fed to the vessel. After 20 hours, the reaction mixture was diluted with non-anhydrous acetonitrile (10 mL) and the liquid phase separated by centrifugation (3 x 5 minutes at 3000 rpm). The solvent was then removed *in vacuo.* Purification by column chromatography (diameter of column = 1.5 cm, product: silica = 1: 19, 1:1 EtOAc:Hex) afforded the cyclic carbonate product (Yield % $_{Me\text{-}TMC}$ = 70% , Yield % $_{DTC}$ = 75%).

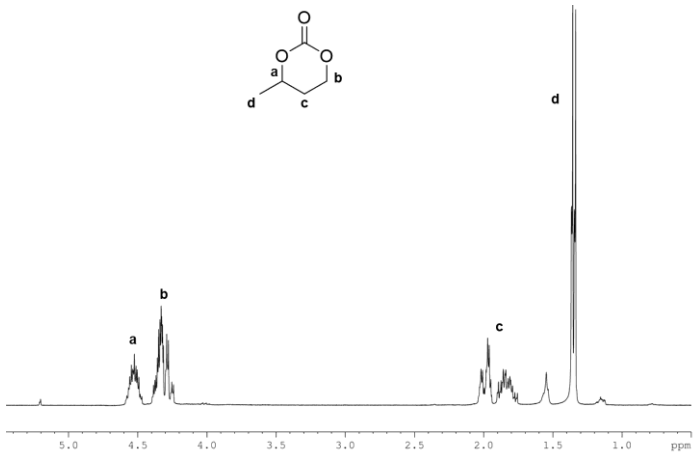

Figure 2.19: ^{1}H-NMR spectrum of the methyl-trimethylenecarbonate (solvent: $CDCl_3$, 400 MHz, 25 °C).

^{1}H NMR (400 MHz, $CDCl_3$, 25 °C): δ 1.35 (d, 3H, CH_3), 1.78-1.88 (m, 1H, CH_2), 2.06-2.00 (m, 1H, CH_2), 4.46-4.21 (m, 2H, OCH_2), 4.68-4.44 (m, 1H, CH).

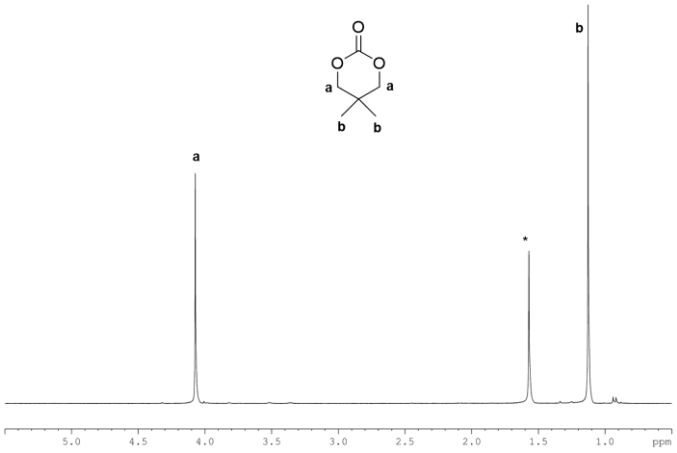

Figure 2.20: ^{1}H-NMR spectrum of the 2,2-dimethyl-trimethylenecarbonate (solvent: $CDCl_3$, 300 MHz, 25 °C).

^{1}H NMR (400 MHz, $CDCl_3$, 25 °C): δ 1.09 (s, 6H, CH_3), 4.04 (s, 4H, CH_2).

2.4.5 Ring-Opening Polymerization of Alkyl Substituted Trimethylene Carbonates

The polymerization experiments in solution were carried out in a glovebox. In a typical procedure, the zinc complex (8 x 10^{-6} mol) was weighed into a 4 mL vial, fitted with a magnetic stirrer, while the monomer was weighed into a 4 mL vial. Both monomer and zinc complex were dissolved in the desired solvent. Subsequently, the solution of the initiator in the same solvent was added to the solution of the complex and left to stir for a few minutes: finally, the monomer solution was added to the reaction mixture. All the used vials were washed with solvent to recover the whole amount of each weighed compound; the total amount of solvent was 0.8 mL.

The polymerization experiments in bulk were carried out in a glovebox or in a thermostated oil bath, at the desired temperature. In a typical procedure, the zinc complex (8 x 10^{-6} mol) was weighed into a vessel: subsequently, the initiator was added

to the complex and left to stir for a few minutes: finally, the monomer, weighed into a 4 mL vial, was added to the reaction mixture.

All the polymerization experiments were stopped using wet dichloromethane, after taking the vial out of the glovebox. The solvent was removed under reduced pressure and the polymer was washed in methanol, dried and characterized by NMR spectroscopy, MALDI mass spectrometry and/or GPC analysis.

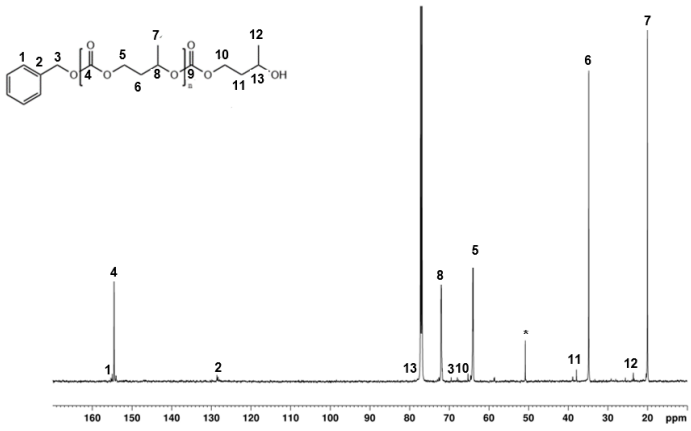

Figure 2.21: ^{13}C-NMR spectrum of the poly-2-methyl-trimethylenecarbonate (solvent: $CDCl_3$,100.6 MHz, 25 °C, Entry 11 of **Table 2.2**). *methanol.

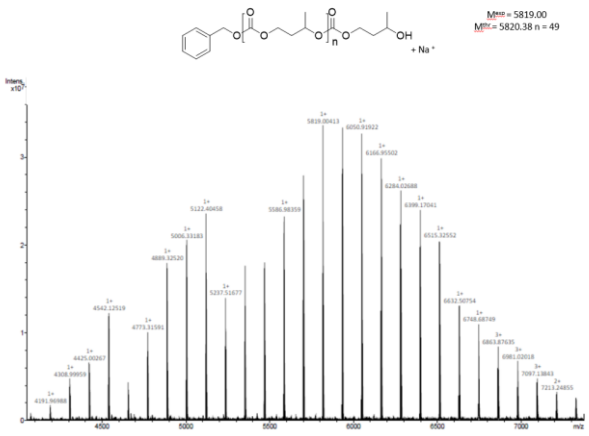

Figure 2.22: MALDI-FT-ICR mass spectrum (matrix: DCTB) of the polymer isolated from methyl-trimethylene carbonate polymerization (Entry 11 of **Table 2.2**). Polymerization conditions: $[Me\text{-}TMC]_0$:$[BnOH]_0$:[**1a**] = 50:1:1, temperature: 20 °C.

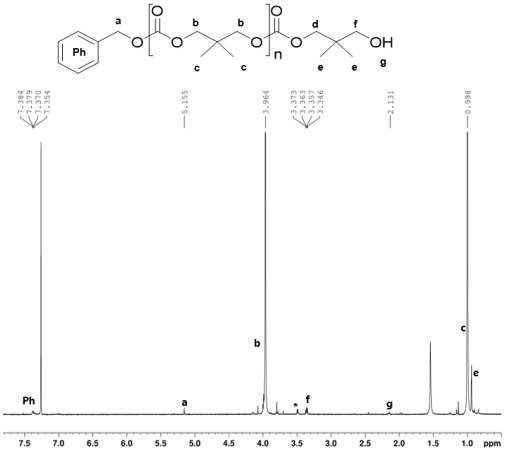

Figure 2.23 ^{1}H-NMR spectrum of the poly-2,2'-dimethyl-trimethylenecarbonate (solvent: $CDCl_3$, 300 MHz, 25°C, Entry 19 of **Table 2.2**) *methanol.

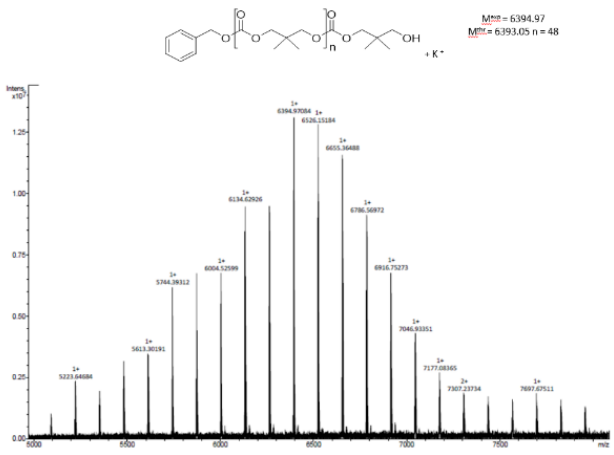

Figure 2.24: MALDI-FT-ICR mass spectrum (matrix: DCTB) of the polymer isolated from 2,2' dimethyltrimethylene carbonate polymerization (Entry 19 of **Table 2.2**). Polymerization conditions: $[DTC]_0$:$[BnOH]_0$:[**1a**] = 50:1:1, temperature 20 °C.

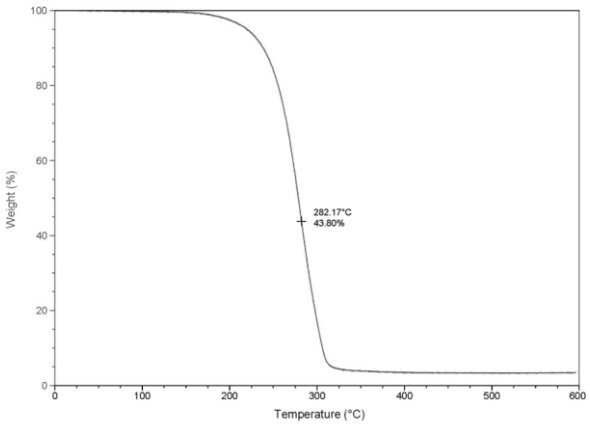

Figure 2.25: TGA of a polydimethylcarbonate sample (Entry 19 of **Table 2.2**).

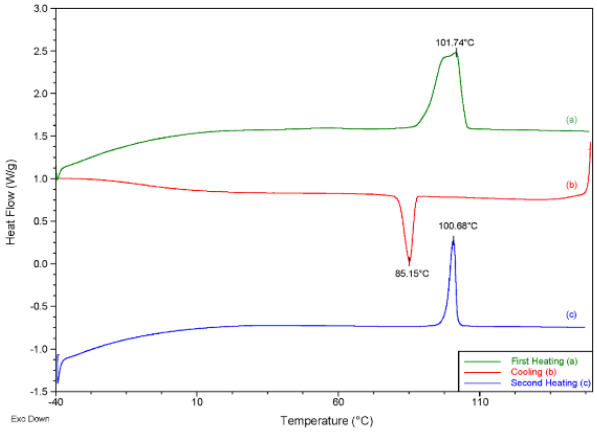

Figure 2.26: DSC of a polydimethylcarbonate sample (Entry 19 of **Table 2.2**).

2.4.6 Synthesis of Copolymers

Synthesis of PEG/PTMC copolymers

The copolymerization experiments were carried out in a glovebox. In a typical procedure, the complex (8.0 x 10^{-6} mol) was weighed into a 4 mL vial, while TMC was weighed into 4 mL vials, fitted with a magnetic stirrer. Both TMC and complex were dissolved. Subsequently, a PEG solution was added to the complex solution and left to stir for a few minutes: finally, the monomer solution was added to the reaction mixture. The copolymerization was stopped using wet dichloromethane, after taking the vial out of the glovebox. The solvent was removed under reduced pressure and the polymer was washed in methanol, dried and characterized by NMR spectroscopy, MALDI mass spectrometry and/or GPC analysis.

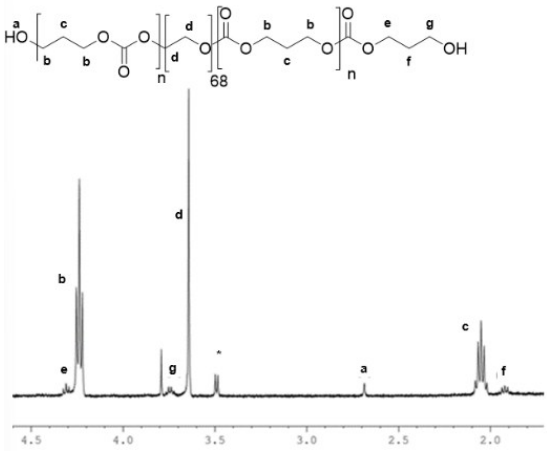

Figure 2.27: ^{1}H-NMR spectrum of PTMC/PEG triblock copolymer with signal assignment (solvent: $CDCl_3$, 300 MHz, 25 °C , Entry 21 of **Table 2.3**).

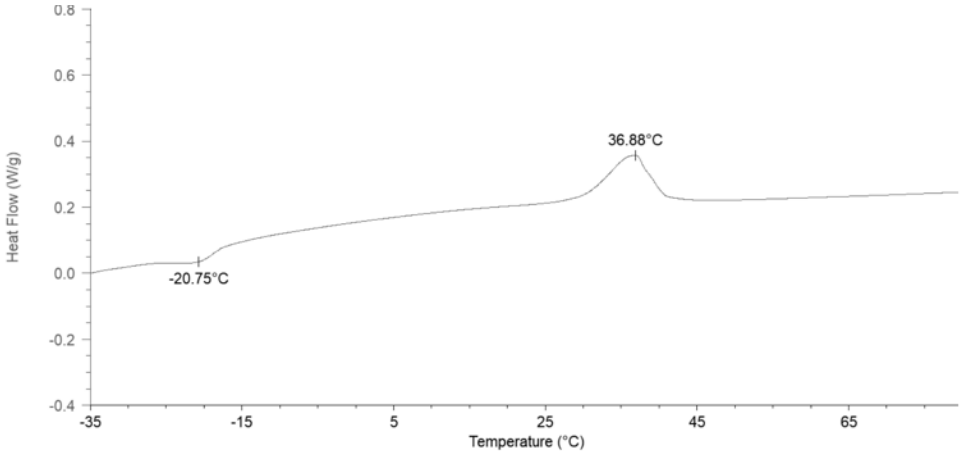

Figure 2.28: DSC of PTMC/PEG triblock copolymer (Entry 21 of **Table 2.3**).

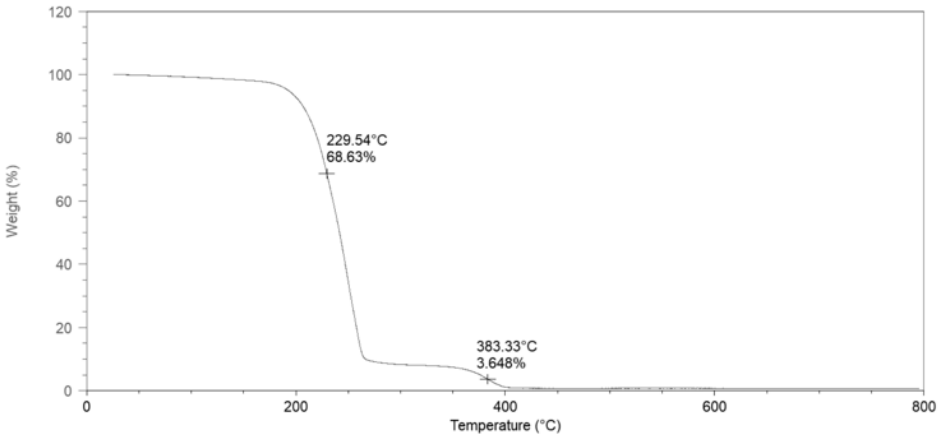

Figure 2.29: TGA of PTMC/PEG triblock copolymer (Entry 21 of **Table 2.3**).

Synthesis of PLLA/PTMC copolymers

The sequential copolymerization experiments were carried out in a glovebox. In a typical procedure, the complex (8.0 x 10^{-6} mol) was weighed into a 4 mL vial, while trimethylene carbonate and lactide were weighed into a 4 mL vial, fitted with a magnetic stirrer. Both monomers and complex were dissolved in solvent. Subsequently, the solution of the initiator was added to the solution of the complex and left to stir for ten minutes. Finally, the solution of trimethylene carbonate was added to the reaction mixture and left to stir. When the TMC was fully consumed, the solution of lactide was added to the reaction mixture. After the necessary time for the LA polymerization, the sequential copolymerization was stopped using wet dichloromethane, after taking the vial out of the glovebox. The solvent was removed under reduced pressure and the polymer was washed in methanol, dried and characterized by NMR spectroscopy, MALDI mass spectrometry and/or GPC analysis.

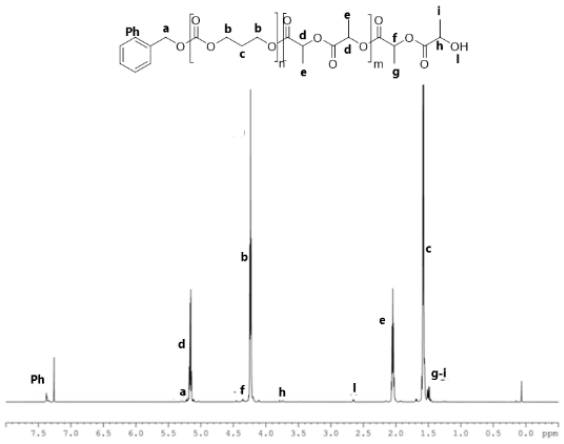

Figure 2.30: ^{1}H-NMR spectrum of the PTMC/PLLA diblock copolymer with signals assignment (solvent: $CDCl_3$, 600 MHz, 25 °C , Entry 23 of **Table 2.3**).

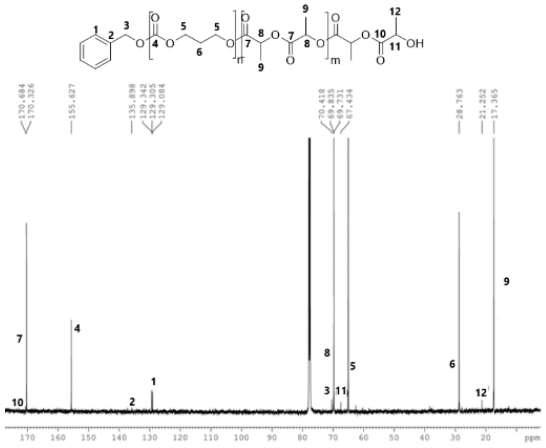

Figure 2.31 ^{13}C-NMR spectrum of the PTMC/PLLA diblock copolymer with signals assignment (solvent: $CDCl_3$, 100,6 MHz, 25 °C , Entry 23 of **Table 2.3**).

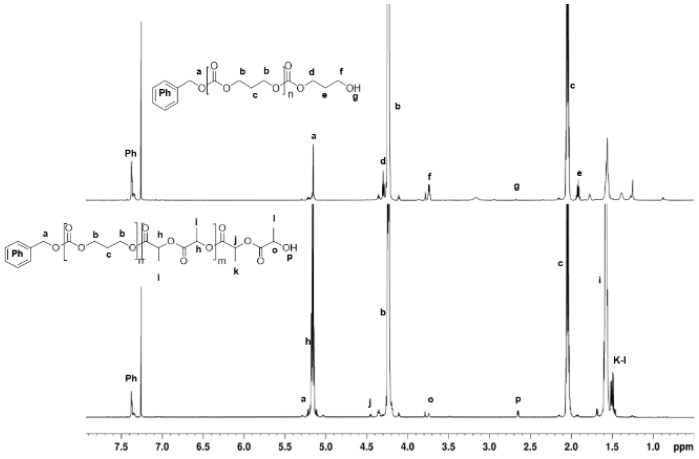

Figure 2.32: Comparison of ^{1}H-NMR spectrum of the PTMC/PLLA diblock copolymer with signals assignment with PTMC (solvent: $CDCl_3$, 600 MHz, 25 °C).

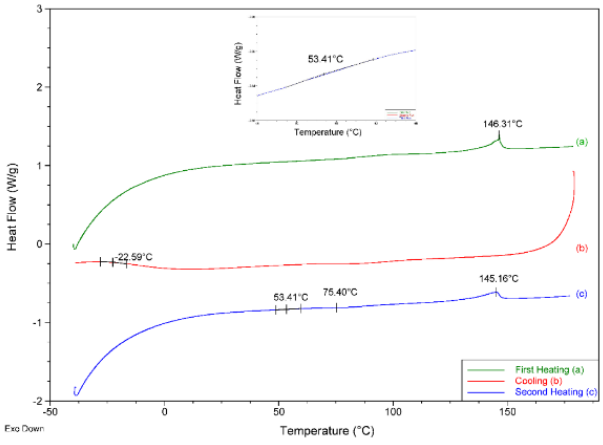

Figure 2.33 DSC of the PTMC/PLLA diblock copolymer (Entry 23 of **Table 2.3**).

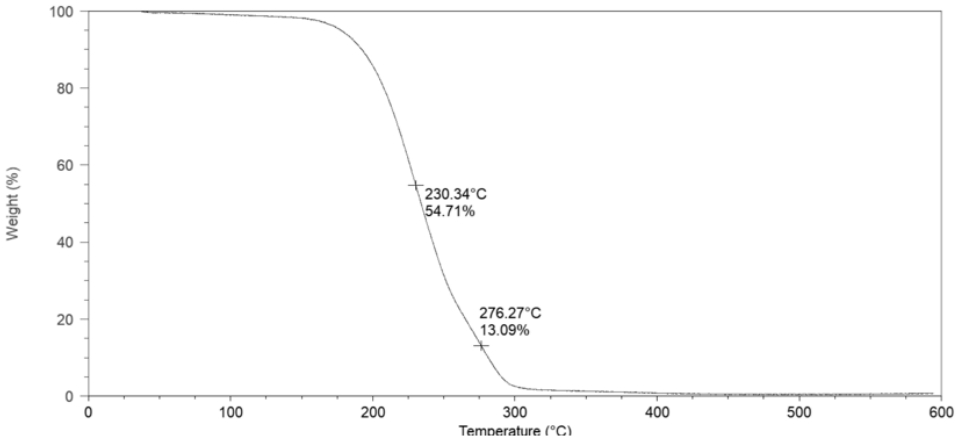

Figure 2.34: TGA of the PTMC/PLLA diblock copolymer (Entry 23 of **Table 2.3**).

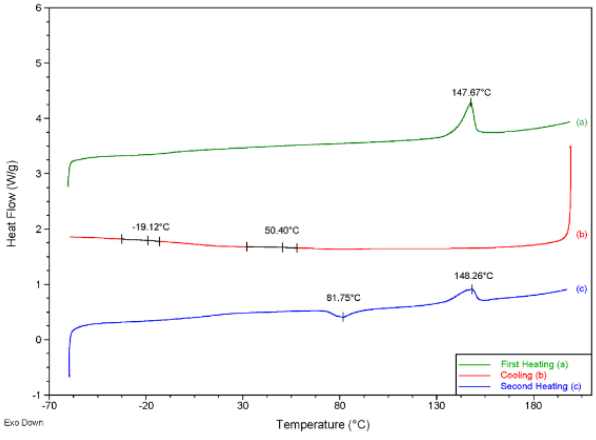

Figure 2.35: DSC of PTMC/PLLA triblock copolymer (Entry 25 of **Table 2.3**).

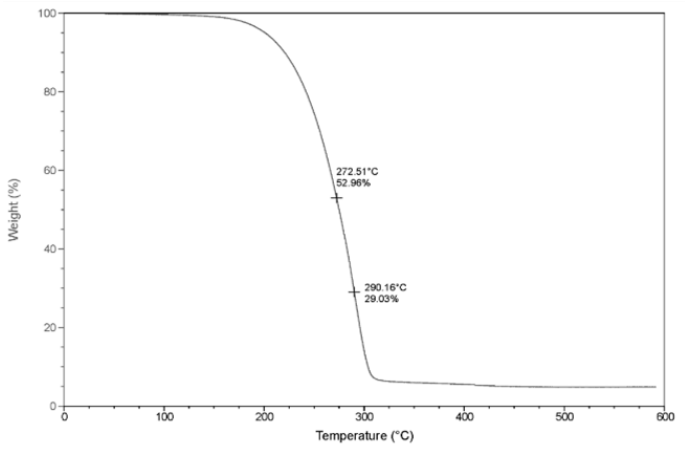

Figure 2.36 TGA of PTMC/PLLA triblock copolymer (Entry 25 of **Table 2.3**).

2.5 References

(1) Yu, W.; Maynard, E.; Chiaradia, V.; Arno, M. C.; Dove, A. P. Aliphatic Polycarbonates from Cyclic Carbonate Monomers and Their Application as Biomaterials. *Chem. Rev.* **2021**, *121* (18), 10865–10907. https://doi.org/10.1021/acs.chemrev.0c00883.

(2) Cui, S.; Borgemenke, J.; Liu, Z.; Li, Y. Recent Advances of "Soft" Bio-Polycarbonate Plastics from Carbon Dioxide and Renewable Bio-Feedstocks via Straightforward and Innovative Routes. *J. CO_2 Util.* **2019**, *34*, 40–52. https://doi.org/10.1016/j.jcou.2019.05.027.

(3) Qin, Y.; Sheng, X.; Liu, S.; Ren, G.; Wang, X.; Wang, F. Recent Advances in Carbon Dioxide Based Copolymers. *J. CO_2 Util.* **2015**, *11*, 3–9. https://doi.org/10.1016/j.jcou.2014.10.003.

(4) Gregory, G. L.; López-Vidal, E. M.; Buchard, A. Polymers from Sugars: Cyclic Monomer Synthesis, Ring-Opening Polymerisation, Material Properties and Applications. *Chem. Commun.* **2017**, *53* (14), 2198–2217. https://doi.org/10.1039/C6CC09578J.

(5) Liu, Q.; Wu, L.; Jackstell, R.; Beller, M. Using Carbon Dioxide as a Building Block in Organic Synthesis. *Nat. Commun.* **2015**, *6* (1), 5933. https://doi.org/10.1038/ncomms6933.

(6) Kricheldorf, H. R.; Stricker, A. Polymers of Carbonic Acid 29. Bu_2SnOct_2—Initiated Polymerizations of Trimethylene Carbonate (TMC, 1,3-Dioxanone-2). *Polymer* **2000**, *41* (20), 7311–7320. https://doi.org/10.1016/S0032-3861(00)00096-3.

(7) Tufano, F.; Santulli, F.; Grisi, F.; Lamberti, M. N-Heterocyclic Carbene-Based Zinc Complexes: Same Precursors for Different Lactide Ring-Opening Polymerization Mechanisms. *ChemCatChem* **2022**, *14* (20), e202200962. https://doi.org/10.1002/cctc.202200962.

(8) Brignou, P.; Carpentier, J.-F.; Guillaume, S. M. Metal- and Organo-Catalyzed Ring-Opening Polymerization of α-Methyl-Trimethylene Carbonate: Insights

into the Microstructure of the Polycarbonate. *Macromolecules* **2011**, *44* (13), 5127–5135. https://doi.org/10.1021/ma200950j.

(9) DeRosa, C. A.; Luke, A. M.; Anderson, K.; Reineke, T. M.; Tolman, W. B.; Bates, F. S.; Hillmyer, M. A. Regioregular Polymers from Biobased (*R*)-1,3-Butylene Carbonate. *Macromolecules* **2021**, *54* (13), 5974–5984. https://doi.org/10.1021/acs.macromol.1c00828.

(10) McGuire, T. M.; López-Vidal, E. M.; Gregory, G. L.; Buchard, A. Synthesis of 5- to 8-Membered Cyclic Carbonates from Diols and CO_2: A One-Step, Atmospheric Pressure and Ambient Temperature Procedure. *J. CO_2 Util.* **2018**, *27*, 283–288. https://doi.org/10.1016/j.jcou.2018.08.009.

(11) Gregory, G. L.; Ulmann, M.; Buchard, A. Synthesis of 6-Membered Cyclic Carbonates from 1,3-Diols and Low CO_2 Pressure: A Novel Mild Strategy to Replace Phosgene Reagents. *RSC Adv.* **2015**, *5* (49), 39404–39408. https://doi.org/10.1039/C5RA07290E.

(12) Contreras-Ramírez, J. M.; Monsalve, M. Ring-Opening Polymerization of 2,2-Dimethyltrimethylene Carbonate Using Samarium Acetate(III) as an Initiator. *Polym. Sci. Ser. B* **2021**, *63* (2), 94–102. https://doi.org/10.1134/S1560090421020044.

(13) Hu, W.; Sun, H.; Pan, L.; Zhang, C.; Shen, X.; Su, F.; Song, J. Poly(Trimethylene Carbonate)-b-Poly(Ethylene Glycol) Diblock Copolymer Micelles for Hydrophobic Drug Delivery: The Effect of Hydrophilic/Hydrophobic Segment Length on Micellar Properties and Drug Loading. *Polym. Adv. Technol.* **2023**, *34* (4), 1209–1219. https://doi.org/10.1002/pat.5963.

(14) Taniguchi, I.; Thao Thi Thu Nguyen; Kinugasa, K.; Masutani, K. A Strategy to Enhance Recyclability of Degradable Block Copolymers by Introducing Low-Temperature Formability. *J. Mater. Chem. A* **2022**, *10* (48), 25446–25452. https://doi.org/10.1039/D2TA06036A.

(15) Jeske, R. C.; Rowley, J. M.; Coates, G. W. Pre-Rate-Determining Selectivity in the Terpolymerization of Epoxides, Cyclic Anhydrides, and CO_2 : A One-Step

Route to Diblock Copolymers. *Angew. Chem. Int. Ed.* **2008**, *47* (32), 6041–6044. https://doi.org/10.1002/anie.200801415.

(16) Zhang, Y.; Zhuo, R. Synthesis and Drug Release Behavior of Poly (Trimethylene Carbonate)–Poly (Ethylene Glycol)–Poly (Trimethylene Carbonate) Nanoparticles. *Biomaterials* **2005**, *26* (14), 2089–2094. https://doi.org/10.1016/j.biomaterials.2004.06.004.

(17) Perfetto, A.; Costabile, C.; Longo, P.; Bertolasi, V.; Grisi, F. Probing the Relevance of NHC Ligand Conformations in the Ru-Catalysed Ring-Closing Metathesis Reaction. *Chem. – Eur. J.* **2013**, *19* (32), 10492–10496. https://doi.org/10.1002/chem.201301540.

Chapter Three

Sustainable Polyesters and Polycarbonates through Ring-Opening Polymerization by NHC-based Zinc and Magnesium Complexes

The results described in this *Chapter* have been published in:

Tufano F., Santulli F., Liguori C., Santoriello G., Ritacco I., Caporaso L., Grisi F., Mazzeo M., and Lamberti M., Versatile NHC-based zinc and magnesium complexes for the synthesis and chemical recycling of aliphatic polyesters and polycarbonates *Catalysis Science & Technology* **2025**,*15*, 822-835.

3.1 Introduction

Alongside aliphatic polycarbonates, aliphatic polyesters represent some of the most promising candidates for sustainable polymers, as they are biodegradable and can be obtained from renewable monomers.[1,2] Their synthesis is typically based on the ring-opening polymerization (ROP) of cyclic monomers catalysed by metal complexes. In this context, the use of abundant, biocompatible, and environmentally friendly metals is essential, especially for biomedical and pharmaceutical applications. Among non-toxic metals, magnesium and zinc stand out for their biological relevance and the catalytic versatility of their compounds. Numerous Mg and Zn complexes, supported by various classes of ligands, have shown excellent activity and control in the ROP of cyclic esters[3–5] and carbonates.[6–9] Zinc complexes, in particular, have also proven effective in chemical recycling processes, such as the alcoholysis of polylactide (PLA).[12–14] N-heterocyclic carbene (NHC) ligands have gained considerable attention due to their unique stereoelectronic properties and high degree of modularity. However, while the use of Zn-NHC complexes in the ROP of esters and cyclic carbonates is widely documented, the chemistry of magnesium-NHC complexes remains less explored. This is mainly due to the high electropositivity of magnesium, which weakens the Mg-NHC bond, limiting catalyst stability.[13,14] As described in *Chapter Two*, our group has previously reported the efficiency of zinc complexes supported by NHC ligands in the ROP of lactides[15] and cyclic carbonates.[16] The introduction of *syn*- or *anti*-phenyl groups on the saturated backbone, combined with N-tolyl substituents, generates a different steric envelope around the metal center, affecting catalytic activity. In this contribution, we extend our study to the synthesis of aliphatic polyesters and polycarbonates mediated by magnesium complexes, presenting a direct comparison of the catalytic activity between zinc-based and magnesium-based systems.

3.2 Results and Discussions

3.2.1 Synthesis and characterization of complexes

Zinc- and magnesium-based complexes were synthesized via a direct reaction in benzene, by combining the respective imidazolium salt, prepared according to procedures reported in the literature,[17] with one equivalent of $M[N(SiMe_3)_2]_2$ (M = Zn, Mg) (**Scheme 3.1**).[15]

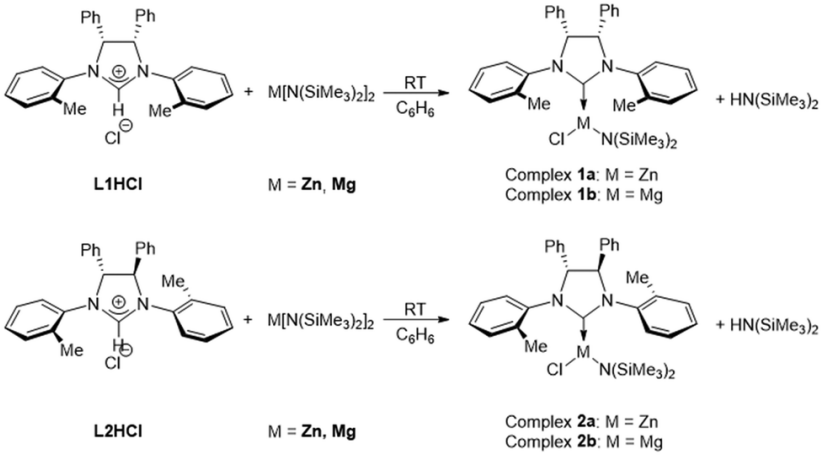

Scheme 3.1 Schematic pathway for the synthesis of NHC–zinc and –magnesium complexes.

After one hour of stirring at room temperature, the solvent was removed under vacuum, yielding each complex as an off-white powder in high yields. A thorough characterization by NMR spectroscopy confirmed their structures (**Figures 3.8-3.16**).

The ^{1}H NMR spectrum of **1b** in C_6D_6 (**Figure 3.1**) is consistent with the symmetry of C_s in solution, showing eight distinct signals for the ligand hydrogens and a singlet for the methyl groups bonded to silicon. The absence of the imidazolium precarbenic proton resonance confirmed NHC coordination to the magnesium center.

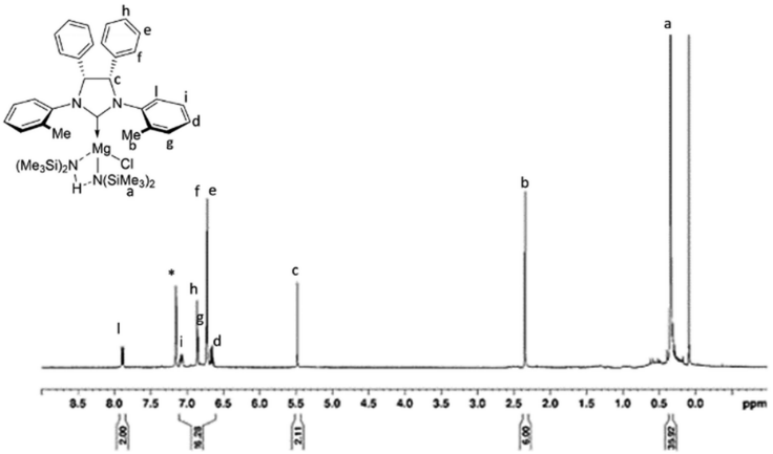

Figure 3.1 ^{1}H NMR spectrum of magnesium complex **1b** (20 °C, 600 MHz, C_6D_6).

Unlike the similar zinc complexes **1a** and **2a**, the singlet for the silicon methyl groups in **1b** showed an integrated intensity twice that expected. This suggests that the amine remains coordinated to the magnesium center, likely stabilized by a hydrogen bond with the amide group, resulting in a dynamic equilibrium as illustrated in the inset of **Figure 3.1**.

To test this hypothesis, the ^{1}H NMR spectrum was acquired in the coordinating solvent THF-d_8: this experiment revealed new low-shift signals, indicating a shift of the coordinated amine, although signal overlap prevented accurate integration. To obtain further structural information, diffusion coefficients (D) for **1b** were determined by DOSY experiments in both C_6D_6 (**Figure 3.2**) and THF-d_8 (**Figure 3.17**), using Tris(trimethylsilyl)silane (TMSS) as an internal standard (**Table 3.6**).

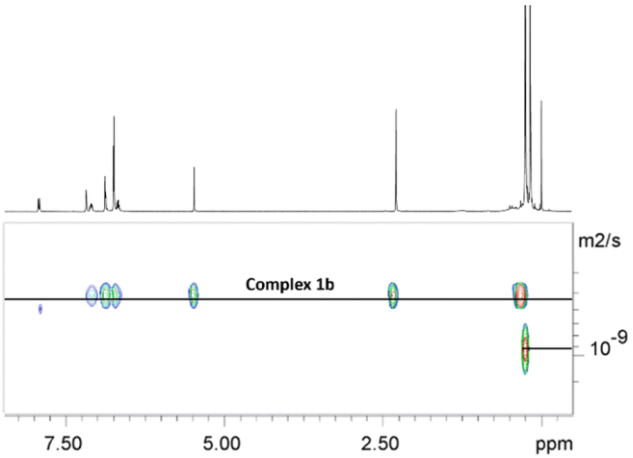

Figure 3.2 DOSY NMR spectrum of complex **1b** with TMSS as an internal standard (400 MHz, 25 °C, C_6D_6).

The diffusion data were converted to estimated molecular masses. In C_6D_6, the experimental mass (886 Da) closely aligned with the theoretical mass of a monomeric complex featuring a coordinated amine molecule (786 Da), corroborating the ^{1}H NMR hypothesis. In contrast, the estimated mass in THF-d_8 (605 Da) was consistent with the monomeric complex (624 Da) or, more plausibly, with a monomer with a coordinated THF molecule (696 Da). Crucially, the amine signal in THF-d_8 showed a distinct diffusion coefficient, corresponding to a molecular mass (190 Da) that matches the free amine (162 Da), confirming its displacement from the metal center. By comparison, DOSY analysis of the zinc complex **1a** in C_6D_6 (**Figure 3.18**) yielded a mass (553 Da) closer to that of the monomeric species (665 Da), indicating the absence of amine coordination.

Thus, we may conclude that in solution of non-coordinating solvents, the amine ($HN(SiMe_3)_2$) formed during the synthesis of the organometallic species remains coordinated to the metal for both magnesium complexes while moving away from the metal for zinc complexes. To rationalize this different behavior of the *syn* and *anti* magnesium (**1b** and **2b**) and zinc (**1a** and **2a**) complexes, density functional theory (DFT) calculations were performed. Therefore, the formation energy

of the monomeric Zn and Mg complexes and those of corresponding complexes with the amine coordinated were computed and compared (**Scheme 3.2** and **Figure 3.3**).

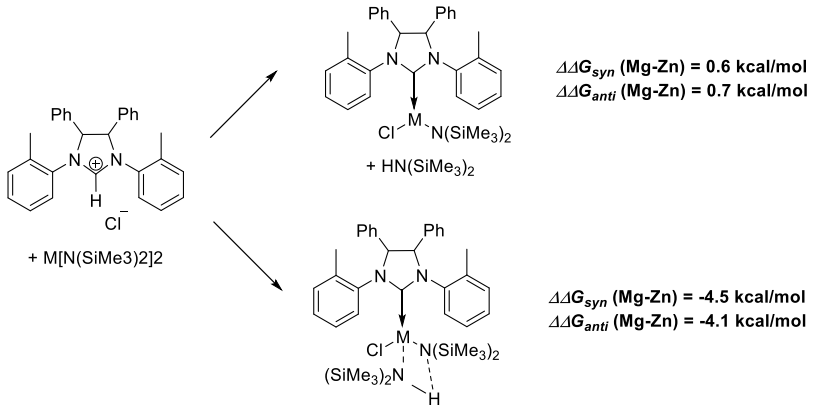

Scheme 3.2 Free energy difference in benzene as a solvent, calculated for the formation of monomeric complexes of M = Zn and Mg ($\Delta\Delta G_{syn}$ (Mg–Zn) and $\Delta\Delta G_{anti}$ (Mg–Zn), respectively) with the reactants and reaction products at an infinite distance.

The calculations, in agreement with the experimental results, show that the formation of the *syn* and *anti* monomeric complexes was favored for Zn by about 1 kcal mol^{-1}, while the formation of the amine coordinated complexes is favored for Mg by about 5 kcal mol^{-1}.

In line with this result, the analysis of the most stable geometries of the *syn* and *anti* complexes of Zn and Mg shows that the interaction of the metal with the nitrogen of the coordinated amine is stronger for the magnesium complexes with a shorter M–N distance (compare 2.33 Å, **Figure 3.3 A, C**, with 2.26/2.27 Å for the corresponding complexes of Mg, **Figure 3.3 B, D**). This is a consequence of the difference in charge of the two metal cations.

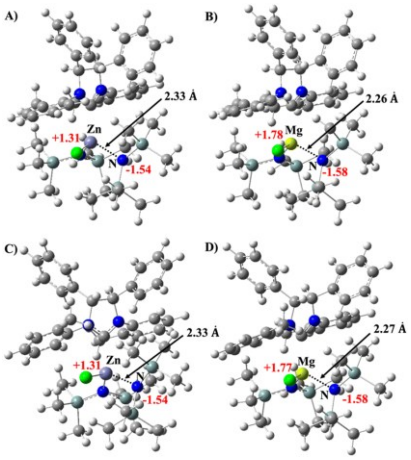

Figure 3.3 Optimized structure of the *syn* (panel A and B) and *anti* (panel C and D) monomeric complexes of Zn and Mg with the coordinated amine.

The positive partial charge of Mg is about 0.5 higher than that of Zn, which increases the interaction of Mg with the amine, favoring coordination at the metal center. Furthermore, calculations carried out on magnesium complex **1b** show that the replacement of the amine coordinated to the metal by the THF solvent molecule is favored by approximately 13 kcal mol^{-1} (**Scheme 3.6**), in agreement with the experimental evidence obtained by NMR analyses.

3.2.2 Polymerization of Cyclic Monomers

Following the behaviour of the magnesium complex in different solvents, we evaluated the catalytic activity of our complexes in the ROP of various monomers. Initial screening of the **1b**/BnOH system for the polymerization of trimethylene carbonate (TMC) in different solvents revealed that the activity decreased in the order: toluene > THF > 1,3-dioxolane > DCM > Me–THF (**Table 3.1**).

Table 3.1: ROP of TMC promoted by complex **1b** in different solvents, at 20°C[a]

Entry [a]	Solvent	Time	Conv[b] (%)	M_n^{th} [c]	M_n^{exp} [d]	$Đ$ [d]
1	THF	1 min	45			
		5 min	70			
		10 min	89			
		20 min	98	10.0	13.9	1.7
2	Toluene	1 min	45			
		5 min	58			
		20 min	95	9.7	11.2	1.1
3	1,3	5 min	48			
	dioxolane	20 min	76			
		35 min	85			
		45 min	90	9.2	11.2	1.7
4	DCM	30 min	78			
		1 h	88	9.0	5.7	1.5
5	Me-THF	1 h	52			
		2 h	65			
		4 h	79			
		9 h	88	9.0	5.6	1.6

[a] General conditions: [**1b**] = 8 µmol, 1 equivalent of BnOH, 100 equiv.of TMC. Volume of solvent = 0.8 mL [b] Conversion determined by ^{1}H NMR ($CDCl_3$) integrals of TMC (δ = 4.45 ppm) and PTMC (δ= 4.23 ppm). [c] M_n^{th} (kDa) = $MM_{monomer}$ × ([monomer]$_0$/[**1b**]$_0$) × monomer conversion. [d] Experimental M_n (in kDa) and M_w/M_n ($Đ$) values were determined by GPC in THF using polystyrene standards and corrected of 0.73 for PTMC (as indicated in the literature for PTMC with theoretical mass in the range 5000-10000).[18]

Encouraged by these results, including the activity also recorded in green solvents, THF was selected as the standard solvent for subsequent comparative studies to evaluate the four complexes (**1a, 2a, 1b, 2b**) in the ROP of various cyclic esters and carbonates.

The polymerization progress was monitored by ^{1}H NMR spectroscopy through the integration of the characteristic resonances of the monomer and the polymer. The complexes were initially evaluated in the ROP of L-lactide (L-LA) and ε-caprolactone (ε-CL) using isopropanol as the initiator (**Table 3.2**, Entries 6–13).

Table 3.2 ROP of the cyclic esters and cyclic carbonates promoted by complexes **1a**, **1b**, **2a** and **2b.** *[a]*

Entry [a]	**Comp**	**Mon. (equ.)**	**Init.**	**T. (°C)**	**t (h)**	**Conv** *[b]* **(%)**	M_n^{th} [c]	M_n^{exp} *[d]*	*Đ* *[d]*	k_{obs} (h^{-1})
6	**1a**	L-LA (100)	^{i}PrOH	20	2.5	84	12.1	8.5	1.3	0.80
7	**1b**	L-LA (100)	^{i}PrOH	20	6	55	7.9	6.3	1.3	0.14
8	**2a**	L-LA (100)	^{i}PrOH	20	6	61	8.8	8.2	1.2	0.23
9	**2b**	L-LA (100)	^{i}PrOH	20	6	49	7.2	6.3	1.2	0.11
10	**1a**	ε-CL (100)	^{i}PrOH	20	7	80	9.1	10.1	1.2	0.17
11	**1b**	ε-CL (100)	^{i}PrOH	20	0.3	99	11.3	10.3	1.9	13.6
12	**2a**	ε-CL (100)	^{i}PrOH	20	9	7	0.8			$9.5x10^{-3}$
13	**2b**	ε-CL (100)	^{i}PrOH	20	0.5	99	11.3	6.7	1.6	8.8
14	**1a**	TMC (100)	BnOH	20	1	92	9.4	10.5	1.5	2.7
15	**1b**	TMC	BnOH	20	0.2	95	9.7	9.9	1.8	42.3

		(100)								
16	**2a**	TMC (100)	BnOH	20	5.5	96	9.8	8.8	1.3	0.6
17	**2b**	TMC (100)	BnOH	20	0.3	96	9.8	12.4	1.6	10.1
18 [e]	**1a**	DTC (50)	BnOH	160	1	79	5.1	*4.6*		
19 [e]	**1b**	DTC (50)	BnOH	160	1	94	6.1	*5.7*		
20 [e]	**1a**	Me-TMC (50)	BnOH	70	1	75	3.8	*5.9*		
21[e]	**1b**	Me-TMC (50)	BnOH	70	3.5	75	4.5	*4.3*		
22[e]	**1a**	Me-TMC (50)	BnOH	160	0.5	91	5.3	*6.2*		
23[e]	**1b**	Me-TMC (50)	BnOH	160	0.5	84	4.9	*5.7*		

[a] General conditions: [Complex] = 8 µmol for cyclic carbonates, 15 µmol for cyclic esters; one equivalent of alcohol. Volume of THF= 1 mL for ROP of cyclic carbonates, 2 mL for ROP of cyclic esters. [b] Determined by ^{1}H NMR spectral data. [c] M_n^{th} (Da) = $MM_{monomer} \times ([monomer]_0/[Complex]_0) \times$ monomer conversion. [d] Experimental M_n (in kDa) and M_w/M_n ($Đ$) values were determined by GPC in THF using polystyrene standards and corrected using a factor of 0.58 for PLA, 0.56 for PCL and 0.73 for PTMC (as indicated in the literature for PTMC with theoretical mass in the range 5000-10000). Experimental M_n (in kDa) indicated in italic have been determined by MALDI analysis. [e] Polymerization experiments carried out in bulk conditions.

All four complexes were active in the production of polylactide (PLLA) and polycaprolactone (PCL). A metal-dependent activity trend was observed: zinc complexes outperformed their magnesium analogues in the polymerization of L-LA, while the reverse was true for ε-CL. Furthermore, for a given metal, the NHC ligand L1 consistently conferred greater activity than L2. A similar trend was observed in the ROP of TMC, initiated by benzyl alcohol (Entries 14–17). Magnesium complexes again demonstrated superior activity to their zinc counterparts for both ligands, maintaining the beneficial effect of ligand L1.

To broaden the scope, the activities of **1a** and **1b** were compared for substituted cyclic carbonates (Me-TMC and DTC) under bulk conditions at elevated temperatures (Entries 18–23). Zinc complex **1a** was more active with Me-TMC at 70°C, while magnesium **1b** was more active with DTC at 160°C. To investigate a potential temperature effect on amine dissociation in the magnesium complex, a polymerization of Me-TMC was also conducted at 160°C. While nearly quantitative conversion was achieved within 30 minutes for both catalysts, zinc complex **1a** maintained slightly higher activity.

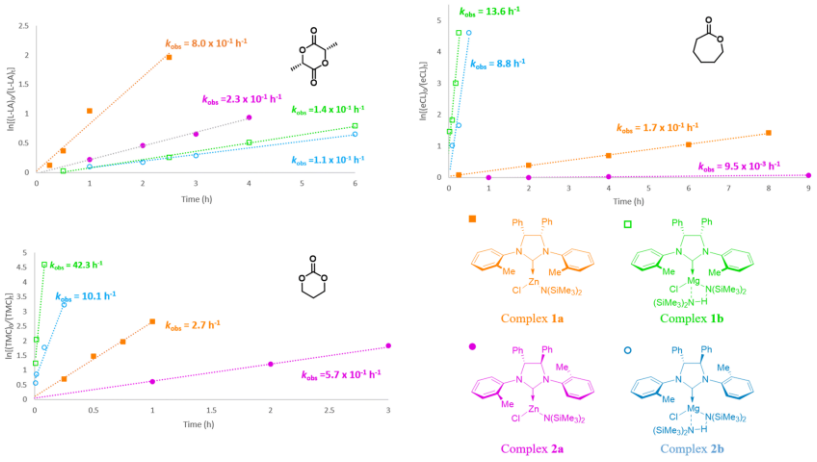

Figure 3.4 First-order kinetic plots for the consumption of L-LA, ε-CL and TMC by complex **1a** (orange full squares, complex **1b** (green empty squares), complex **2a** (purple full circles) and complex **2b** (blue empty circles) in combination with an equivalent of BnOH or ^{i}PrOH as initiators, in tetrahydrofuran at room temperature.

Semi-logarithmic plots of monomer conversion versus time were linear in all cases (**Figure 3.4**), indicating first-order kinetics in monomer concentration. The apparent rate constants derived from these plots (**Table 3.2**) confirmed the activity trends: for L-LA, activity decreased as **1a > 2a > 1b > 2b**, while for ε-CL and TMC, the order was **1b > 2b > 1a > 2a.**

To get more information on the behaviour of zinc and magnesium complexes with the different monomers, complexes **1a** and **1b** were tested in the polymerization of glycolide (GA). Structurally, GA is the simplest cyclic ester and serves as a lactide analogue, distinguished only by the absence of methyl substituents adjacent to the carbonyl group.

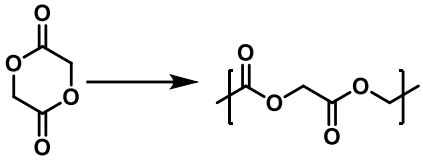

Scheme 3.3: ROP of glycolide.

Due to poor solubility of monomer in THF at room temperature, the polymerisations were carried out in toluene at 85°C with a low monomer concentration. The results are summarized in **Table 3.3**

Table 3.3. ROP of GA promoted by complex **1a** and **1b**

Entry[a]	**Comp.**	**Mon. (equ.)**	**Init.**	**T (°C)**	**Time (min)**	**Conv** [b] **(%)**	M_n^{th} [c]
24	**1a**	GA (30)	BnOH	85	5	89	2.9
25	**1b**	GA (30)	BnOH	85	5	15	0.5

[a]General conditions: [Complex] = 15 µmol for cyclic esters; one equivalent of alcohol. Volume of toluene= 3 mL. [b] Determined by ^{1}H NMR spectral data. [c] M_n^{th} (KDa) = $MM_{monomer}$ × ($[monomer]_0/[Complex]_0$) × monomer conversion.

Under these reaction conditions, the zinc complex showed high activity, reaching 89% conversion in only 5 min. In sharp contrast, the magnesium analogue achieved only 15% conversion in the same time frame. These experimental results highlight a clear divergence in catalytic performance between the two metal systems. Zinc-based complexes show superior activity in the ring-opening polymerization (ROP) of lactide, glycolide, and methyltrimethylene carbonate. In contrast, magnesium complexes are more efficient for trimethylene carbonate, ε-caprolactone, and dimethyltrimethylene carbonate.

This difference can be explained by the steric and electronic effects. The magnesium complexes appear particularly sensitive to congestion caused by substituents near the monomer's carbonyl moiety, which hinders coordination and slows polymerization. On the other hand, magnesium, being a stronger Lewis acid, forms stronger metal-alkoxide interactions with the reaction intermediates. The resulting stabilization reduces its lability and slows monomer insertion, decreasing the overall propagation rate. Furthermore, the ability of lactide and glycolide to form stable chelate intermediates limits access to the metal site, contributing to the slower propagation rates.

Although the absolute activities of our systems are lower than those of state-of-the-art catalysts reported in the literature,[19–21] they are comparable or superior to other NHC-supported Zn and Mg complexes.[8,13,22,23] In particular, the observed metal-dependent reversal of activity based on the monomeric substrate is unusual. In most works in the literature, Mg complexes typically outperform their Zn analogues in various cyclic esters and carbonates,[24–26] regardless of the monomer structure.

The resulting polymers have been extensively characterized by NMR, MALDI-FT-ICR and GPC. ^{1}H NMR analysis of the end groups confirmed that polymerization proceeded via initiation by alcohol (isopropanol or benzyl alcohol) and termination by hydrolysis, for both polyesters and polycarbonates.

MALDI-FT-ICR analysis revealed a primary distribution corresponding to polymer chains with the expected initiator and hydrolytic end groups. However, polymers derived from magnesium-based catalysts showed additional minor distributions attributable to side reactions of transesterification and/or hydrolysis, which were largely absent in polymers derived from zinc-based catalysts. This was corroborated by GPC analysis, which consistently showed higher dispersity (*Đ*) values for polymers obtained with magnesium complexes. Despite this, the experimental molecular weights for all polymers were in reasonable agreement with the theoretical values (**Table 3.2**).

3.2.3 Mechanistic Studies

Previous studies have established that the NHC-zinc complex **1a** reacts with one equivalent of alcohol to form a carbene-alcohol adduct and a zinc-based species.[15,16] To study the behaviour of the magnesium system, we treated complex **1b** with one equivalent of benzyl alcohol in three deuterated solvents; for comparison, the same reactions were performed with the zinc complex **1a** (**Figure 3.5**, **3.32, 3.33**).

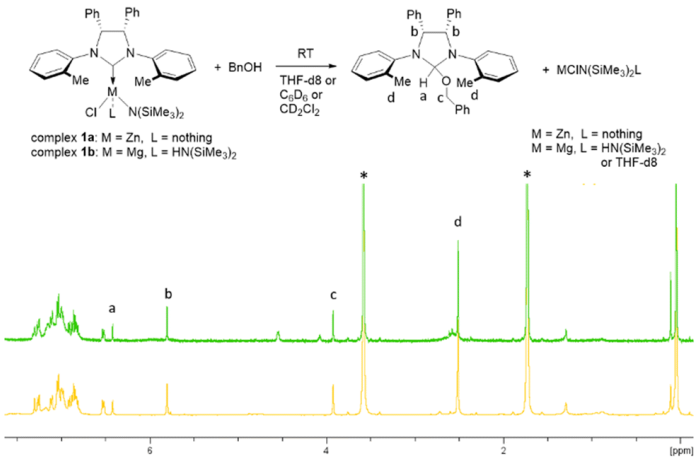

Figure 3.5 Top: Schematic reaction of complexes **1a** and **1b** with BnOH in different deuterated solvents. Bottom: ^{1}H NMR spectra of the products obtained from the reaction of complex **1a** (green spectrum) and complex **1b** (orange spectrum) with one equivalent of BnOH in THF-d_8 (peaks denoted with *) (400 MHz, 20 °C).

In all cases, a quantitative and immediate conversion of the metal complexes into the corresponding adducts occurred, identified by its characteristic signal pattern. To confirm the participation of this adduct in the polymerization, 15 equivalents of TMC were added to the preformed mixture of **1b** and BnOH in THF-d_8. NMR acquisition shows rapid consumption of both the adduct and the monomer, with the concomitant appearance of new signals attributable to a species in which the benzoxide group is replaced by a growing poly(TMC) chain (**Figure 3.6**).

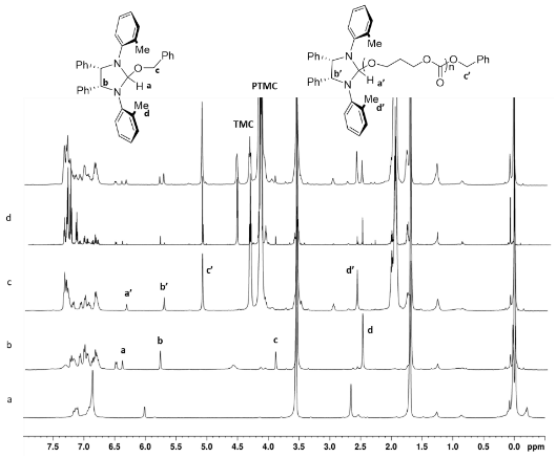

Figure 3.6: ^{1}H NMR spectra of the sequential addition of one equivalent of BnOH and 15 equiv. of TMC to complex **1b** in THF-d_8 (400 MHz, 20 °C). In order the spectrum of L1Mg complex (**a**), addition of BnOH (**b**), addition of TMC (**c**), addition of another equivalent of BnOH (**d**) and TMC.

To rationalize the catalytic mechanism and decouple the intrinsic effect of the metal from the influence of the coordinated amine in **1b**, several controlled polymerization experiments were performed (**Table 3.4**). Using L-LA and TMC as reference monomers, we initially determined that the L1HO^{i}Pr adduct was completely inactive in ROP, highlighting the need for a metal co-catalyst. We then evaluated three distinct catalytic systems for each metal: the metal complex with one equivalent of ^{i}PrOH; the L1HO^{i}Pr adduct with a 0.5:0.5 equivalent mixture of $ZnCl_2$ and $Zn[N(SiMe_3)_2]_2$ (or $Mg[N(SiMe_3)_2]_2$ for Mg), designed to generate the mixed halide/amide species; and finally, the L1HO^{i}Pr adduct with a full equivalent of the metal amide.

Table 3.4. ROP of L-LA and TMC promoted by complex **1a** and **1b**, alcohol adduct and its combination with Zn and Mg precursors in THF, 20°C.[a]

Entry	Cat. System	Mon.	Time	Conv[b] (%)	$M_n^{th[c]}$	$M_n^{exp[d]}$	$Đ^{[d]}$	k_{obs} (h^{-1})
26	L1HO^{i}Pr	TMC	20 min	-				
27	**1a** + ^{i}PrOH	TMC	30 min 2.5 h 5 h	16 58 85	8.7	7.5	1.3	0.34
28	**L1**HO^{i}Pr + 0.5 $ZnCl_2$ + 0.5 $Zn(N(SiMe_3)_2)_2$	TMC	15 min 30 min 1 h 2.5 h	12 37 57 85	8.7	8.8	1.5	0.79
29	L1HO^{i}Pr + $Zn(N(SiMe_3)_2)_2$	TMC	15 min	78	8.0	19.2	2.3	
30	**1b** + ^{i}PrOH	TMC	1 min 5 min 15 min	34 75 92	9.4	12.6	2.2	13.0
31	L1HO^{i}Pr + 0.5 $MgCl_2$ + 0.5 $Mg(N(SiMe_3)_2)_2$	TMC	5 min 10 min 15 min 20 min	45 60 85 90	9.2	7.4	2.1	7.1
32	L1HO^{i}Pr + $Mg(N(SiMe_3)_2)_2$	TMC	15 min	94	9.6	33.3	1.9	
33	$Mg(N(SiMe_3)_2)_2$	TMC	15 min	99	10.1	24.4	2.3	
34	L1HO^{i}Pr	LLA	20 min	-				
Table 1	**1a** + ^{i}PrOH	LLA	15 min 30 min 1 h 2.5 h	12 31 65 84	12.1	8.5	1.3	0.80
36	L1HO^{i}Pr	LLA	15 min	39				

	+ 0.5 $ZnCl_2$ + 0.5 $Zn(N(SiMe_3)_2)_2$		30 min 45 min 1 h	58 70 80	11.5			1.6
37	L1HO^{i}Pr + $Zn(N(SiMe_3)_2)_2$	LLA	15 min	39	5.6	14.7	1.8	
38	**1b** + ^{i}PrOH	LLA	30 min 2.5 h 4 h 6 h	3 23 40 55	7.9	6.0	1.2	0.14
39	L1HO^{i}Pr + 0.5 $MgCl_2$ + 0.5 $Mg(N(SiMe_3)_2)_2$	LLA	30 min 4 h 6 h 8 h	6 37 54 75	10.8	8.1	1.4	0.13
40	L1HO^{i}Pr + $Mg(N(SiMe_3)_2)_2$	LLA	15 min	93	13.4	16.4	3.0	
41	$Mg(N(SiMe_3)_2)_2$	LLA	15 min	77	11.1	24.4	2.3	

[a] General conditions: [**cat**] = 15 µmol for L-LA, 8 µmol for TMC, 100 equiv.of monomer. [b] Conversion determined by ^{1}H NMR ($CDCl_3$) integrals of L-LA (δ = 5.08 ppm) and PLLA (δ = 5.15 ppm) , TMC (δ = 4.45 ppm) and PTMC (δ= 4.23 ppm). [c] M_n^{th} (kDa) = $MM_{monomer}$ × ([monomer]$_0$/[cat]$_0$) × monomer conversion. [d] Experimental M_n (in kDa) and M_w/M_n ($Đ$) values were determined by GPC in THF using polystyrene standards and corrected of 0.73 for PTMC (as indicated in the literature[28] for PTMC with theoretical mass in the range 5000-10000) and of 0.56 for PLLA.

The results highlight a critical cooperative effect between the organic adduct and the metal species. The systems combining the adduct with the equimolar metal mixture mirrored the activity and control of the original metal complex/^{i}PrOH systems. In contrast, systems using the metal amide alone showed the highest activity but poor control over polymerization. This loss of control was particularly evident when $M(N(SiMe_3)_2)_2$ was used alone, producing polymers with broad molecular weight distributions.

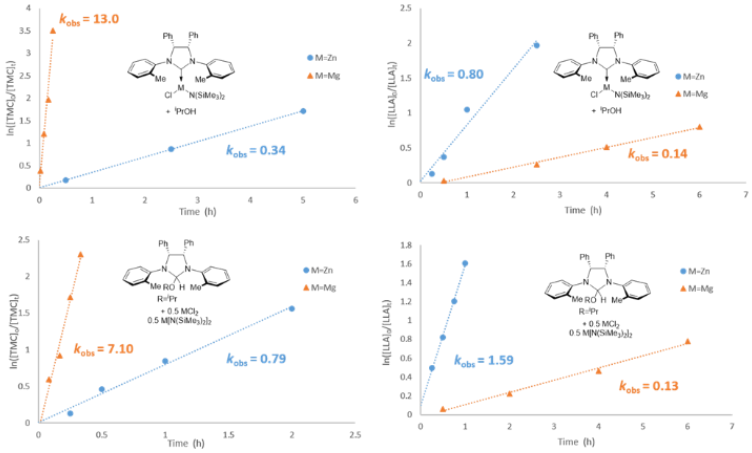

Figure 3.7 First-order kinetic plots for the consumption of TMC (left) and L-LA (right) by the catalytic systems depicted in the insets.

Critically, the trend toward metal-dependent activity is confirmed in this series of targeted experiments: magnesium-based systems were more active for TMC polymerization, while zinc-based systems were superior for L-LA (**Figure 3.7**). This confirms that the order of activity is an intrinsic property of the metal center itself, not an artifact of the coordinated amine in the magnesium precatalyst. In light of these results, we hypothesized that both the magnesium- and zinc-based systems operate via a dual catalytic mechanism (**Scheme 3.4**), similar to that reported for other NHC-based systems[18,27,28] and for our complex **1a**.

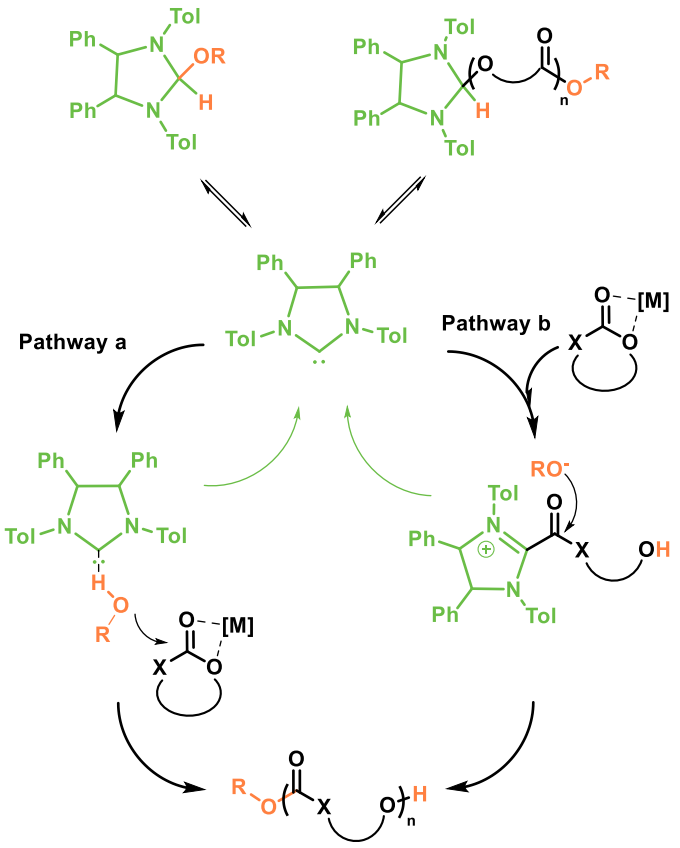

Scheme 3.4 Proposed mechanism for the ROP of cyclic monomers promoted by zinc and magnesium complexes in combination with an alcohol. In "Pathway a", the free NHC acts as a base while in "Pathway b" the NHC acts as a nucleophile. In both cases the metal species operates as the Lewis acid which activates the monomer.

This mechanism involves an initial monomer activation step, through coordination of the carbonyl oxygen to the Lewis acid metal species, followed by an organocatalytic cycle initiated by the free carbene, which exists in equilibrium with the alcohol adduct (which

drives the growing isopropoxy or polymer chain). This cycle can be divided into two concurrent pathways: the carbene can act as a base (Path **a**) or as a nucleophile (Path **b**) in a monomer-activated mechanism, with both pathways producing polymers with identical end groups.

3.2.4 Chemical Recycling of PLLA

Zinc complexes (**1a, 2a**) and magnesium complex (**2b**) were further evaluated as catalysts for the chemical recycling of poly(L-lactide) (PLLA) via methanolysis. This process typically occurs via random chain scission in solution, progressively depolymerizing the polymer into oligomers, and ultimately producing methyl lactate (Me-LA), a valuable eco-friendly solvent (**Scheme 3.5**).

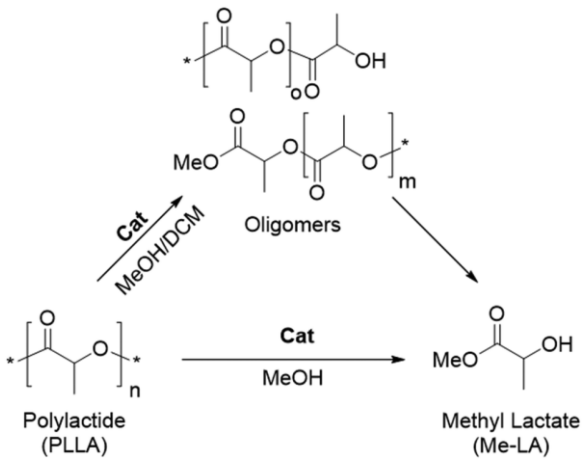

Scheme 3.5 Methanolysis reactions promoted by complexes **1a**, **2a** and **2b**.

The species formed during the reaction can be easily quantified by analysis of the methine region (*ca.* δ = 4.2–5.2 ppm) of the ^{1}H NMR spectra. The efficiency of the process can be estimated by parameters such as conversion, selectivity, and yield of methyl lactate (X_{Int}, $S_{Me\text{-}LA}$, $Y_{Me\text{-}LA}$, respectively) that are evaluated by sample checks of the reaction mixtures (section **3.4.6**). Initial experiments were conducted using a purified PLLA sample (M_n = 30 kDa, $Đ$ = 1.2) in a DCM/MeOH mixture at room

temperature, following the same reaction conditions described in the literature for the NHC zinc complexes [complex: ester units of the PLLA: methanol molar ratio of 1: 200: 100] (**Table 3.5**).

Table 3.5 Methanolysis reactions of PLLA samples.

Entry[a]	Cat (µmol)	DCM (mL)	Time (h)	X_{Int}[b] (%)	S_{MeLA}[b] (%)	Y_{MeLA}[b] (%)
42	**1a**	1.4	24	6	<1	<1
43	**2a**	1.4	24	56	36	19
44	**2b**	1.4	24	15	10	2
45[c]	**1a**	-	24	57	100	57
46[c]	**2a**	-	19	92	100	92
47[c,d]	**2a**	-	19	70	100	70
48[c,d]	**2b**	-	19	100	100	100
49[c]	L_1HO^iPr	-	2	5	100	5
50[c]	$Zn[N(SiMe_3)_2]_2$	-	2	40	100	40
51[c]	L_1HO^iPr/ $Zn[N(SiMe_3)_2]_2$	-	2	95	100	95

[a] All reactions were carried out by using 14 µmol of catalyst (0.5 mol % relative to ester linkages) and 2.8 mmol of PLLA, with 0.56 mL of MeOH in 1.4 mL of DCM at room temperature. [b] Determined by ^{1}H NMR spectroscopy. [c] 10 µmol of catalyst (1 mol % relative to ester linkages) and 1 mmol of PLLA in 1.0 mL of MeOH. [d] PLLA from a commercial plastic cup.

Complex **1a** was found to be scarcely active: after 24 hours only 6% of the polymer was converted to oligomeric species, while no evidence of the formation of methyl lactate emerged from the ^{1}H NMR spectrum of the reaction mixture. In contrast, complex **2a** achieved 56% oligomerization, with a yield of 20% of Me-LA in the same period (Entry 43), a performance comparable to other reported NHC-zinc systems. Magnesium complex **2b** showed lower activity (Entry 44), mirroring its relative performance in the ROP of L-LA (**Table 3.5**, Entries 44–45). In all reactions in solution, the product mixture was composed of oligomers and Me-LA, consistent with a random chain scission mechanism (**Scheme 3.5)**. On the other hand, when the alcoholysis reactions were performed in neat methanol, Me-LA was produced selectively, even at low conversions, as a consequence of the unzipping mechanism of the polymer starting from the chain ends. Interestingly, in the absence of DCM, the performance of both catalysts improved significantly. Zinc complex **2a** achieved quantitative conversion of PLLA to Me-LA within 19 hours (Entry 46) and maintained high activity even with a post-consumer PLLA sample (M_n = 53 kDa, Entry 47). Surprisingly, magnesium complex **2b** also showed superior performance in pure methanol. This result is noteworthy given the paucity of well-defined Mg(II) catalysts for polyester solvolysis, with recent studies showing lower conversions at elevated temperatures.[29]

As previously described, it has been hypothesized that the active catalytic system in methanolysis arises from the reaction of the metal complex with the alcohol, generating an equilibrium mixture of the carbene-alcohol adduct and the metal amide species (e.g., $ZnClN(SiMe_3)_2$). Control experiments confirmed this cooperative effect: the isolated L1HO^{i}Pr adduct was largely inactive (5% conversion in 2 hours, Entry 49), while $Zn[N(SiMe_3)_2]_2$ was highly active (Entry 50). However, the highest activity was obtained with an equimolar mixture of the two (Entry 51), clearly demonstrating their synergistic cooperation in depolymerization catalysis.

Interestingly, the order of activity of complexes supported by *ant*i-ancillary ligands is higher than that of the analogues with the *syn*-ligand in methanolysis. This trend appears to be completely opposite to that observed in the ROP of lactide. Both electronic and steric aspects could be responsible for the observed behavior. As previously studied,[15]

the different stereochemistry of the phenyls on the backbone influences the donating capacity of the carbene ligands towards the zinc atom, as well as that of the carbon atom between the two nitrogen atoms in the corresponding alcohol adduct. The *syn*- and *anti*-symmetric alcohol adducts, deriving from complexes **1a** and **2a**, respectively, would interact differently with the s-*cis* lactones and the s-*trans* esters of the interchain esters, favouring the interaction with the monomer or the polymer chain. At the same time, steric factors could be involved, related to the binding of complexes with different symmetry of the backbone substituents on the NHC ligand, to the different substrates (i.e., the monomer and the polymer chain)

3.3 Conclusions

This chapter explores the study of NHC ligand-supported catalysts, describing the synthesis and characterization of four zinc and magnesium complexes. NMR and DFT studies highlighted a first difference between these complexes: the amine formed in situ during synthesis persists in the coordination sphere of magnesium, unlike zinc complexes. This phenomenon is a direct consequence of the greater positive charge of magnesium, which effectively stabilizes this interaction. Subsequently, all the complexes were evaluated in the ring-opening polymerization of cyclic esters and carbonates derived from renewable sources. All the complexes exert a fair control in the polymerization processes. Kinetic studies confirmed a first-order dependence on monomer concentration, while NMR studies led us to hypothesize a dual activation mechanism, in which the cooperation between the alcohol adduct and the mixed metal species is essential for controlling the polymerization process. The activity order of zinc and magnesium complexes depend on the nature of the monomer: the former showed better performance with lactide, glycolide, and methyl-trimethylene carbonate (Me-TMC), while the latter were more active with ε-caprolactone, trimethylene carbonate (TMC), and dimethyl-trimethylene carbonate (DTC). These differences have been tentatively attributed to a combination of steric and electronic effects: future in-depth computational studies will be conducted to confirm monomer structure-activity relationships. Finally, the versatility of these complexes has been demonstrated in the

chemical recycling of poly(L-lactide) (PLLA) via methanolysis, efficiently converting the polyester to methyl lactate.

3.4 Experimental Part

All the operations of synthesis and handling of air-sensitive chemicals were performed in an inert atmosphere, using Schlenk techniques and/or a glovebox in nitrogen atmosphere. The used glassware was dried in an oven at 120 °C and subsequently subjected to vacuum-nitrogen cycles. Solvents used for polymerization experiments and for the synthesis of substances instable toward air and moisture, were distilled prior to use on the opportune drying agent. In particular, THF, toluene, and benzene were dried by refluxing over sodium and benzophenone and stored under nitrogen. Dichloromethane was dried over calcium hydride and distilled prior to use. Benzyl alcohol and isopropanol were dried by refluxing over sodium. Deuterated solvents were purchased from Sigma–Aldrich and dried over activated 3-Å molecular sieves prior to use. All the reagents used for the synthesis of the complexes were purchased from Sigma Aldrich, while trimethylene carbonate was purchased from TCI. L-LA was crystallized in toluene and then dried over P_2O_5, ε-caprolactone was dried over CaH_2 and distilled under nitrogen, while TMC was purified twice by recrystallization from dry THF and stored in a glovebox before use. The NMR spectra were recorded with BRUKER AVANCE instruments operating at 600, 400 and 300 MHz for ^1H. Molecular masses (M_n and M_w) and their dispersities (M_w/M_n) were measured by GPC, using THF as the eluent (1.0 mL min^{-1}) and narrow polystyrene standards as the reference. MALDI mass spectra were recorded using a Bruker solariX XR Fourier transform ion cyclotron resonance (FT-ICR) mass spectrometer (Bruker Daltonik GmbH,Bremen, Germany) equipped with a 7 T refrigerated actively shielded superconducting magnet (Bruker Biospin, Wissembourg, France). The samples were prepared at the concentration of 1.0 mg mL^{-1} in THF, while the matrix (DCTB) was mixed at a concentration of 10.0 mg mL^{-1}.

3.4.1 Synthesis of the Complexes

The reaction was carried out in a glovebox: in a vial, 0.100 g (2.273×10^{-4} mol) of NHC proligand was weighed, dissolved in 4 mL of anhydrous benzene and transferred into a 20 mL vial, equipped with a magnetic stirrer. In another vial, 1 equiv.of $M[N(SiMe_3)_2)]_2$ (2.273×10^{-4} mol) was weighed and dissolved in 4 mL of anhydrous benzene. The solution of the metal precursor was transferred to the solution of the salt and the mixture was left stirring for one hour at room temperature. The solvent was subsequently removed under reduced pressure and the complex obtained was a white powdery solid. The formation of the desired species was confirmed by NMR analysis.

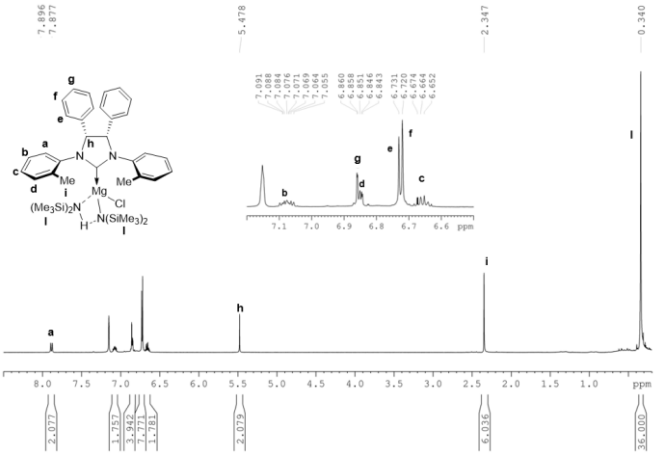

Figure 3.8 ^{1}H spectrum of complex **1b**. (Solvent: C_6D_6, 400 MHz, 25°C).

^{1}H NMR (400 MHz, C_6D_6, 25°C): δ 0.34 (s, 36H, $Si(CH_3)_3$), 2.35 (s, 6H, CH_3), 5.48 (s, 2H, N-CH), 6.66 (t, 2H, Ar-H), 6.72 (t, 4H, Ar-H), 6.73 (d, 4H, Ar-H), 6.84 (d, 2H, Ar-H), 6.86 (d, 2H, Ar-H), 7.07 (m, 2H, Ar-H), 7.88 (d, 2H, Ar-H).

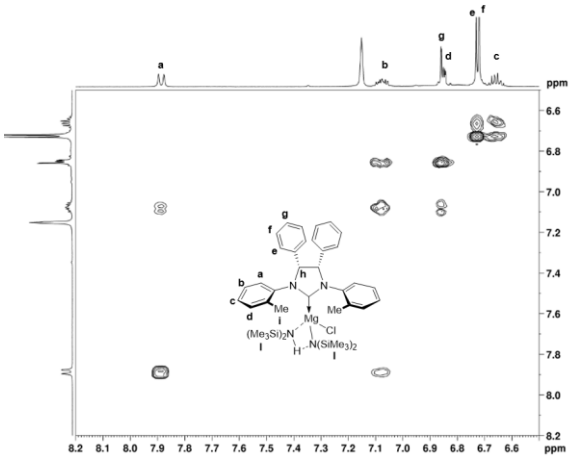

Figure 3.9: Aromatic region of the 2D-COSY spectrum of complex **1b** (Solvent: C_6D_6, 400 MHz, 25°C.)

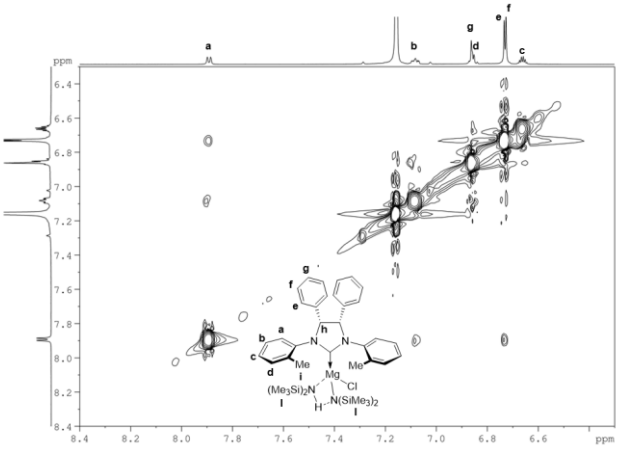

Figure 3.10: Aromatic region of the 2D-NOESY spectrum of complex **1b**. (Solvent: C_6D_6, 400 MHz, 25°C.)

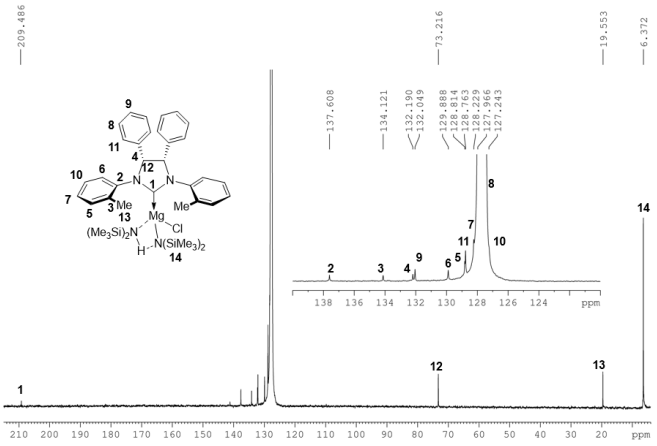

Figure 3.11: ^{13}C spectrum of complex **1b**. (Solvent: C_6D_6, 100,6 MHz, 25°C).

^{13}C NMR (100.6 MHz, C_6D_6, 25°C): δ 6.37 ($Si(CH_3)_3$), 19.55 (2 CH_3), 73.22 (2 CH), 127.24 (2 CH) 127.97 (2 CH), 128.23 (2 CH) 128.76 (2 CH), 128.81 (2 CH), 129.89 (2 CH), 132.05 (2 CH), 132.19 (2 Cq), 134.12 (2 Cq), 137.61 (2 CqN), 209.49 (C Carbenic).

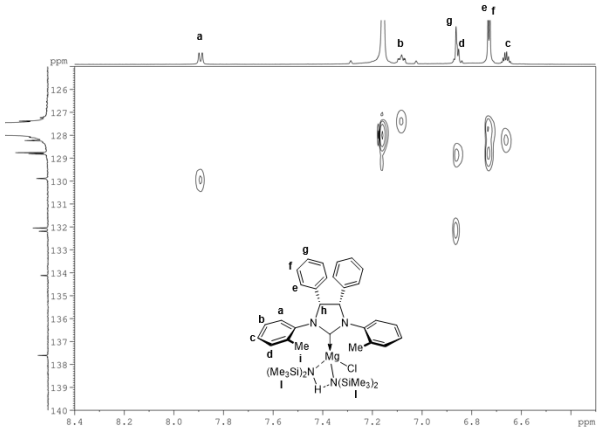

Figure 3.12: Aromatic region of 2D-HSQC spectrum of complex **1b**. (Solvent: C_6D_6, 600 MHz, 25°C.)

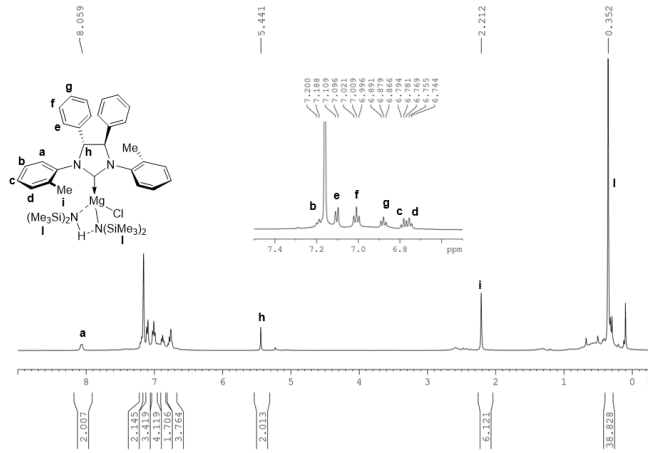

Figure 3.13: ^{1}H-NMR spectrum of complex **2b**. (Solvent: C_6D_6 400 MHz, 25°C.)

^{1}H NMR (400 MHz, C6D6, 25°C): δ 0.35 (s, 36H, $Si(CH_3)_3$), 2.21 (s, 6H, CH_3), 5.44 (s, 2H, N-CH), 6.76 (d, 2H, Ar-H), 6.80 (t, 2H, Ar-H), 6.88 (t, 2H, Ar-H), 7.01 (t, 4H, Ar-H), 7.10 (d, 4H, Ar-H), 7.19 (d, 2H, Ar-H), 8.06 (d, 2H, Ar-H).

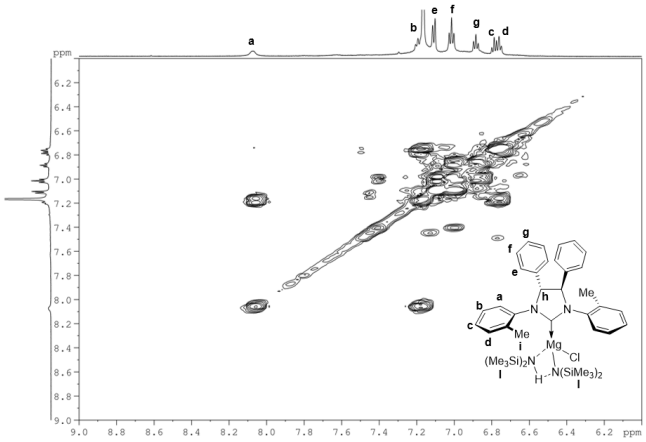

Figure 3.14: Aromatic region of 2D-COSY spectrum of complex **2b** (Solvent: C_6D_6, 400 MHz, 25°C.)

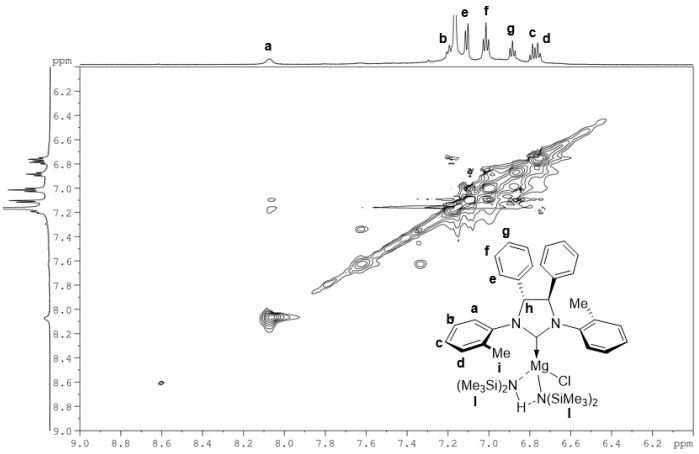

Figure 3.15: Aromatic region of 2D-NOESY spectrum of complex **2b.** (Solvent: C_6D_6, 400 MHz, 25°C.)

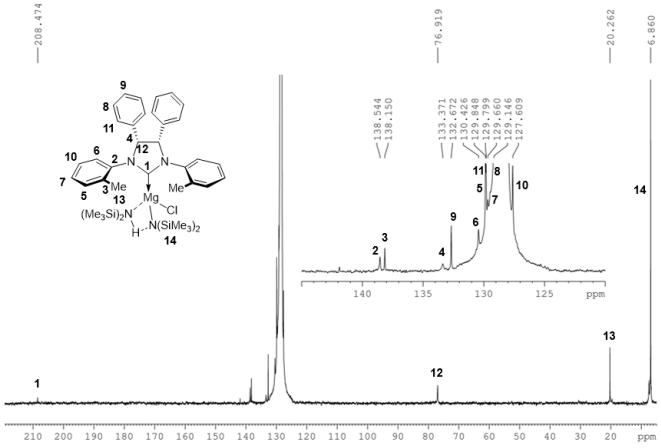

Figure 3.16: ^{13}C spectrum of complex **2b**. (Solvent: C_6D_6, 100.6 MHz, 25°C.)

^{13}C NMR (100.6 MHz, C_6D_6, 25°C): δ 6.86 ($Si(CH_3)_3$), 20.26 (2 CH_3), 76.92 (2 CH), 127.61 (2 CH) 129.15 (2 CH), 129.66 (2 CH), 129.80 (2 CH), 129.85 (2 CH), 130.43 (2 CH), 132.67 (2 CH), 133.37 (2 Cq), 138.15 (2 Cq), 138.54 (2 CqN), 208.45 (C Carbenic).

3.4.2 DOSY-NMR experiments details

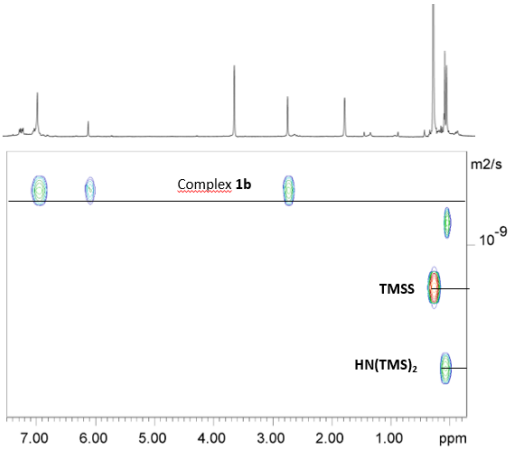

Figure 3.17: DOSY spectrum (THF-d^8, 25°C, 400 MHz) of complex **1b** (D = 8.8 10^{-10} m^2 /s) in the presence of TMSS as standard (D = 1.10 x 10^{-9} m^2/s), with the formation of free amine $HN(SiMe_3)_2$ (D= 1.42 x 10^{-9} m^2/s).

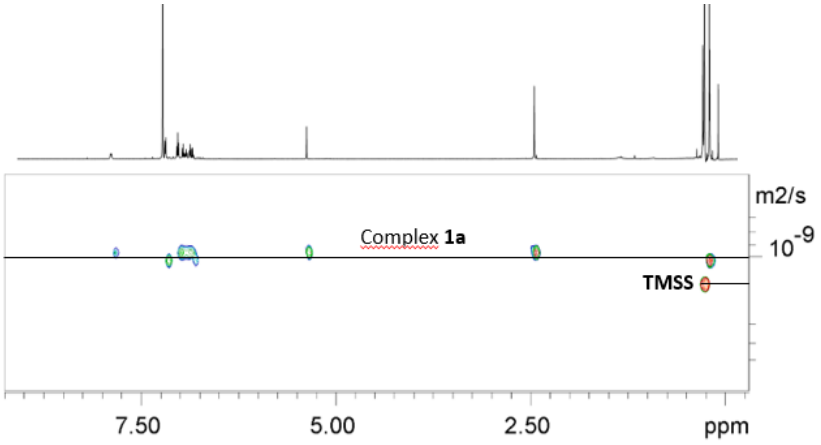

Figure 3.18: DOSY spectrum (C_6D_6, 25°C, 400 MHz) of complex 1a (D = 9.9 10-10 m^2 /s) in the presence of TMSS as standard (D = 1.3 x 10 -9 m^2/s).

Table 3.6: Diffusion coefficients and estimated molecular mass of complex **1b**, using TMSS as internal reference species

Complex	D_{Sample} ($x10^{-10}$ m^2 / s)	D_{TMSS} ($x10^{-10}$ m^2 /s)	MM^{est} (Da)	MM (Da)	MM_{amine} (Da)	MM_{THF} (Da)	MM_2 (Da)
[a]**1b**	5.4	9.3	886	624	**786**	-	1410
[b]**1b**	8.8	11	605	624	786	**696**	1410
[a]**1a**	9.9	13	553	**665**	827	-	1330

[a]C_6D_6 at 25 °C . [b]THF-d8 at 25 °C . MM^{est} = estimated molecular mass, MM = formula weight.

3.4.3 DFT Section

All the DFT geometry optimizations were performed by using the Gaussian16 package[30] at the B3LYP-D3(BJ)[31,32] level of theory, using the quasi relativistic LANL2DZ ECP effective core potential for Zn and Mg and the 6-311g (d,p) basis set for C, H, N, Cl, and Si atoms. The reported free energies were obtained by adding the thermal correction in the gas-phase to the electronic energy in solvent (SMD model) calculated *via* single point energy calculations in benzene (ΔG_{BENZ}) at the M06[33] level. The electronic configuration of the systems was described by using the standard triple-ζ TZVP[34] basis set with a polarization function of Ahlrichs and co-worker for the atoms of the main groups and LANL2DZ ECP pseudopotential for Zn and Mg. The $\Delta\Delta G$ values in benzene as a solvent were computed as the energy difference between the ΔGs of the Mg complexes and the ΔGs of the Zn complexes. The charge distribution in the complexes was calculated using the natural bond orbital (NBO) analysis.

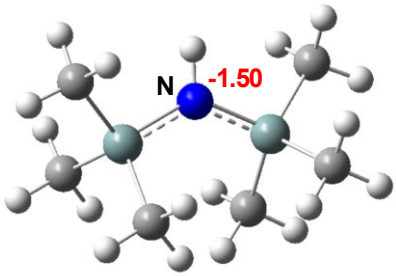

Figure 3.19. NBO charge values of the nitrogen atom in the produced $HN(SiMe_3)_2$. The structures are represented in balls and sticks. C, H, N and Si, are depicted in gray, white, blue and light green, respectively. The NBO charge values of the metals are in red.

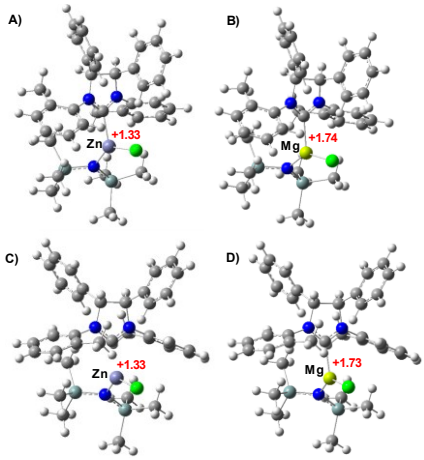

Figure 3.20. NBO charge values of the metals in the *syn* and *anti* monomeric Zn and Mg complexes **1a, 1b** (panel A and B) and **2a, 2b** (panel C and D), respectively. The structures are represented in balls and sticks. C, H, N, Si, Cl, Zn and Mg are depicted in grey, white, blue, light green, green, light purple and yellow, respectively. The NBO charge values of the metals are in red.

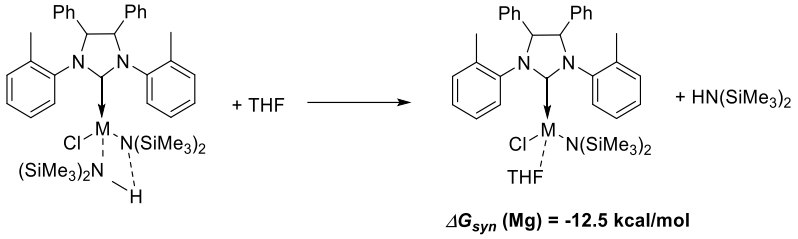

Scheme 3.6. Free energy difference in THF as solvent between the syn Mg complex interacting with $HN(SiMe_3)_2$ and with a THF molecule (ΔG_{syn} (Mg)).

3.4.4 Ring-Opening Polymerization (ROP) of Cyclic Monomers.

Polymerization experiments at room temperature were performed in a glovebox: in a 4 mL vial, the complex was weighed and dissolved in the desired solvent. Subsequently, the solution of the alcohol was added to the solution of the complex and left to stir for 5 min. Finally, the monomer solution was added to the reaction mixture. Conversions were determined by analyzing aliquots taken during the reaction. The polymerization was stopped using wet dichloromethane, and then the solvent was removed under reduced pressure. The polymer was washed with methanol to remove the non-reacted monomer. Most of the samples were characterized by NMR spectroscopy, MALDI-FT-ICR mass spectrometry and/or GPCanalysis both before and after washing with methanol.

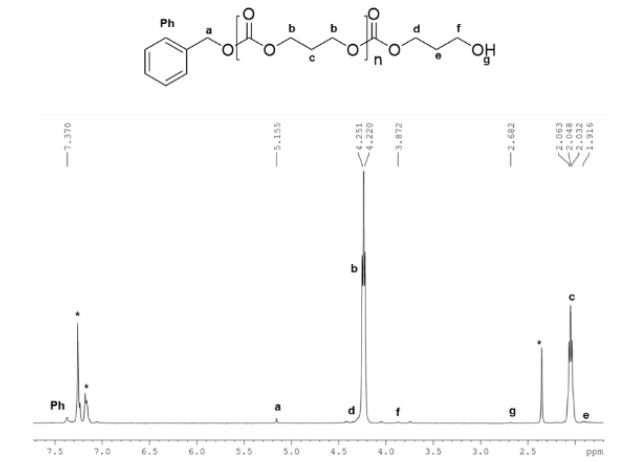

Figure 3.21: ^{1}H-NMR spectrum of polytrimethylene carbonate (solvent: $CDCl_3$, 400 MHz, 25°C). * = toluene.

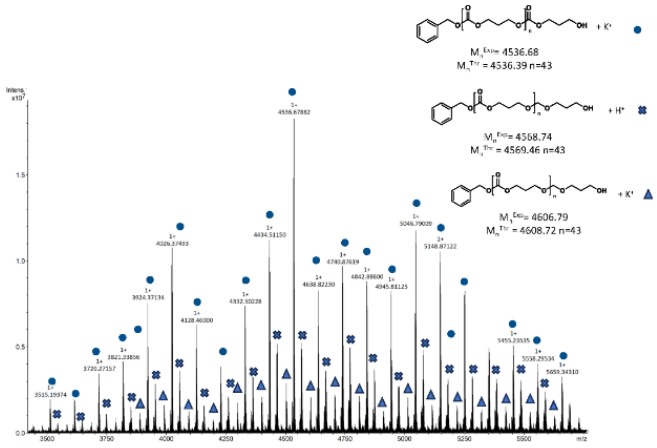

Figure 3.22: MALDI-FT-ICR mass spectrum (matrix DCTB) of the isolated polymer from TMC polymerization. Polymerization conditions: $[TMC]_0$:$[BnOH]_0$:[**1b**] = 50:1:1, Temperature: 25°C, Solvent: THF.

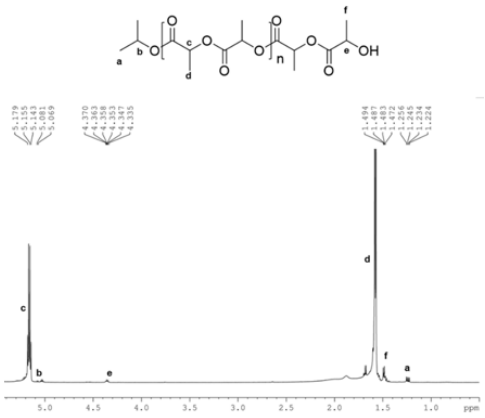

Figure 3.23: ^{1}H-NMR spectrum of polylactide (solvent: $CDCl_3$, 600 MHz, 25°C).

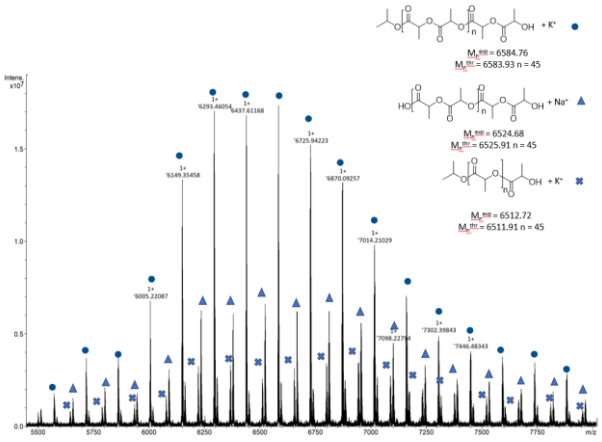

Figure 3.24: MALDI-FT-ICR mass spectrum (matrix: DCTB) of the isolated polymer from L-LA polymerization (Entry 2 in Table 1). Polymerization conditions: $[L\text{-}LA]_0$:$[iPrOH]_0$:[**1b**] = 100:1:1, Temperature: 25°C, Solvent: THF.

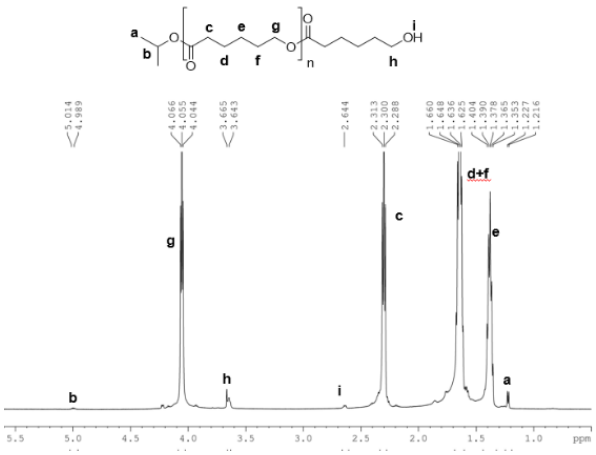

Figure 3.25: ^{1}H-NMR spectrum of polycaprolactone (solvent: $CDCl_3$, 400 MHz, 25°C*).*

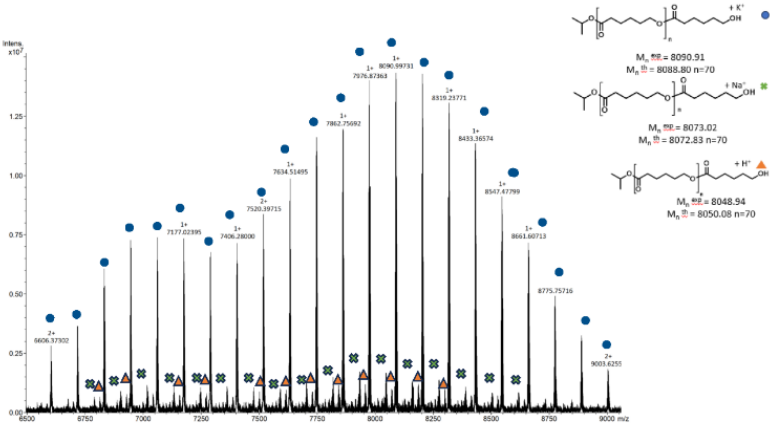

Figure 3.26 MALDI-FT-ICR mass spectrum (matrix: DCTB) of the isolated polymer from ε-caprolactone polymerization (Entry 5 in **Table 3.1**). Polymerization conditions: [ε-CL]$_0$:[iPrOH]$_0$:[**1a**] = 100:1:1, Temperature: 25°C, Solvent: THF.

In a typical procedure, the complex (8.0×10^{-6} mol) was weighed into a vial, one equivalent of the alcohol was added to the complex and left to stir for 5 minutes, then the desired equivalents of monomer, synthesized according to the literature, were added to the reaction mixture and the vial was immersed in a thermostated oil bath at the desired temperature. After the reaction time, the polymerization was stopped using dichloromethane and the solvent was removed under reduced pressure. In all cases, the polymers were washed with methanol, dried, and then characterized by NMR spectroscopy, MALDI-FT-ICR mass spectrometry, and/or GPCanalysis.

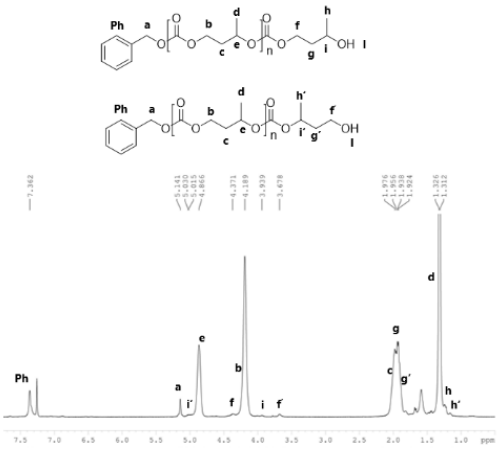

Figure 3.27: ^{1}H-NMR spectrum of poly-methyl-trimethylenecarbonate (Solvent: $CDCl_3$, 600 MHz, 25 °C).

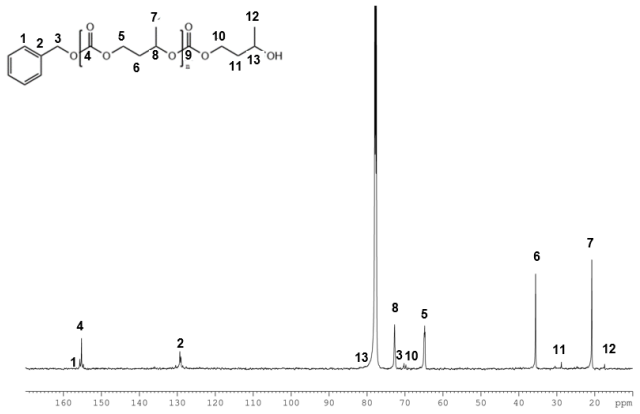

Figure 3.28: ^{13}C-NMR spectrum of poly-methyl-trimethylenecarbonate (Solvent: $CDCl_3$, 100.6 MHz, 25 °C).

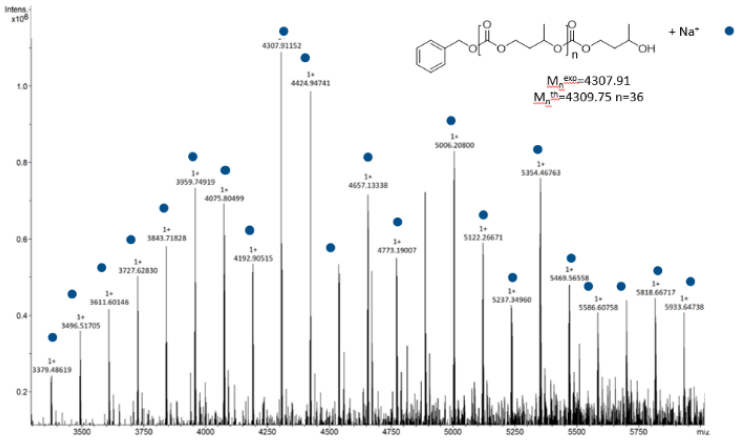

Figure 3.29: MALDI-FT-ICR mass spectrum (matrix: DCTB) of the isolated polymer from 2,2-dimethyl-trimethylene carbonate polymerization (Entry 16 in **Table 3.1**). Polymerization conditions: $[Me\text{-}TMC]_0$:$[BnOH]_0$:[**1b**] = 50:1:1, Temperature: 70 °C.

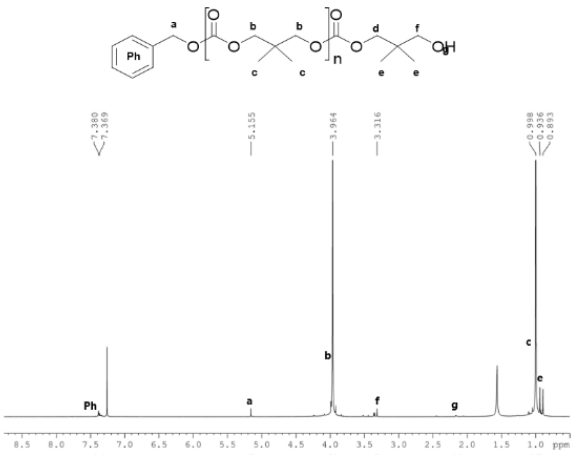

Figure 3.30 ^{1}H-NMR spectrum of poly-2,2-dimethyl-trimethylenecarbonate (Solvent: $CDCl_3$, 600 MHz, 25°C).

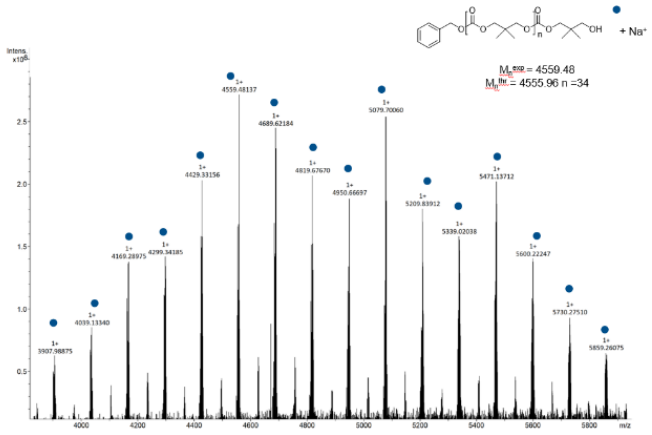

Figure 3.31: MALDI-FT-ICR mass spectrum (matrix: DCTB) of the isolated polymer from 2,2-dimethyl-trimethylene carbonate polymerization (Entry 13 in **Table 3.1**). Polymerization conditions: $[DTC]_0$: $[BnOH]_0$:[**1a**] = 50:1:1, Temperature: 160 °C.

3.4.5 Mechanistic Studies via NMR Analysis

A deuterated solution (0.5 mL) of BnOH (1.63 mg, 1.51 x 10^{-5} mol) was added to a deuterated solution (0.3 mL) of complex (1.51 x 10^{-5} mol). Once the addition was complete, the reaction mixture was left to stir for a few minutes and transferred to the J-Young tube at room temperature. The formation of the corresponding alcohol adduct was observed.

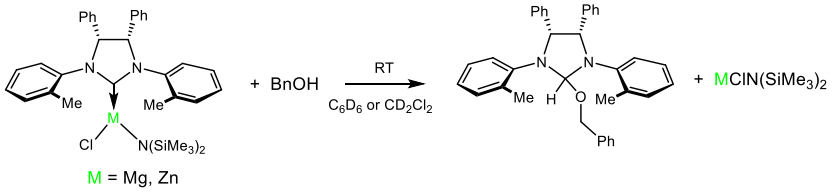

Scheme 3.7: Synthesis of the alcohol adduct L1HOBn from complex **1a** and **1b.**

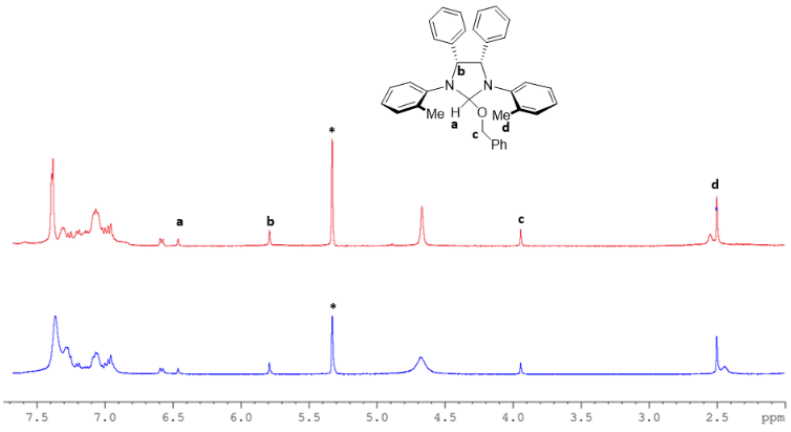

Figure 3.32: ^{1}H NMR spectra of the products obtained from the reaction of complex **1a** (top spectrum) and complex **1b** (bottom spectrum) with one equivalent of BnOH in CD_2Cl_2 (400 MHz, 20 °C).* = benzyl alcohol.

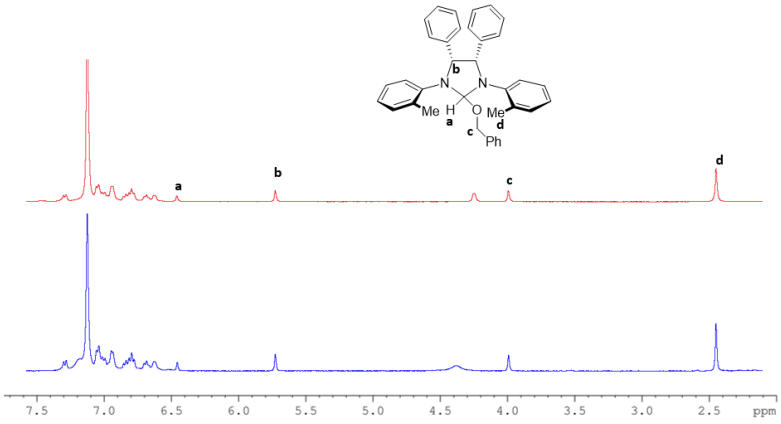

Figure 3.33: ^{1}H NMR spectra of the products obtained from the reaction of complex **1a** (top spectrum) and complex **1b** (bottom spectrum) with one equivalent of BnOH in C_6D_6 (400 MHz, 20 °C).

3.4.6 Chemical recycling of PLLA

Methanolysis performed in DCM solution

In a 4 mL vial, the complex (14.0×10^{-6} mol) was weighed and dissolved in 0.4 mL of DCM. The polymer (200 mg, 2.8×10^{-3} mol) was weighted into another vial and then dissolved in 1 mL of DCM. The solution of the complex was added to the solution of the polymer and left to stir for 5 min. After this time, methanol (56.3 µL, 1.4 mmol) was added and the reaction mixture was stirred at room temperature for 24 h. The reaction was stopped using wet dichloromethane, and an aliquot of the reaction mixture was dissolved in wet CD_2Cl_2 and analysed by ^{1}H NMR spectroscopy.

The conversion of internal methine units (X_{Int}), Selectivity ($S_{Me\text{-}La}$) and Yield ($Y_{Me\text{-}La}$) of methyl lactate were calculated by the following equations[5]:

Conversion $X_{int} = \frac{Int_0 - Int}{Int_0}$

Selectivity $S_{MeLa} = \frac{MeLa}{Int_0 - Int}$

Yield $Y_{MeLa} = S_{MeLa} X_{Int}$

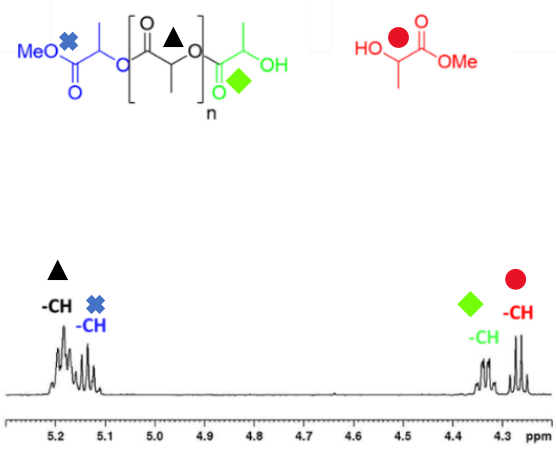

Figure 3.34: ^{1}H NMR spectrum of PLA methanolysis with assignment of internal (black triangle), chain end (blue cross and green diamond), and methyl lactate (red circle) alkyl protons. (Solvent = CD_2Cl_2, 400 MHz, 25°C).

Methanolysis performed under solvent free conditions

In a 4 mL vial, the complex (10.0×10^{-6} mol) was weighed then the polymer and 1 mL of methanol were added. The reaction mixture was left to stir for the desired time then stopped using wet dichloromethane. An aliquot of the reaction mixture was dissolved in wet CD_2Cl_2 and analysed by ^{1}H NMR spectroscopy.

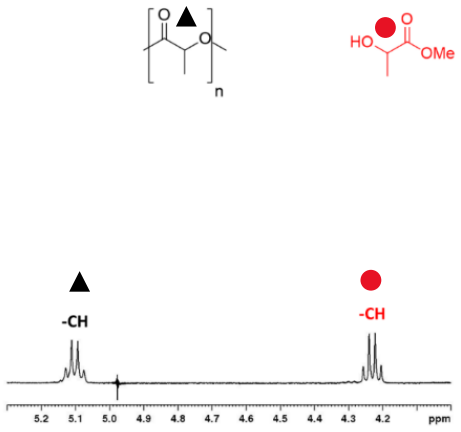

Figure 3.35: ^{1}H NMR spectrum of PLA methanolysis with assignment of internal (black triangle), and methyl lactate (red circle) alkyl protons. (Solvent = CD_2Cl_2, 400 MHz, 25°C).

3.4.7 Synthesis of the alcoholic adduct

The adduct (L_1HOiPr) was prepared from the corresponding imidazolium salt by deprotonation with potassium hydride and subsequent reaction with isopropanol. The product was characterized by NMR analysis. The ^{1}H-NMR spectrum of $L_1HO^{i}Pr$ showed a pattern in agreement with the formation of the desired product and attributable to the presence of a symmetrical species in solution.

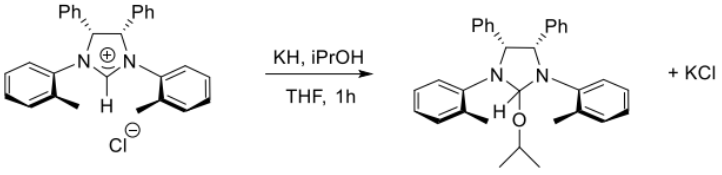

Scheme 3.8: Synthesis of the alcohol adduct $L_1HO^{i}Pr$.

The reaction was carried out in the glovebox in a nitrogen atmosphere. A THF suspension (1.25 mL) of KH (0.0238 g, 5.93 x 10^{-4} mol) was added to a THF suspension (4.4 mL) of

the L1HCl salt (0.200 g, 4.55 x 10^{-4} mol). Once the addition was complete, the reaction mixture was left to stir for 5 minutes at room temperature. Subsequently, a solution of ^{i}PrOH (0.0251 g, 4.2 x 10^{-4} mol) in THF (1.0 mL) was added and the reaction mixture was left under stirring for 1 hour. Then, the reaction mixture was filtered to remove residual salts and the solvent removed under vacuum. The product was obtained as a white powdery solid.

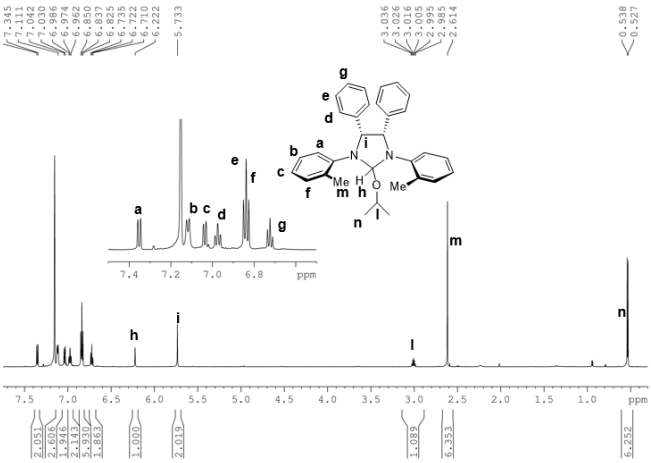

Figure 3.36: ^{1}H NMR spectra of the alcohol adduct $L_1HO^{i}Pr$. (Solvent = C_6D_6, 400 MHz, 25°C).

^{1}H NMR (400 MHz, C_6D_6, 25°C): δ 0.53 (d, 6H, CH_3), 2.61 (s, 6H, CH_3), 3.00 (m, H, CH), 5.73 (s, 2H, CH), 6.22 (s, H, CH), 6.72 (t, 2H, Ar-H), 6.83 (t, 6H, Ar-H), 6.97 (t, 2H, Ar-H), 7.02 (t, 2H, Ar-H), 7.13 (t, 2H, Ar-H), 7.35 (d, 2H, Ar-H).

3.5 References

(1) Zhang, X.; Fevre, M.; Jones, G. O.; Waymouth, R. M. Catalysis as an Enabling Science for Sustainable Polymers. *Chem. Rev.* **2018**, *118* (2), 839–885. https://doi.org/10.1021/acs.chemrev.7b00329.

(2) Getzler, Y. D. Y. L.; Mathers, R. T. Sustainable Polymers: Our Evolving Understanding. *Acc. Chem. Res.* **2022**, *55* (14), 1869–1878. https://doi.org/10.1021/acs.accounts.2c00194.

(3) Chamberlain, B. M.; Cheng, M.; Moore, D. R.; Ovitt, T. M.; Lobkovsky, E. B.; Coates, G. W. Polymerization of Lactide with Zinc and Magnesium β-Diiminate Complexes: Stereocontrol and Mechanism. *J. Am. Chem. Soc.* **2001**, *123* (14), 3229–3238. https://doi.org/10.1021/ja003851f.

(4) Jones, M. D.; Davidson, M. G.; Keir, C. G.; Hughes, L. M.; Mahon, M. F.; Apperley, D. C. Zinc(II) Homogeneous and Heterogeneous Species and Their Application for the Ring-Opening Polymerisation of Rac-Lactide. *Eur. J. Inorg. Chem.* **2009**, *2009* (5), 635–642. https://doi.org/10.1002/ejic.200801049.

(5) Santulli, F.; Lamberti, M.; Mazzeo, M. A Single Catalyst for Promoting Reverse Processes: Synthesis and Chemical Degradation of Polylactide. *ChemSusChem* **2021**, *14* (24), 5470–5475. https://doi.org/10.1002/cssc.202101518.

(6) Helou, M.; Miserque, O.; Brusson, J.-M.; Carpentier, J.-F.; Guillaume, S. M. Poly(Trimethylene Carbonate) from Biometals-Based Initiators/Catalysts: Highly Efficient Immortal Ring-Opening Polymerization Processes. *Adv. Synth. Catal.* **2009**, *351* (9), 1312–1324. https://doi.org/10.1002/adsc.200800788.

(7) Darensbourg, D. J.; Choi, W.; Ganguly, P.; Richers, C. P. Biometal Derivatives as Catalysts for the Ring-Opening Polymerization of Trimethylene Carbonate. Optimization of the Ca(II) Salen Catalyst System. *Macromolecules* **2006**, *39* (13), 4374–4379. https://doi.org/10.1021/ma0603433.

(8) Fliedel, C.; Mameri, S.; Dagorne, S.; Avilés, T. Controlled Ring-Opening Polymerization of Trimethylene Carbonate and Access to PTMC-PLA Block Copolymers Mediated by Well-Defined N-Heterocyclic Carbene Zinc Alkoxides.

Appl. Organomet. Chem. **2014**, *28* (7), 504–511. https://doi.org/10.1002/aoc.3154.

(9) Gregory, G. L.; Sulley, G. S.; Kimpel, J.; Łagodzińska, M.; Häfele, L.; Carrodeguas, L. P.; Williams, C. K. Block Poly(Carbonate-Ester) Ionomers as High-Performance and Recyclable Thermoplastic Elastomers. *Angew. Chem. Int. Ed.* **2022**, *61* (47), e202210748. https://doi.org/10.1002/anie.202210748.

(10) D'Aniello, S.; Laviéville, S.; Santulli, F.; Simon, M.; Sellitto, M.; Tedesco, C.; Thomas, C. M.; Mazzeo, M. Homoleptic Phenoxy-Imine Pyridine Zinc Complexes: Efficient Catalysts for Solvent Free Synthesis and Chemical Degradation of Polyesters. *Catal. Sci. Technol.* **2022**, *12* (20), 6142–6154. https://doi.org/10.1039/D2CY01092E.

(11) Becker, T.; Hermann, A.; Saritas, N.; Hoffmann, A.; Herres-Pawlis, S. Open- and Closed-Loop Recycling: Highly Active Zinc Bisguanidine Polymerization Catalyst for the Depolymerization of Polyesters. *ChemSusChem* **2024**, *17* (18), e202400933. https://doi.org/10.1002/cssc.202400933.

(12) *Effective Ligand Design: Zinc Complexes with Guanidine Hydroquinoline Ligands for Fast Lactide Polymerization and Chemical Recycling*. https://chemistry-europe.onlinelibrary.wiley.com/doi/epdf/10.1002/cssc.202201075 (accessed 2025-10-22).

(13) Ferrentino, N.; Franco, F.; Grisi, F.; Pragliola, S.; Mazzeo, M.; Costabile, C. Ring Opening Polymerization of Lactide Promoted by Zinc and Magnesium Complexes with a N-Heterocyclic Carbene-Phenoxy-Imine Hybrid Non-Innocent Ligand. *Mol. Catal.* **2022**, *533*, 112799. https://doi.org/10.1016/j.mcat.2022.112799.

(14) Nesterov, V.; Reiter, D.; Bag, P.; Frisch, P.; Holzner, R.; Porzelt, A.; Inoue, S. NHCs in Main Group Chemistry. *Chem. Rev.* **2018**, *118* (19), 9678–9842. https://doi.org/10.1021/acs.chemrev.8b00079.

(15) Tufano, F.; Santulli, F.; Grisi, F.; Lamberti, M. N-Heterocyclic Carbene-Based Zinc Complexes: Same Precursors for Different Lactide Ring-Opening

Polymerization Mechanisms. *ChemCatChem* **2022**, *14* (20), e202200962. https://doi.org/10.1002/cctc.202200962.

(16) Tufano, F.; Napolitano, C.; Mazzeo, M.; Grisi, F.; Lamberti, M. CO_2-Based Polycarbonates through Ring-Opening Polymerization of Cyclic Carbonates Promoted by a NHC-Based Zinc Complex. *Biomacromolecules* **2024**. https://doi.org/10.1021/acs.biomac.4c00532.

(17) Perfetto, A.; Costabile, C.; Longo, P.; Bertolasi, V.; Grisi, F. Probing the Relevance of NHC Ligand Conformations in the Ru-Catalysed Ring-Closing Metathesis Reaction. *Chem. – Eur. J.* **2013**, *19* (32), 10492–10496. https://doi.org/10.1002/chem.201301540.

(18) McGraw, M. L.; Chen, E. Y.-X. Lewis Pair Polymerization: Perspective on a Ten-Year Journey. *Macromolecules* **2020**, *53* (15), 6102–6122. https://doi.org/10.1021/acs.macromol.0c01156.

(19) Thevenon, A.; Romain, C.; Bennington, M. S.; White, A. J. P.; Davidson, H. J.; Brooker, S.; Williams, C. K. Dizinc Lactide Polymerization Catalysts: Hyperactivity by Control of Ligand Conformation and Metallic Cooperativity. *Angew. Chem. Int. Ed.* **2016**, *55* (30), 8680–8685. https://doi.org/10.1002/anie.201602930.

(20) *Next Generation of Zinc Bisguanidine Polymerization Catalysts towards Highly Crystalline, Biodegradable Polyesters*. https://onlinelibrary.wiley.com/doi/epdf/10.1002/anie.202008473 (accessed 2025-10-22).

(21) Zhang, J.; Lui, K. H.; Zunino, R.; Jia, Y.; Morodo, R.; Warlin, N.; Hedrick, J. L.; Talarico, G.; Waymouth, R. M. Highly Selective *O* -Phenylene Bisurea Catalysts for ROP: Stabilization of Oxyanion Transition State by a Semiflexible Hydrogen Bond Pocket. *J. Am. Chem. Soc.* **2024**, *146* (32), 22295–22305. https://doi.org/10.1021/jacs.4c04740.

(22) Fliedel, C.; Vila-Viçosa, D.; Calhorda, M. J.; Dagorne, S.; Avilés, T. Dinuclear Zinc–N-Heterocyclic Carbene Complexes for Either the Controlled Ring-Opening Polymerization of Lactide or the Controlled Degradation of Polylactide Under

Mild Conditions. *ChemCatChem* **2014**, *6* (5), 1357–1367. https://doi.org/10.1002/cctc.201301015.

(23) Arnold, P. L.; Casely, I. J.; Turner, Z. R.; Bellabarba, R.; Tooze, R. B. Magnesium and Zinc Complexes of Functionalised, Saturated N-Heterocyclic Carbene Ligands: Carbene Lability and Functionalisation, and Lactide Polymerisation Catalysis. *Dalton Trans.* **2009**, No. 35, 7236. https://doi.org/10.1039/b907034f.

(24) Slattery, R. M.; Stahl, A. E.; Brereton, K. R.; Rheingold, A. L.; Green, D. B.; Fritsch, J. M. Ring Opening Polymerization and Copolymerization of L-Lactide and ε-Caprolactone by Bis-Ligated Magnesium Complexes. *J. Polym. Sci. Part Polym. Chem.* **2019**, *57* (1), 48–59. https://doi.org/10.1002/pola.29280.

(25) D'Auria, I.; Tedesco, C.; Mazzeo, M.; Pellecchia, C. New Homoleptic Bis(Pyrrolylpyridiylimino) Mg(Ⅱ) and Zn(Ⅱ) Complexes as Catalysts for the Ring Opening Polymerization of Cyclic Esters via an "Activated Monomer" Mechanism. *Dalton Trans.* **2017**, *46* (36), 12217–12225. https://doi.org/10.1039/C7DT02445B.

(26) Huang, M.; Pan, C.; Ma, H. Ring-Opening Polymerization of Rac-Lactide and α-Methyltrimethylene Carbonate Catalyzed by Magnesium and Zinc Complexes Derived from Binaphthyl-Based Iminophenolate Ligands. *Dalton Trans.* **2015**, *44* (27), 12420–12431. https://doi.org/10.1039/C5DT00158G.

(27) Naumann, S.; Scholten, P. B. V.; Wilson, J. A.; Dove, A. P. Dual Catalysis for Selective Ring-Opening Polymerization of Lactones: Evolution toward Simplicity. *J. Am. Chem. Soc.* **2015**, *137* (45), 14439–14445. https://doi.org/10.1021/jacs.5b09502.

(28) Balint, A.; Naumann, S. A Comparison of Zwitterionic and Anionic Mechanisms in the Dual-Catalytic Polymerization of Lactide. *Polym. Chem.* **2021**, *12* (37), 5320–5327. https://doi.org/10.1039/D1PY00992C.

(29) Payne, J. M.; Kociok-Köhn, G.; Emanuelsson, E. A. C.; Jones, M. D. Zn(II)- and Mg(II)-Complexes of a Tridentate {ONN} Ligand: Application to Poly(Lactic Acid) Production and Chemical Upcycling of Polyesters. *Macromolecules* **2021**, *54* (18), 8453–8469. https://doi.org/10.1021/acs.macromol.1c01207.

(30) Hugo, V.-V. V.; Alejandro, H.-S. M.; María, V.-S. A.; María, R.-H.; Antonio, L.-R. M.; Guadalupe, P.-O. M.; Antonio, M.-G. M.; Fernando, A.-H.; Víctor, A.; Diego, C.-A.; Enrique, Á. Molecular Modeling and Synthesis of Ethyl Benzyl Carbamates as Possible Ixodicide Activity. *Comput. Chem.* **2019**, *07* (01), 1–26. https://doi.org/10.4236/cc.2019.71001.

(31) Allouche, A.-R. Gabedit—A Graphical User Interface for Computational Chemistry Softwares. *J. Comput. Chem.* **2011**, *32* (1), 174–182. https://doi.org/10.1002/jcc.21600.

(32) Grimme, S.; Antony, J.; Ehrlich, S.; Krieg, H. A Consistent and Accurate Ab Initio Parametrization of Density Functional Dispersion Correction (DFT-D) for the 94 Elements H-Pu. *J. Chem. Phys.* **2010**, *132* (15), 154104. https://doi.org/10.1063/1.3382344.

(33) Wadt, W. R.; Hay, P. J. Ab Initio Effective Core Potentials for Molecular Calculations. Potentials for Main Group Elements Na to Bi. *J. Chem. Phys.* **1985**, *82* (1), 284–298. https://doi.org/10.1063/1.448800.

(34) Schäfer, A.; Huber, C.; Ahlrichs, R. Fully Optimized Contracted Gaussian Basis Sets of Triple Zeta Valence Quality for Atoms Li to Kr. *J. Chem. Phys.* **1994**, *100* (8), 5829–5835. https://doi.org/10.1063/1.467146.

Chapter Four

Sustainable Polymers obtained by Naphtoxy-imino-pyridine Zn and Mg Complexes

The results described in this *Chapter* have been published in:

Tufano, F., Galotto, M.V., D'Elia, A., Santulli, F., Mazzeo, M. and Lamberti, M., Recyclable, Biobased Polycarbonates and Polyesters by Naphthoxy-Imine Zinc and Magnesium Complexes. *Chem. Eur. J.,* **2025,** *31,* e202501271.

4.1 Introduction

The growing demand for sustainable polymers requires the development of catalytic systems that are not only efficient but also highly versatile. This versatility is essential for achieving sophisticated microstructures by combining different classes of monomers, an essential strategy for obtaining polymers with tailored properties. Furthermore, to be truly competitive, these catalytic systems must also be able to promote the chemical recycling of the resulting materials. Among the numerous catalysts described in the literature, zinc and magnesium complexes stand out for their high activity, and remarkable ability to maintain precise control over polymerization processes. The high versatility of amino- and imino-phenolate ligands made them a common choice as ancillary ligands for both magnesium and zinc, resulting in efficient catalysts in polymerization and in chemical recycling.

Some of us developed zinc and magnesium complexes bearing phenoxy-imino-pyridinic ligands that are easy to synthesize, cost-effective, and exhibit outstanding activity both in the production of polylactic acid (PLA) and in its chemical recycling.[1,2] Having verified that the substituents on the ligand play a significant role on the catalytic activity, we decided to move to a naphthoxy-imino-pyridinic ligand, as coordinative environment. To demonstrate the versatility of these new systems, the study extends from the homopolymerization of cyclic esters and carbonates, to their copolymerization, allowing for the fine-tuning of chemical and physical properties. Finally, the performance of the zinc complex was also evaluated in the depolymerization of PTMC and its copolymers, utilizing microwaves as a more sustainable alternative to conventional heating methods.

4.2 Results and Discussions

4.2.1 Synthesis of the complexes

The proligand was synthesized via a condensation reaction between 2-hydroxy-1-naphthaldehyde and 2-aminoethylpyridine under reflux in ethanol.[3] The product was isolated and characterized by NMR spectroscopy (**Figures 4.7,4.8**). Subsequently, the corresponding zinc and magnesium complexes (**3** and **4**, respectively) were synthesized by treating the proligand with one equivalent of the respective metal bis(trimethylsilyl)amide, $M[N(SiMe_3)_2]_2$ (M = Zn, Mg), in benzene (**Scheme 4.1**). The resulting complexes were purified by washing with hexane to remove the liberated amine byproduct and dried under vacuum (**Figures 4.9-4.11** for complex **3**; **4.12-4.17** for complex **4)**.

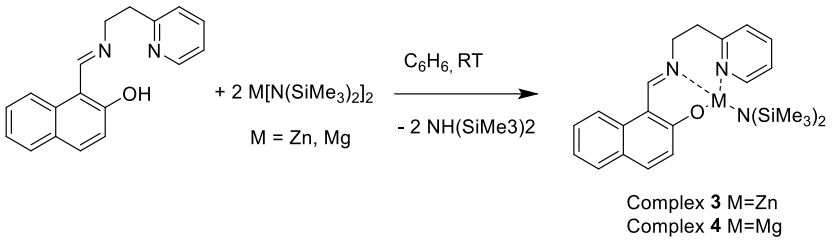

Scheme 4.1: Synthesis of complexes **3** and **4**.

The ^1H NMR spectrum of the zinc complex (**3**) is consistent with the formation of a tetracoordinated species, as illustrated in **Figure 4.1**. Key evidence for coordination includes the presence of broadened signals for the methylene protons, suggesting fluxional behaviour of the six-membered metallacycle formed following coordination of the pyridine nitrogen to the zinc centre. A characteristic low-chemical-shift signal was assigned to the methyl protons of the coordinated trimethylsilylamido ligand. Further confirmation of the coordination environment was obtained from a Nuclear Overhauser Effect (NOE) correlation observed between the pyridine α-proton and the amido methyl protons (**Figure 4.1**).

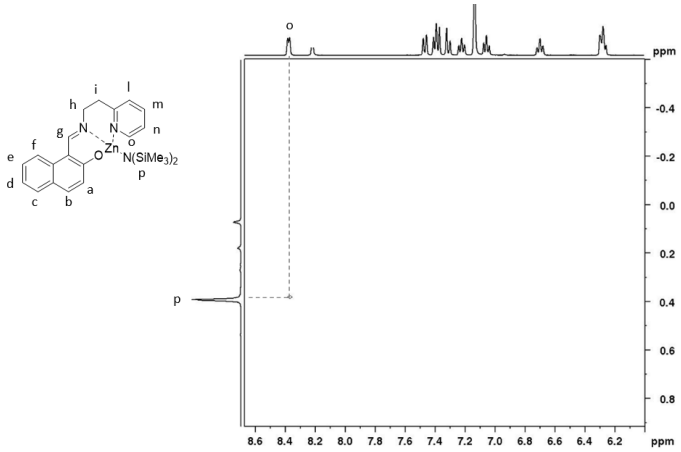

Figure 4.1. Enlargement of the 2D-NOESY spectrum of complex **3** (Solvent:C_6D_6, 400 MHz, 25°C).

Characterization of the magnesium complex (**4**) yielded similar results, albeit with significantly broader signals in both the aromatic and methylene regions of the ^{1}H NMR spectrum.

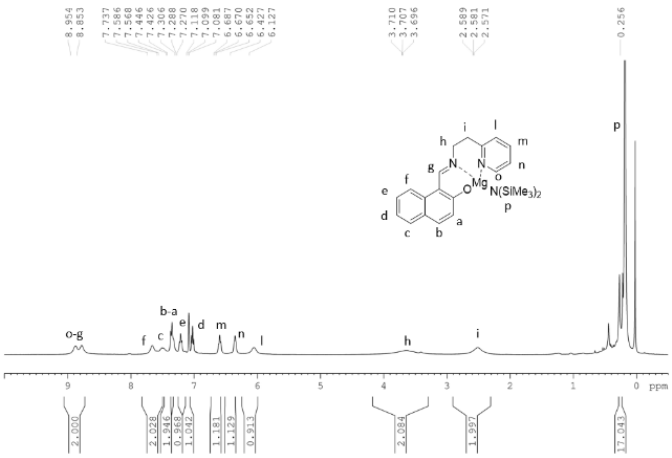

Figure 4.2. ^{1} H-NMR spectrum of complex **4** (Solvent: C_6D_6, 400 MHz, 25°C).

This line broadening indicates a greater degree of fluxionality in solution for complex **4** compared to its zinc counterpart. Variable-temperature ^{1}H NMR studies supported this hypothesis; upon cooling to –40 °C, fluxional equilibrium was slowed down on the NMR time scale, revealing a resolved AA'BB' cleavage pattern for the ligand backbone methylene protons.

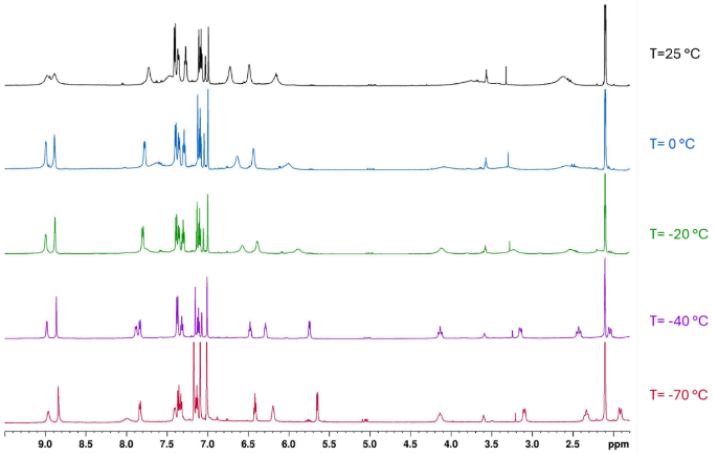

Figure 4.3. ^{1}H-NMR spectra of complex **4** with acquisition at different temperatures (Solvent: tol-d^{8}, 600 MHz).

4.2.2 ROP of Lactones and Cyclic Carbonates

The efficiency of complexes was evaluated in the ring-opening polymerization (ROP) of various cyclic lactones and carbonates under different conditions, with key results summarized in **Table 4.1**.

Table 4.1. ROP of cyclic esters and carbonates by complexes **3** and **4**.

Entry[a]	Comp.	Mon. (equiv)	Init. (equiv)	Temp (°C)	Solvent (vol)	Time	Conv[b] (%)	M_n^{th}[c]	M_n^{exp}[d]	$Đ$[d]
1	**3**	L-LA (100)	^{i}PrOH	20	DCM (2 mL)	1 min	90	13.0	14.7	1.1
2	**3**	L-LA (5000)	BnOH (50)	150	-	5 min	88	12.7	13.6	1.1
3	**4**	L-LA (100)	^{i}PrOH	20	DCM (2 mL)	1.5 h	80	11.5	11.5	1.3
4	**3**	β-BL (100)	^{i}PrOH	70	Toluene (2 mL)	6 h	62	5.3	*4.9*	
5	**4**	β-BL (100)	^{i}PrOH	70	Toluene (2 mL)	6 h	< 1	-	-	
6	**3**	β-BL (100)	^{i}PrOH	70	-	30 min	98	8.4	8.5	1.4
7	**4**	β-BL (100)	^{i}PrOH	70	-	2 h	56	4.8	*3.9*	
8	**3**	ε-CL (100)	^{i}PrOH	20	DCM (2 mL)	1.5 h	85	9.7	8.7	1.3
9	**4**	ε-CL (100)	^{i}PrOH	20	DCM (2 mL)	45 min	90	10.3	8.6	1.4
10	**3**	TMC (200)	BnOH	20	DCM (0.4 mL)	1 min 5 min	85 89	18.1	16.3	1.6
11	**4**	TMC (200)	BnOH	20	DCM (0.4 mL)	1 min 5 min	82 95	19.4	20.3	1.7

12	**3**	TMC (200)	BnOH	20	dioxolane (0.4 mL)	30 min 1.5 h	52 87	17.8	11.8	2.1
13	**4**	TMC (200)	BnOH	20	dioxolane (0.4 mL)	30 min 1.5 h	73 87	16.7	16.5	1.7
14	**3**	TMC (500)	BnOH (5)	70	-	10 min	100	10.2	19.2	2.0
15	**4**	TMC (500)	BnOH (5)	70	-	10 min	97	9.9	6.0	1.8
16	**4**	TMC (500)	BnOH	70	-	1 h	98	50.0	52.2	2.2
17	**3**	Me-TMC (50)	BnOH	20	-	30 min	72	4.2	*3.1*	
18	**4**	Me-TMC (50)	BnOH	20	-	1 h	70	4.1	*5.2*	

[a] General conditions: metal complex = 4 µmol for cyclic carbonates, 5 µmol for cyclic esters; one equivalent of alcohol, except when differently specified. [b] Determined by ^{1}H NMR spectral data. [c] M_n^{th} (kDa) = $MM_{monomer}$ × ([monomer]$_0$/[Cat]$_0$) × monomer conversion)/10^3 Da/kDa. [d] Experimental M_n and M_w/M_n ($Đ$) values were determined by GPC in THF using polystyrene standards and corrected using a factor of 0.58 for PLA, 0.54 for PBL, 0.56 for PCL and 0.73 for PTMC with theoretical mass in the range 5-10 kDa and 0.88 for PTMC with theoretical mass > 10 kDa. Experimental M_n indicated in italic have been determined by MALDI analysis.

First, our studies focused primarily on L-LA polymerization under previously established conditions with analogous zinc phenoxy-imino-pyridine complexes.[4] Complex **3**, containing the naphthoxy-imino-pyridine ligand, showed a marked increase in activity,

reaching a turnover frequency (TOF) of 9800 h^{-1} (**Table 4.1**, Entry 1) at 30 s, approximately double the highest value previously reported (5050 h^{-1}).[1] Furthermore, complex **3** demonstrated exceptional stability and activity under industrially relevant conditions using unpurified molten L-lactide (L-LA, 5000 equiv.) at 150 °C with a high initiator loading (BnOH, 50 equiv.). The recorded TOF of 52,800 h^{-1} (Entry 2) underscores the catalyst's robustness against both protic impurities and elevated temperatures. Comparing the zinc and magnesium complexes revealed different behaviour depending on the nature of the monomer. For cyclic esters, complex **3** was more active than **4** in the ROP of L-LA, exhibiting two orders of magnitude higher activity. While complex **3** successfully polymerized β-butyrolactone (β-BL) at 70 °C in toluene (Entry 4), the magnesium analogue was found to be inactive under these conditions (Entry 5). When run in pure monomer, complex **4** promoted the ROP of β-BL, although with substantially lower activity than complex **3** (Entries 6 and 7). In contrast, the magnesium complex showed a slight activity advantage in the ROP of ε-caprolactone (ε-CL, Entries 8 and 9).

Kinetic studies of ε-CL polymerization in CD_2Cl_2 at 25 °C (**Figure 4.4**) revealed pseudo-first-order kinetics for both catalysts. Complex **4** showed an induction period of approximately 0.6 h, suggesting a slower initiation phase, but ultimately demonstrated a slightly higher observed rate constant ($k_{obs} = 6.06 \times 10^{-1}$ h^{-1}) than complex **3** ($k_{obs} = 3.71 \times 10^{-1}$ h^{-1}). The higher activity of zinc compared to magnesium in the ROP of lactide is consistent with previous observations for phenoxy-imino-pyridine ligands,[5] with the enhanced activity for both metals in this study attributed to the superior electron-donating character of the napthoxy-based ligand.

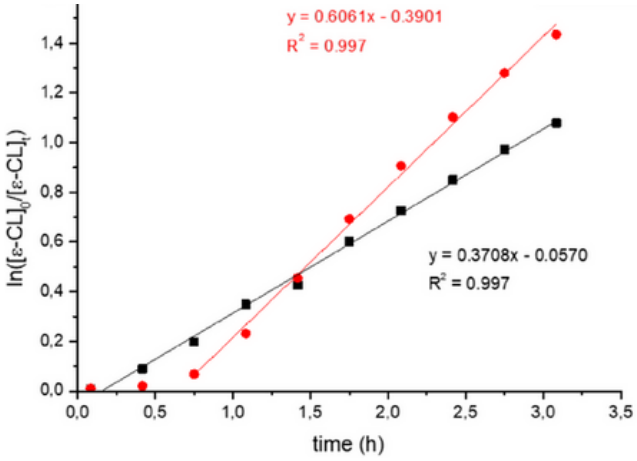

Figure 4.4. Pseudo first-order kinetic plots for the consumption of ε-CL (100 equiv) in CD_2Cl_2 at 20 °C by complex **3** (black square) and complex **4** (red circles) in combination with ^{i}PrOH.

Under the selected conditions, both complexes showed similarly high activity in the TMC ROP, both in solution at 20 °C and in bulk at 70 °C (Entries 10-11, 14-15). High molecular weight (~50 kDa) PTMC was obtained at 70 °C (Entry 16). Both catalysts also remained active in the green dioxolane solvent, although with reduced activity compared to dichloromethane (Entries 12-13). In contrast, for the ROP of the bulk asymmetric monomer 1-methyl-TMC (1-Me-TMC) at 20 °C, complex **3** demonstrated approximately twice the activity of complex **4** (Entries 17–18). The polymerization of 1-Me-TMC, synthesized from renewable CO_2 and 1,3-butanediol,[6] allowed for the investigation of regioselectivity. The resulting polymeric microstructures were analysed by ^{13}C NMR spectroscopy. The regioselectivity (X_{reg} = HT/(HT+HH+TT)) was found to be slightly higher for the magnesium complex (X_{reg} = 0.87, **Figure 4.27**) than for the zinc complex (X_{reg} = 0.80). Analysis of the terminal groups (**Figure 4.28**) indicated that initiation proceeds via both primary and secondary insertion with comparable probability, confirming that initiation is not regiocontrolled, a behaviour consistent with other catalytic systems. Overall, the experimental molecular weights of the obtained polymers, determined by GPC, showed good agreement with theoretical values. Polymers produced from the zinc

complex showed slightly lower dispersity (*Đ*) values, indicating a higher level of control over the polymerization process across all monomers. Analysis of the terminal groups by ^{1}H NMR and MALDI-FT-ICR spectrometry (**Figures 4.18-4.24**) confirmed initiation by the metal–alkoxide bond and termination by hydrolysis. The presence of a single distribution in all MALDI-FT-ICR spectra indicates the absence of side reactions, such as transesterification in polyesters or decarboxylation in polycarbonates, further corroborating the well-controlled nature of these polymerization processes.

4.2.3 ROCOP of Lactones with TMC

Motivated by the high activity and versatility of complex **3**, we next investigated the performance of complex **3** as a catalyst for the ROCOP of TMC with ε-caprolactone and L-lactide (**Table 4.2**). Initially, diblock copolymers were synthesized by sequential monomer addition.

Table 4.2. Sequential and simultaneous copolymerization reactions of TMC with *ε* -CL and L-LA by complex **3**.

Entry[a]	**TMC equiv**	**Mon2 equiv**	**Conv**[b] **TMC (%)**	**Conv**[b] **Mon2 (%)**	**L_{TMC}**[c]	**L_{Mon2}**[c]	**M_n^{th}** [d] **(kDa)**	**M_n^{exp}** [e] **(kDa)**	***Đ*** [e]	**T_g (°C)**
19	200	L-LA 200	90	83	Diblock copolymer		43.3	48.4	2.3	-20.0, 53.2
20	100	ε-CL 100	74	100	Diblock copolymer		19.0	30.2	1.7	-21.0
21	100 + 100	L-LA	88	95	2.6	2.6	22.7	25.1	1.7	17.0
22	250 + 250	L-LA	57	82	2.2	3.8	45.9	-	-	29.6

23	ε-CL 250 + 250	86	65	2.6 (2.3)[e]	1.8 (1.8)[e]	40.4	47.3	1.7	- 42.8
24	ε-CL 500 + 500	96	66	2.5 (2.5)[e]	1.6 (1.7)[e]	86.6	53.3	1.8	- 36.7

[a] General conditions: Polymerization experiments carried out in bulk conditions. [**3**] = 4 µmol; one equivalent of benzyl alcohol (0.0185 M in THF). [b] Determined by ^{1}H NMR spectral data. [c] Average lengths of carbonate and caproyl blocks in chains for a completely random distribution of units calculated for the experimental molar fraction of TMC in the copolymer. [d] M_n^{th} = (102.03 x $[TMC]_0$: $[I]_0$ x C_{TMC}%) + (144.13 x $[L\text{-}LA]_0$: $[I]_0$ x $C_{L\text{-}LA}$%) or M_n^{th} = (102.03 x $[TMC]_0$: $[I]_0$ x C_{TMC}%) + (114.14 x $[\varepsilon\text{-}CL]_0$: $[I]_0$ x $C_{\varepsilon\text{-}CL}$%). [e] Experimental M_n (kDa) and M_w/M_n ($Đ$) values were determined by GPC in THF.

First, diblock copolymers were prepared by sequential polymerization: the TMC block fails to form after the polymerization of the lactide, so in this case the cyclic carbonate was polymerized first and then lactide was added (**Table 4.2**, Entry 19). In contrast, the order of monomer addition was irrelevant for TMC/ε-CL combinations, with the second monomer introduced after the first was completely consumed (**Table 4.2**, Entry 20). The formation of diblock copolymers was confirmed by product masses and DOSY (**Figures 4.30,4.33**). DSC revealed a glass transition temperature (T_g) of approximately −20 °C for the poly(TMC) block in both copolymers. For the second block, the PLA segment exhibited a T_g of 53.2 °C and a melting temperature (T_m) of 169.88 °C, while the PCL segment exhibited only a T_m of 57.79 °C (**Figures 4.31, 4.33**).

Subsequently, complex **3** was employed for simultaneous one-pot ROCOP of TMC with LLA and bulk ε-CL at 110 °C). The molecular weights of the copolymer were determined by gel permeation chromatography (GPC), and the compositions were ascertained by ^{1}H NMR spectroscopy by integrating the signals corresponding to TMC (δ = 4.0–4.2, 1.95–2.10 ppm), LA (δ = 1.4–1.6 ppm), and ε-CL (δ = 2.27–2.35 ppm). The ^{1}H NMR spectra (**Figure 4.5**) confirmed the copolymer structure, with the random copolymers showing additional signals indicative of heterodyads. The lack of signals near δ = 3.1 ppm in all copolymer spectra indicates the absence of ether bonds, due to carbonate decarboxylation. In all cases, the absence of signals around 3.1 ppm in the ^{1}H NMR

spectra of the copolymers ruled out the formation of ether units due to decarboxylation of carbonate linkages, even at 110 °C.

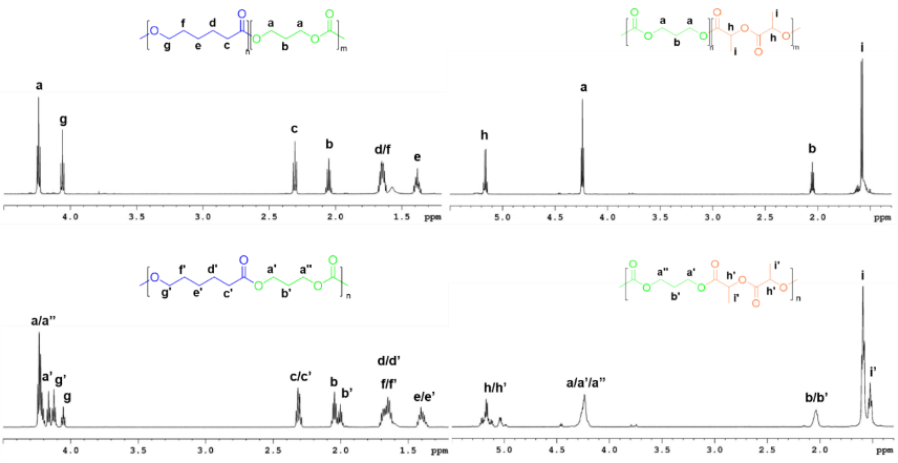

Figure 4.5. ^{1}H NMR spectra of the diblock (top) and random (bottom) copolymers synthesized in this work (600 MHz, $CDCl_3$, 25°C)

Using a [TMC]:[L-LA]:[**3**]:[BnOH] ratio of 100:100:1:1, high conversions of TMC (88%) and L-LA (95%) were achieved within 12 min (**Table 4.2**, Entry 21). With 250 equivalents of each monomer, conversions of 57% (TMC) and 82% (L-LA) were observed within 10 min (Entry 22). The deviation of the copolymer composition from the feed ratio indicates a catalytic preference for L-LA incorporation. This selectivity is further supported by the calculated average block length of the lactyl units from ^{1}H and ^{13}C NMR analysis at low conversion (Entry 22).[7] The ^{13}C NMR spectrum of copolymer Entry 4 (**Figure 4.36**) showed no signals for either isolated or odd-numbered lactyl sequences, indicating the absence of transesterification, however small signals have been observed for copolymer of Entry 21 and their intensities increase when reactions were conducted beyond the time required for the complete consumption of the monomers.

Subsequently, one-pot copolymerizations of ε-CL and TMC were also conducted at [monomer]:[**3**]:[BnOH] ratios of 250:250:1:1 and 500:500:1:1 at 110 °C (Entries 23, 24).

After 5 minutes a conversion of 90% and 60% was calculated for TMC and ε-CL, respectively; similar conversions were registered for the copolymerization of 500 eq of monomers after the same time. For these copolymerizations a greater propensity of complex **3** to polymerize the TMC is observed compared to the ε-CL. The experimental average lengths of the carbonate (L_{TMC}) and caproyl (L_{CL}) units were determined from the carbonyl regions in the ^{13}C NMR spectra (**Figure 4.39)**, according to the equations reported in the literature.[8] As expected, the lengths of the TMC blocks are slightly longer than those of CL. However, the calculated block lengths are in all cases close to the values determined for copolymers containing the molar fraction of TMC evaluated by ^{1}H NMR, and with a completely random distribution of carbonate and caproyl units. Also, worthy of note are the molecular masses of the obtained copolymers that can be adjusted in a satisfactory manner by varying the number of equivalents of the two monomers in the feeds.

The thermal properties of these four copolymers were analyzed by differential scanning calorimetry (DSC). All samples were amorphous and no crystalline phase was found in these copolymers (**Figures 4.37, 4.40**). The measured T_g values (**Table 4.2**) are in good agreement with those found in the literature for copolymers of similar compositions and similar masses. As expected, these values are intermediate between the T_g's of the respective homopolymers.[8]

4.2.4 Chemical Recycling

Building on previous demonstrations of high efficiency for this class of zinc complexes in the chemical recycling of polylactide,[9] we investigated their utility in the depolymerization of PTMC and its copolymers into their constituent monomers, using microwave irradiation as a heating source. The first depolymerization tests were conducted on a synthesized PTMC sample (M_n = 15 kDa, $Đ$ = 1.7). Using a solution in anhydrous acetonitrile, the zinc complex (15 mol%, pretreated with one equivalent of 1,3-propanediol to avoid product mixture complexity) efficiently catalysed the reaction at 95 °C. This system converted PTMC to TMC monomer in 88% yield within 2 hours (**Table 4.3**, Entry 25).

Table 4.3. Depolymerization reactions of PTMC by complex **3**.

Entry[a]	Complex 3 (eq)	Propanediol (eq)	Time (h)	TMC Conversion[b] (%)
25	0.15	0.15	2	88
26	0.15	0.15	0.5	30
27	0.15	0.15	1	73
28	0.15	0.15	1.5	81
29	0.075	0.075	2	66
30	0.05	0.05	2	11
31	0.15	0.45	2	86
32	0.15	-	2	<1
33	-	0.15	2	<1

[a] General conditions: depolymerization experiments were carried out by using 0.1 mmol of PTMC (12 mg), 15 µmol of catalyst (0.15 equiv. relative to carbonate linkages) and 15 µmol of propanediol, except when differently specified; solvent: 1 mL of CH_3CN; temperature: 95 °C by microwave irradiation (20 W power). [b] Determined by ^1H NMR spectral data.

Reaction kinetics (**Table 4.3**, Entries 25–28; **Figure 4.6**) revealed a linear increase in depolymerization yield over time, eventually reaching a plateau consistent with the

established monomer-polymer equilibrium. Further optimization showed that increasing the alcohol loading did not improve performance, while reducing the catalyst loading to 0.05 equiv. significantly hindered the reaction (**Table 4.3**, Entries 29–31).

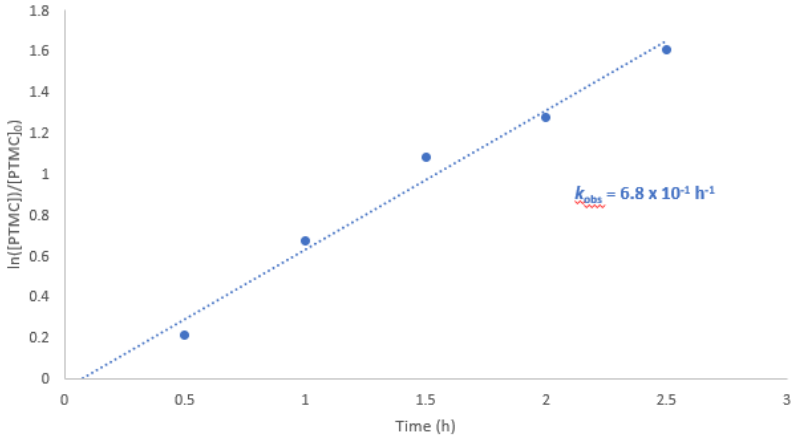

Figure 4.6: Pseudo first-order kinetic plots for the consumption of PTMC by complex **3** and 1,3 propanediol.

Control experiments confirmed the synergistic role of the catalytic system: neither the zinc complex nor propanediol alone produced any conversion under standard conditions (**Table 4.3**, Entries 32–33). Furthermore, complex **3** performed better than the organocatalyst 1,5,7-triazabicyclo[4.4.0]dec-5-ene (TBD), which produced only 35% conversion under identical conditions.[10]

Finally, the zinc complex was used in the depolymerization of the previously synthesized PTMC-PLLA diblock copolymer (**Table 4.4**).

Table 4.4: Depolymerization of copolymers with complex **3**

Entry[a]	[b]Polymer[b] (Mn, *Đ*)	Time	$Conv_{TMC}$[c] (%)	$Conv_{LLA}$[c] (%)	$Conv_{\varepsilon\text{-}CL}$[c] (%)
34	PTMCbPLLA (10.0 kDa, 1.32)	0.5 h	0	>99	-
35	PTMCbPCL (19.0 kDa, 1.72)	2 h	59	-	0
36	PCL (10.1 kDa, 1.69)	2 h	-	-	0

[a]The reactions were performed using 14 µmol of complex **1** (0.15 equiv. with respect to the functional groups in the chain) in 1 mL of CH_3CN at 95 °C by microwave irradiation. [b]The polymers used for the depolymerization reactions were synthesized *ad hoc* and washed with methanol to remove all the catalytic residues. The values of M_n and *Đ* were determined by GPCin THF. [c]Determined by ^1H NMR spectral data.

It was observed that operating in the same conditions as Entry 26 in **Table 4.3**, after 0.5 hour the PLLA was completely depolymerized to the corresponding monomer, while the PTMC block remained completely intact (Entry 34). Following the removal of L-LA from the reaction mixture, the depolymerization of PTMC was successfully carried out using the same catalyst. The selective depolymerization of the diblock copolymer highlights the feasibility of separately recovering both starting monomers, establishing an efficient chemical recycling process. In contrast, the depolymerization of the PTMC-PCL diblock copolymer leads to the formation of TMC, while the PCL block remains intact (Entry 35). The same reaction carried out on a polycaprolactone homopolymer confirmed that complex **e** is unable to depolymerize PCL (Entry 36). As a result, even in copolymers formed from these two monomers, selective recycling of the TMC monomer from the unaffected PCL block is possible.

4.3 Conclusions

This chapter reports the development of zinc and magnesium complexes coordinated by a naphthoxy-imino pyridine ligand, detailing their characterization and their use as catalysts for the synthesis of aliphatic polyesters and polycarbonates. Both complexes promoted efficient ROP of L-LA, ε-caprolactone and β-butyrolactone, as cyclic esters, and TMC and 1-methyl-trimethylene carbonate, as cyclic carbonates. All polymerizations occurred in a well-controlled manner, as demonstrated by molecular weights consistent with theoretical predictions and the excellent fidelity of the end groups, confirmed by GPC, NMR, and MALDI-FT-ICR analyses. Specifically, in the polymerization of L-lactide, β-butyrolactone, and 1-methyltrimethylene carbonate, the zinc complex showed significantly higher activity than its magnesium analogue, while similar activities for the two complexes were recorded with ε-caprolactone and TMC. Based on these results, we tentatively hypothesize that steric and electronic effects play a role in slowing down the polymerization promoted by the magnesium complex. Kinetic studies on the polymerization of ε-caprolactone also revealed an induction period for the magnesium catalyst, absent in the zinc-mediated process. Such different performances of zinc and magnesium complexes undoubtedly merit further investigation. Due to its superior activity, the zinc complex was further employed for the synthesis of well-defined diblock and random copolymers of TMC with L-lactide and ε-caprolactone. NMR and DSC characterization confirmed the microstructure of diblock and random copolymers, revealing a high degree of control with the copolymer composition. Finally, the same zinc complex was successfully applied to the microwave-assisted depolymerization of these materials, achieving selective and efficient conversion into the corresponding monomers. Remarkably, this process enabled the selective depolymerization of individual blocks within the diblock copolymers, demonstrating the potential of these systems.

4.4 Experimental Part

All the operations of synthesis and handling of air-sensitive chemicals were performed in an inert atmosphere, using Schlenk techniques and/or a glove-box in nitrogen atmosphere. The used glassware was dried in an oven at 120 °C and subsequently subjected to vacuum-nitrogen cycles. Solvents used for polymerization experiments and for the synthesis of substances instable toward air and moisture, were distilled prior to use on the opportune drying agent. In particular, THF, toluene, and benzene were dried by refluxing over sodium and benzophenone and stored under nitrogen. Dichloromethane was dried over calcium hydride and distilled prior to use. Benzyl alcohol and isopropanol were dried by refluxing over sodium. Deuterated solvents were purchased from Sigma–Aldrich and dried over activated 3-Å molecular sieves prior to use. All the reagents used for the synthesis of the complexes were purchased from Sigma Aldrich, while trimethylene carbonate was purchased from TCI. L-LA was crystallized in toluene and then dried over P_2O_5, ε-caprolactone and β-butyrolactone were dried over CaH_2 and distilled under nitrogen, while TMC was purified twice by recrystallization from dry THF. The NMR spectra were recorded with BRUKER AVANCE instruments operating at 600, 400 and 300 MHz for ^1H. Molecular masses (M_n and M_w) and dispersity values (M_w/M_n) were measured by GPC, using THF as the eluent (1.0 mL min^{-1}) and narrow polystyrene standards as the reference. MALDI mass spectra were recorded using a Bruker solariX XR Fourier transform ion cyclotron resonance (FT-ICR) mass spectrometer (Bruker Daltonik GmbH,Bremen, Germany) equipped with a 7 T refrigerated actively shielded superconducting magnet (Bruker Biospin, Wissembourg, France). The samples were prepared at the concentration of 1.0 mg mL^{-1} in THF, while the matrix (DCTB) was mixed at a concentration of 10.0 mg mL^{-1}. Thermal analysis was carried out by using a TA-DSC Q20 apparatus manufactured by Waters/TA instruments (Waters, New Castle, DE, USA) in flowing N_2. Polymer samples was placed into aluminium crucibles and heated/cooled runs were carried out in the range -40 - 180 °C at 10 °C/min or in the range -100 – 110 °C at 10 °C/min. All the microwave assisted reactions were performed using a microwave synthesizer from CEM Corporation (Discover 2.0).

4.4.1 Synthesis and Characterization of the Ligand

The ligand was synthetized by condensation of the 2-hydroxy-1-naphthaldehyde (0.172 g, 1 mmol) with the 2-(2-pyridyl)ethylamine (0.122 mg, 1 mmol). The reaction was performed in reflux of ethanol (30 mL) for 4 h. The solvent was removed under vacuum, forming an orange oil. (Yield= 98%)

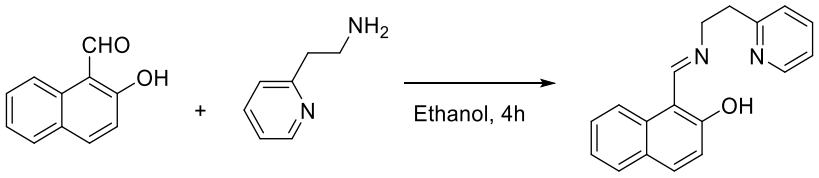

Scheme 4.2: Synthesis of the ligand LH.

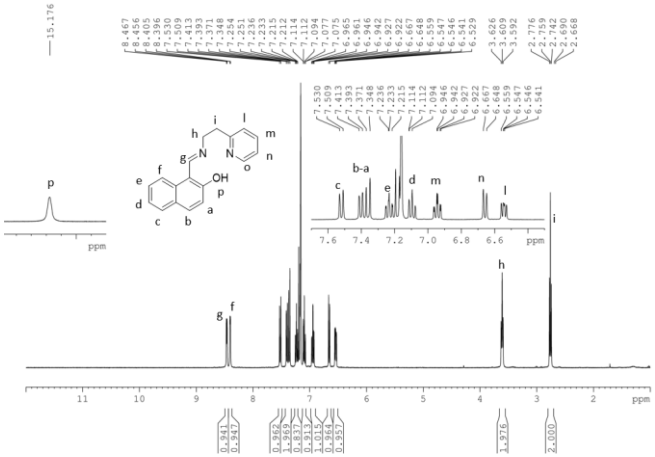

Figure 4.7. ^{1}H NMR spectrum of the ligand LH (Solvent: C_6D_6, 400 MHz, 25°C).

^{1}H NMR (400 MHz, C_6D_6, 25°C): δ 15.2 (br, 1H, -OH), 8.46 (d, J = 4.5 Hz, 1H, CH-Py), 8.39 (s, 1H, CH=N), 7.51 (d, J = 8.2 Hz, 1H, CH-Ar), 7.39 (d, J = 8.0 Hz, 1H, CH-Ar), 7.34 (d, J = 9.3 Hz, 1H, CH-Ar), 7.23 (t, J = 8.0 Hz, 1H, CH-Ar), 7.17 (d, J = 9.3 Hz, 1H, CH-Ar), 7.11 (t, J = 8.0 Hz, 1H, CH-Ar), 6.93 (t, J = 7.6 Hz, 1H, CH-Ar), 6.65 (d, J = 8.2 Hz, 1H, CH-Ar), 6.55

(dd, J_1 = 12.1 Hz, J_2 = 5.1 Hz, 1H, CH-Ar), 3.61 (t, J = 6.7 Hz, 2H, -CH_2), 2.74 (t, J = 6.7 Hz, 2H, -CH_2).

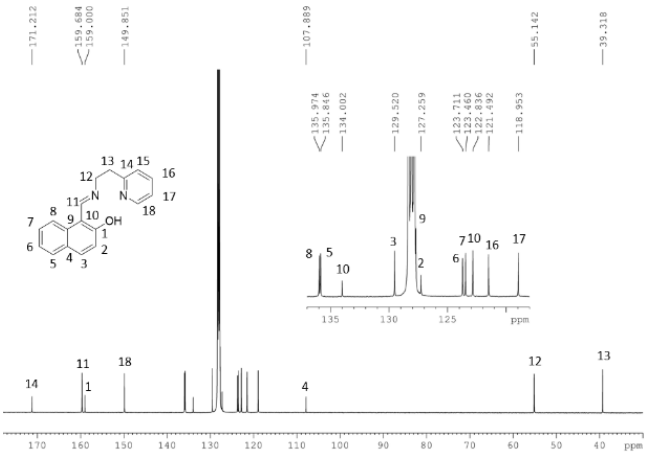

Figure 4.8. ^{13}C NMR spectrum of the ligand LH (Solvent: C_6D_6, 150 MHz, 25°C).

^{13}C NMR (150 MHz, C_6D_6, 25°C): δ 171.21 (Cq), 159.68 (CH=N), 159.00 (Cq), 149.95 (Cp), 135.97 (CH), 135.84 (Cq), 134.00 (Cq), 129.52 (CH), 127.70 (Cq), 127.26 (CH), 123.71 (CH), 123.46 (CH), 122.83 (CH), 121.49 (CH), 118.95 (CH), 107.89 (Cq), 55.14 (CH_2), 39.31 (CH_2).

4.4.2 Synthesis and Characterization of the Complexes

The reactions were carried out in a glovebox in a nitrogen atmosphere. A benzene solution (8 mL) of $M[N(SiMe_3)_2]_2$ (4.54 x 10^{-4} mol) was added to a benzene solution (8 mL) of the ligand LH (0.200 g, 4.54 x 10^{-4} mol). Once the addition was complete, the reaction mixture was left to stir for 1h at room temperature. The solvent was then removed under reduced pressure. The obtained complex is a whitish powdery solid (Yield = 80%). Confirmation of the formation of the desired complex was obtained from the NMR spectra.

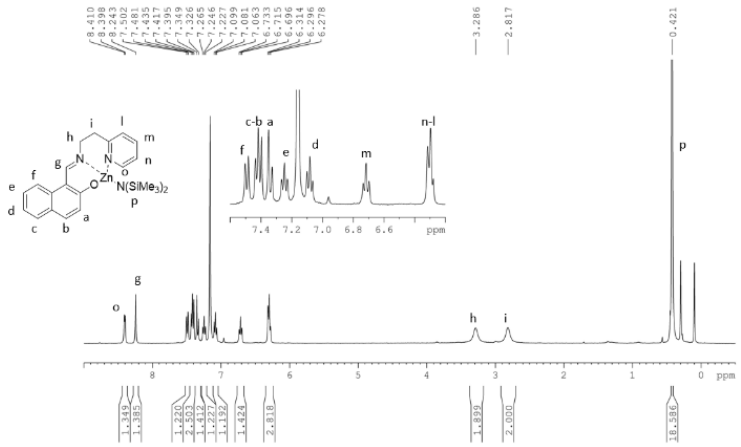

Figure 4.9. ^{1}H NMR spectrum of **3** (Solvent: C_6D_6, 400 MHz, 25°C).

^{1}H NMR (400 MHz, C_6D_6, 25°C): δ 8.40 (d, J = 5.2 Hz, 1H, CH-Py), 8.24 (s, 1H, CH=N), 7.49 (d, J = 8.2 Hz, 1H, CH-Ar), 7.41 (d, J = 8.0 Hz, 1H, CH-Ar), 7.40 (d, J = 9.1 Hz, 1H, CH-Ar), 7.33 (d, J = 9.2 Hz, 1H, CH-Ar), 7.25 (t, J = 7.8 Hz, 1H, CH-Ar), 7.08 (t, J = 8.0 Hz, 1H, CH-Ar), 6.71 (t, J = 7.6 Hz, 1H, CH-Ar), 6.30 (m, 2H, CH-Ar), 3.29 (br, 2H, -CH_2), 2.82 (br, 2H, -CH_2), 0.42 (s, 18H, $Si(CH_3)_3$).

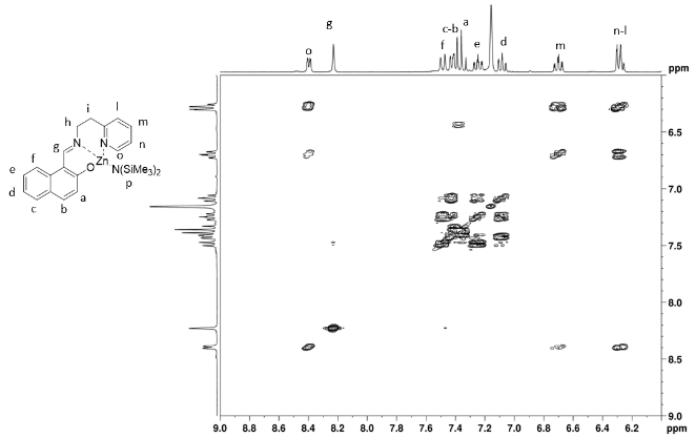

***F*igure 4.10**. 2D COSY spectrum of complex **3** (Solvent: C_6D_6, 400 MHz, 25°C).

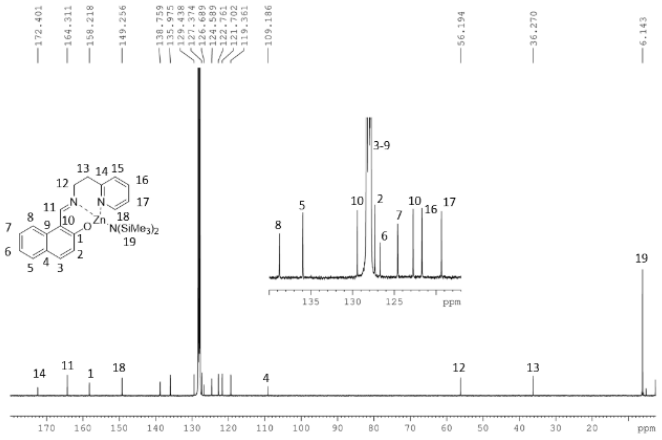

Figure 4.11. ^{13}C NMR spectrum of complex **3** (Solvent: C_6D_6, 150 MHz, 25°C).

^{13}C NMR (150 MHz, C_6D_6, 25°C): δ 172.40 (Cq), 164.31 (CH=N), 158.22 (Cq), 149.26 (Cp), 138.76 (CH), 135.98 (Cq), 129.44 (Cq), 128.18 (CH), 127.95 (Cq), 127.37 (CH), 126.69 (CH), 124.59 (CH), 122.76 (CH), 121.70 (CH), 119.36 (CH), 109.19 (Cq), 56.19 (CH_2), 36.27 (CH_2), 6.14 ($Si(CH_3)_3$).

Figure 4.12. ^{1}H-NMR spectrum of complex **4** (Solvent: C_6D_6, 400 MHz, 25°C).

^{1}H NMR (400 MHz, C_6D_6, 25°C): δ 8.95-8.85 (m, 2H, CH-Ar, CH=N), 7.76 (m, 1H, CH-Ar), 7.61 (m, 1H, CH-Ar), 7.42 (m, 2H, CH-Ar), 7.30 (t, J = 7.6 Hz, 1H, CH-Ar), 7.10 (t, J = 7.8 Hz, 1H, CH-Ar), 6.67 (m, 1H, CH-Ar), 6.42 (m, 1H, CH-Ar), 6.42 (m, 1H, CH-Ar), 3.71 (br, 2H, -CH2), 2.58 (br, 2H, -CH2), 0.26 (s, 18H, $Si(CH_3)_3$).

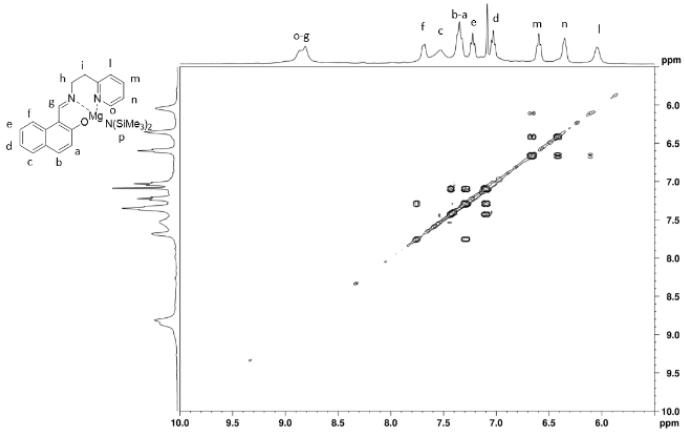

Figure 4.13 Aromatic region of the 2D-COSY spectrum of complex **4** (Solvent: C_6D_6, 400 MHz, 25 °C).

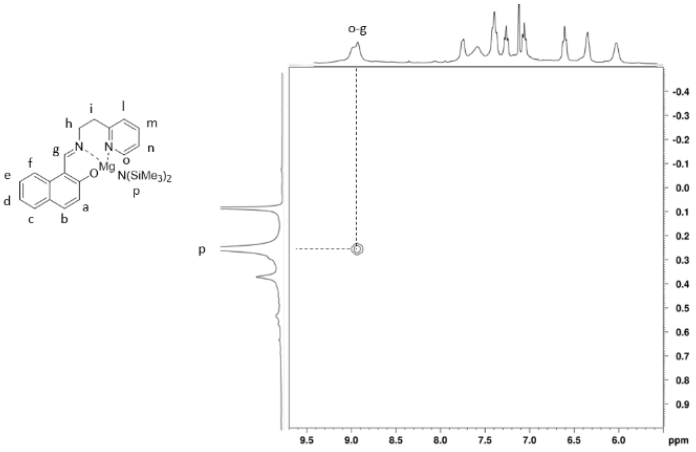

Figure 4.14 Enlargement of the 2D-NOESY spectrum of complex **4** (Solvent:C_6D_6, 400 MHz, 25°C).

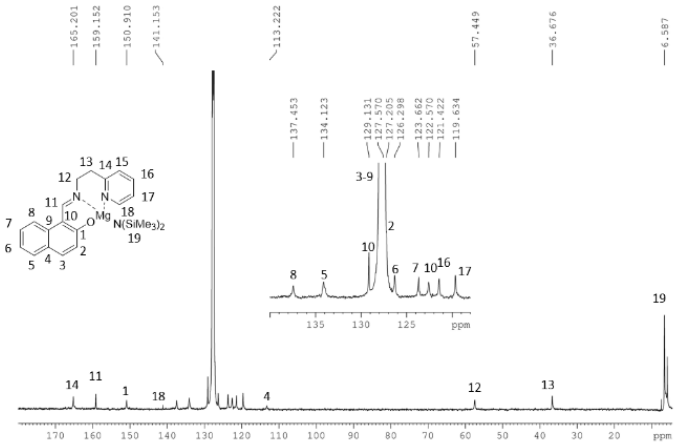

Figure 4.15. ^{13}C NMR spectrum of complex **4** (Solvent: C_6D_6, 150 MHz, 25°C).

^{13}C NMR (150 MHz, C_6D_6, 25°C): δ 165.20 (Cq), 159.15 (CH=N), 150.91 (Cq), 141.15 (Cp), 137.45 (CH), 134.12 (Cq), 129.13 (Cq), 128.18 (CH), 127.57 (Cq), 127.20 (CH), 126.30 (CH), 123.66 (CH), 122.57 (CH), 121.42 (CH), 119.63 (CH), 113.22 (Cq), 57.45 (CH_2), 36.68 (CH_2), 6.59 ($Si(CH_3)_3$).

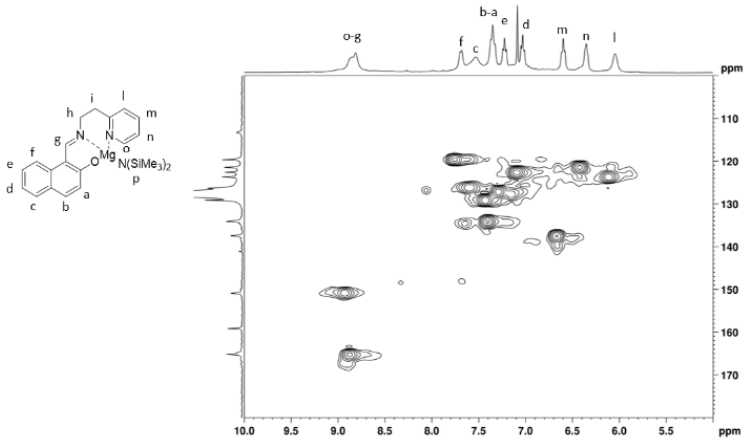

Figure 4.16. Aromatic region of the 2D HSQC spectrum of complex **4** (Solvent: C_6D_6, 400 MHz, 25 °C).

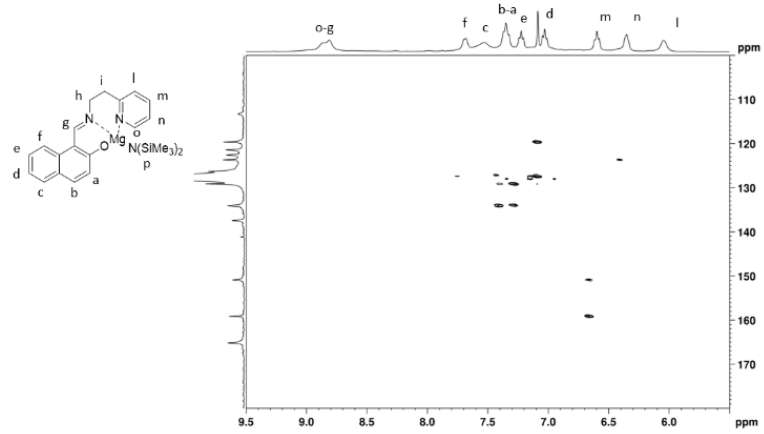

Figure 4.17. Aromatic region of the 2D HMBC spectrum of complex **4** (Solvent: C_6D_6, 400 MHz, 25 °C).

4.4.3 Ring-Opening Polymerization (ROP) of Cyclic Monomers.

Polymerization in solution

The polymerization experiments were carried out in a glovebox. In a typical procedure, the complex and the monomer were weighed into two different 4 mL vials, fitted with magnetic stirrers. Both monomer and complex were dissolved in the desired solvent. Subsequently, the solution of the initiator in the same solvent used to dissolve monomer and complex, was added to the solution of the complex and left to stir for a few minutes: finally, the monomer solution was added to the reaction mixture. All the used vials were washed with solvent to recover the whole amount of each weighed compound, the total amount of solvent was 0.8 mL.

Polymerization in bulk

In a typical procedure, the complex was weighed into a vessel: subsequently, the initiator was added to the complex and left to stir for a few minutes, then the monomer, weighed into a 4 mL vial, was added to the reaction mixture. For the polymerization experiments conducted at higher temperature, the same procedure was followed and after the addition, the vial was closed, pulled out of the glove box and immersed in a thermostated oil bath at the desired temperature.

All the polymerization experiments were stopped using wet dichloromethane, after taking the vial out of the glovebox. The solvent was removed under reduced pressure and the polymer was washed in methanol, dried and characterized by NMR spectroscopy, MALDI mass spectrometry and/or GPC analysis.

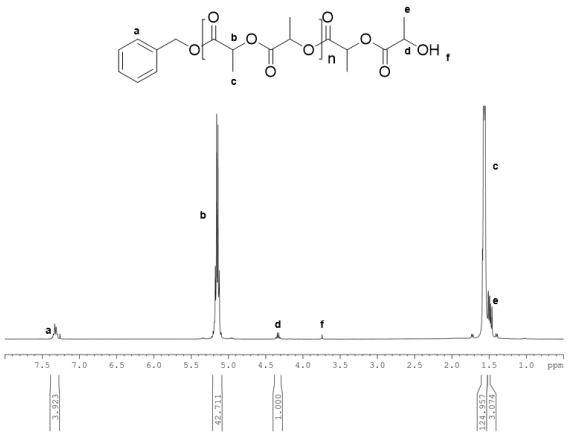

Figure 4.18 ^{1}H NMR spectrum of polylactide (solvent: $CDCl_3$, 400 MHz, 25°C).

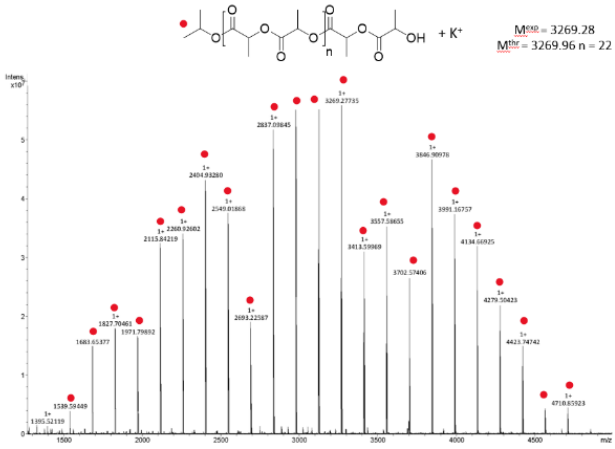

Figure 4.19 MALDI-FT-ICR mass spectrum (matrix DCTB) of the isolated polymer from L-LA polymerization. Polymerization conditions: $[L\text{-}LA]_0$:$[^{i}PrOH]_0$:[**3**] = 50:1:1; Solvent =DCM; Temperature= 25 °C.

Figure 4.20: ^{1}H NMR spectrum of polycaprolactone (solvent: $CDCl_3$, 400 MHz, 25°C) * = methanol.

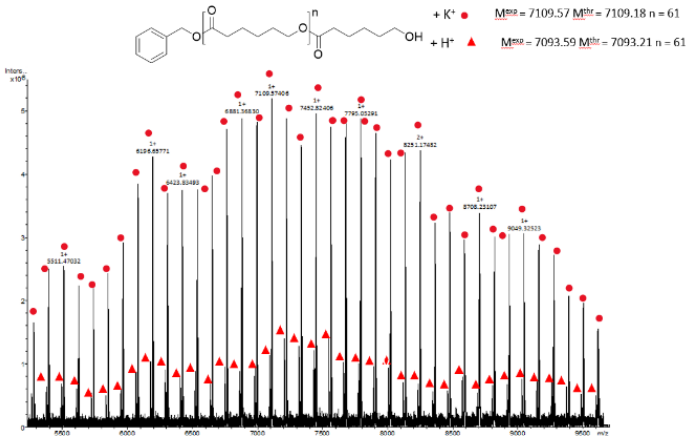

Figure 4.21: MALDI-FT-ICR mass spectrum (matrix DCTB) of the isolated polymer from ε-CL polymerization. Polymerization conditions: $[\varepsilon\text{-CL}]_0$:$[BnOH]_0$:[**4**] = 200:1:1; Solvent = DCM; Temperature= 25 °C.

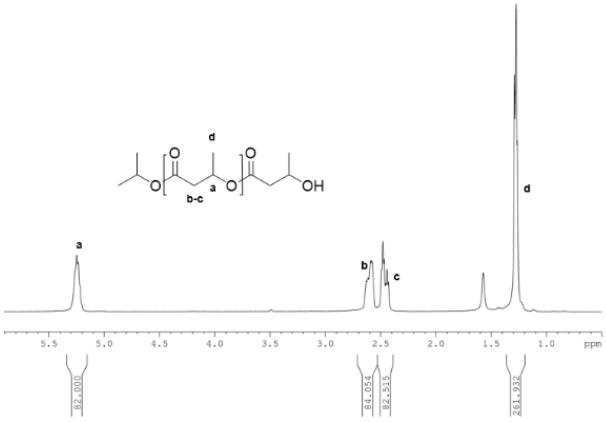

Figure 4.22: ^{1}H NMR spectrum of poly β-butyrolactone (solvent: $CDCl_3$, 400 MHz, 25°C).

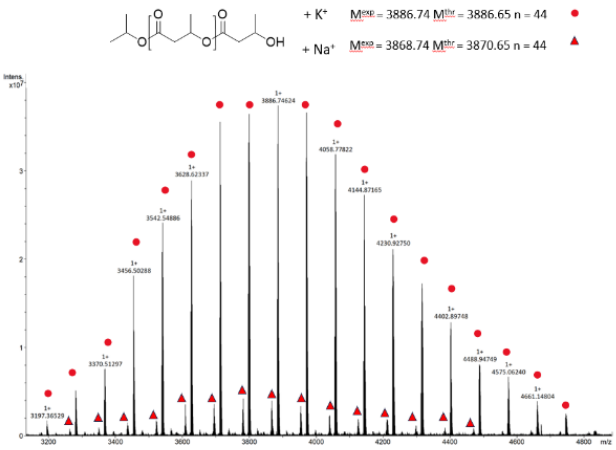

Figure 4.23: MALDI-FT-ICR mass spectrum (matrix DCTB) of the isolated polymer from β-BL polymerization. Polymerization conditions: $[\beta\text{-BL}]_0$: $[^{i}\text{PrOH}]_0$: [**3**] = 100:1:1; Solvent = Toluene, Temperature = 70 °C.

Table 4.5: ROP of TMC with complexes **3** and **4**

Entry[a]	Complex (µmol)	TMC (equiv) [mol/L]	Time	Conv (%)	M_n^{thr} [b] (kDa)	M_n^{exp} *[c] (kDa)	$Đ$[c]	Solvent (mL)	TOF (h^{-1})
37	**4** 8 µmol	100 [1]	1 min 5 min	82 88	8.4 9.0	8.8	1.6	CH_2Cl_2 (0.8)	4920
38	**4** 4 µmol	200 [1]	1 min 7 min 15 min	69 86 89	18.1	16.7	1.5	CH_2Cl_2 (0.8)	8280
39	**4** 4 µmol	200 [2]	1 min 5 min	82 95	19.4	20.3	1.7	CH_2Cl_2 (0.4)	9840 2289
40	**3** 4 µmol	200 [2]	5 min	89	18.1	16.3	1.6	CH_2Cl_2 (0.4)	2145
41	**4** 4 µmol	200 [2]	30 min 1.5 h	73 82	16.7	16.5	1.6	Dioxolane (0.4)	292
42	**3** 4 µmol	200 [2]	30 min 1.5 h	52 87	17.8	11.8	2.0	Dioxolane (0.4)	208

[a] General conditions: initiator BnOH= 1 equiv., [b] M_n^{th}= 102.09 x ([TMC]/[BnOH]) x conversion TMC; [c] M_n^{expC}*= M_n^{exp}corrected by a factor of 0.73 for 5 <M_n<10 kDa, 0.88 for M_n>10 kDa; [d]TOF= equiv. x conv/time

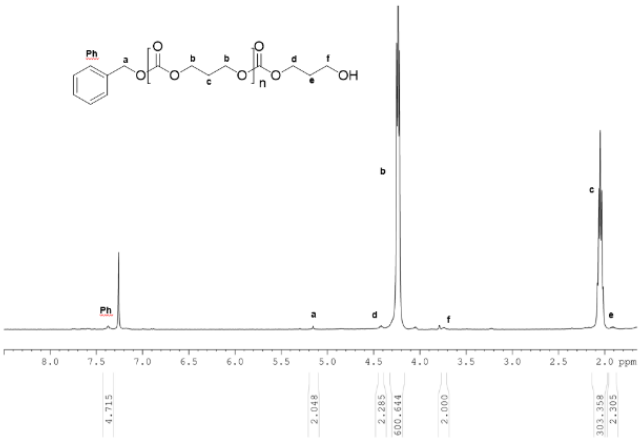

Figure 4.24: ^{1}H NMR spectrum of polytrimethylene carbonate (solvent: $CDCl_3$, 400 MHz, 25°C).

4.4.4 Kinetic Studies for ε-caprolactone Polymerization

ε-caprolactone (250 µmol, 28.5 mg, 100 equiv) was weighed into a 4 mL vial, dissolved in 0.4 mL CD_2Cl_2, and transferred to a J-Young NMR tube. The complex (2.5 µmol, 1 equiv.) was weighed into a 4 mL vial and dissolved in 0.5 mL CD_2Cl_2. Subsequently, 0.1 mL of ^{i}PrOH solution (0.025 M in CD_2Cl_2, 2.5 µmol, 1 equiv.) was added to the complex solution and allowed to stir for 5 min. The reaction mixture was added to the monomer solution, and NMR acquisition was performed every 15 min.

Table 4.6: Kinetic studies of ε-caprolactone polymerization with complexes **3** and **4**

Entry[a]	Complex	Time (h)	Conv (%)
43	**3**	0.08	0.007
		0.41	0.085
		0.75	0.18
		1.08	0.29
		1.42	0.35
		1.75	0.45
		2.08	0.52
		2.42	0.57
		2.75	0.62
		3.08	0.66
44	**4**	0.08	0.01
		0.42	0.02
		0.75	0.06
		1.08	0.21
		1.42	0.36
		1.75	0.50
		2.08	0.60
		2.42	0.67

		2.75 3.08	0.72 0.76

The reactions were performed with 2.5 µmol of complex with [ε-CL]: [complex]: [^{i}PrOH]= 100: 1: 1 in 1.0 mL of CD_2Cl_2 at 25 °C.

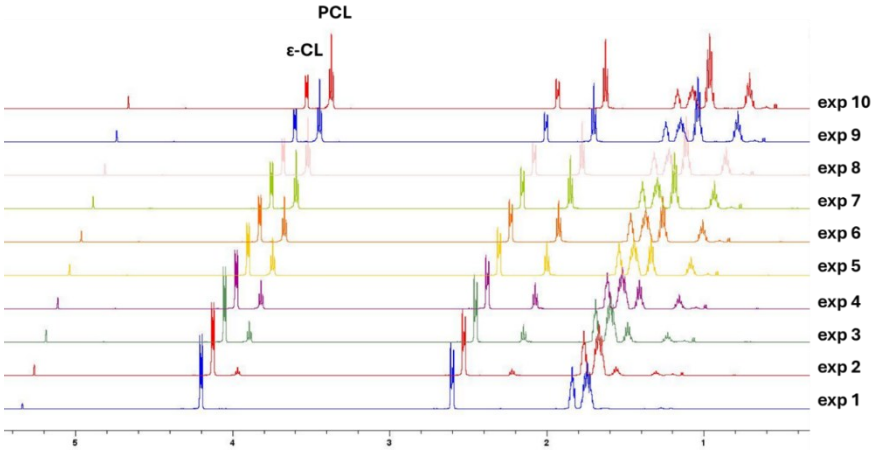

Figure 4.25. ^{1}H NMR spectra of ε-caprolactone polymerization with complex **3**. Acquisitions every 15 min (bottom up). (Solvent: CD_2Cl_2, 600 MHz, 25 °C).

4.4.5 Ring Opening Polymerization (ROP) of 1-Methyl-Trimethylene Carbonate

The polymerization experiments in bulk were carried out in a glovebox or in a thermostated oil bath, at the desired temperature. In a typical procedure, the complex (4 x 10^{-6} mol) was weighed into a vessel. Subsequently, the initiator was added to the complex and left to stir for a few minutes and the monomer, weighed into a 4 mL vial, was added to the reaction mixture. Conversions have been determined by ^{1}H NMR spectroscopy, with the quantities of polymers and monomers determined by integrating the proper resonances (MeTMC: δ = 4.65 ppm; P(MeTMC): δ = 4.90 ppm). All the polymerization experiments were stopped using wet dichloromethane, after taking the vial out of the glovebox. The solvent was removed under reduced pressure and the

polymer was washed with methanol, dried and characterized by NMR spectroscopy, MALDI FT-ICR mass spectrometry and/or GPC analysis.

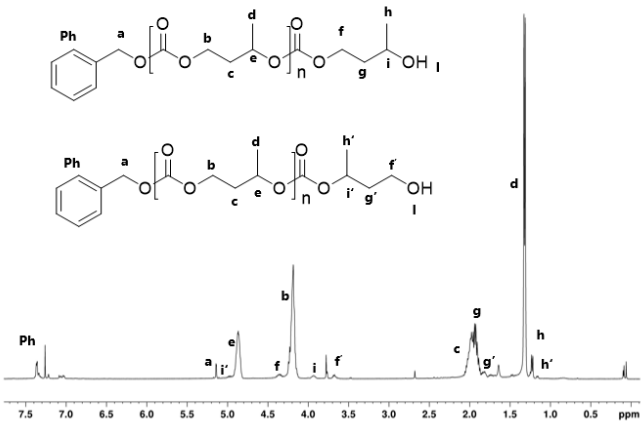

Figure 4.26: ^{1}H-NMR spectrum of poly-methyl-trimethylenecarbonate (Solvent: $CDCl_3$, 600 MHz, 25 °C).

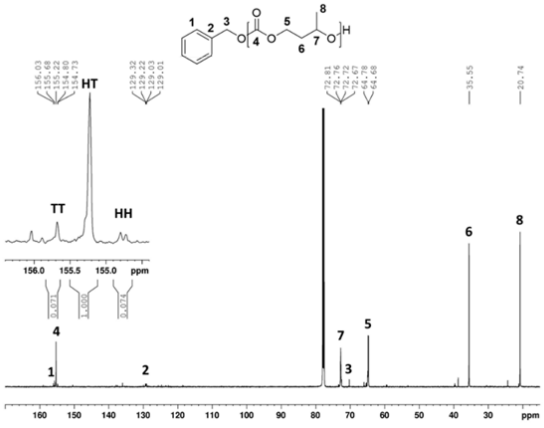

Figure 4.27: ^{13}C NMR spectra of poly-methyl-trimethylenecarbonate synthesized using magnesium complex **4** (Solvent: $CDCl_3$, 100.6 MHz, 25 °C).

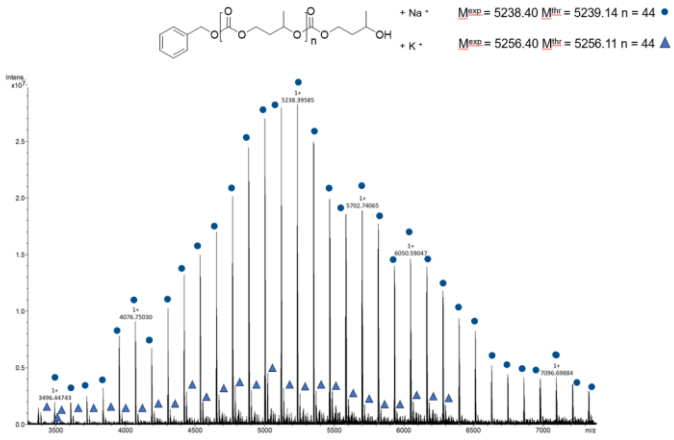

Figure 4.28 MALDI-FT-ICR mass spectrum (matrix: DCTB) of the isolated polymer from methyl-trimethylene carbonate polymerization. Polymerization conditions: [Me-TMC]$_0$:[BnOH]$_0$:[**4**] = 50:1:1; Temperature : 25 °C.

4.4.6 Synthesis of Copolymers

Complex **3** (4.0 x 10^{-6} mol) and both monomers were weighed into three different 4 mL vials, fitted with magnetic stirrers. Monomers and complex were dissolved in DCM (0.8 mL total). 0.08 mL of a solution of BnOH (0.05 M in DCM) was added to the solution of the complex and left to stir for ten minutes. Subsequently, the trimethylene carbonate solution was introduced into the reaction mixture and allowed to stir for 5 minutes, during which the polymerization of TMC took place. Then, the solution of the second monomer was added to the reaction mixture. After further time necessary for the second monomer polymerization, the sequential copolymerization was stopped using wet dichloromethane. The solvent was removed under reduced pressure and the polymer was washed in methanol, dried and characterized by NMR spectroscopy, MALDI mass spectrometry and/or GPC analysis.

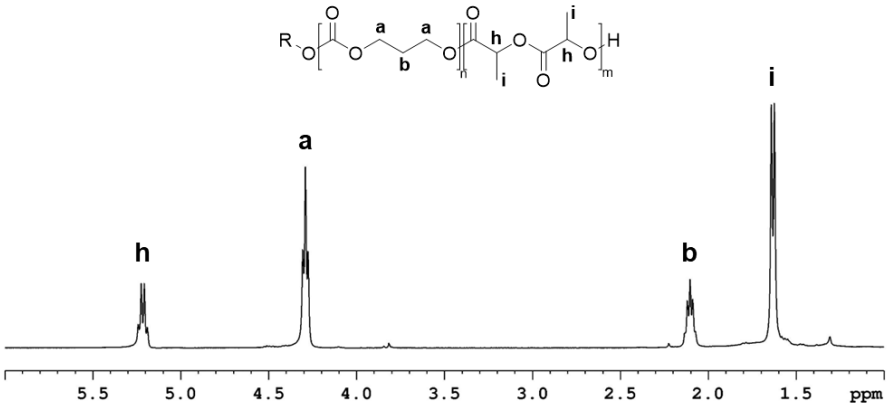

Figure 4.29: ^{1}H-NMR spectrum of PTMC-b-PLA (Solvent: $CDCl_3$, 400 MHz, 25 °C).

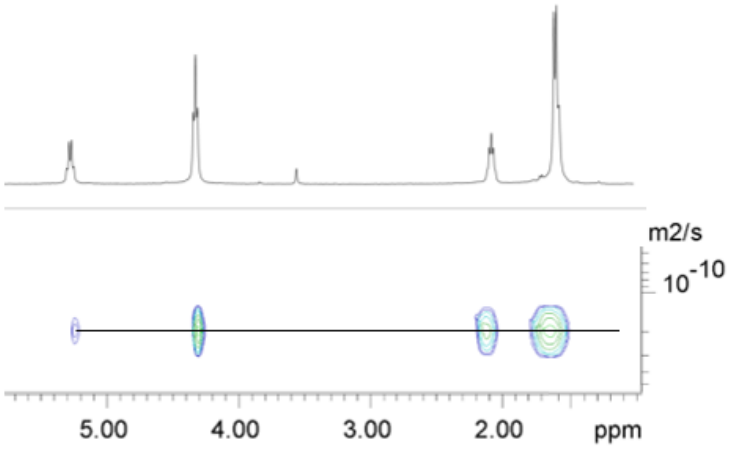

Figure 4.30: DOSY spectrum of PTMC-b-PLA (Solvent: $CDCl_3$, 400 MHz, 25 °C)

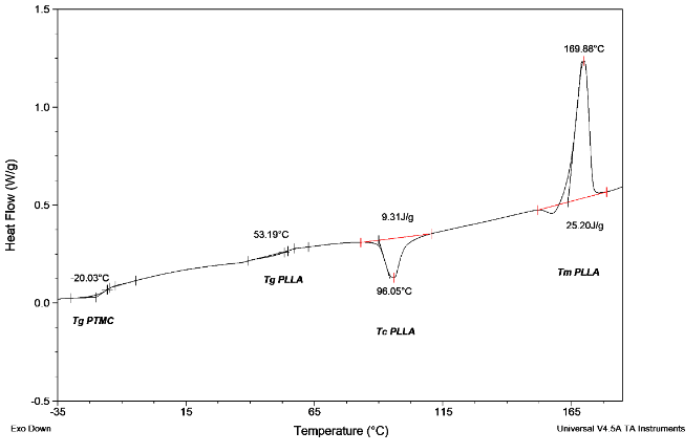

Figure 4.31: DSC thermogram of PTMC-b-PLA sample (third run).

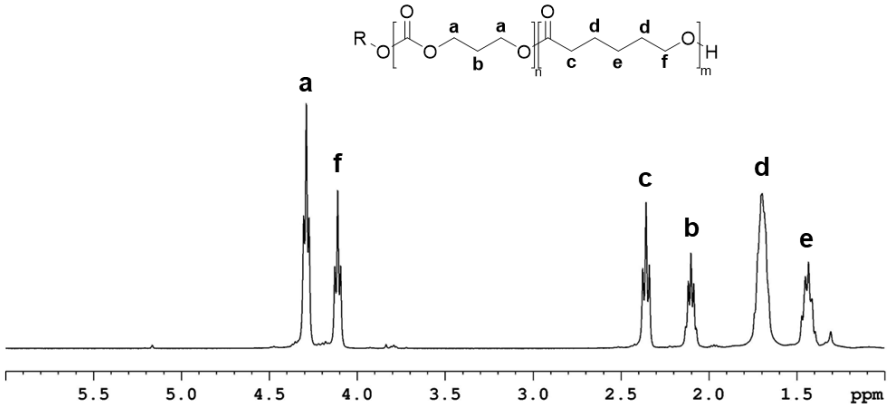

Figure 4.32 ^{1}H-NMR spectrum of PTMC-b-PCL (Solvent: $CDCl_3$, 400 MHz, 25 °C).

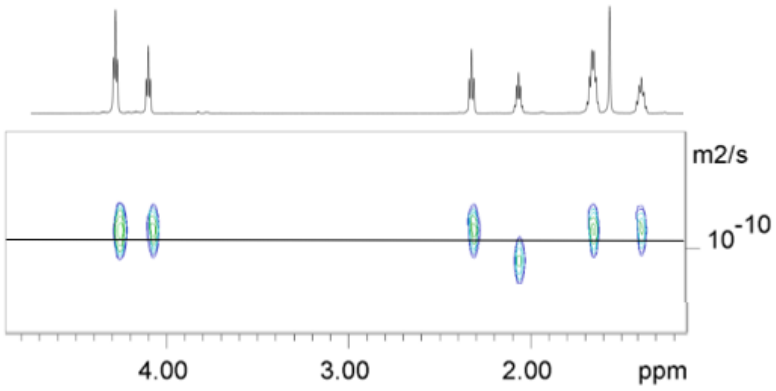

Figure 4.33: DOSY spectrum of PTMC-b-PCL (Solvent: $CDCl_3$, 400 MHz, 25 °C)

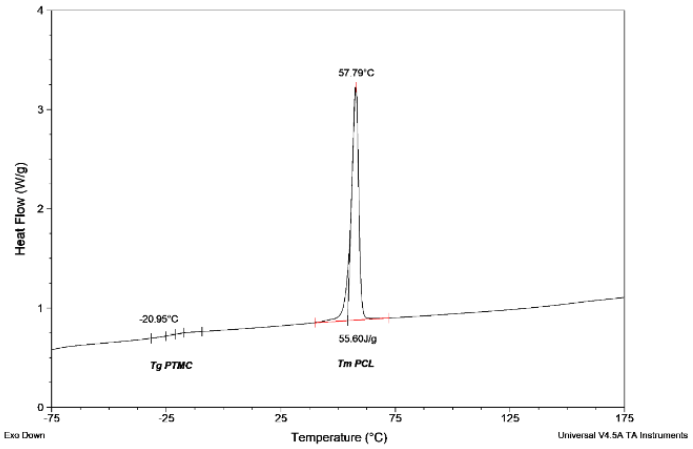

Figure 4.34: DSC thermogram of PTMC-b-PCL sample (third run).

In the one-pot one-step copolymerisation, complex **3** was weighed into a 4 mL vial (2 mg, 4.0 x 10^{-6} mol), and one equivalent of benzyl alcohol (stock solution in THF, 0.0185 M) was added to the complex and left to stir for few minutes. Subsequently, TMC and the other monomer (ε-CL or L-LA) were weighed into a 4 mL vial and placed into a thermostated oil bath at 110°C. After melting the contents of the vial, the solution of the complex and the initiator was added to the reaction mixture and left to stir, until the end

of the reaction and finally cooled rapidly at 0°C. The copolymers thus obtained were purified by dissolution in minimal amount of chloroform and precipitation into cold methanol, dried and characterized by NMR spectroscopy, GPC and DSC analysis.

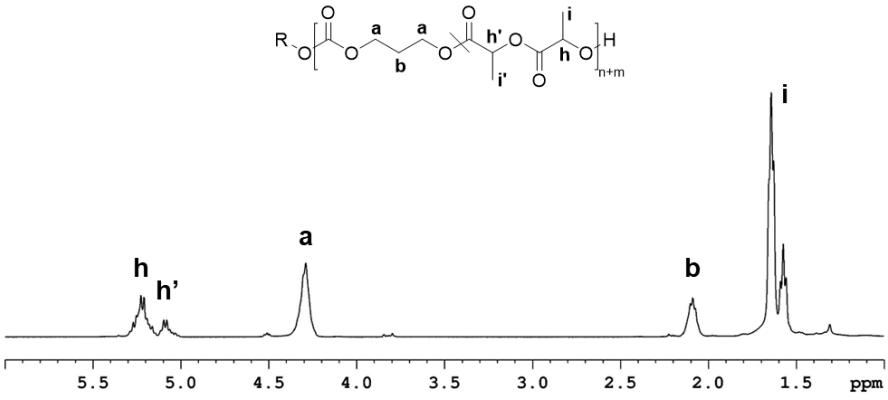

Figure 4.35: ^{1}H-NMR spectrum of PTMC-co-PLA (Solvent: $CDCl_3$, 400 MHz, 25 °C).

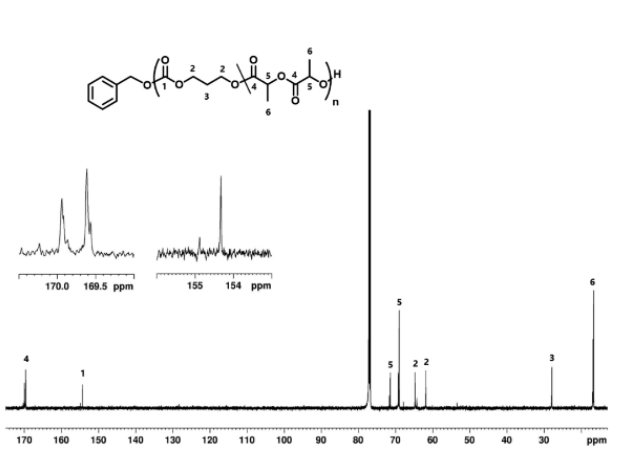

Figure 4.36: ^{13}C NMR spectrum of PTMC-co-PLA (Solvent: $CDCl_3$, 100.5 MHz, 25 °C)

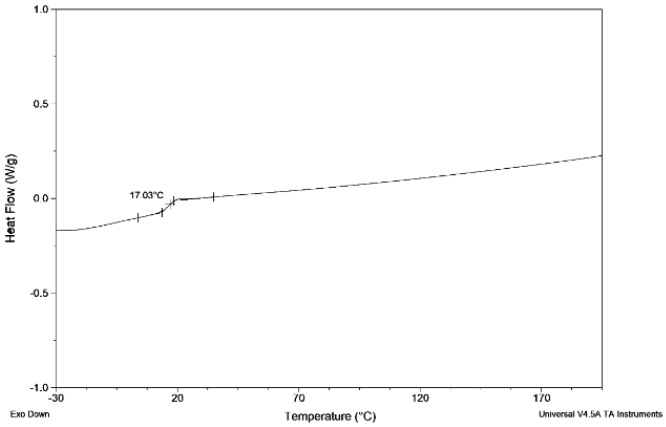

Figure 4.37: DSC thermogram of PTMC-co-PLA sample (third run).

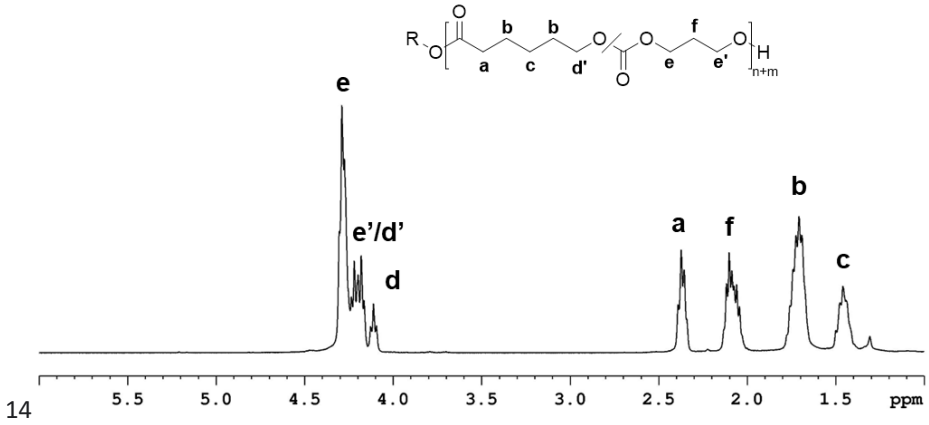

14

Figure 4.38: ^{1}H NMR spectrum of PTMC-co-PCL (Solvent: $CDCl_3$, 400 MHz, 25 °C).

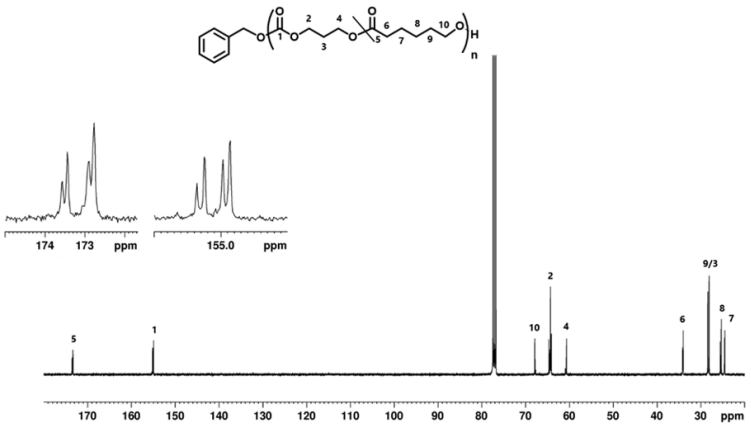

Figure 4.39: ^{13}C NMR spectrum of PTMC-co-PCL (Solvent: $CDCl_3$, 100.5 MHz, 25 °C).

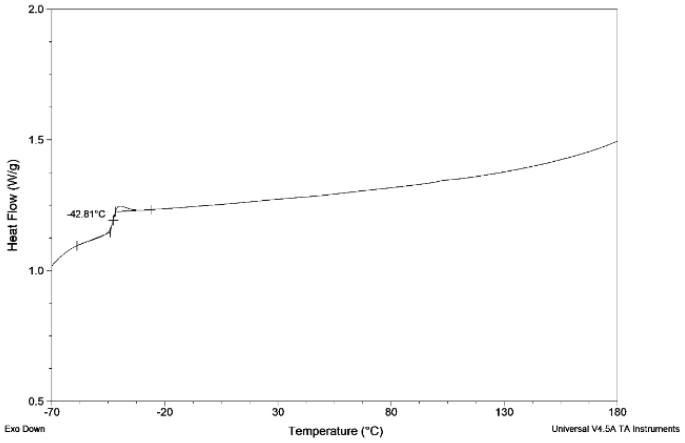

Figure 4.40: DSC thermogram of PTMC-co-PCL sample (third run).

4.4.7 Chemical Recycling of PTMC using Microwave Irradiation

Depolymerization experiments were performed: the complex (1.4×10^{-5} mol) was weighed into a 4 mL vial and dissolved in 0.4 mL of CH_3CN. Subsequently, a solution of 1,3-propanediol (1.4×10^{-5} mol) in anhydrous acetonitrile was added and left stirring for few minutes. The polymer (12 mg, 10^{-4} mol) was weighted into another vial and dissolved in 0.6 mL of acetonitrile. Finally, the polymer solution was transferred into vessel, closing and taking to a microwave reactor. All the depolymerization experiments were stopped using wet dichloromethane. The suspension was characterized by NMR spectroscopy.

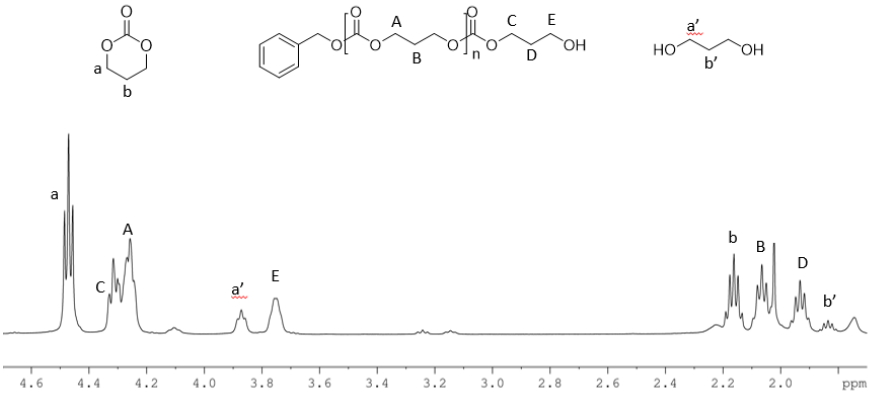

Figure 4.41: ^{1}H NMR spectrum of PTMC depolymerization with assignment of internal alkyl protons, TMC and 1,3 propanediol. (Solvent = $CDCl_3$, 400 MHz, 25°C).

4.5 References

(1) Santulli, F.; Pappalardo, D.; Lamberti, M.; Amendola, A.; Barba, C.; Sessa, A.; Tepedino, G.; Mazzeo, M. Simple and Efficient Zinc Catalysts for Synthesis and Chemical Degradation of Polyesters. *ACS Sustain. Chem. Eng.* **2023**, *11* (43), 15699–15709. https://doi.org/10.1021/acssuschemeng.3c04927.

(2) Fuchs, M.; Schäfer, P. M.; Wagner, W.; Krumm, I.; Walbeck, M.; Dietrich, R.; Hoffmann, A.; Herres-Pawlis, S. A Multitool for Circular Economy: Fast Ring-Opening Polymerization and Chemical Recycling of (Bio)Polyesters Using a Single Aliphatic Guanidine Carboxy Zinc Catalyst. *ChemSusChem* **2023**, *16* (12), e202300192. https://doi.org/10.1002/cssc.202300192.

(3) Naskar, B.; Modak, R.; Maiti, D. K.; Kumar Mandal, S.; Kumar Biswas, J.; Kumar Mondal, T.; Goswami, S. Syntheses and Non-Covalent Interactions of Naphthalene-Bearing Schiff Base Complexes of Zn(II), Co(III), Cu(II) and V(IV): Selective Detection of Zn(II). *Polyhedron* **2016**, *117*, 834–846. https://doi.org/10.1016/j.poly.2016.07.018.

(4) Santulli, F.; Lamberti, M.; Mazzeo, M. A Single Catalyst for Promoting Reverse Processes: Synthesis and Chemical Degradation of Polylactide. *ChemSusChem* **2021**, *14* (24), 5470–5475. https://doi.org/10.1002/cssc.202101518.

(5) Santulli, F.; Gravina, G.; Lamberti, M.; Tedesco, C.; Mazzeo, M. Zinc and Magnesium Catalysts for the Synthesis for PLA and Its Degradation: Clues for Catalyst Design. *Mol. Catal.* **2022**, *528*, 112480. https://doi.org/10.1016/j.mcat.2022.112480.

(6) McGuire, T. M.; López-Vidal, E. M.; Gregory, G. L.; Buchard, A. Synthesis of 5- to 8-Membered Cyclic Carbonates from Diols and CO_2: A One-Step, Atmospheric Pressure and Ambient Temperature Procedure. *J. CO_2 Util.* **2018**, *27*, 283–288. https://doi.org/10.1016/j.jcou.2018.08.009.

(7) Dobrzynski, P.; Kasperczyk, J. Synthesis of Biodegradable Copolymers with Low-Toxicity Zirconium Compounds. V. Multiblock and Random Copolymers of L-Lactide with Trimethylene Carbonate Obtained in Copolymerizations Initiated with Zirconium(IV) Acetylacetonate. *J. Polym. Sci. Part Polym. Chem.* **2006**, *44* (10), 3184–3201. https://doi.org/10.1002/pola.21428.

(8) Pastusiak, M.; Dobrzynski, P.; Kasperczyk, J.; Sobota, M.; Kaczmarczyk, B.; Janeczek, H. Synthesis of Trimethylene Carbonate/ϵ-Caprolactone Copolymers Initiated with Zinc Alkoxide: Influence of Copolymer Chain Microstructure on Thermal and Mechanical Properties. *Polym. Int.* **2017**, *66* (9), 1259–1268. https://doi.org/10.1002/pi.5379.

(9) Santulli, F.; Pappalardo, D.; Lamberti, M.; Amendola, A.; Barba, C.; Sessa, A.; Tepedino, G.; Mazzeo, M. Simple and Efficient Zinc Catalysts for Synthesis and Chemical Degradation of Polyesters. *ACS Sustain. Chem. Eng.* **2023**, *11* (43), 15699–15709. https://doi.org/10.1021/acssuschemeng.3c04927.

(10) Gregory, G. L.; Sulley, G. S.; Kimpel, J.; Łagodzińska, M.; Häfele, L.; Carrodeguas, L. P.; Williams, C. K. Block Poly(Carbonate-Ester) Ionomers as High-Performance and Recyclable Thermoplastic Elastomers. *Angew. Chem. Int. Ed.* **2022**, *61* (47), e202210748. https://doi.org/10.1002/anie.202210748.

Chapter Five

Synthesis of Aliphatic and Semi-Aromatic Polyesters Promoted by Schiff-base Binuclear Zinc Complexes

The results described in this *Chapter* have been published in:

Tufano F., Santulli F., Cozzolino M., D'Auria I., Strianese M., Mazzeo M., and Lamberti M Cooperative effects of Schiff base binuclear zinc complexes on the synthesis of aliphatic and semi-aromatic polyesters *Dalton Transactions* **2023**, *52*, 14400-14408.

5.1 Introduction

In the development of new catalytic systems, binuclear complexes have assumed a central role, often demonstrating superior activity and selectivity compared to their mononuclear counterparts. This enhanced performance is primarily attributed to cooperative interactions between spatially close metal centers, a phenomenon that requires precise molecular engineering.[1] From this perspective, the role of the ancillary ligand becomes crucial: it must be designed to position the two metal centers at the optimal distance to promote catalytic synergy. Among the various classes of ligands, Salen-type systems can fulfil this requirement, thanks to the wide availability of precursors that allows for the fine tuning of steric and electronic properties. It is possible to modify the nature of the bridge between the nitrogen atoms, systematically vary the substituents on the aromatic rings, and even introduce donor atoms to expand the coordination environment, thus stabilizing multinuclear structures.

In this context, this chapter describes the synthesis and characterization of Salen ligands, functionalized with sulfur atoms as additional donors and their use for the preparation of mono- and bimetallic zinc complexes. These systems, which have already used as active catalysts for the synthesis of aliphatic polycarbonates via copolymerization of CO_2 with cyclohexene oxide,[2] are evaluated here for the synthesis of aliphatic polyesters obtained via ROP of cyclic esters and in the ROCOP of cyclohexene oxide with phthalic anhydride.

5.2 Results and Discussions

5.2.1 Synthesis of the ligands

The Salen-type hexadentate ligands, OSNNSO, feature two anionic phenolic oxygen donors and four neutral donors, namely two thioether sulfur atoms and two aldimine nitrogen atoms. They were prepared following a three-step synthetic protocol (**Scheme 5.1**), already reported in literature.[2] By varying the amine used in the final step, the same strategy also allows access to tridentate OSN ligands.

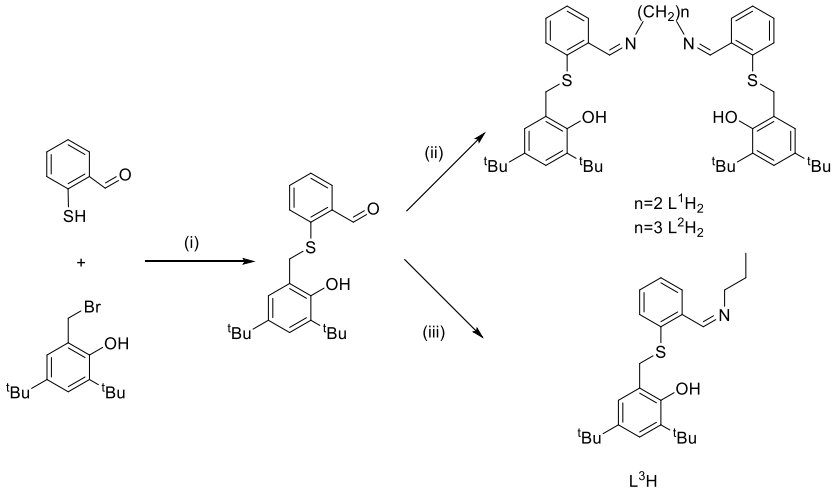

Scheme 5.1: Synthesis of the ligand precursors L^1H_2, L^2H_2 and L^3H (i) DMF; (ii) 0.5 equivalents of ethylenediamine or 1,3-propanediamine in CH_3CN; (iii) 1 equivalent of propanamine in CH_3CN.

In the first step, thiophenol, previously complexed with N,N,N',N'-tetramethylethylenediamine (TMEDA), was deprotonated using n-butyllithium, and the resulting species was subsequently converted to 2-mercaptobenzaldehyde by reaction with anhydrous dimethylformamide in hexane. In the second step, the resulting 2-mercaptobenzaldehyde was reacted with 2-(bromomethyl)-4,6-di-tert-butylphenol pre-synthesized in anhydrous dimethylformamide. Finally, the condensation of two

equivalents of the resulting 2-(3,5-di-tert-butyl-2-hydroxybenzyl)sulfanyl benzaldehyde with the appropriate diamine in anhydrous acetonitrile yielded the desired bis(aldimine-thioether-phenolate) ligand precursors.

5.2.2 Synthesis of the bimetallic complexes

Zinc complexes based on OSNNSO ligands, reported in **Scheme 5.2**, were synthesized according to the general strategy, adapting previously reported procedures.[2] Their synthesis consists in the reaction among the corresponding ligands with two equivalents of zinc bis[bis(trimethylsilyl)amide] for L^1H_2 and L^2H_2, or one equivalent for L^3H, in benzene. After stirring for 2 h at room temperature, the solvent was removed under vacuum, and the resulting products were washed with cold hexane to remove impurities, including the byproduct bis(trimethylsilyl)amine (**Scheme 5.3-5.5**).

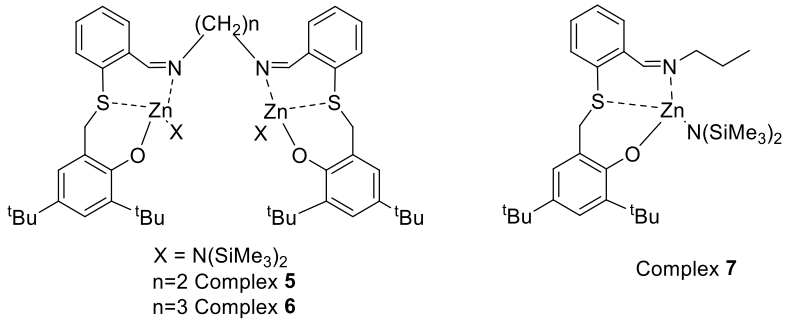

Scheme 5.2 Zinc complexes **5–7**.

Structural characterization was performed by ^{1}H NMR spectroscopy (**Figures 5.6-5.8**). In the spectrum of complex **5,** the disappearance of the hydroxyl proton signal and the appearance of two new broad peaks at 0.14 and 0.04 ppm (integrating for 36 protons) confirmed the presence of silylamido groups. Furthermore, methylene protons bonded to sulfur (SCH_2Ar) and nitrogen (NCH_2CH_2N) appeared as three broad signals at 4.98, 4.51, and 3.57 ppm, with respective integrations of two, four, and two protons, consistent with coordination-induced deshielding. The remaining ligand proton signals

were recognizable but generally shifted downward upon complexation. Complex **6** displayed a similar ^{1}H NMR pattern, although all methylene protons appeared as broad signals in the 2.5–4.5 ppm region, and a single broad resonance was observed at 0.08 ppm for the 36 silylamido protons. These spectral features support the coordination of two zinc centers per complex, each adopting a tetracoordinate geometry involving a phenolic oxygen, a sulfur donor, an aldimine nitrogen, and a silylamido ligand. The similarity of the spectral patterns suggests maintenance of ligand symmetry in solution, while the broad methylene resonances indicate fluxional behaviour. For complex **7**, the disappearance of the hydroxyl proton, the presence of a high-field resonance integrating 18 methyl amide protons, and two broad methylene signals at 3.5 and 4.0 ppm confirmed successful complexation.

Given the propensity of tetracoordinated zinc complexes to form dimeric species in solution, thereby increasing the coordination number of the metal, the nuclearity of complex **7** was further investigated using diffusion-ordered spectroscopy (DOSY). The DOSY experiment (**Figure 5.9-5.10**) performed in C_6D_6 with tetramethylsilane (TMS) as an internal standard yielded diffusion coefficients (D) of 1.56×10^{-9} m^2 s^{-1} for TMS and 5.76×10^{-10} m^2 s^{-1} for complex **7**. Based on these values and the known molecular mass (MM) of TMS (88.23 Da), the molecular mass of the zinc species was estimated to be 647 Da.[3,4] This value aligns well with the theoretical MM of 622.38 Da for the monomeric form, indicating that complex **7** exists as a monomeric species in solution.

5.2.3 Ring-opening polymerization of Cyclic Esters

The catalytic performance of zinc complexes based on OSNNSO ligands in the ROP of L-LA was studied under various temperature, solvent, and co-initiator conditions. The representative results were summarized in **Table 5.1**.

Table 5.1 Ring-opening polymerization of L-lactide by complexes **5**-**7**.

Entry[a]	Comp.	$[L\text{-}LA]_0$: $[Zn]_0$: $[^iPrOH]_0$	Temp (°C)	Time (h)	Conv [b](%)	M_n th[c]	M_n exp[d]	$Đ$ [d]
1	**5**	200:2:0	25	24	76	21.9	21.1	1.2
2	**6**	200:2:0	25	24	69	19.9	21.0	1.3
3	**7**	100:1:0	25	9	61	8.8	34.4	1.3
4	**5**	200:2:0	60	4	86	24.8	28.8	1.2
5	**6**	200:2:0	60	2	85	24.6	24.7	1.2
6	**7**	100:1:0	60	1	82	11.8	31.3	1.5
7	**5**	200:2:2	25	0.5 3	31 71	10.2	7.3	1.1
8	**6**	200:2:2	25	0.5 1	75 90	13.0	11.4	1.2
9	**7**	100:1:1	25	0.5 3	18 67	9.7	6.5	1.1
10	**6**	200:2:4	25	0.5 1	61 83	6.0	7.3	1.4
11	**6**	800:2:10	25	0.5 1	27 53	6.1	3.7	1.4

[a] General conditions: All reactions were carried out in 1 mL of THF. $[\mathbf{5}]_0$-$[\mathbf{6}]_0 = 5.0 \times 10^{-6}$ mol; $[\mathbf{7}]_0 = 1.0 \times 10^{-5}$ mol, (i.e. $[Zn]_0 = 1.0 \times 10^{-2}$ M). [L-LA] = 1.0 M except in Entries 11 and 12). [b] Determined

by ^{1}H NMR spectral data. [c] M_n^{th} (kDa) 144,13 x ([L-LA]$_0$/[Cat]$_0$) x L-LA conversion (for Entries 1-6), M_n^{th} (kDa) 144,13 x ([L-LA]$_0$/[iPrOH]$_0$) x L-LA conversion (for Entries 7-11). [d] Experimental M_n (in kDa) and M_w/M_n ($Đ$) values were determined by GPC in THF using polystyrene standards and corrected using the factor of 0.58.

Initial screening was conducted with 100 equivalents of L-LA per metal center in the absence of a co-initiator: bimetallic complexes **5** and **6** showed moderate and comparable activity, reaching 76% and 69% monomer conversion, respectively, after 24 hours. In contrast, monometallic complex **7** demonstrated greater activity, reaching 61% conversion in just 9 hours. As expected, raising the temperature to 60 °C improved the activity of all catalysts: complex **6** showed double the activity with respect to the complex **5**, while complex **7** remained the most active. Analysis of the polymers revealed distinct mechanistic behaviors: a good agreement among the experimental and the theoretical molecular masses is achieved for bimetallic complexes, assuming the growth of a single polymer chain per bimetallic complex. This suggests that, after initiation at a zinc center, propagation is favored over initiation at the second site. A linear increase in molecular weight with conversion and a constant dispersity for a polymerization catalysed by **6** (**Figure 5.12, Table 5.5**) confirmed a well-controlled and living character. In contrast, for the highly active monometallic complex **7**, M_n^{exp} values are approximately three times higher than calculated, with wider dispersities ($Đ$ = 1.34–1.47). This indicates a slower rate of initiation relative to propagation, a characteristic of less controlled systems. Addition of one equivalent of ^{i}PrOH per metal center significantly increased the activity of all complexes [5]: under these conditions, the activity trend was **6 > 5 > 7**. The superior performance of the bimetallic complexes suggests that a cooperative mechanism between the two metal centers is operative in their alkoxide forms. In particular, the twice as high activity of **6** compared to **5** highlights the critical influence of the length of the diimine bridge and the resulting intermetallic distance of the complex on this cooperativity.[6] In these systems, the M_n^{exp} values agreed well with theory, and the low dispersities confirmed a controlled polymerization.

To clarify the nature of the active species, an alcoholysis experiment was performed by adding 2 equivalents of ^{i}PrOH to complex **6** in C_6D_6. The ^{1}H NMR spectrum of the

reaction mixture (**Figure 5.1**) showed the disappearance of the amide proton signal and the appearance of a signal corresponding to a free amine, consistent with the protonolysis of both Zn–N bonds. Integration of the resulting isopropoxide signals confirmed the quantitative formation of a new bis(alkoxide) species.

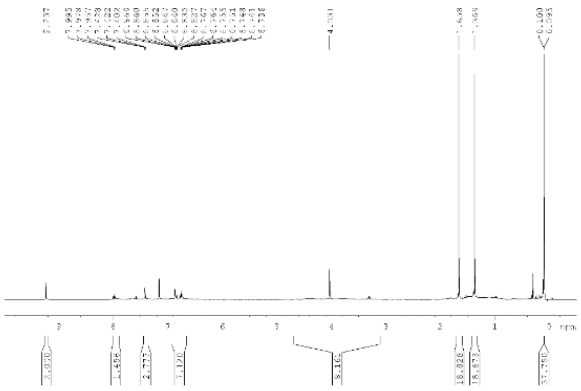

Figure 5.1. ^{1}H NMR spectrum (C_6D_6, 25°C, 400 MHz) of the reaction mixture composed by complex **6** and 2 equivalents of isopropanol.

Scalability of the most active system, **6**/^{i}PrOH, was demonstrated using higher monomer/catalyst ratios (Entries 10–11, **Table 5.1**), maintaining high activity and control. Analysis of the PLA end groups revealed the exclusive presence of HO–CH(CH_3)–CO– and –O–CH(CH_3)$_2$ chain termini. This, combined with MALDI-FT-ICR-MS analysis (**Figure 5.14**) showing a series of linear oligomers with integral LA units, confirms a coordination-insertion mechanism initiated by the isopropoxide group and the absence of significant transesterification side reactions.

Subsequently, the efficiency of bimetallic complexes **5** and **6** in the absence of a co-initiator in the polymerization of *rac*-lactide was also studied using the more sterically hindered bimetallic complexes **5** and **6** at 25 °C (**Table 5.6**). The activities and molecular weight control are fully comparable to those observed with L-LA: in particular, analysis of the PLA microstructure by homocoupled ^{1}H NMR spectroscopy (**Figure 5.15**) revealed

an atactic microstructure. The signal intensities of the methine tetrad were not consistent with theoretical values for either the enantiomorphic site or the chain end control mechanisms (**Tables 5.7–5.8**), confirming the absence of stereocontrol under these conditions.

Finally, the effect of solvent on the polymerization catalysed by complex **6** was explored (**Table 5.9**). Activities in dichloromethane and THF at 25 °C were comparable, while in toluene a lower activity was observed, which was attributed to monomer solubility issues.

In summary, the less sterically hindered monometallic complex proves more active than bimetallic complexes in the absence of a co-initiator, due to steric reasons. Conversely, the alkoxide derivatives of in situ-generated bimetallic complexes exhibit a cooperative effect, making them more active than their monometallic counterpart. Additionally, the length of the diimine bridge is a critical parameter for this cooperativity, with the propylene bridge in **6** producing approximately double the activity of the ethylene-bridged complex **5**.

The catalytic efficacy of zinc complexes **5–7** was subsequently evaluated in the ROP of ε-CL, with key results reported in **Table 5.2**. All complexes demonstrated good activity, successfully converting 100 to 400 equivalents of monomer at room temperature.[7]

Table 5.2 Ring-opening polymerization of ε-caprolactone by complexes **5**-**7**.

Entry [a]	**Comp.**	**[ε-CL]$_0$: [Zn]$_0$: [^{i}PrOH]$_0$**	**Solvent**	**Time (h)**	**Conv**[b]ù **(%)**	M_n^{th} [c]	M_n^{exp} [d]	$Đ$[d]
12	**5**	400:2:2	THF	0.5 2	54 92	21.0	21.8	1.4
13	**5**	200:2:2	THF	0.5 1.5	53 88	10.0	7.8	1.5

14	**6**	400:2:2	THF	0.5 2	27 79	18.0	12.1	1.3
15	**6**	200:2:2	THF	0.5 2	18 89	10.1	5.9	1.3
16	**7**	200:1:1	THF	0.5 1.5	14 61	13.7	12.9	1.3
17	**7**	200:1:1	Tol	0.5 1	63 80	18.3	17.2	1.2
18	**7**	200:1:1	CH_2Cl_2	0.5 3	18 79	18.0	18.2	1.2
19	**7**	200:1:0	Tol	0.5 5	6 45	10.3	32.9	1.6

[a] General conditions: All reactions were carried out in 2 mL of solvent. $[\mathbf{5}]_0$-$[\mathbf{6}]_0$ = 5.0 x 10^{-6} mol; $[\mathbf{7}]_0$ = 1.0 x 10^{-5} mol (i.e. [Zn]= 5mM) [b] Determined by ^{1}H NMR spectral data. [c] M_n^{th} (Da) =114.13 x ([ε-CL] /[^{i}PrOH]) x ε-CL conversion. [d] Experimental M_n (in Da) and M_w/M_n ($Đ$) values were determined by GPC in THF using polystyrene standards and corrected using the factor of 0.56.

Polymerization was conducted in THF using one equivalent of ^{i}PrOH per metal center. Under these conditions, the bimetallic complexes showed higher activity than the monometallic complex **3**. Interestingly, the activity trend for the polymerization of ε-CL was **5 > 6 > 7**: this result confirms that bimetallic cooperativity increases activity, as in the lactide case.

However, the reversal of reactivity between complexes **5** and **6**, compared to polymerization with LA, indicates that the optimal ligand architecture and intermetallic distance for cooperativity could depend on the steric nature of the monomer.[8] Kinetic analysis revealed a first-order concentration dependence , as reported in **Figure 5.2**

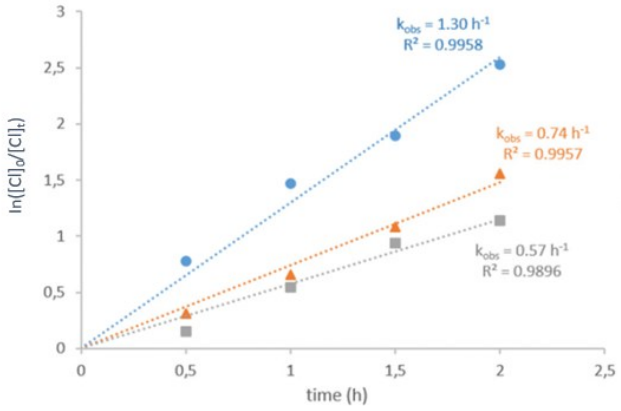

Figure 5.2 First-order kinetic plots for the consumption of ε-CL in THF at 20 °C by complex **5** (blue circles), complex **6** (orange triangles) and complex **7** (grey squares) in combination with ^{i}PrOH.

A solvent screening for complex **7** showed comparable activity in THF and dichloromethane, but a significant rate increase in the less polar toluene (Entries 16–18). In most cases, the experimental molecular weights of PCL samples are well aligned with the theoretical ones, indicating a well-controlled polymerization. Compared to observations with lactide, polymerization with complex **7** in the absence of ^{i}PrOH was slower and less controlled (Entry 19). Analysis of the end groups of a PCL sample, prepared using ^{i}PrOH (from Entry 15, **Table 5.2**) by ^{1}H NMR and MALDI-FT-ICR-MS (**Figures 5.16-5.17**) confirmed the exclusive presence of the HO–$(CH_2)_5$–CO– and –O–$CH(CH_3)_2$ chain terminal. This supports a coordination-insertion mechanism initiated by the isopropoxide group. The molecular weights determined by ^{1}H-NMR and MALDI-FT-ICR are in excellent agreement, although lower than the theoretical value. The GPC-derived molecular weight (M_n^{exp} = 5.9 kDa) was higher, a discrepancy often attributed to the different calibration standards used in GPC versus absolute techniques.

5.2.4 Ring Opening COPolymerization of Phthalic Anhydride and Cyclohexene Oxide

The catalytic performance of complexes **5–7** in ROCOP was evaluated using various cocatalysts. The polymer composition was determined by ^{1}H NMR spectroscopy, quantifying the relative integrals of the signals corresponding to the epoxide-anhydride sequences versus those of the polyether sequences. The resulting polyesters were further characterized by GPC and MALDI-FT-ICR, the main results of which are summarized in **Table 5.3**.

Table 5.3 Ring-opening copolymerization of cyclohexene oxide and phthalic anhydride by complexes **5**-**7**.[a]

Entry [a]	Comp.	$[CHO]_0$: $[PA]_0$: $[Zn]_0$: $[cocat]_0$	Cocat	Time (h)	Conv [b](%)	Ester content [c] (%)	M_n^{th} [c]	M_n^{exp} [d]	$Đ$[d]
20	**5**	250:250:2:2	^{i}PrOH	24	92	78	28.3	8.1	1.4
21	**5**	250:250:2:2	TBAB	16 24	58 76	>99 >99	23.4	11.8	1.3
22	**5**	250:250:2:2	DMAP	16	84	>99	25.9	25.2	1.2
23	**6**	250:250:2:2	DMAP	16 24	70 87	>99 >99	26.8	14.5	1.3
24	**7**	125:125:1:1	DMAP	16 24	54 67	>99 >99	20.6	14.1	1.3

[a]General conditions: $[\mathbf{5}]_0$-$[\mathbf{6}]_0$ = 1x10^{-5} mol; $[\mathbf{7}]_0$ = 2x10^{-5} mol; CHO = 2.5x10^{-3} mol (245 mg); PA = 2.5x10^{-3} mol (370 mg); toluene = 1 mL. Temperature: 110°C. [b]Determined by ^{1}H NMR spectroscopy ($CDCl_3$) by integrating the normalized resonances for PA (7.97 ppm) and the phenylene signals in PE (7.30–7.83 ppm). [c]Determined by ^{1}H NMR spectroscopy ($CDCl_3$)

integrating the normalized resonances for ester linkages (4.80–5.40 ppm) and ether linkages (3.28–3.86 ppm). [d] M_n^{th} (kDa) =246.36 x ([PA]/[^{i}PrOH]) x PA conversion [e] Experimental M_n (in kDa) and M_w/M_n ($Đ$) values were determined by GPC in THF using polystyrene standards and corrected using the factor of 1.85.

Initial investigations focused on complex **5** at 110 °C in toluene, using a CHO/PA/catalyst ratio of 250:250:1 with two equivalents of cocatalyst. The choice of cocatalyst significantly influenced both activity and selectivity. Screening of ^{i}PrOH, tetra-n-butylammonium bromide (TBAB), and 4-(N,N-dimethylamino)pyridine (DMAP) revealed DMAP to be the most efficient, achieving 84% PA conversion in 16 hours (Entry 20). Both the less active TBAB cocatalyst and DMAP produced an exclusively alternating polyester structure with an ester linkage content of >99%. Due to its high selectivity, TBAB was selected for a comparative study of complexes **5–7** under identical conditions (Entries 22–24). The observed activity profile was **5 > 6 > 7**, mirroring the results for the polymerization of ε-caprolactone. This consistency suggests that bimetallic cooperativity is also critical in ROCOP, with the shorter ethylene bridge in complex **5** proving more effective for this specific monomer pair than the propylene bridge in complex **6**. All complexes, including monometallic complex **7**, demonstrated high selectivity for polyester formation over polyether (**Figure 5.18**). GPC analysis of the resulting polyesters showed monomodal molecular weight distributions with narrow dispersities, indicative of well-controlled polymerization. The number-average molecular weights (M_n^{exp}) were consistently lower than theoretical values, a common feature in these systems often attributed to the presence of protic impurities, which act as chain transfer agents.

5.3 Conclusions

This chapter illustrates the catalytic performance of mono- and bimetallic zinc complexes supported by aldimine-thioetherphenolate ligands in the synthesis of aliphatic and semi-aromatic polyesters. In the ROP of cyclic esters, conducted in the presence of isopropyl alcohol as initiator, the systems ensured excellent control, producing polymers with predictable molecular weights, narrow dispersities, and high end-group fidelity. Similarly, in the ROCOP of cyclohexene oxide and phthalic anhydride, the three complexes, in combination with DMAP as the co-catalyst, provided polyesters with complete selectivity.

We observed that for the bimetallic complexes with different metal–metal distances, the order of activity depends on the nature of the monomers. Specifically, the complex characterized by the propylene bridge proved to be the most active for lactide polymerization. Conversely, the complex with the ethylene bridge, characterized by a shorter intermetallic distance and different flexibility, proved more active in the ROP of ε-caprolactone and in the ROCOP of cyclohexene oxide and phthalic anhydride. These results could be explained on the basis of different steric hindrances and/or coordination modes of the explored monomers, where a larger catalytic pocket is required to activate bulky monomer, while for less bulky monomers the proximity of metal centers becomes the governing factor.

5.4 Experimental Part

All reactions with substances that are sensitive toward air or moisture were carried out in dried glassware (24 h at 150 °C in an oven or 5 min at 650 °C in a vacuum) under a positive pressure of nitrogen (ca. 1.2 bar). Solvents and reagents were obtained from Merck and used as received unless stated otherwise. Methylene chloride, tetrahydrofuran, benzene, toluene, isopropyl alcohol and hexane used for polymerization experiments and the synthesis of substances unstable toward air and moisture, were distilled prior to use on an opportune drying agent. In particular, THF,

toluene, benzene and hexane were dried by refluxing over sodium and benzophenone and stored under nitrogen. Dichloromethane and isopropanol were dried over calcium hydride and distilled prior to use. Methanol, ethanol, n-hexane, and tetrahydrofuran (HPLC grade) were used without further purification. The lactide monomers (L-LA and *rac*-LA) were crystallized in toluene and then dried over P_2O_5. Cyclohexene oxide (CHO) and ε-caprolactone were dried over CaH_2 and distilled under nitrogen. Phthalic anhydride was purified by dissolving it in toluene, filtering off impurities, recrystallizing and then subliming. All dry solvents and monomers were stored under nitrogen. Deuterated solvents for NMR experiments were stored at 20 °C over molecular sieves. NMR spectra were measured with 300/400/600 MHz Bruker AVANCE spectrometers at 20 °C. Chemical shifts δ are given in ppm relative to the residual solvent peak of the used deuterated solvent. Molecular masses (M_n and M_w) and their dispersities (M_w/M_n) were measured by GPC, using THF as the eluent (1.0 mL min^{-1}) and narrow polystyrene standards were used as the reference. MALDI-FT-ICR mass spectra were recorded using a Bruker solariX XR Fourier transform ion cyclotron resonance (FT-ICR) mass spectrometer (Bruker Daltonik GmbH, Bremen, Germany) equipped with a 7 T refrigerated actively shielded superconducting magnet (Bruker Biospin, Wissembourg, France). The samples were prepared at a concentration of 1.0 mg mL^{-1} in THF, while the matrix (DCTB) was mixed at a concentration of 10.0 mg ml^{-1}.

5.4.1 Synthesis of ligands

To a stirred solution of TMEDA (1.5 mL, 10 mmol; 2.2 equiv.) and thiophenol (0.46 mL, 4.54 mmol; 1.0 equiv.) in hexane (15 mL) at 0 °C was added dropwise a solution a 1.8 M nBuLi in cyclohexane (5.5 mL, 10 mmol; 2.2 equiv.). The resulting solution was left to stir at room temperature for 17 h. DMF (0.9 mL, 11.35 mmol; 2.5 equiv.) was then added dropwise at room temperature and the resulting solution was allowed to stir at r.t. for 20 h. Et_2O (20 mL) was added and stirred for another 20 min. The reaction mixture was washed with 1 M HCl (50 mL) and the aqueous layer was back-extracted with Et_2O (2 × 20 mL). The combined organic layer was dried over $MgSO_4$ and concentrated in vacuo to obtain orange oil.

To a stirred solution of 2-mercaptobenzaldehyde (1.041 g, 7.535 x 10^{-6} mol) and K_2CO_3 (4.165 g, 30.1 mmol) in DMF (83 mL) at room temperature was added dropwise a solution of 2-(bromomethyl)-4,6-di-tert-phenol (2.255g, 7.535 x 10^{-6} mol) in dry DMF (18 mL). The flask was left to stir at room temperature for 3 h. 50 mL of water and 50 mL of diethyl ether were added. The organic layer was washed with water (3 x 30 mL) and brine (3 x 30 mL). The solution was dried over sodium sulfate and then filtered. The solvent was removed under vacuum yielding a white yellow solid that was recrystallized from pentane as a white solid, and collected by vacuum filtration (Yield = 63%).

To a stirred solution of 2-(3,5 di-tert-butyl-2-hydroxybenzyl) sulfanyl benzaldehyde (1.628 g, 4.565 x 10^{-6} mol) in dry acetonitrile (33 mL) at room temperature was added dropwise a solution of ethylenediamine (153 µL, 2.289 x 10^{-6} mol), in dry acetonitrile (24 mL). The flask was left to stir at room temperature for 2 h. After this time a white solid was precipitated. It was washed with cold pentane and dried using the trap-by trap system. The formation of the desired species was confirmed by NMR analysis and MALDI FT ICR mass spectrometry. (Yield = 51%).

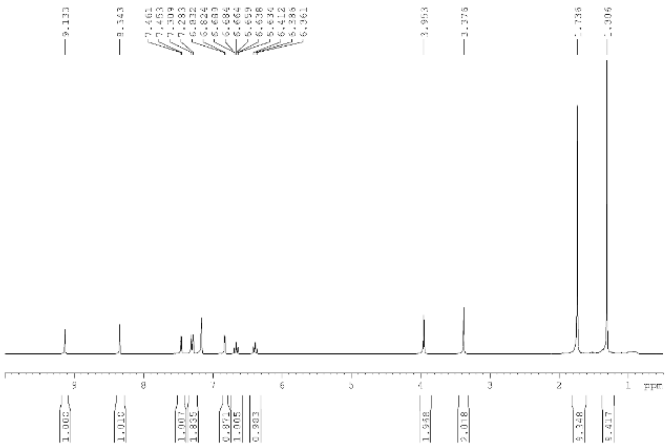

Figure 5.3 ^{1}H NMR spectrum of ligand L^1H_2(400 MHz, C_6D_6, 25 °C).

^{1}H NMR (400 MHz, C_6D_6, 25°C): δ 1.29 (s, 18H, ^{t}Bu), 1.71 (s, 18H, ^{t}Bu), 3.42 (s, 4H, N-CH_2), 3.97 (s, 4H, S-CH_2),6.44 (t, 2H, Ar-H), 6.67 (t, 2H, Ar-H), 6.82 (d, J= 2.44, 2H, Ar-H), 7.27

(d, J=7.84; 2H, Ar-H), 7.37 (d, J=7.79, 1H, Ar-H), 7.44 (d, J= 2.41, 1H, Ar-H), 8.10 (s, 1H, OH) 9.07 (s, 1H, CH=N).

To a stirred solution of 2-(3,5 di-tert-butyl-2-hydroxybenzyl) sulfanyl benzaldehyde (0.7050 g, 1.9774 x 10^{-3} mol) in dry acetonitrile (14 mL) at room temperature was added dropwise a solution of 1,3-propanediamine (83.3 µL, 9.887 x 10^{-4} mol), in dry acetonitrile (10 mL). The flask was left to stir at room temperature for 2 h. After this time a white solid was precipitated. It was washed with cold pentane and dried using the trap-by trap system. The formation of the desired species was confirmed by NMR analysis. (Yield = 54%).

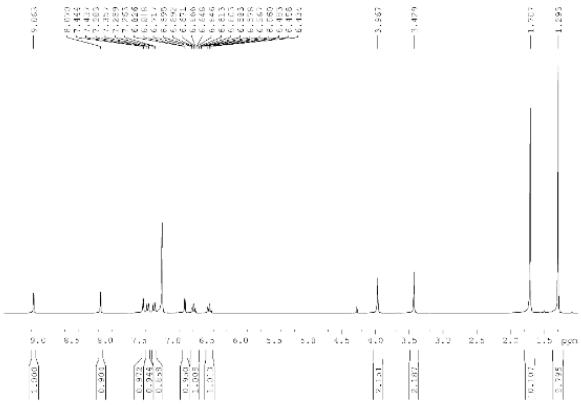

Figure 5.4. ^{1}H NMR spectrum of ligand $L^{2}H_{2}$(400 MHz, C_6D_6, 25 °C).

^{1}H NMR (400 MHz, C_6D_6, 25°C): δ 1.23 (s, 9H, ^{t}Bu), 1.58 (s, 9H, ^{t}Bu), 2.20 (m, 2H, N-CH_2),3.72 (t, 2H, N-CH_2), 3.81 (s, 2H, S-CH_2), 6.76 (s, 1H, OH), 6.82, (d, J= 2.36, 1H, Ar-H), 6.86 (t, 1H, Ar-H), 6.91 (t, 1H, Ar-H), 7.24 (d, J= 7.76, 1H, Ar-H), 7.39 (d, J= 2.43, 1H, Ar-H), 7.82 (d, J= 7.90, 1H, Ar-H), 8.60 (s, 1H, CH=N).

To a stirred solution of 2-(3,5 di-tert-butyl-2-hydroxybenzyl) sulfanyl benzaldehyde (0.5028 g, 1.41 x 10^{-3} mol), in dry acetonitrile (10 mL) at room temperature was added dropwise a solution of propylamine (116 µL, 1.41 x 10^{-3} mol), in dry acetonitrile (10 mL). The flask was left to stir at room temperature for 2 h. After this time the solution was

dried over $MgSO_4$ and then filtered and was concentrated in vacuo. The result is a yellow oil. The crude product was recrystallized from pentane to give a white solid, which was washed with cold pentane and dried using the trap-by-trap system. The formation of the desired species was confirmed by NMR analysis. (Yield = 62%).

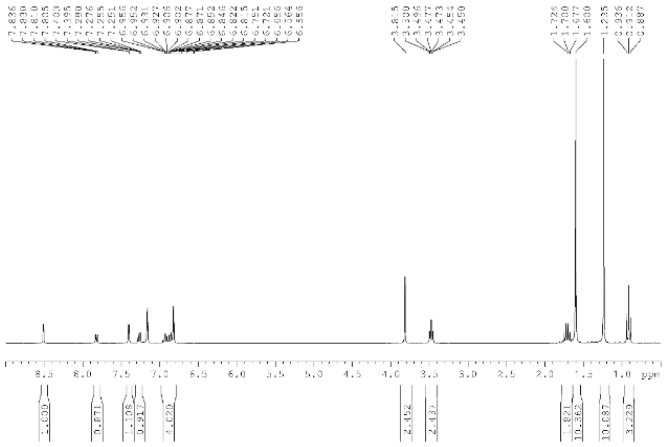

Figure 5.5 ^{1}H NMR spectrum of ligand L^3H (400 MHz, C_6D_6, 25 °C).

^{1}H NMR (400 MHz, C_6D_6, 25°C): δ 0.91 (t, 3H, CH_3) 1.23 (s, 9H, ^{t}Bu), 1.59 (s, 9H, ^{t}Bu), 1.70 (m, 2H, CH_2), 3.47 (t, 2H, N-CH_2), 3.81 (s, 2H, S-CH_2), 6.77 (s, 1H, OH), 6.81 (s, 1H, Ar-H), 6.85 (t, 1H, Ar-H), 6.91 (t, 1H, Ar-H), 7.25 (d, J= 7.62 Hz, 1H, Ar-H), 7.39, (s, 1H, Ar-H), 7.82 (d, J= 7.55 Hz, 1H, Ar-H), 8.52 (s, 1H, CH=N).

5.4.2 Synthesis of complexes

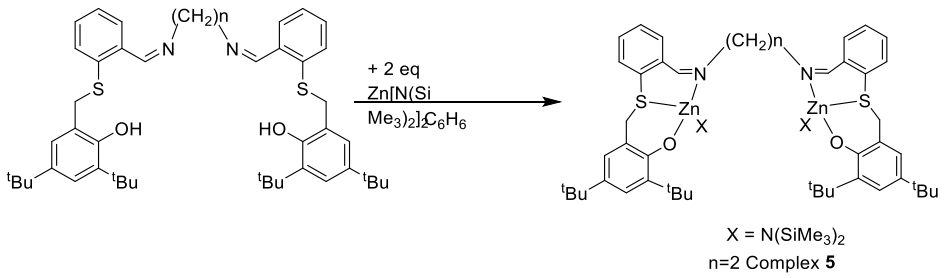

Scheme 5.3: Synthesis of di-Zinc complex **5**.

The synthesis was carried out in a glovebox under a nitrogen atmosphere. In a 20 mL vial with a magnetic stirrer bar, 157.2 mg (4.07×10^{-4} mol) of $Zn[N(SiMe_3)_2]_2$ was dissolved in 3 mL of dry benzene. In a 5 mL vial 150 mg (2.03×10^{-4} mol) of ligand L^1H_2 were dissolved in 6 mL of dry benzene. The ligand solution was slowly added dropwise in the solution containing $Zn[N(SiMe_3)_2]_2$ and other 0.5 mL of dry benzene were used to wash the vial containing the ligand. The resulting mixture was stirred at room temperature for 2 hours. The solvent was then removed under vacuum and the solid residue was washed with hexane. Complex **1** was obtained as a yellow powder. (Yield = 95%).

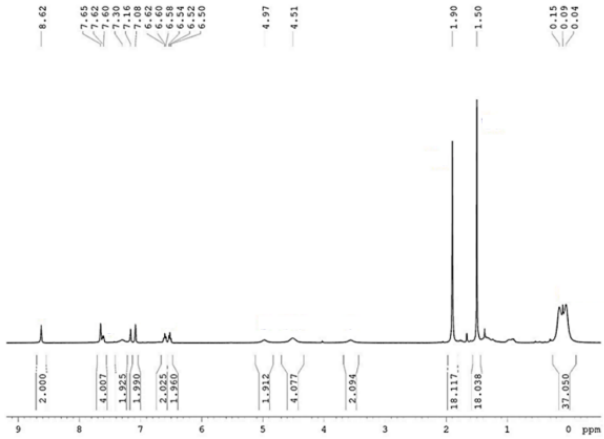

Figure 5.6. ^{1}H NMR spectrum of complex **5**. (C_6D_6, 25°C, 400 MHz)

^{1}H NMR (400 MHz, C_6D_6, 25°C): δ 0.14 (br, 36H, $Si(CH_3)_3$), 1.50 (s, 18H, CCH_3), 1.90 (s, 18H, CCH_3), 3.57 (br, 2H, N-CH_2), 4.51 (br, 4H, S-CH_2), 4.98 (br, 2H, N-CH_2), 6.49 (t, 2H, Ar-H), 6.58 (t, 2H, Ar-H), 7.08 (d, J=2.48 Hz, 2H, Ar-H), 7.29 (br, 2H, Ar-H). 7.60 (d, J= 7.88 Hz, 2H, Ar-H), 7.63 (d, J=2.53 Hz, 2H, Ar-H), 8.62 (s, 2H, CH=N)

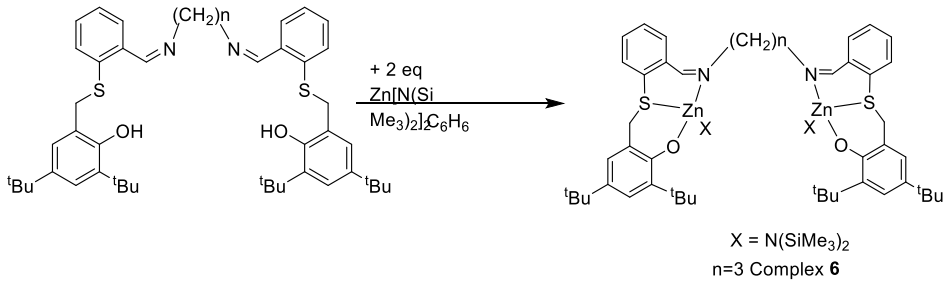

Scheme 5.4: Synthesis of di-Zinc complex **6**.

The synthesis was carried out in a glovebox under a nitrogen atmosphere. In a 20 mL vial with a magnetic stirrer bar, 212 mg (5.33×10^{-4} mol) of $Zn[N(SiMe_3)_2]_2$ was dissolved in 3 mL of dry benzene. In a 5 mL vial 200 mg (2.67×10^{-4} mol) of ligand L^2H_2 were dissolved

in 6 mL of dry benzene. The ligand solution was slowly added dropwise in the solution containing $Zn[N(SiMe_3)_2]_2$ and other 0.5 mL of dry benzene were used to wash the vial containing the ligand. The resulting mixture was stirred at room temperature for 2 hours. The solvent was then removed under vacuum and the solid residue was washed with hexane. Complex **6** was obtained as a yellow powder. Yield: 91%.

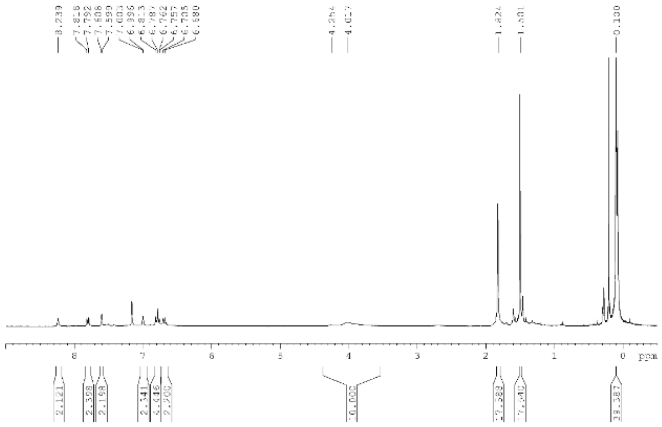

Figure 5.7. ^{1}H NMR spectrum of Complex **6**. (C_6D_6, 25°C, 400 MHz)

^{1}H NMR (400 MHz, C_6D_6, 25°C): δ 8.62 (s, 2H, CH=N), 7.63 (d, J=2.53 Hz, 2H, Ar-H), 7.60 (d, J= 7.88 Hz, 2H, Ar-H), 7.29 (br, 2H, Ar-H), 7.08 (d, J=2.48 Hz, 2H, Ar-H), 6.58 (t, 2H, Ar-H), 6.49 (t, 2H, Ar-H), 4.98 (br, 2H, N-CH_2), 4.51 (br, 4H, S-CH_2), 3.57 (br, 2H, N-CH_2), 1.90 (s, 18H, CCH_3), 1.50 (s, 18H, CCH_3), 0.14 (br, 36H, $Si(CH_3)_3$).

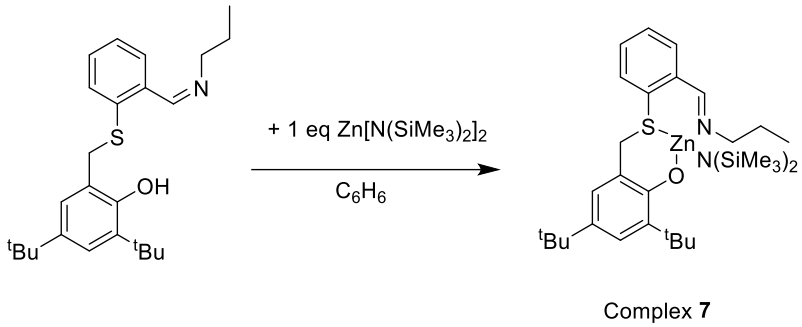

Scheme 5.5: Synthesis of Zinc complex **7.**

The synthesis was carried out in a glovebox under a nitrogen atmosphere. In a 20 mL vial with a magnetic stirrer bar, 152 mg (3.77 x 10^{-4} mol) of $Zn[N(SiMe_3)_2]_2$ were dissolved in 3 mL of dry benzene. In a 5 mL vial 150 mg (3.77 x 10^{-4} mol) of ligand L^3H were dissolved in 6 mL of dry benzene. The ligand solution was slowly added dropwise in the solution containing $Zn[N(SiMe_3)_2]_2$ and other 0.5 mL of dry benzene were used to wash the vial containing the ligand. The resulting mixture was stirred at room temperature for 2 hours. The solvent was then removed under vacuum and the solid residue was washed with hexane. Complex **7** was obtained as a yellow powder. (Yield = 97%).

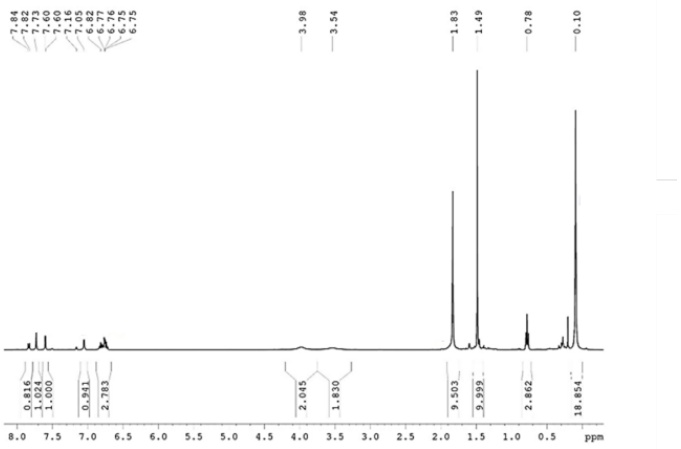

Figure 5.8. ^1H NMR spectrum of complex **7** (C_6D_6, 25°C, 400 MHz).

^{1}H NMR (400 MHz, C_6D_6, 25°C): δ 7.84 (d, J= 7.90 Hz 2H, Ar-H), 7.73 (s, 1H, CH=N), 7.59(s, 1H, Ar-H), 7.05 (s, 1H, Ar-H), 6.75 (m, 3H, Ar-H), 3.98 (br, 2H, S-CH_2), 3.54 (br, 2H, N-CH_2), 1.83 (s, 9H, CCH_3), 1.49 (s, 9H, CCH_3), 0.78 (t, 3H, CH_3), 0.10 (s, 18H, $Si(CH_3)_3$).

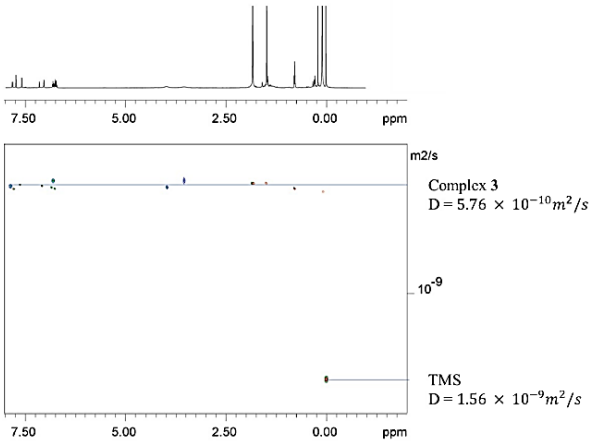

Figure 5.9. DOSY spectrum (C_6D_6, 25°C, 600 MHz) of complex **7** (D = 5.76 10^{-10} m^2 /s) in the presence of SIME3 as standard (D = 1.56 10^{-9} m^2/s).

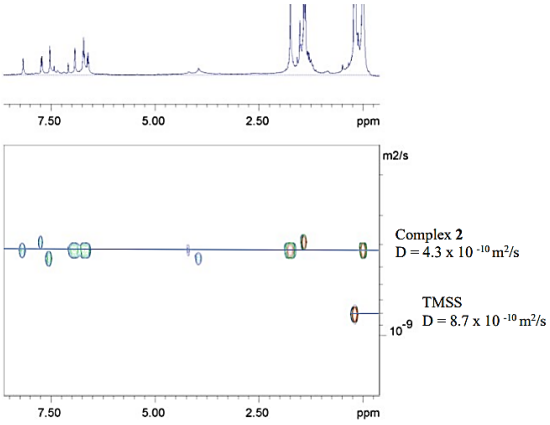

Figure 5.10 DOSY spectrum (C_6D_6, 25°C, 600 MHz) of complex **6** (D = 4.3 10^{-10} m^2 /s) in the presence of TMSS as standard (D = 8.7 10^{-10} m^2 /s). (Molecular weight of TMSS = 320.84 Da; estimated mass for complex **6** = 1300; Molecular weight for complex **6** = 1200.67 Da).

5.4.3 Ring-Opening Polymerization of Lactide

The polymerization experiments were carried out in a glove box. The complex was weighed and added to a 4 ml vial, fitted with a magnetic stirrer (5.0×10^{-6} mol for complexes **5** and **6** and 1.0×10^{-5} mol for complex **7**): subsequently, a solution of the co-catalyst (0.1 M of ^{i}PrOH in the reaction solvent) was added and stirred for 5 minutes. In a 4 mL vial, the monomer was weighed and dissolved in the same solvent. Finally, the monomer solution was added to the solution of the catalytic system. The polymerization experiments were stopped by taking the 4 ml vial out of the glove box and adding dichloromethane. The solvent was removed under reduced pressure, and the polymer was dried in a vacuum oven and characterized by NMR spectroscopy and GPC.

Table 5.4. Ring-opening polymerization of L-lactide by complexes **5-7**

Entry[a]	Comp.	$[LA]_0$: $[Zn]_0$: $[iPrOH]_0$	Temp (°C)	Time (h)	Conv[b](%)	M_n^{th} [c]	M_n^{exp} [d]	$Đ$[d]
25	**5**	200:2:0	25	2 4 7 24	0 5 11 76	21.9	21.1	1.2
26	**6**	200:2:0	25	2 4 7 24	0 7 20 69	19.9	21.0	1.3
27	**7**	100:1:0	25	2 4 7 9	8 20 40 61	8.8	34.4	1.3
28	**5**	200:2:0	60	2 3 4	57 74 86	24.8	28.8	1.2
29	**6**	200:2:0	60	2	85	24.6	24.7	1.2
30	**7**	100:1:0	60	0.5 1	50 82	11.8	31.3	1.5

[a] General conditions: All reactions were carried out in 1 mL of THF. $[\mathbf{5}]_0$-$[\mathbf{6}]_0$ = 5.0 x 10^{-6} mol; $[\mathbf{7}]_0$ = 1.0 x 10^{-5} mol, (i.e. $[Zn]_0$ = 1.0 x 10^{-2} M). [L-LA] = 1.0 M). [b] Determined by ^{1}H NMR spectral data. [c] M_n^{th} (kDa) 144,13 x ($[\text{L-LA}]_0/[Cat]_0$) x L-LA conversion (for Entries 1-6). [d] Experimental M_n (in

kDa) and M_w/M_n ($Đ$) values were determined by GPC in THF using polystyrene standards and corrected using the factor of 0.58.

Table 5.5. Polymerization of L-LA by complex **6.**

Time (h)	Conv[a] (%)	M_n^{th}[b]	M_n^{exp}[c]	$Đ$[c]
6	20	5.8	8.8	1.2
16	70	20.2	23.4	1.2
20	80	23.1	26.2	1.2
24	84	24.2	26.2	1.3

The polymerization was carried out in 1 mL of THF. $[\mathbf{6}]_0$ = 5.0 x 10^{-6} mol. [L-LA] = 1.0 M. $[\text{L-LA}]_0$:$[\mathbf{6}]_0$:$[\text{iPrOH}]_0$ = 200:2:0. [a] Determined by ^{1}H-NMR spectral data. [b] M_n^{th} (kDa) = 144.13 x ($[\text{L-LA}]_0/[\mathbf{2}]_0$) x L-LA conversion. [c] M_n^{exp} (in kDa) and M_w/M_n ($Đ$) values were determined by GPC in THF using polystyrene standards and corrected using the factor of 0.58.

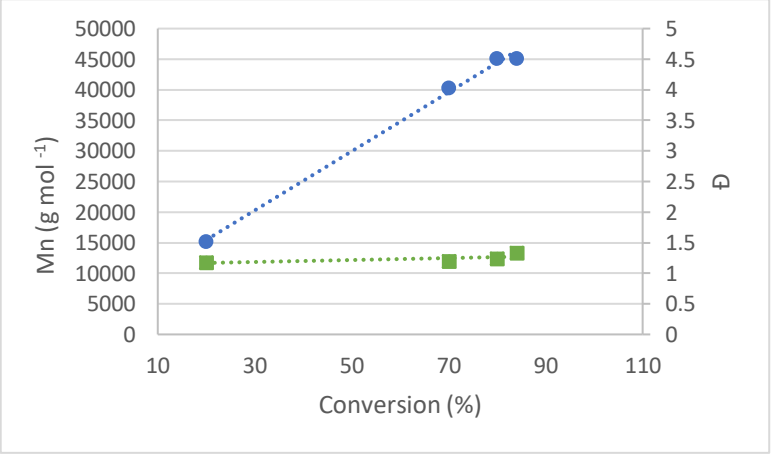

Figure 5.11. Molecular weights and molecular weights distribution (determined by GPC analysis) in function of the conversion for the polymerization experiment detailed in **Table 5.5** $(\text{L-LA})_0$:$[\mathbf{6}]_0$ = 200:2 in THF as solvent).

Table 5.6. Polymerization of L-LA by complex **6** and iPrOH

Time (h)	Conv[a] (%)	M_n^{th}[b]	M_n^{exp}[c]	Đ[c]
0.5	32	4.6	2.5	1.2
1	42	6.1	4.1	1.1
1.5	55	7.9	5.3	1.2
2	69	9.9	7.0	1.2

The polymerization experiment was carried out in 1 mL of THF. $[\mathbf{6}]_0 = 5.0 \times 10^{-6}$ mol. [L-LA] = 1.0 M. $[\text{L-LA}]_0:[\mathbf{6}]_0:[\text{iPrOH}]_0 = 200:2:2$. [a]Determined by ^{1}H-NMR spectral data. [b]M_n^{th} (kDa) = 144.13 x ($[\text{L-LA}]_0/[\text{iPrOH}]_0$) x L-LA conversion. [c] M_n^{GPC} (in kDa) and M_w/M_n (Đ) values were determined by GPC in THF using polystyrene standards and corrected using the factor of 0.58.

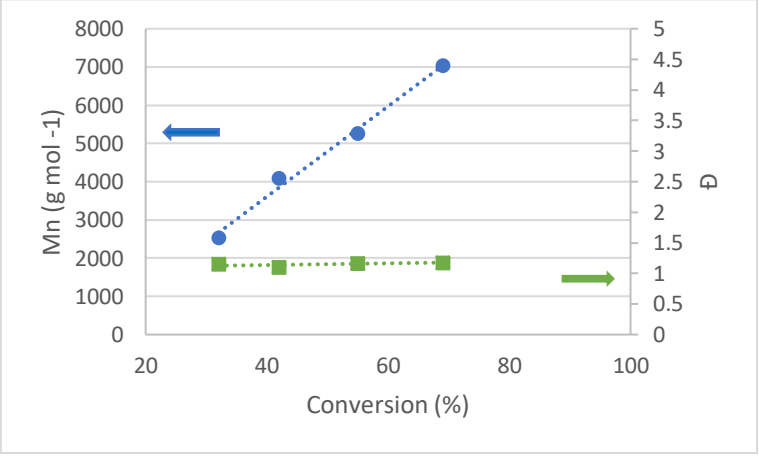

Figure 5.12. Molecular weights and molecular weights distribution (determined by GPC analysis) in function of the conversion for the polymerization experiment detailed in **Table 5.6** $(\text{L-LA})_0:[\mathbf{6}]_0:[^i\text{PrOH}]_0 = 200:2:2$ in THF as solvent).

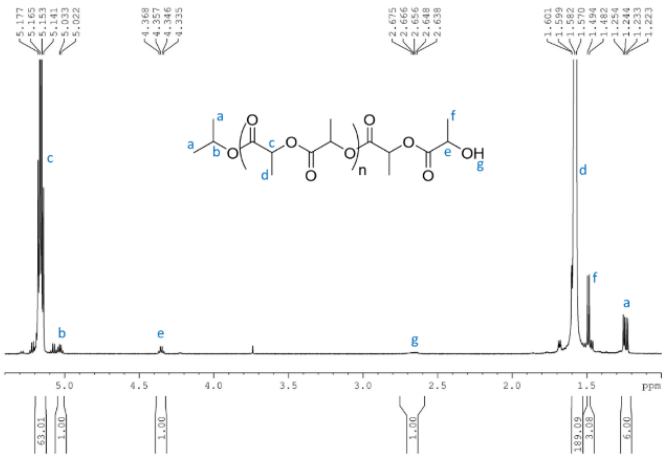

Figure 5.13. ^{1}H NMR spectrum (600 MHz, $CDCl_3$, 25 °C) of a PLA sample (run 10 in **Table 5.1**).

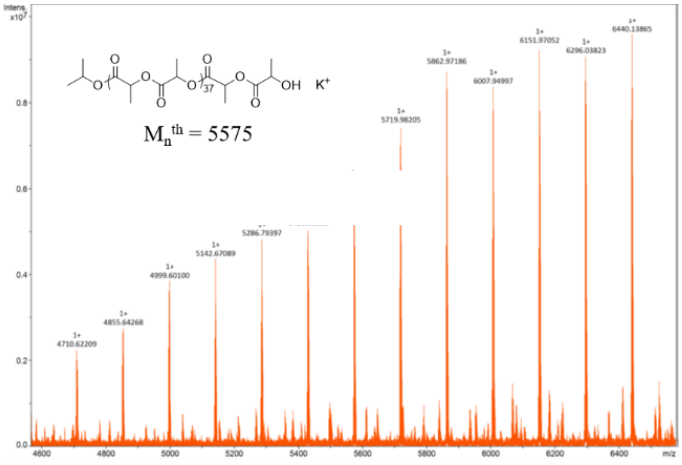

Figure 5.14. MALDI-FT-ICR spectrum of a PLA sample (M_n^{Thr} = 5575 Da) (run 9, **Table 5.1**).

Table 5.7 Ring-opening polymerization of *rac*-lactide by complexes **5** and **6**.

Entry[a]	Comp.	$[LLA]_0$: $[Zn]_0$: $[^iPrOH]_0$	Conv[b] (%)	M_n^{th}[c]	M_n^{exp}[d]	$Đ$[d]
31	**5**	200:2:0	66	19.0	16.3	1.4
32	**6**	200:2:0	77	22.2	25.6	1.4

[a]Reactions were carried out in 1 mL of solvent (THF), complexes **5**-**6** = 5.0 x 10^{-6} mol; *rac*-lactide was used as monomer. Temperature = 25 °C; time = 24 h. [b]Determined by ^{1}H NMR spectral data. [c]M_n^{th} (kDa) = 144,13 x ($[LA]_0/[^iPrOH]_0$) x LA conversion. [d]Experimental M_n (in kDa) and M_w/M_n ($Đ$) values were determined by GPC in THF using polystyrene standards and corrected using the factor of 0.58.

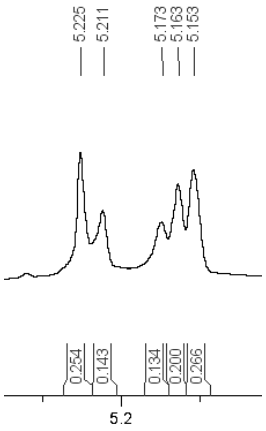

Figure 5.15. Methine region of the homonuclear decoupled ^{1}H NMR spectrum ($CDCl_3$, 25 °C, 400K) of P(rac-LA) (run 30 in **Table 5.7).**

Table 5.8 Tetrad probabilities based on Bernoullian Statistics (Th) and experimental values (Exp) as obtained by NMR analysis of polymeric sample obtained in Entry 30 of **Table 5.7**

Tetrad	**Formula**	**Th**	**Exp**
[*rmm*]	$P_m^2/2$	0.254	0.254
[*rmm*]	$P_rP_m/2$	0.102	0.143
[*mrr*]	$P_rP_m/2$	0.102	0.134
[*mmm*]	$P_r^2+P_rP_m/2$	0.185	0.200
[*mrm*]	$(P_m^2+P_rP_m)/2$	0.356	0.266

Table 5.9 Tetrad probabilities based on Enantiomorphic Site Control Statistics (Th) and experimental values (Exp) as obtained by NMR analysis of polymeric sample obtained in Entry 31 of **Table 5.7.**

Tetrad	**Formula**	**Th**	**Exp**
[*rmm*]	$[\alpha^2(1-\alpha)+\alpha(1-\alpha)^2]/2$	0.113	0.254
[*rmm*]	$[\alpha^2(1-\alpha)+\alpha(1-\alpha)^2]/2$	0.113	0.143
[*mrr*]	$[\alpha^2(1-\alpha)+\alpha(1-\alpha)^2]/2$	0.113	0.134
[*mmm*]	$[\alpha^2+(1-\alpha)^2+\alpha^3+(1-\alpha)^3]/2$	0.435	0.200
[*mrm*]	$[\alpha(1-\alpha)+\alpha(1-\alpha)]/2$	0.226	0.266

Table 5.10. Ring-opening polymerization of L-lactide by complex **6**, using different solvents.

Entry[a]	**Solvent (V, mL)**	**Temp (°C)**	**Time (h)**	**Conv**[b] **(%)**
Entry 2 Table 5.1	THF (1 mL)	25	24	69
33	DCM (1 mL)	25	24	74
Entry 5 Table 5.1	THF (1 mL)	60	2	85
34	Toluene (1 mL)	60	1 2	36 59
35	Toluene (2.5 mL)	60	1 2 4 6	24 37 63 77
36	THF (2.5 mL)	60	1 2 4 6	20 39 57 75

[a]All reactions were carried out with complex **6** = 5.0 x 10^{-6} mol; ^{i}PrOH = 1.0 x 10^{-5} mol; L-LA = 1.0 x 10^{-3} mol (200 eq, i.e. 100 eq/Zn). [b]Determined by ^{1}H NMR spectral data.

5.4.4 Ring-Opening Polymerization of ε-caprolactone

The polymerization experiments were carried out in a glovebox. The zinc complex was weighed (5.0×10^{-6} mol for complexes **5** and **6** and 1.0×10^{-5} mol for complex **7**) and added to a 4 mL vial, fitted with a magnetic stirrer. Subsequently, a solution of the co-catalyst (0.1 M of ^{i}PrOH in the reaction solvent) was added and stirred for 5 minutes. In another 4 mL vial, the monomer was weighed and dissolved in the reaction solvent. Finally, the monomer solution was added to the first solution. The polymerization was stopped using dichloromethane after taking the vial out of the glove box. The solvent was removed under reduced pressure, and the polymer was dried in a vacuum oven and characterized by NMR spectroscopy and GPC analysis.

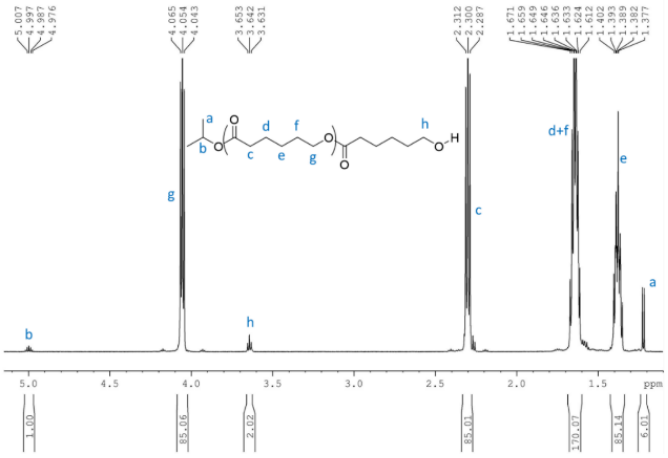

Figure 5.16 ^{1}H NMR spectrum (600 MHz, $CDCl_3$, 25 °C) of PCL.

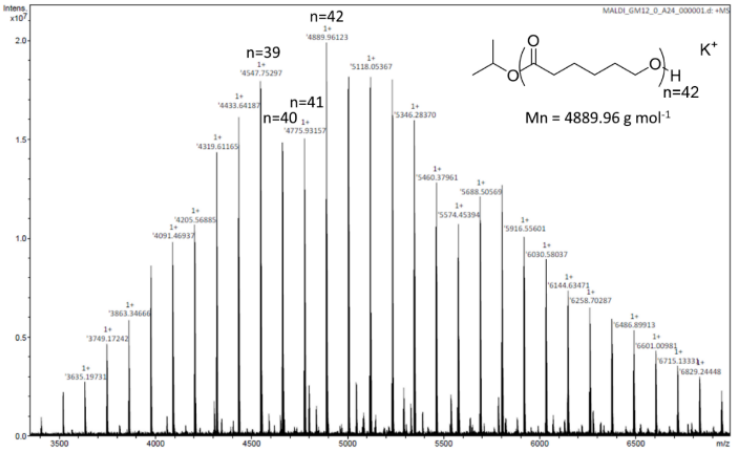

Figure 5.17 MALDI-FT-ICR spectrum of PCL.

5.4.5 Ring-Opening COPolymerization of Phthalic Anhydride and Cyclohexene Oxide

In a glovebox, the previously weighed monomer and the co-catalyst were transferred into a 10 mL Schlenk tube, equipped with a magnetic stirrer, and dissolved in 0.5 mL of toluene. In a 2 mL vial, the complex was weighed and dissolved in 0.5 mL solvent. Subsequently, the complex solution was transferred into the Schlenk tube: the latter was closed, taken out of the glove box and immersed in a thermostated oil bath at a temperature of 110 °C. The polymerizations were stopped after the prescribed time using dichloromethane. The solvent was removed under reduced pressure and the polymer was coagulated in methanol, filtered, dried in a vacuum oven and characterized by NMR spectroscopy and GPC analysis.

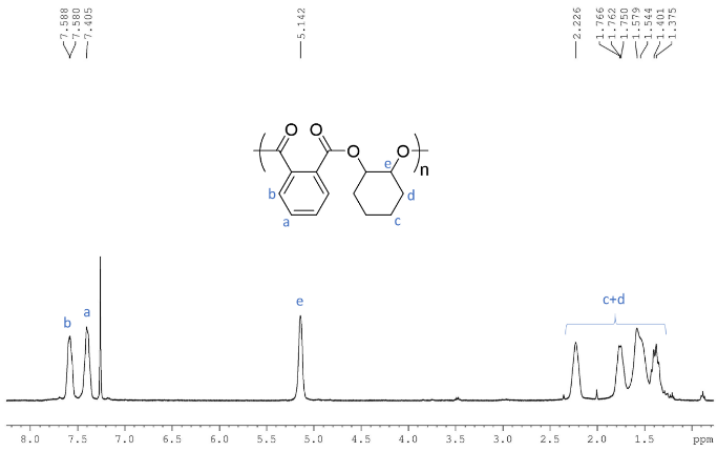

Figure 5.18. ^{1}H NMR spectrum (600 MHz, $CDCl_3$, 25 °C) of P(CHO-PA).

5.5 References

(1) Wu, L.-J.; Lee, W.; Kumar Ganta, P.; Chang, Y.-L.; Chang, Y.-C.; Chen, H.-Y. Multinuclear Metal Catalysts in Ring-Opening Polymerization of E-caprolactone and Lactide: Cooperative and Electronic Effects between Metal Centers. *Coord. Chem. Rev.* **2023**, *475*, 214847. https://doi.org/10.1016/j.ccr.2022.214847.

(2) Cozzolino, M.; Melchionno, F.; Santulli, F.; Mazzeo, M.; Lamberti, M. Aldimine-Thioether-Phenolate Based Mono- and Bimetallic Zinc Complexes as Catalysts for the Reaction of CO_2 with Cyclohexene Oxide. *Eur. J. Inorg. Chem.* **2020**, *2020* (17), 1645–1653. https://doi.org/10.1002/ejic.202000119.

(3) *Zinc Complexes Bearing Dinucleating Bis(imino- pyridine)binaphthol Ligands: Highly Active and Robust Catalysts for the Lactide Polymerization*. https://chemistry-europe.onlinelibrary.wiley.com/doi/epdf/10.1002/cctc.202300498 (accessed 2025-10-25).

(4) Pilone, A.; Lamberti, M.; Mazzeo, M.; Milione, S.; Pellecchia, C. Ring-Opening Polymerization of Cyclic Esters by Phenoxy-Thioether Complexes Derived from Biocompatible Metals. *Dalton Trans.* **2013**, *42* (36), 13036. https://doi.org/10.1039/c3dt51219c.

(5) Stasiw, D. E.; Luke, A. M.; Rosen, T.; League, A. B.; Mandal, M.; Neisen, B. D.; Cramer, C. J.; Kol, M.; Tolman, W. B. Mechanism of the Polymerization of *Rac* -Lactide by Fast Zinc Alkoxide Catalysts. *Inorg. Chem.* **2017**, *56* (22), 14366–14372. https://doi.org/10.1021/acs.inorgchem.7b02544.

(6) Isnard, F.; Lamberti, M.; Lettieri, L.; D'auria, I.; Press, K.; Troiano, R.; Mazzeo, M. Bimetallic Salen Aluminum Complexes: Cooperation between Reactive Centers in the Ring-Opening Polymerization of Lactides and Epoxides. *Dalton Trans.* **2016**, *45* (40), 16001–16010. https://doi.org/10.1039/C6DT02592G.

(7) Arbaoui, A.; Redshaw, C. Metal Catalysts for ε-Caprolactone Polymerisation. *Polym. Chem.* **2010**, *1* (6), 801. https://doi.org/10.1039/b9py00334g.

(8) Isnard, F.; Carratù, M.; Lamberti, M.; Venditto, V.; Mazzeo, M. Copolymerization of Cyclic Esters, Epoxides and Anhydrides: Evidence of the Dual Role of the Monomers in the Reaction Mixture. *Catal. Sci. Technol.* **2018**, *8* (19), 5034–5043. https://doi.org/10.1039/C8CY01174E.

Chapter Six

Ring Opening Polymerisation of Trimethylene Carbonate and Macrolactones through Heterometallic Zinc-Alkali Complexes

During my PhD, I carried out a visiting research period at the School of Chemistry of the University of Edinburgh, under the supervision of Dr. Jennifer Garden.

6.1 Introduction

Metal-metal cooperativity is a fundamental element in the design of efficient catalysts. In these systems, the proximity of two identical metal centers improves catalytic performance through an activation mechanism where one metal coordinates the monomer, while the other activates the growing polymer chain .[1] While the homometallic synergy has been extensively studied and established, the potential of heterometallic cooperativity remains largely unexplored. This emerging strategy relies on the combination of metals with distinct electronic properties to enable the rational design of tailored catalysts.[2]

In this context, a significant contribution by Dr. Garden's research has been given, which has investigated the benefits of heterometallic cooperation in polymerization, with the aim of improving catalytic performance.[2,3] In detail, the Garden group have reported the synthesis of heterometallic complexes, based on zinc in combination with Lewis acidic alkali metals, such as sodium and potassium: these metals were selected not only for their high activity but also because they are earth-abundant, non-toxic, and economically viable. Studies on the ROP of various cyclic esters revealed improved activity compared to their homometallic counterparts: the enhancement of polymerisation rate relies on electronic communication between metal centers along the bond Zn–O–M (M = Na, K), in which the hard alkali metal utilizes its greater Lewis acidity to facilitate coordination of the monomer, simultaneously increasing the nucleophilicity of the zinc-alkoxide group (Zn–OR) (**Figure 6.1**).[4]

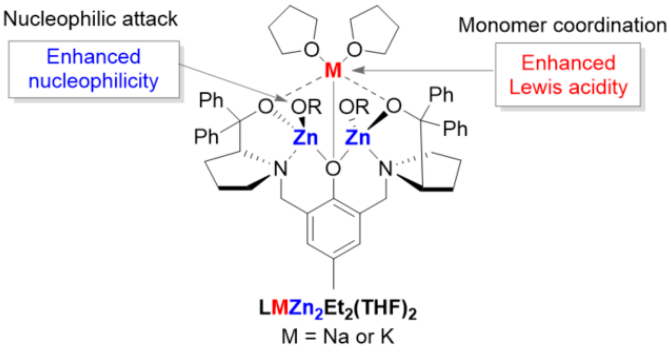

Figure 6.1 Heterometallic cooperativity of complex **$LMZn_2Et_2(THF)_2$** through an "ate" activation
(L = ProPhenol ligand, and M = Na or K).

Despite these clear advantages, the application of heterometallic catalysts in ROP remains relatively underexplored. During the six months that I spent in Garden's research group, as will be illustrated through this *Chapter,* we expanded the scope of these catalysts, testing for the first time the heterometallic complexes in the polymerization of trimethylene carbonate (TMC) and large-ring macrolactones, specifically pentadecalactone (PDL) and globalide (GLO).

6.2 Results and Discussions

6.2.1 Synthesis of Homo- and Heterometallic Complexes

The synthetic strategy for preparing both homometallic and heterometallic complexes, previously reported in the literature,[5] involves the use of the commercially available chiral ProPhenol ligand. This scaffold, originally developed by Trost and colleagues,[6,7] is particularly advantageous for the construction of multinuclear species: the specific arrangement of donor atoms N_2O_3 creates adjacent coordination pockets, strengthening the proximity of the metal centers required for cooperative catalysis.[7]

As a first step, the homobimetallic species was synthesized through triple deprotonation of the ligand with 2 equivalents of diethylzinc: the reaction was carried out in tetrahydrofuran for 16 hours, proceeding through the elimination of ethane to produce the target ethyl-zinc complex (**Scheme 6.1**).

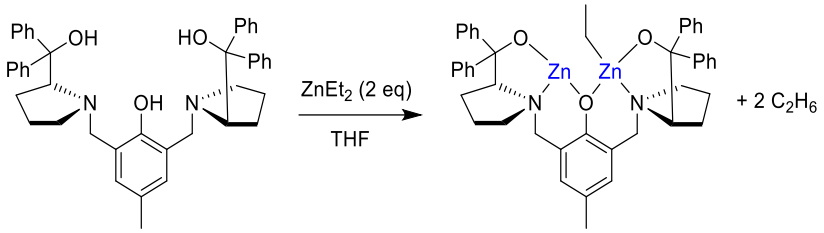

Scheme 6.1: Synthesis of LZn_2Et complex **8**.

After the solvent was removed, the LZn_2Et complex was obtained as a yellow solid (97%) and characterized by NMR spectroscopy: the observed resonances corresponded well with those reported in the literature.[5]

The ^1H NMR spectrum (**Figure 6.2**) highlights the asymmetry of the molecular structure, suggesting the presence of two non-equivalent zinc centers: one zinc site bears a nucleophilic ethyl substituent (resonances at 0.9 and 1.2 ppm), while the second zinc atom is coordinated to a THF molecule, as confirmed by diagnostic NMR resonances at 3.8 and 1.5 ppm.

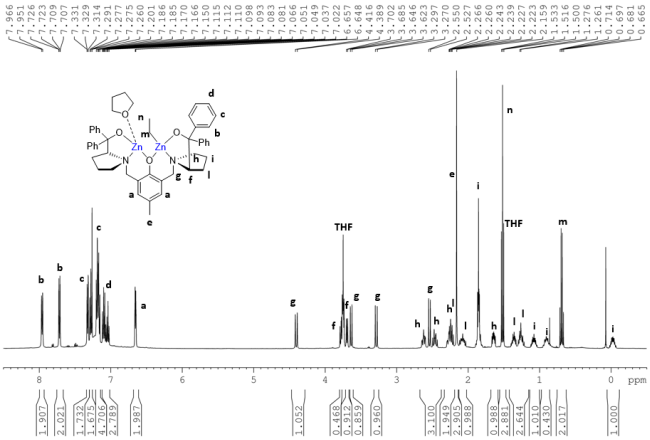

Figure 6.2: ^{1}H-NMR of LZn_2Et complex **8** (Solvent: $CDCl_3$, 500 MHz, 25°C).

The protons in the *ortho* position of the phenyl groups bonded to the chiral centers, labeled **b**, appear as two distinct, deshielded signals around 7.7 and 8.0 ppm, suggesting different chemical environments due to the rigid coordination of the complex. The protons in meta (**c**) and para (**d**) resonate as multiplets around 7.3 ppm and 7.1 ppm, respectively. The singlet signal at 6.7 ppm is assigned to the two aromatic protons **a** on the central ring. The central region of the spectrum identifies the benzene protons and those bonded to the heteroatoms. The **g** protons, which form the methylene bridges between the central phenolic ring and the nitrogen atoms, appear as an AB system at approximately 4.4 ppm and 3.3 ppm: this strong separation indicates that the protons are diastereotopic due to the rigidity of the structure. In the same region, around 3.7 ppm, the **f** signal is found, attributable to protons in the backbone or near the nitrogen. The aliphatic region hosts the remaining signals from the alkyl groups and the saturated backbone. The intense singlet at 2.2 ppm corresponds to the methyl group **e** on the central aromatic ring. Finally, the protons belonging to the saturated rings of the ligand structure, designated **h, l**, and **i**, appear as a series of distributed multiplets.

Subsequently, the tri-heterometallic zinc-based complexes were synthetised, according to the procedure reported in literature (**Scheme 6.2**).[4] First, the monometallic

precursors were synthesized via selective mono-deprotonation of the phenolic –OH group with NaH or KH, respectively, and left to react for one hour, in tetrahydrofuran. After this time, 2 equivalents of diethyl zinc were added to the reaction mixture and left to stir for 1 hour. After removed the solvent, the complexes [$LNaZn_2Et_2(THF)_2$] **9** and [$LKZn_2Et_2(THF)_2$] **10** were obtained as a yellow solid in high yield (90%, 95%, respectively) and characterized by ^{1}H-NMR spectroscopy (**Figure 6.3, 6.4)**.

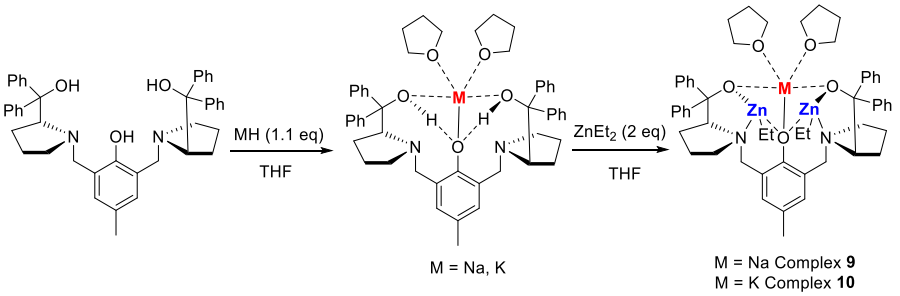

Scheme 6.2: Synthesis of mono and heterometallic complexes.

Both spectra (**Figure 6.3-6.4**) are consistent with the symmetry of C_s, suggesting that each Et_2Zn deprotonates one benzylic O*H* and retains one ethyl group.

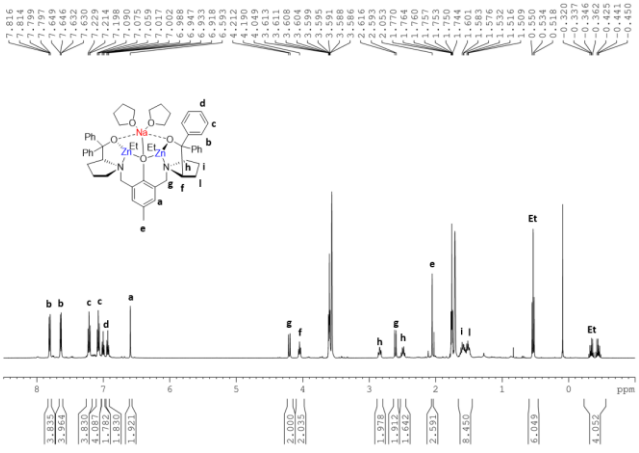

Figure 6.3: ^{1}H-NMR of LZn_2NaEt complex **9** (Solvent: THF-d^8, 500 MHz, 25°C).

In the region between 6.5 and 8.0 ppm, there are signals related to aromatic protons. The protons **b, c**, and **d** on the lateral phenyl rings appear as two distinct signals, due to the asymmetry of the chiral complex. The singlet labeled **a** at approximately 6.6 ppm is attributed to the two aromatic protons on the central phenyl ring. Moving to the region between 2.0 and 4.5 ppm, we observe the methylene protons of the bridge **g**, appearing as two distinct peaks, due to the structural rigidity, following the coordination with the metal precursors. In the same region, we find signals attributable to the protons of the heterocycle. The intense, singlet peak **e** at approximately 2.05 ppm unequivocally corresponds to the methyl group bonded to the central aromatic ring. Finally, signals from the ethyl group (**Et**) bonded directly to the zinc are identified. The peak at around 0.6 ppm is attributable to the terminal methyl group, while the signal that falls in the negative range, around -0.4 ppm, corresponds to the methylene protons directly bound to the metal. Spectra also show coordinated THF signals, which completes the saturation of the alkali metal.

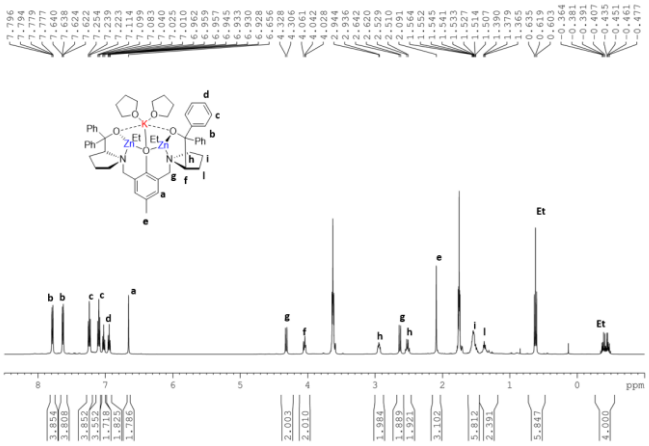

Figure 6.4: ^{1}H-NMR of LZn_2KEt complex **10** (Solvent: THF-d^8, 500 MHz, 25°C).

NMR analysis of the potassium complex confirms its structural similarity to the corresponding sodium analogue. The spectrum is characterized by distinct resonances for the phenyl side groups and the benzyl protons of the methylene bridges, due to the

coordination-induced rigidity of the ligand; furthermore, in this case too, it is possible to distinguish the signals related to the THF coordinated to the alkali metal. However, the replacement of sodium with the bulkier potassium cation induces slight geometric distortions, which cause slight chemical shift changes. This effect is particularly significant for the protons closest to the metal center: specifically, the benzyl protons **g** shifted to 4.3 ppm, compared to 4.2 ppm for the sodium complex, while the methylene protons directly coordinated to the zinc **Et** are further shielded, toward negative values.

6.2.2 Polymerisation of Trimethylene Carbonate

The catalytic investigation began by evaluating the complexes' performance in the ROP of trimethylene carbonate. The experimental data, summarized in **Table 6.1**, highlight the impact of metal cooperativity on reaction efficiency.

Table 6.1. Ring-opening polymerization of TMC by homometallic and heterometallic complexes.

Entry [a]	Comp.	$[TMC]_0$: $[Comp]_0$: $[BnOH]_0$	Temp (°C)	Solvent	Time (min)	Conv [b] (%)	M_n th[c]	M_n exp[d]	$Đ$ [d]
1	**8**	100:1:1	70	Tol	0.2	97	9.9	12.4	1.6
2	**8**	100:1:1	60	THF	5	91	9.3	12.4	1.2
3	**8**	100:1:1	25	THF	5	84	8.6	-	-
4	**9**	100:1:2	25	THF	1	99	5.0	5.7	1.8
5	**10**	100:1:2	25	THF	1	99	5.0	2.3	1.7
6	**8**	500:1:1	25	THF	120	96	49.0	17.4	1.3
7	**9**	500:1:2	25	THF	0.2	99	25.2	12.5	1.7
8	**10**	500:1:2	25	THF	0.5	99	25.3	14.3	1.6
9	**LNa**	500:1:1	25	THF	0.5	16	8.2	3.3	2.2
10	**LK**	500:1:1	25	THF	0.5	76	38.8	21.6	1.5

[a] General conditions: All reactions were carried out in 1.3 mL of solvent; [TMC] = 1.0 M. [**Cat**] = 13.8 x 10^{-6} for Entries 1-4, 2.8 x 10^{-6} for Entries 5-9 [b]Determined by ^{1}H NMR spectral data. [c]M_n^{th} (kDa) = (102,13 x ($[TMC]_0/[Cat]_0$) x TMC) / $[BnOH]_0$. [d]Experimental M_n (in kDa and M_w/M_n ($Đ$)

values were determined by GPC in THF using polystyrene standards and corrected using a factor of 0.56, 0.73 and 0.88 for PTMC (as indicated in the literature for PTMC with theoretical mass lower than 5000, in the range 5000-10000, higher than 10000).[8]

The catalytic performance of the homometallic complex **8** was initially evaluated in toluene at 70 °C, using benzyl alcohol (BnOH) as the initiator. Under these conditions, the system showed remarkable activity, achieving quantitative conversion in just 20 seconds. Next, we tested the complex in solvent of different polarity, such as THF (Entry 2): in this case, we recorded a slight decrease in activity. This is attributed to competitive coordination of the solvent to the metal centers, which compromises monomer coordination. Further experiments performed at 25 °C (Entry 3) confirmed that high conversions (84% in 5 minutes) were maintained: consequently, these milder conditions were selected to evaluate the catalytic performance of the heterometallic complexes.

The introduction of an alkali metal into the molecular scaffold increased the catalytic activity: at 25°C in THF, the heterometallic complexes reached 99% conversions in times less than a minute (Entries 4–5). To assess any differences in activity, the catalyst loading was reduced (Entries 6–8): again, the homometallic complex proved to be the least active, reaching 96% conversion after 2 hours. The heterometallic system **9** achieved complete conversion in only 0.2 minutes (12 seconds), while the analogous **10** showed similar performance, completing the reaction in 0.5 minutes (30 seconds). To rule out the possibility that this activity was driven exclusively by the alkali metals, control experiments were conducted with the monometallic species LNa and LK (Entries 9–10). The low activity observed for these species confirms that the reaction rates of the heterometallic systems result from a cooperative effect between the zinc centers and the alkali metals.

To highlight electronic differences between heterometallic complexes, FT-IR analysis of complex **9** and **10** was performed, in combination with 4-trifluoromethylbenzoic acid. This acid allows the formation of stable carboxylate complexes, which serve as diagnostic indicators. Furthermore, the carboxylate group is extremely sensitive to the electronic environment of the metal and provides clear signals, free from spectral interference.

The analysis focused on the frequency difference Δ between the asymmetric and symmetric stretching modes of the carboxylate group: as reported in the literature,[9–11] this parameter is directly related to the character of the alkali metal-oxygen bond (**Figure 6.5**).

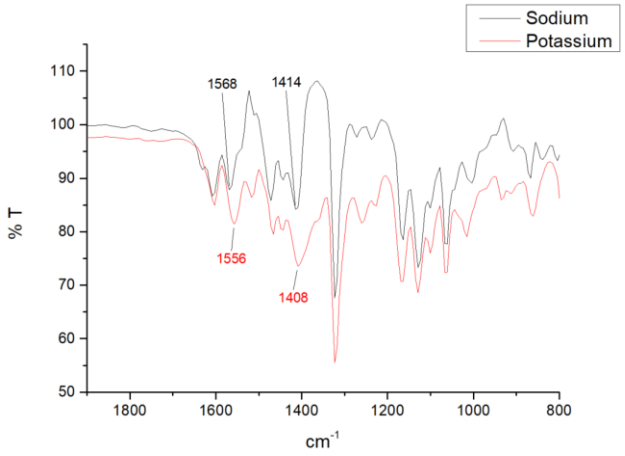

Figure 6.5 FT-IR spectrum of LZn_2NaEt_2 **9** and LZn_2KEt_2 **10** complex, in combination with 4-trifluoromethyl benzoic acid.

For the omplex **9**, the carboxylate bands appeared at 1568.37 cm^{-1} and 1414.38 cm cm^{-1} (Δ = 154.0), while the potassium derivative **10** showed absorptions at 1556.96 cm^{-1} and 1408.68 cm^{-1} (Δ= 148.3 cm). The higher Δ value observed for the sodium-based system indicates a higher charge density and polarizing power compared to potassium. Consequently, after coordination of the monomer, sodium exerts a strong polarizing effect that increases the electrophilicity of the carbonyl carbon, which is more susceptible to nucleophilic attack by the zinc alkoxide group. In contrast, the lower activity of the potassium analogue is attributed to the larger ionic radius and lower charge density. This results in a weaker polarization of the substrate, resulting in less efficient activation of the monomer and a slower polymerization rate.

It is noteworthy that the activity of the complexes could be strongly influenced by the nature of the monomer: actually, in case of the ring-polymerization of L-LA and ε-CL, the

potassium complex exhibits higher reactivity than the sodium analogue, [12] differently from the case of ROP of TMC. This phenomenon highlights the need for further investigation.

Despite the significant catalytic activity, the complexes showed poor control over the polymerization process, evidenced by dispersity values and the substantial discrepancy between the theoretical and experimental molecular weights: this phenomena has been already reported for other ROP polymerisation catalysed by heterobimetallic Trost-ligand complexes.[13]

Further insights were provided by MALDI-FT-ICR analysis, conducted on a PTMC sample at low molecular weight, obtained from using complex **8** in combination with BnOH. The spectrum revealed a primary distribution, with mass difference between adjacent peaks of 102.03 Da, confirming the regular incorporation of TMC units: this corresponds to linear chains with benzyloxy chain end-groups. A second, lower-intensity distribution was also detected, corresponding to linear PTMCs with hydroxyl groups at both chain ends (**Figure 6.6**).

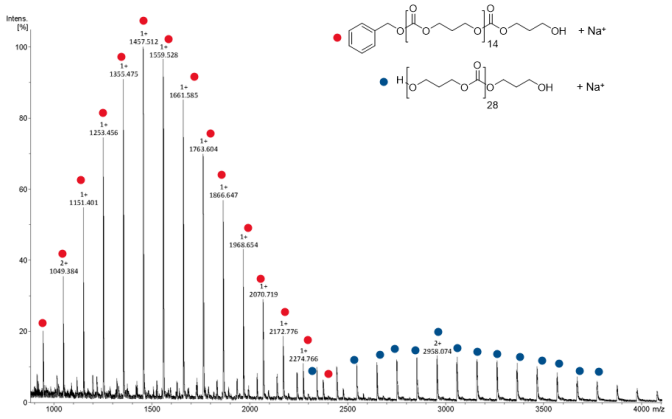

Figure 6.6: MALDI-FT-ICR mass spectrum of the isolated polymer from TMC polymerization. Polymerization conditions: $[TMC]_0$:$[BnOH]_0$:[**8**] = 20:1:1 at 25 °C in THF.

The presence of this second distribution is likely attributed to initiation by the auxiliary ligand, due to the similarity between the Zn-O(ligand) bond and the Zn-OBn species (**Scheme 6.3).** However, following quenching, hydrolysis of the bond between the polymer and the ligand prevents the chain ends from being identified, generating the observed hydroxyl-terminated species.

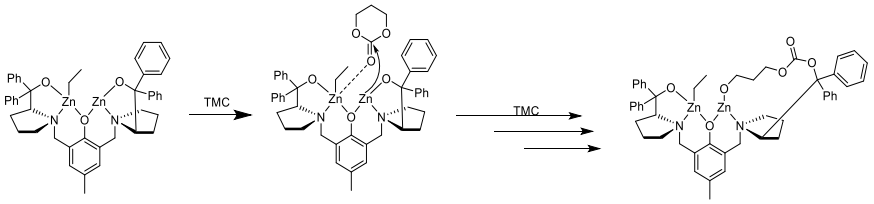

Scheme 6.3: Proposed ligand-mediated polymerisation of PTMC.

A similar ligand involvement has been reported for PLA;[5] however, a notable difference is that, while this exchange typically occurs in the advanced stages of PLA polymerization, our data suggest that in this system the phenomenon occurs during the early stages.

NMR analysis of the isolated polymers ruled out the occurrence of decarboxylation phenomena, as the resonances at 1.8 and 3.4 ppm, characteristic of ether bond signals associated with CO_2 elimination, were absent (**Figure 6.7**). Instead, the spectra displayed the typical polycarbonate pattern (triplet at 4.2 ppm and quintet at 2.0 ppm), with main resonances arising from the polymer backbone. Minor resonances with comparable intensities were attributable to the end groups: signals at 1.9, 3.7, and 4.3 ppm were assigned to the methylene protons at the ω chain end (**Figure 6.7**, protons **d**, **e**, and **f**), while signals at 5.2 and 7.4 ppm were associated with the benzyloxy α chain end (**Figure 6.7**, signals **a** and **Ph**).

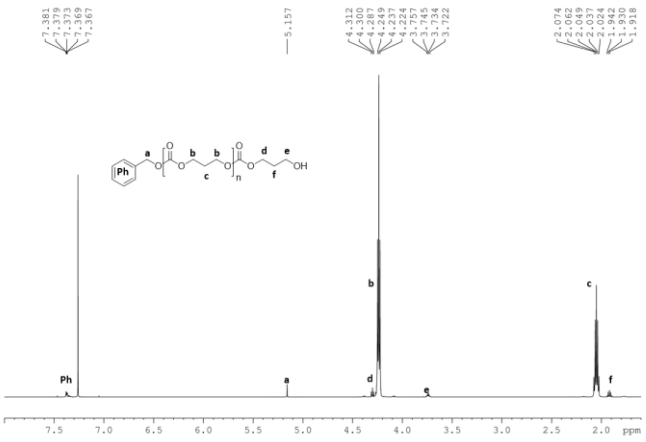

Figure 6.7: ^{1}H NMR spectrum of PTMC with benzyloxy and hydroxylic terminal groups (Solvent $CDCl_3$, 500 MHz, 20 °C).

6.2.3 Polymerisation of Macrolactones

Based on the catalytic activities observed with smaller cyclic esters, the investigation of heterometallic complexes **9** and **10** was extended to the ring-opening polymerization of macrolactones. These bio-derived compounds, traditionally used in the fragrance industry, have attracted considerable attention as monomers for sustainable materials. Through ROP, they produce polyesters with long methylene sequences, conferring thermal and mechanical properties comparable to high-density polyethylene (HDPE), with the crucial added benefit of biodegradability. Since macrolactones exhibits minimal ring strain, the enthalpic contribution during ROP is negligible, and the main driving force is the entropic gain achieved through ring-opening thanks to a greater chain rotation.

We first evaluated the polymerization of pentadecalactone (PDL), a 15 membered saturated macrolactone, promoted by homometallic and heterometallic complexes **(Scheme 6.3)**.

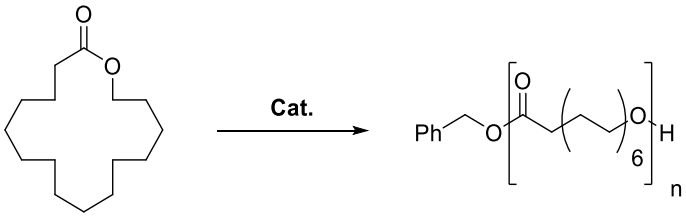

Scheme 6.3: Ring-opening Polymerisation of pentadecalactone (PDL).

Table 6.2. Ring-opening polymerization of pentadecalactone, promoted by complexes **8**-**10**.

Entry[a]	Comp.	$[Mon]_0$: $[Comp.]_0$: $[BnOH]_0$	Mon.	Time (h)	Conv [b] (%)	M_n^{th} [c]	M_n^{exp} [d]	$Đ$[d]
11	**8**	50:1:1	PDL	66	72	8.6	24.6	1.7
12	**9**	50:1:2	PDL	6	93	5.6	16.7	1.6
13	**10**	50:1:2	PDL	17	90	5.4	7.7	1.6
14	**LNa**	50:1:1	PDL	10	60	7.2	8.3	2.5
15	**LK**	50:1:1	PDL	10	-	-	-	-

[a] General conditions: All reactions were carried out in 0.6 mL of Toluene. [Mon] =1 M; [**Cat**] = 13.8 x 10^{-6} mol [b] Determined by ^{1}H NMR spectral data. [c] M_n^{th} (kDa) = (MM_{mon} x ($[Mon]_0/[Cat]_0$) x Conversion) / $[BnOH]_0$. [d] Experimental M_n (in kDa) and M_w/M_n ($Đ$) values were determined by GPC in THF using polystyrene standards.

Initially, the homometallic complex LZn_2Et was evaluated using benzyl alcohol (BnOH) as the initiator in toluene at 70 °C (Entry 11). This system displayed moderate activity, achieving 66% conversion after 72 hours. Upon introducing alkali metals into the scaffold, a pronounced enhancement was observed: the heterometallic LZn_2Na system (Entry 12) reached 93% conversion in just 6 hours, while the LZn_2K complexes reached

90% in 17 hours. As for the polymerisation of TMC, the sodium complex **9** outperforms its potassium analogue **10**, due to sodium's greater charge density and Lewis acidity, which promote monomer coordination. Interestingly, the catalytic activity depends on the substrate: potassium proves more efficient for L-LA and ε-CL,[4] whereas sodium shows higher activity for TMC and PDL. This highlights that catalytic activity relies on a specific match between the metal center and the monomer.

To prove that the increase of polymerisation rate depends on the synergy of different metal centres, the monometallic complexes were tested: in detail, the sodium complex LNa (Entry 14) showed significantly lower performance (60% conversion in 10 hours), while LK complex was totally inactive (Entry 15). This underscores the essential role of zinc in the catalytic cycle.

Kinetic studies on PDL polymerization were conducted by monitoring the reaction via NMR spectroscopy (**Table 6.4**). As shown in **Figure 6.8**, a linear relationship indicates a first-order dependence on monomer concentration for all complexes.

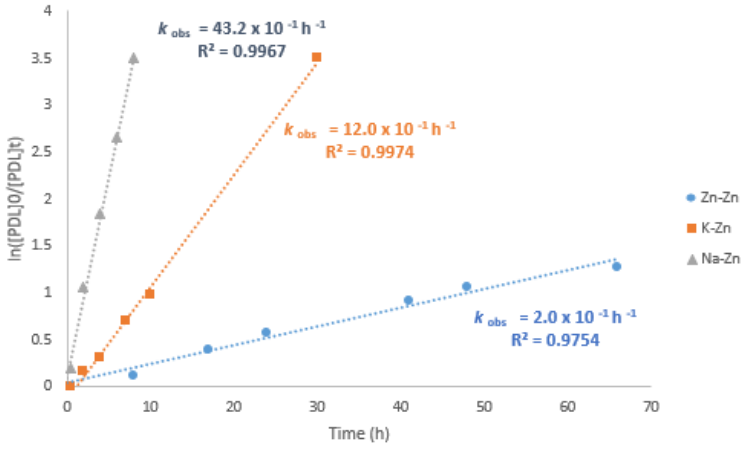

Figure 6.8: First-order kinetic plots for the consumption of PDL by complex **8** (blue circles), **9** (grey triangle) and **10** (orange square), in combination with BnOH.

The resulting polymers were characterized by NMR spectroscopy (**Figure 6.9** and **Figure 6.14**): minor resonances were attributable to the end groups, such as signals at 7.4 ppm

and 5.1 ppm, related the benzyloxy α chain end, derived from the initiator (signals **a** and **Ph**), and at 3.7 ppm, related to the methylene protons at the ω chain end. The main resonances resonate at 4.1 ppm and 2.3 ppm, associated to the methylene protons near the carbonyl groups and oxygen atom, while methylene protons of long aliphatic chain are centered at 1.6 and 1.3 ppm.

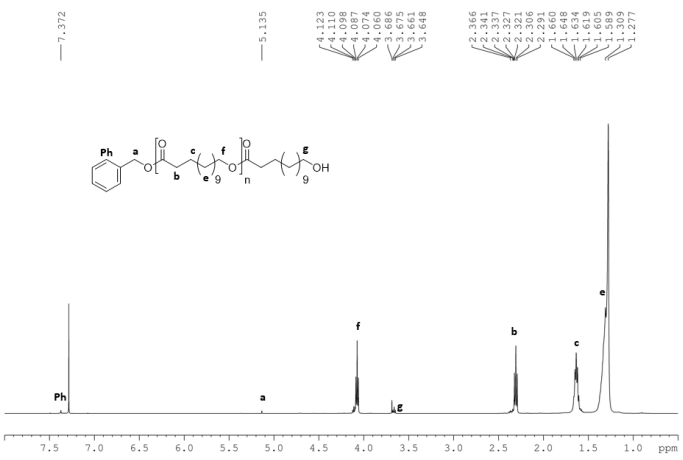

Figure 6.9: ^{1}H NMR spectrum of poly(PDL) with benzyloxy and hydroxylic terminal groups (Solvent $CDCl_3$, 500 MHz, 20 °C).

As detailed in **Table 6.2**, experimental molecular weights are higher than theoretical values, accompanied by high dispersity. This discrepancy is well documented in the literature for these classes of monomers, [14] where the high flexibility of the aliphatic polymer chain makes these systems susceptible to concomitant transesterification processes, such as intramolecular backbiting and intermolecular chain redistribution. To verify the presence of these species, MALDI-FT-ICR analysis was performed on low molecular weight poly(pentadecalactone) samples (**Figure 6.10**).

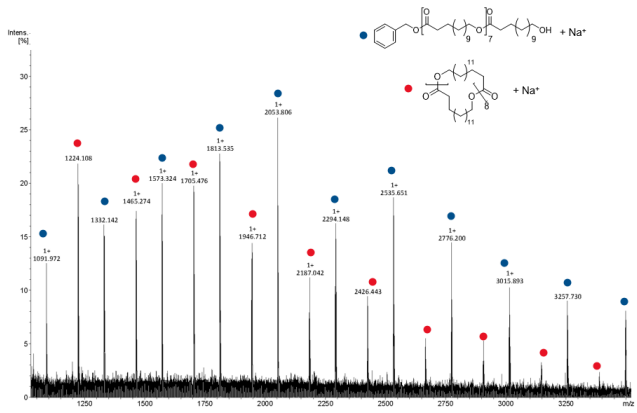

Figure 6.10: MALDI-FT-ICR mass spectrum of the isolated polymer from PDL polymerization. Polymerization conditions: $[PDL]_0$:$[BnOH]_0$:[**8**] = 20:1:1 at 70 °C in Toluene.

The mass spectrum reveals two distinct distributions, each separated 240 Da, consistent with the repeating unit of PDL. The predominant series is attributed to linear PPDL chains end-capped with a benzyloxy group, while a secondary, less intense distribution corresponds instead to cyclic PPDLs lacking terminal groups. The occurrence of these cyclic species confirmed the coexistence of cyclic oligomers, formed via intramolecular transesterification.

Encouraged by the catalytic performance obtained with PDL, the scope of the study was extended to globalide (GLO), a 15-membered macrolactone with an internal C=C double bond, at the C4 position **(Scheme 6.4)**. This monomer represents a highly interesting target because its polymerization yields unsaturated polyesters, which are valuable materials whose internal double bonds provide unique sites for post-polymerization functionalization.

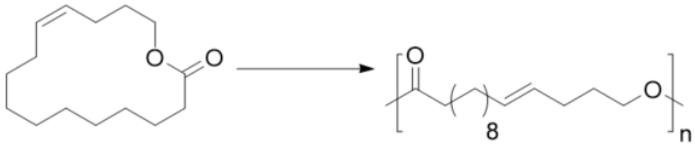

Scheme 6.4: Ring-opening Polymerization of globalide (GLO).

It is worthy to know that the polymerisation of this compound has been widely explored just using enzymatic systems or Brønsted acid catalysis, while the application of organometallic compounds remains unexplored. [15] Therefore, the results presented herein represent the first example of homo- and heterometallic catalysts successfully applied to the polymerization of this unsaturated macrolactone.

Table 6.3. Ring-opening polymerization of globalide catalysed by complexes **8-10.**

Entry[a]	Comp.	$[Mon]_0$: $[Comp]_0$: $[BnOH]_0$	Mon.	Time (h)	Conv [b] (%)	M_n^{th} [c]	M_n^{exp} [d]	$Đ$[d]
16	**8**	50:1:1	GLO	10	40	4.8	-	-
17	**9**	50:1:2	GLO	13	88	10.5	10.2	1.8
18	**10**	50:1:2	GLO	10	83	9.8	8.3	1.8
19	**LNa**	50:1:1	GLO	8	6	-	-	-
20	**LK**	50:1:1	GLO	8	0	-	-	-

[a]General conditions: All reactions were carried out in 0.6 mL of Toluene. [Mon] =1 ; [**Comp**] = 13.8 x 10^{-6} mol [b]Determined by ^{1}H NMR spectral data. [c]M_n^{th} (kDa) = (MM_{mon} x ($[Mon]_0/[Cat]_0$) x Conversion) / $[BnOH]_0$. [d]Experimental M_n (in kDa) and M_w/M_n ($Đ$) values were determined by GPC in THF using polystyrene standards.

First, the homometallic zinc complex **8** (Entry 16) was tested in toluene at 70 °C, reaching 40% of conversion. A marked improvement was observed switching to the heterometallic complexes. Both heterometallic complexes achieved conversions exceeding 80%, demonstrating the powerful synergistic effect of the heterometallic core. Specifically, complex **9** reached 88% conversion in 13 hours (Entry 17), while complex **10** reached 83% conversion in just 10 hours (Entry 18). To verify that these results depend on cooperative effects, monometallic complexes were tested under identical conditions (Entries 19-20). The almost complete lack of reactivity confirms that alkali metal centers alone are insufficient to activate the macrolactone, highlighting that the combination with a zinc center is essential for the catalysis.

Resulting poly(globalide) were characterized by NMR spectroscopy and GPC analysis (**Figure 6.11**). The aromatic protons of the benzyl initiator appear at 7.4 ppm (**Ph**), while the benzylic methylene protons adjacent to the ester group are observed at 5.1 ppm (**a**). This signal unambiguously confirms the presence of the benzyl ester end group derived from the initiator. A distinctive feature of this polymer backbone is the presence of unsaturation, confirmed by the signals at 5.3–5.5 ppm (**d-e**), which are assigned to the olefinic protons of the double bond. The methylene protons adjacent to the ester oxygen atom resonate at 4.1 ppm (**h**), whereas the methylene protons alpha to the carbonyl group are detected at 2.3 ppm (**b**). Furthermore, the allylic methylene protons are observed at 2.0 ppm and at 1.6 ppm (**c**-**f**). Finally, the broad signals centered at 1.3 ppm (**g**) corresponds to the long aliphatic segments of the repeating unit.

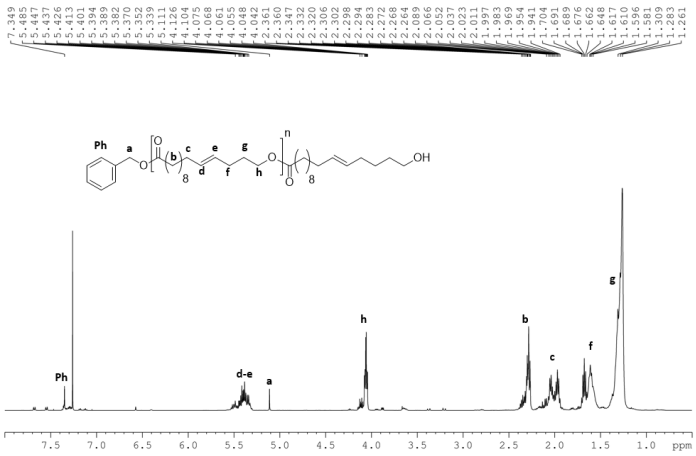

Figure 6.11: ^{1}H NMR spectrum of poly(GLO) with benzyloxy and hydroxylic terminal groups (Solvent $CDCl_3$, 500 MHz, 20 °C).

Experimental molecular weights, determined relative to polystyrene standards, showed a remarkably close agreement with theoretical values. However, since these values are uncorrected, future work will aim to determine specific correction factors to probe the absolute molecular masses and assess the degree of polymerization control.

Kinetic studies were performed by monitoring monomer consumption via NMR (**Table 6.5**). The linear plots confirm a pseudo first-order dependence on monomer concentration for the active species. (**Figure 6.12**)

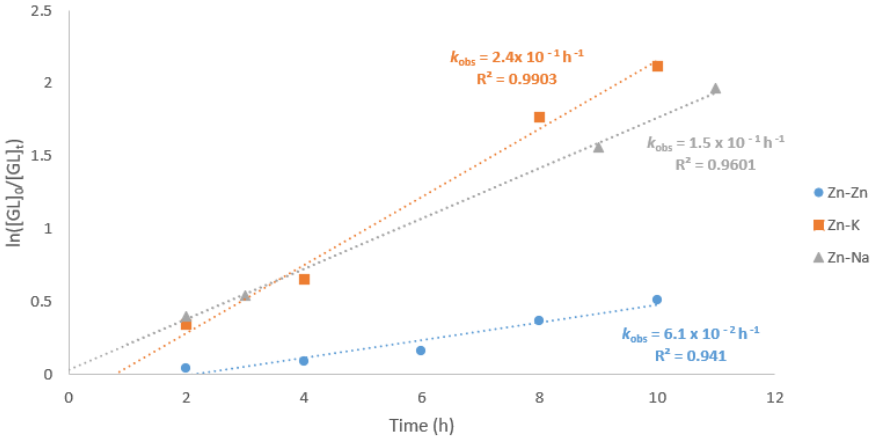

Figure 6.12: First-order kinetic plots for the consumption of globalide by complex LZn_2Et **8** (blue circles), LZn_2NaEt_2 **9** (grey triangle) and LZn_2KEt_2 **10** (orange square), in combination with BnOH.

In the case of PDL, the sodium-based heterobimetallic complex was the most active, while for globalide, this trend was reversed, with the potassium-based catalyst being slightly more efficient. This result led us to hypothesize that the presence of unsaturation critically alters the activation mechanism: in particular, potassium, with its larger ionic radius and softer Lewis acid character, is uniquely able to efficiently coordinate both the carbonyl oxygen and the olefinic moiety through π interactions.[16] This extensive double-site coordination may allow the large macrocyclic monomer to be guided toward an optimal conformation for nucleophilic attack. In contrast, sodium, although a stronger Lewis acid for the carbonyl, has a smaller ionic radius that imposes a significantly narrower and more constrained coordination sphere. We propose that, as polymerization proceeds, this spatial constraint leads to excessive steric crowding around the metal center, not able to accommodate both the monomer and the growing polymer chain, resulting in decreased activity.

6.3 Conclusions

This chapter describes the synthesis of a family of zinc-based homo- and heterometallic complexes, supported by the chiral ligand ProPhenol, and their evaluation in the ring-opening polymerization (ROP) of cyclic carbonates and macrolactones. These heterometallic systems LZn_2NaEt and LZn_2KEt outperform their homometallic analogues homo-bimetallic complex LZn_2Et, as recorded in the case of other cyclic monomers, such as lactide, caprolactone and valerolactone.[4] This marked superiority is attributed to a synergistic cooperation between the two metal centers, where alkali metal increases the electrophilicity of the carbonyl carbon of the monomer, which became more susceptible to nucleophilic attack by the zinc alkoxide group.

For the polymerization of trimethylene carbonate (TMC), the LZn_2NaEt_2 heterobimetallic complex achieved complete monomer conversion in a few seconds at room temperature, ranking among the most active heterometallic catalysts reported: however, all complexes showed a discrepancy between theoretical and experimental molecular weights. The study was subsequently extended to the polymerization of macrolactones: the LZn_2NaEt_2 system showed higher activity for pentadecalactone, while the LZn_2KEt_2 system showed greater activity for globalide. This reversal in activity is attributed to the presence of the double bond in globalide, which serves as an additional coordination site. In the case of sodium, the interaction with the double bond induces steric congestion, due to its smaller coordination sphere. Conversely, the more expanded coordination sphere of potassium allows the metal to accommodate the π interaction with the double bond, minimizing steric hindrance.

6.4 Experimental Part

All manipulations requiring inert conditions were performed under an argon atmosphere using standard Schlenk techniques or in a glove box. All reagents and solvents were obtained from Sigma Aldrich, Fischer Scientific, Honeywell or Acros Organics and were used without further purification unless described otherwise. Dry THF, toluene and hexane were collected from a solvent purification system (Innovative Technologies), dried over activated 4 Å molecular sieves and stored under argon. THF-d^8 and toluene-d^8 NMR solvents for NMR were degassed by three freeze-pump-thaw cycles and stored over activated 4 Å molecular sieves under argon. Trimethylene carbonate (TMC) and pentadecalactone (PDL) was purified by double recrystallisation from tetrahydrofuran and toluene, respectively. Globalide (GLO) and benzyl alcohol (BnOH) were dried over CaH_2 and distilled under reduced pressure prior to use. ^1H, ^{13}C and ^{2D} NMR (COSY, HSQC and DOSY) spectra were recorded on a Bruker AVA500, PRO500, AVA400 and AVA600 spectrometers at 25°C at 400 MHz, 500 MHz and 600 MHz and referenced to the residual solvent peaks (^1H: δ 3.58 for THF- d^8 and δ 2.08 for toluene- d^8, ^{13}C: δ 67.21 for THF- d^8 and δ 137.48 for toluene- d^8). APPI-MS analysis was performed using a Bruker Daltonics 12T SolariX Fourier Transform Ion Cyclotron Resonance Mass Spectrometer using atmospheric pressure photoionisation (APPI). GPC analyses of the filtered polymer samples were carried out in GPC grade THF at a flow rate of 1 mL min^{-1} at 35 °C on a 1260 Infinity II GPC/GPCsingle detection system with mixed bed C PLgel columns (300 x 7.5 mm). MALDI-FT-ICR MS analyses were performed using a Bruker Daltonics UltrafleXtreme™ MALDITOF/TOF MS instrument. The sample to be analysed, dithranol matrix and KI (cationising agent) were dissolved in THF at 10 mg mL^{-1} and the solutions were mixed in a 2:2:1 volume ratio, respectively. A droplet (2 µL) of the resultant mixture was spotted on to the sample plate and submitted for MALDI-FT-ICR MS analysis.

6.4.1 Synthesis of complexes

For the synthesis of LZn_2Et complex, (S,S)-(+)-2,6-bis[2-(hydroxydiphenylmethyl)-1-pyrrolidinyl-methyl]-4-methylphenol (1.00 g, 1.57 mmol) was weighed into a Schlenk flask and dissolved in dry THF (15 mL) in the glove box. $ZnEt_2$ (0.32 mL, 3.13 mmol) was added dropwise into a vial with dry THF (5 mL) in the glove box. The resulting $ZnEt_2$ solution was then added dropwise into the ligand solution and the resulting mixture was stirred for 21 h at ambient temperature under an argon atmosphere. THF was subsequently removed *in vacuo* resulting in a pale yellow powder (Yield = 94%). This high isolated yield is in good agreement with previously reported literature values for this complex.[5]

^{1}H NMR (500 MHz, $CDCl_3$) δ 7.96 (d, 2 H), 7.72 (d, 2 H), 7.28-7.33 (m, 4 H), 7.15-7.20 (m, 6 H), 7.02-7.11 (m, 4 H), 6.66 (d, 2 H), 4.41 (d, 1 H), 3.69 (d, 1 H), 3.63 (d, 1 H), 3.28 (d, 1 H), 2.60-2.65 (m, 1 H), 2.54 (d, 1 H), 2.43-2.49 (m, 1 H), 2.20-2.29 (m, 3 H), 2.16 (s, 3 H), 2.03-2.12 (m, 2 H), 1.62-1.66 (m, 1 H), 1.52 (t, 3 H), 1.33-1.40 (m, 1 H), 1.22-1.29 (m, 2 H), 1.05-1.11 (m, 1 H), 0.88-0.95 (m, 1 H), 0.68 (q, 2 H), -0.07-0.01 (m, 1 H).

For the synthesis of LZn_2NaEt_2, (S,S)-(+)-2,6-bis[2-(hydroxydiphenylmethyl)-1-pyrrolidinyl-methyl]-4-methylphenol (1.00 g, 1.57 mmol) was weighed into a Schlenk flask and dissolved in dry THF (20 mL) in the glove box. NaH (41.4 mg, 1.73 mmol) was slowly added into the ligand solution. The resulting mixture was stirred for 2 h at ambient temperature under an argon atmosphere in the glove box. Subsequently, $ZnEt_2$ (154 mg, 1.24 mmol) was added dropwise into a vial with dry THF (2.5 mL) in the glove box and the resulting solution was added dropwise to the reaction mixture. The reaction mixture was stirred for 1 h at ambient temperature under an argon atmosphere in the glove box. THF was subsequently removed in vacuo, resulting in a pale yellow powder (Yield = 64 %) This high isolated yield is in good agreement with previously reported literature values for this complex.[17]

^{1}H NMR (500 MHz, THF-d8) δ 7.82 (dd, 4 H), 7.65 (dd, 4 H), 7.23 (t, 4 H), 7.09 (t, 4 H), 7.02 (t, 2 H), 6.95 (t, 2 H), 6.61 (s, 2 H), 4.22 (d, 2 H), 4.07 (t, 2 H), 3.61-3.63 (m, 8 H), 2.86

(dt, 2 H), 2.62 (d, 2 H), 2.52 (q, 2 H), 2.07 (s, 3 H), 1.76-1.79 (m, 8 H), 1.49-1.66 (m, 8 H), 0.55 (t, 6 H), -0.46- -0.30 (ddq, 4 H).

For the synthesis of LZn_2KEt_2, (S,S)-(+)-2,6-bis[2-(hydroxydiphenylmethyl)-1-pyrrolidinyl-methyl]-4-methylphenol (1.00 g, 1.57 mmol) was weighed into a Schlenk flask and dissolved in dry THF (20 mL) in the glove box. KH (69.3 mg, 1.73 mmol) was slowly added into the ligand solution. The resulting mixture was stirred for 2 h at ambient temperature under an argon atmosphere in the glove box. Subsequently, $ZnEt_2$ (151 mg, 1.22 mmol) was added dropwise into a vial with dry THF (2.5 mL) in the glove box and the resulting solution was added dropwise to the reaction mixture. The reaction mixture was stirred for 1 h at ambient temperature under an argon atmosphere in the glove box. THF was subsequently removed in vacuo, resulting in a dark yellow powder (Yield = 60 %). This high isolated yield is in good agreement with previously reported literature values for this complex. [17]

^{1}H NMR (500 MHz, THF-d8) δ 7.77 (dd, 4 H), 7.61 (dd, 4 H), 7.22 (t, 4 H), 7.08 (t, 4 H), 7.01 (t, 2 H), 6.93 (t, 2 H), 6.64 (s, 2 H), 4.30 (d, 2 H), 4.03 (dd, 2 H), 3.61-3.63 (m, 8 H), 2.93 (dt, 2 H), 2.62 (d, 2 H), 2.52 (q, 2 H), 2.08 (s, 3 H), 1.76-1.78 (m, 8 H), 1.46-1.58 (m, 6 H), 1.33-1.38 (m, 2 H), 0.58 (t, 6 H), -0.52- -0.38 (ddq, 4 H).

6.4.2 Ring-opening Polymerisation of Trimethylene Carbonate

In the glovebox, in an air-tight vial with a magnetic stirrer bar, TMC (100 equiv., 1.39 mmol) and complex (13.9 µmol) were dissolved in dry THF (1.3 mL). The polymerisation was initiated by addition of BnOH, added in a ratio relative to the total number of zinc centers across all complexes. The reaction was subsequently stirred using DrySyn heating blocks at the appropriate temperature for the required time. Upon completion, the reaction was quenched with wet chloroform. The volatiles were removed under compressed air and an aliquot was dissolved in $CDCl_3$ for NMR spectroscopic analysis.

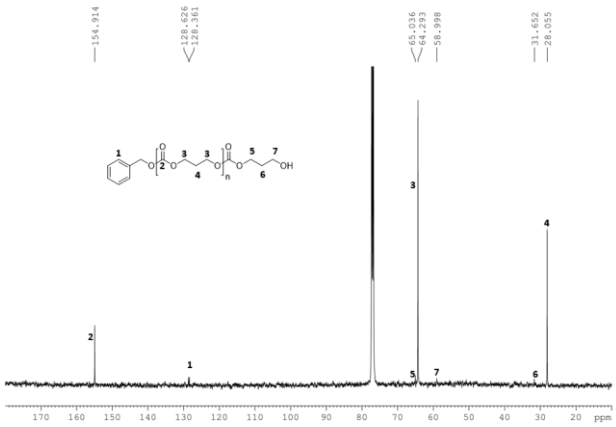

Figure 6.13: ^{13}C-NMR spectrum of poly(TMC) with benzyloxy and hydroxylic terminal groups (Solvent $CDCl_3$, 100 MHz, 20 °C).

6.4.3 Ring-opening Polymerisation of Macrolactones

In the glovebox, in an air-tight vial with a magnetic stirrer bar, macrolactone and complex (13.9 µmol) were dissolved in dry toluene (1.3 mL). The polymerisation was initiated by addition of BnOH, added in a ratio relative to the total number of zinc centers across all complexes. The reaction was subsequently stirred using DrySyn heating blocks at the appropriate temperature for the required time. Upon completion, the reaction was quenched with wet chloroform. The volatiles were removed under compressed air and an aliquot was dissolved in $CDCl_3$ for NMR spectroscopic analysis.

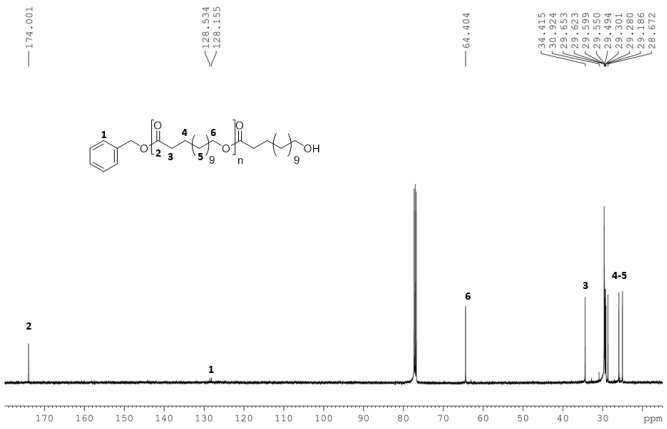

Figure 6.14: ^{13}C-NMR spectrum of poly(PDL) with benzyloxy and hydroxylic terminal groups (Solvent $CDCl_3$, 100 MHz, 20 °C).

Table 6.4. Kinetics of PDL with homo and heterometallic complexes.

Entry	Comp.	$[Mon]_0$: $[Comp]_0$: $[BnOH]_0$	Mon.	Time (h)	Conv[a] (%)
21	**8**	50:1:1	PDL	8	10
				17	32
				24	43
				41	60
				48	65
				66	72
22	**9**	50:1:2	PDL	0.5	18
				2	65
				4	84
				6	93
23	**10**	50:1:2	PDL	0.5	0
				2	15

				4	26
				7	50
				10	62
				17	93
24	**LNa**	50:1:1	PDL	2	12
				4	25
				6	30
				8	47
				10	60

General conditions: All reactions were carried out in 0.6 mL of Toluene. [Mon] =1 ; [**Cat**] = 13.8 x 10^{-6} mol [a]Determined by ^{1}H NMR spectral data.

Table 6.5. Kinetics of GLO with homometallic and heterometallic complexes.

Entry	**Comp.**	**$[Mon]_0$: $[Comp.]_0$: $[BnOH]_0$**	**Mon.**	**Time (h)**	**Conv[a] (%)**
25	**8**	50:1:1	GLO	2	4
				4	9
				6	15
				8	31
				10	40
26	**9**	50:1:2	GLO	1	11
				2	39
				3	45
				7	65
				11	73
				13	88
27	**10**	50:1:2	GLO	1	11
				2	28

				4	50
				6	61
				10	83

General conditions: All reactions were carried out in 0.6 mL of Toluene. [Mon] =1 M ; [**Comp**] = 13.8 x 10^{-6} mol [a]Determined by ^{1}H NMR spectral data.

6.5 References

(1) Kremer, A. B.; Mehrkhodavandi, P. Dinuclear Catalysts for the Ring Opening Polymerization of Lactide. *Coord. Chem. Rev.* **2019**, *380*, 35–57. https://doi.org/10.1016/j.ccr.2018.09.008.

(2) Gruszka, W.; Garden, J. A. Advances in Heterometallic Ring-Opening (Co)Polymerisation Catalysis. *Nat. Commun.* **2021**, *12* (1), 3252. https://doi.org/10.1038/s41467-021-23192-y.

(3) Fazekas, E.; Lowy, P. A.; Abdul Rahman, M.; Lykkeberg, A.; Zhou, Y.; Chambenahalli, R.; Garden, J. A. Main Group Metal Polymerisation Catalysts. *Chem. Soc. Rev.* **2022**, *51* (21), 8793–8814. https://doi.org/10.1039/D2CS00048B.

(4) Gruszka, W.; Lykkeberg, A.; Nichol, G. S.; Shaver, M. P.; Buchard, A.; Garden, J. A. Combining Alkali Metals and Zinc to Harness Heterometallic Cooperativity in Cyclic Ester Ring-Opening Polymerisation. *Chem. Sci.* **2020**, *11* (43), 11785–11790. https://doi.org/10.1039/D0SC04705H.

(5) Gruszka, W.; Walker, L. C.; Shaver, M. P.; Garden, J. A. In Situ Versus Isolated Zinc Catalysts in the Selective Synthesis of Homo and Multi-Block Polyesters. *Macromolecules* **2020**, *53* (11), 4294–4302. https://doi.org/10.1021/acs.macromol.0c00277.

(6) Trost, B. M.; Hung, C.-I. (Joey); Mata, G. Dinuclear Metal-ProPhenol Catalysts: Development and Synthetic Applications. *Angew. Chem. Int. Ed.* **2020**, *59* (11), 4240–4261. https://doi.org/10.1002/anie.201909692.

(7) Trost, B. M.; Bartlett, M. J. ProPhenol-Catalyzed Asymmetric Additions by Spontaneously Assembled Dinuclear Main Group Metal Complexes. *Acc. Chem. Res.* **2015**, *48* (3), 688–701. https://doi.org/10.1021/ar500374r.

(8) *Unprecedented Polymerization of Trimethylene Carbonate Initiated by a Samarium Borohydride Complex: Mechanistic Insights and Copolymerization with ε-Caprolactone - Palard - 2007 - Chemistry – A European Journal - Wiley Online Library*. https://chemistry-

europe.onlinelibrary.wiley.com/doi/10.1002/chem.200600843 (accessed 2025-11-29).

(9) Koczoń, P.; Hrynaszkiewicz, T.; Świsłocka, R.; Samsonowicz, M.; Lewandowski, W. Spectroscopic (Raman, FT-IR, and NMR) Study of Alkaline Metal Nicotinates and Isonicotinates. *Vib. Spectrosc.* **2003**, *33* (1), 215–222. https://doi.org/10.1016/j.vibspec.2003.09.005.

(10) Świsłocka, R.; Samsonowicz, M.; Regulska, E.; Lewandowski, W. Theoretical and Experimental IR, Raman and NMR Spectra in Studying the Electronic Structure of 2-Nitrobenzoates. *Mol. Spectrosc. Mol. Struct. 2006* **2007**, *834–836*, 389–398. https://doi.org/10.1016/j.molstruc.2006.11.044.

(11) Świsłocka, R.; Samsonowicz, M.; Regulska, E.; Lewandowski, W. Molecular Structure of 4-Aminobenzoic Acid Salts with Alkali Metals. *8th Pol. Mol. Spectrosc. Conf.* **2006**, *792–793*, 227–238. https://doi.org/10.1016/j.molstruc.2005.10.060.

(12) Gruszka, W.; Sha, H.; Buchard, A.; Garden, J. A. Heterometallic Cooperativity in Divalent Metal ProPhenol Catalysts: Combining Zinc with Magnesium or Calcium for Cyclic Ester Ring-Opening Polymerisation. *Catal. Sci. Technol.* **2022**, *12* (4), 1070–1079. https://doi.org/10.1039/D1CY01914G.

(13) Abdul Rahman, M.; Neal, T. J.; Garden, J. A. Cooperative Heterometallic Catalysts: Balancing Activity and Control in PCL- *Block* -PLA Copolymer Synthesis. *Chem. Commun.* **2024**, *60* (42), 5530–5533. https://doi.org/10.1039/D4CC01664E.

(14) Pepels, M. P. F.; Hermsen, I.; Noordzij, G. J.; Duchateau, R. Molecular Structure–Catalytic Activity Relationship in the Ring-Opening Polymerization of (Macro)Lactones. *Macromolecules* **2016**, *49* (3), 796–806. https://doi.org/10.1021/acs.macromol.5b02391.

(15) Nifant'ev, I.; Afanaseva, A.; Vinogradov, A.; Ivchenko, P. Unsaturated Macrolactones from Renewable Feedstocks: Synthesis, Ring-Opening Polymerization and Application Prospects. *Int. J. Mol. Sci.* **2025**, *26* (11), 5039. https://doi.org/10.3390/ijms26115039.

(16) Davidson, M. G.; Garcia-Vivo, D.; Kennedy, A. R.; Mulvey, R. E.; Robertson, S. D. Exploiting σ/π Coordination Isomerism to Prepare Homologous Organoalkali Metal (Li, Na, K) Monomers with Identical Ligand Sets. *Chem. – Eur. J.* **2011**, *17* (12), 3364–3369. https://doi.org/10.1002/chem.201003493.

(17) Gaston, A. J.; Greindl, Z.; Morrison, C. A.; Garden, J. A. Cooperative Heterometallic Catalysts for Lactide Ring-Opening Polymerization: Combining Aluminum with Divalent Metals. *Inorg. Chem.* **2021**, *60* (4), 2294–2303. https://doi.org/10.1021/acs.inorgchem.0c03145.

Chapter Seven

Zinc Complexes Supported by Salen-like Ligands for the Synthesis of Aliphatic Polyesters

7.1 Introduction

It is now well established that bimetallic catalysts often outperform their monometallic counterparts:[1 2] this increased activity is primarily attributed to the cooperation between the two metal centers, made possible by the presence of an adequate scaffold capable of optimising it.

Salen-type ligands represent an ideal platform for building these complex systems, as they possess a highly adaptable intrinsic structure that can be tailored to bind two metal centers in a precise and customized geometry.[3] In this context, this chapter describes the design of a new class of hexadentate ligands, characterized by specific dangling amino arms designed to create a secondary coordination pocket. The chapter then describes the first synthetic attempts to isolate the corresponding homo- and heterobimetallic complexes, highlighting their structural differences. Finally, we present preliminary studies on the catalytic performance of the metal complexes in model reactions of interest, such as the ring-opening copolymerization (ROCOP) of anhydrides and epoxides.

7.2 Results and Discussions

7.2.1 Synthesis of the Ligands

The synthetic strategy for the preparation of the hexadentate dianionic ligands is illustrated in **Scheme 7.1.** The ligand design incorporates a flexible achiral bridge, derived from 2,2-dimethyl-1,3-propandiamine, and introduces additional nitrogen donors at the *ortho* position of the phenoxy group. To evaluate the steric and electronic effects of the pendant amino groups, ethyl and methyl groups were chosen as substituents.

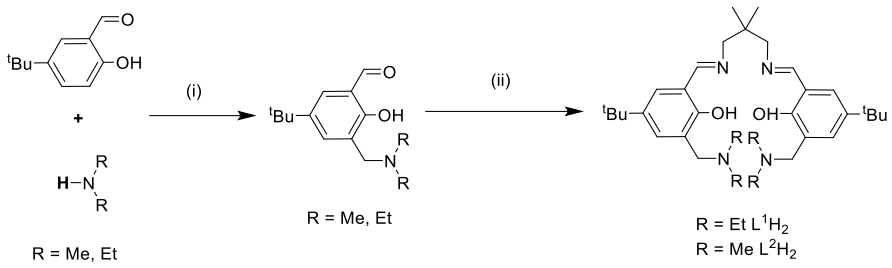

Scheme 7.1. Synthesis of the dianionic hexadentate NONNON ligands. (i) Mannich reaction to introduce the pendant substituent in *ortho* position to the phenolic OH; (ii) condensation with 2,2-dimethyl-1,3-diaminopropane.

The synthesis proceeded via a two-step protocol: first, functionalized salicylaldehyde precursors were prepared via a Mannich reaction according to literature procedures (**Figure 7.9-7.10**).[4] Subsequently, condensation of these aldehydes with 2,2-dimethyl-1,3-diaminopropane yielded the desired proligands L^1H_2 and L^2H_2. Both species were isolated in good yields and fully characterized by ^1H (**Figures 7.1 and 7.2**) and ^{13}C NMR spectroscopy.

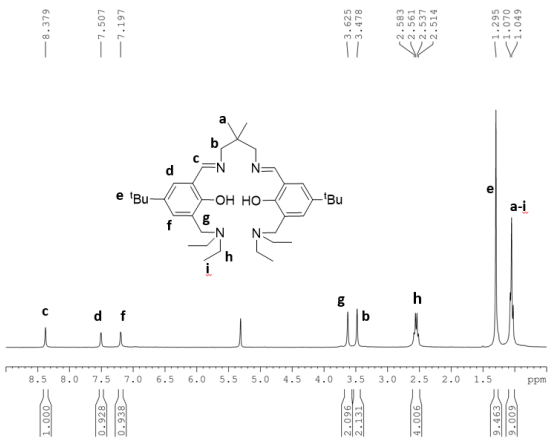

Figure 7.1. ^1H-NMR of L^1H_2 ligand (Solvent CD_2Cl_2, 300 MHz, 25°C).

For ligand L^1H_2, the ^1H NMR spectrum (**Figure 7.1**) reveals a highly symmetric species. In detail, the diagnostic imine proton resonates at 8.4 ppm, while aromatic protons appear at 7.5 and 7.2 ppm. The benzyl methylene protons adjacent to the amino group resonate at 3.6 ppm, while the methylene groups of the propylene bridge appear at 3.5 ppm. The ethyl groups bonded to the amino nitrogen resonate at 2.6 ppm and 1.1 ppm, and the tert-butyl substituent appears at 1.3 ppm. Finally, the dimethyl groups of the backbone resonate at 1.1 ppm.

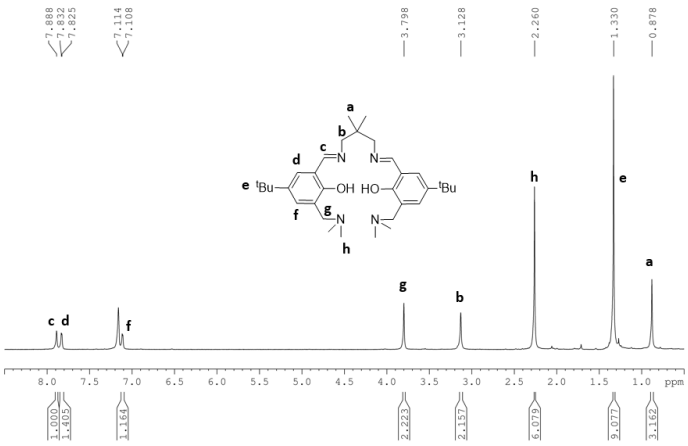

Figure 7.2. ^1H-NMR of L^2H_2 ligand (Solvent $CDCl_3$, 300MHz, 25°C).

Similarly, the ^1H NMR spectrum (**Figure 7.2**) of L^2H_2 showed the imine proton signal at 7.9 ppm. Aromatic protons appear at 7.8 and 7.1 ppm. The benzyl methylene protons adjacent to the amino group resonate at 3.8 ppm, while the methylene groups of the propylene bridge appear at 3.1 ppm. The methyl groups bonded to the amino nitrogen resonate at 2.3 ppm, and the tert-butyl substituents appear at 1.3 ppm. Finally, the dimethyl groups of the aliphatic backbone resonate at 0.9 ppm.

7.2.2 Synthesis of the complexes

The proligands L^1H_2 and L^2H_2 were used to prepare the corresponding homo and heterometallic complexes, represented in the following **Scheme 7.2**.

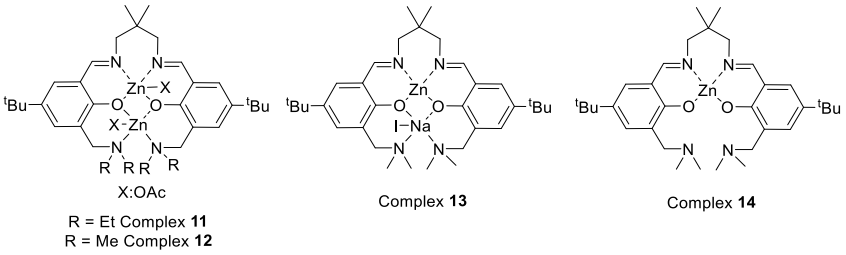

Scheme 7.2 Complexes proposed in this chapter.

The synthesis of the zinc complexes **11** and **12** was accomplished by treating the ligands with 2 equivalents of $Zn(OAc)_2$ in methanol. After 16 hours at room temperature, the methanol was removed under vacuum and the product was crystallized with hexane/THF to remove any impurities including the acetic acid formed as a co-product. The zinc complexes **11-12** appeared as yellow powders (yields: 67 % and 65 %, respectively). The corresponding homobimetallic complexes were characterized by NMR spectroscopy (**Figures 7.3-7.4** and **Figures 7.13-7.22**).

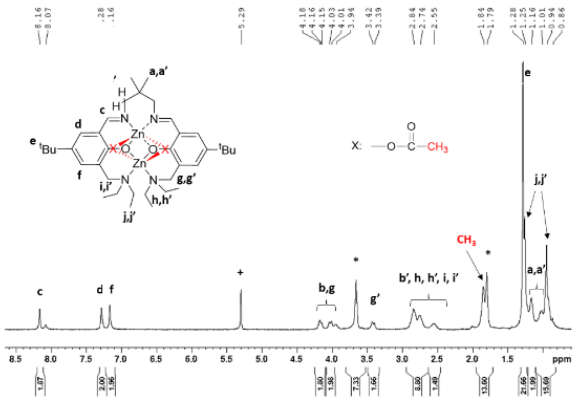

Figure 7.3. ^{1}H NMR spectrum of di-zinc complex **11** (Solvent:CD_2Cl_2, ***THF**, 400 MHz, 25°C).

The ^{1}H NMR spectrum (**Figure 7.3**) of complex **11** showed shifting downfield with respect to the same signals in the spectrum of the free ligand. Particularly, the imine proton resonates at 8.2 ppm, while aromatic protons appear at 7.3 ppm and 7.2 ppm, respectively. The methyl protons of the acetate group coordinated to the zinc of the complex resonates at 1.8 ppm. Finally, the peak at 1.3 ppm corresponds to the protons of ^{t}Bu. The number of signals observed indicates that the complex retains a symmetric structure in solution.

Of particular note is the region between 2.6 and 4.2 ppm, where AB-type patterns relating to the methylene protons are observed. Following complex formation, the coordination of the imino nitrogens induces a structural rigidity that renders the methylene protons and the methyl groups on the aliphatic backbone chemically nonequivalent (**Figure 7.4**).

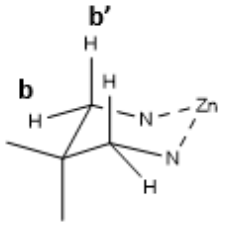

Figure 7.4. 6-membered metallacycle of the first coordination pocket

A similar situation can be observed in the second coordination pocket (**Figure 7.5**), where the coordination of the amino nitrogens to the zinc increases the structural rigidity, also making the methylene protons diastereotopic. This conformational rigidity is clearly reflected in the appearance of two distinct methyl signals between 0.9 and 1.3 ppm, corresponding to ethyl substituents.

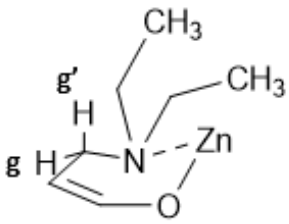

Figure 7.5 6-membered metallacycle of the second coordination pocket.

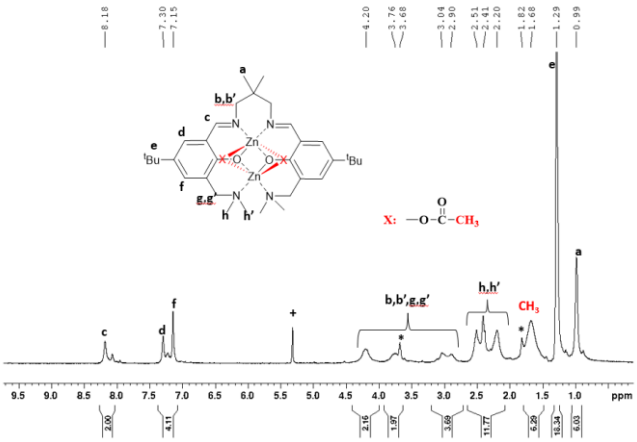

Figure 7.6 ^{1}H NMR spectrum of di-zinc complex **12** (Solvent CD_2Cl_2, *****THF, 300 MHz, 25°C).

In the ^{1}H NMR spectrum of complex **12** (**Figure 7.6**), the imino proton resonates at 8.2 ppm, while the aromatic signals are found at 7.3 and 7.2 ppm, respectively. At 1.7 ppm, the signal of the methyl protons of the acetate is visible. At 1.3 ppm the singlet of the ^{t}Bu group appeared, while at 1.0 ppm the signal of the methyl protons of the aliphatic backbone is observed. As for the previously case, the aliphatic region between 2.9 and 4.2 ppm showed broader signals, related to the methylene protons (**b** and **g**), partially overlapping with the resonances of the residual THF (*). Similarly to what was observed for the previous complex, the coordination of the imino nitrogens generates a rigid pocket, that makes these protons diastereotopic. In the region between 2.2 and 2.5 ppm, the signals of the methyl protons linked to the amino nitrogen (**h, h'**) are identified: also in this case, the coordination of the nitrogen to the zinc blocks the conformation, making the two methyl groups non-equivalent.

A direct comparison between complex **11** and **12** shows that the signals of complex **12** are broader, suggesting a more fluxional behaviour. This dynamism is attributed to the methyl substituents on the additional donors, which introduce both less steric hindrance and a weaker electron-donor effect compared to ethyl groups.

Subsequently, we expanded our investigation by synthesizing the heterobimetallic complex **13**. The procedure consisted of reacting the L^2H_2 ligand with diethylzinc in tetrahydrofuran for 1 hour, followed by the sequential addition of a THF solution of sodium iodide. After solvent removal, the complex was obtained as a white powder (70%) and characterized by ^1H NMR and ^{13}C NMR spectroscopy (**Figure 7.23).**

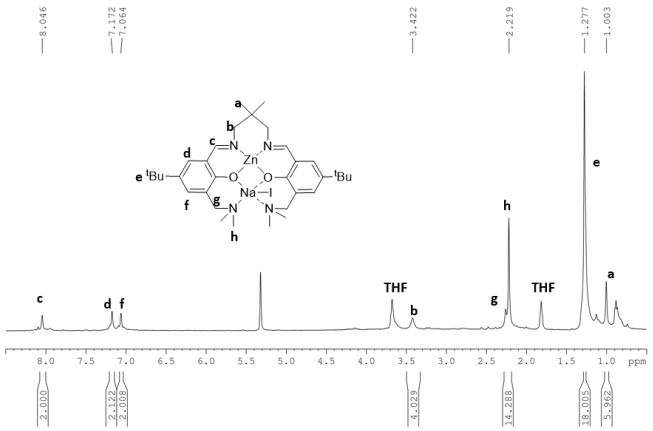

Figure 7.7 ^1H NMR spectrum of zinc-sodium complex **13** (Solvent CD_2Cl_2, 300 MHz, 25°C).

The ^1H NMR spectrum (**Figure 7.7**) shows the imine proton at 8.1 ppm, while in the aromatic region, signals at 7.2 ppm and 7.1 ppm are distinct. In the aliphatic region, the methylene protons bonded to the pendant nitrogen are observed at 3.4 ppm. The methylene protons of the propyl bridge resonate at approximately 2.3 ppm, close to the signal attributable to the methyl groups bonded to the amino nitrogen at 2.2 ppm. At higher fields, the singlet at 1.3 ppm is assigned to the tert-butyl group, while the central methyl protons of the bridge resonate at 1. 0 ppm.

In contrast to the homobimetallic complexes, these spectra do not exhibit signal broadening. This observation supports the hypothesis of a more labile coordination of the zinc center, resulting in a structure with higher fluxionality in solution. Additionally, the persistence of THF signals, observable even after hours of drying, points to a robust

coordination of the solvent to the metal center, which is essential for stabilizing the solution structure.

To exclude the formation of monometallic species in the reactions described above, the analogous monometallic complex was synthesized. The synthesis was accomplished by treating the ligand L^2H_2 with one equivalent of diethylzinc in benzene, for one hour: after solvent removal, the complex was obtained as a yellow powder (yield: 57%) and characterized by ^{1}H NMR (**Figure 7.8**) and ^{13}C NMR spectroscopy (**Figure 7.26**).

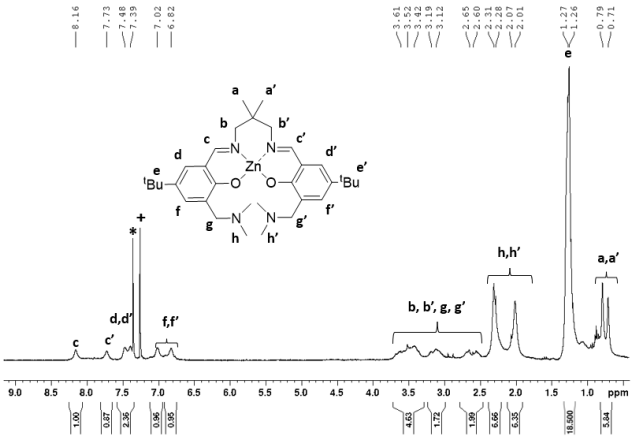

Figure 7.8 ^{1}H NMR spectrum of zinc complex **14** (Solvent: $CDCl_3$, 300 MHz, 25°C).

In the ^{1}H NMR spectrum, the imine protons resonate as two distinct signals at 8.2 and 7.7 ppm. In the aromatic region, the **d** and **d'** protons are found between 7.4 and 7.5 ppm, while **f** and **f'** fall at 6.8 and 7.0 ppm, respectively. The methylene protons of the backbone cover the range 2.6–3.6 ppm. The methyl groups bonded to the amines resonate between 2.0 and 2.3 ppm, while the tert-butyls appear as closely spaced singlets at 1.3 ppm. Finally, the methyls of the propyl bridge (**a** and **a'**) differ markedly at 0.8 ppm.

7.2.3 Studies of Reactivity of Complexes in ROCOP with Phthalic Anhydride and Cyclohexene Oxide

The catalytic potential of the synthesized complexes was evaluated in the Ring-Opening Copolymerization (ROCOP) of phthalic anhydride (PA) and cyclohexene oxide (CHO). The results are summarized in **Table 7.1**.

Table 7.1 Ring-opening copolymerization of cyclohexene oxide and phthalic anhydride by complexes **11-14**.

Entry [a]	**Comp.**	**$[CHO]_0$: $[PA]_0$: $[Comp.]_0$: $[Cocat]_0$**	**Solv. (mL)**	**Cocat**	**Time (h)**	**Conv** [b]**(%)**	**Ester content** [c]**(%)**	M_n th[d]	M_n exp[e]	$Đ$ [e]
1	**11**	100:100:1:0	Tol (1)	/	1.5 24	2 87	- 57	- 21.4	- 5.2	- 1.3
2	**11**	1000:100:1:0	/	/	0.5	99	24	24.6	7.1	1.8
3	**12**	1000:100:1:0	/	/	3 5 7	25 60 82	47 30 26	20.2	4.8	1.8
4	**13**	1000:100:1:0	/	/	3 5 7	30 53 70	99 99 99	19.0	6.8	1.2

5	**13**	1000:100:1:1	/	PPNCl	0.5 1	64 99	99 99	24.6	4.9	1.6
6	**14**	1000:100:1:0	/	/	1 3 4	20 85 99	99 99 99	24.6	7.3	1.4

[a]General conditions: Temperature: 100 °C, cat: 10 µmol. [b]Determined by ^{1}H-NMR spectroscopy ($CDCl_3$) by integrating the normalized resonances for PA (7.97 ppm) and the phenylene signals in the polyester (7.30–7.83 ppm). [c]Determined by ^{1}H-NMR spectroscopy by integrating the normalized resonances for the ester (4.80–5.40 ppm) and ether (3.28–3.86 ppm) bonds. [d]M_n^{th} (kDa) = 246.36 x ([PA]/[CAT]) x PA conversion. [e]The experimental values of M_n (in kDa) and MW/Mn ($Đ$) were determined by GPC in THF using polystyrene standards and corrected using a factor of 1.85.

An initial screening was conducted with the ethyl-substituted homobimetallic complex **11** (Entries 1–2). In the first trial (Entry 1), the reaction was performed in toluene at 100 °C, achieving 87% conversion in 24 hours with moderate selectivity toward the polyester (57%). Subsequently, complex **11** was tested in neat CHO at the same temperature (Entry 2): this resulted in an increase for the activity, reaching 99% of conversion in just 30 minutes. However, under these concentration conditions, a reduction in selectivity to 24% was observed. In both cases, the experimental molecular weights are lower than the theoretical values: this discrepancy, typical of the ROCOP of anhydrides and epoxides, is generally attributed to trace amounts of protic impurities (e.g., 1,2-cyclohexanediol) that act as chain transfer agents, limiting their growth.

Under the same conditions, the methyl-substituted analogue **12** (Entry 3) was significantly slower, reaching 82% conversion in 7 hours, with a similar polyester selectivity (26%). This difference in activity is attributable to the electronic effect of the substituents: the ethyl groups in complex **11** are stronger donors than the methyl groups in complex **12**. This electronic enrichment is believed to enhance the nucleophilicity of the zinc-carboxylate propagating species. Consequently, this facilitates a more rapid

nucleophilic attack on the coordinated epoxide monomer, thereby accelerating the overall polymerization rate.[5]

A surprising result emerged with the heterobimetallic complex **13** (Entry 4). Although the activity was comparable to that of the homobimetallic analogue, the complex showed almost perfect selectivity towards the polyester (99%). This result strongly supports the hypothesis of a synergistic cooperation between the different metal centers, which effectively favours the alternating insertion of monomers while suppressing the formation of ether bonds. Furthermore, the addition of PPNCl as a co-catalyst led to a further increase in activity (99% conversion in 1 h), maintaining high selectivity and highlighting the beneficial role of the external nucleophile in the ring-opening step.

Finally, the monometallic zinc complex **14** was evaluated to clarify the role of the second metal center (Entry 6). Unexpectedly, this system showed greater activity (85% conversion in 3 h) than bimetallic complexes under identical conditions. This behaviour could be due to steric factors: the absence of a second metal center reduces the hindrance around the active site, facilitating monomer coordination. Furthermore, the dangling amino arms, being uncoordinated, can act as internal co-catalysts, promoting the reaction through a cooperative intramolecular mechanism.

7.3 Conclusions

In this chapter, we described the synthesis of a new class of hexadentate dianionic ligands, characterized by a flexible propylene bridge and additional donor nitrogens *ortho* to the phenolic moieties, substituted with an ethyl or methyl group. These scaffolds NONNON allowed the isolation of zinc-based complexes, such as homobimetallic (Zn-Zn), heterobimetallic (Zn-Na), and monometallic species. Preliminary tests of the activity of the four complexes were carried out for the copolymerization of phthalic anhydride (PA) and cyclohexene oxide (CHO). The superior performance of the ethyl-substituted complex compared to the methyl-substituted analogue confirmed that stronger electron-donating groups enhance the nucleophilicity

of the active species, accelerating the polymerization rate. The Zn-Na heterobimetallic complex exhibited higher selectivity than homobimetallic analogue, strongly supporting the hypothesis of a cooperative synergy between the different metals that favours the alternating insertion of the monomers. In contrast, the monometallic complex showed the highest activity among all the tested systems, maintaining high selectivity towards the polyester. This superior performance is attributed to a dual cooperative effect: a significant reduction in steric hindrance caused by the absence of the second metal center, which facilitates monomer coordination, coupled with the intervention of the amino arms as internal co-catalysts, promoting the reaction through a cooperative mechanism.

7.4 Experimental Part

All reactions with substances that are sensitive toward air or moisture were carried out in dried glassware (24 h at 150 °C in an oven or 5 min at 650 °C in a vacuum) under a positive pressure of nitrogen (ca. 1.2 bar). Solvents and reagents were obtained from Merck and used as received unless stated otherwise. Methylene chloride, tetrahydrofuran, benzene, toluene, isopropyl alcohol and hexane used for polymerization experiments and the synthesis of substances unstable toward air and moisture, were distilled prior to use on an opportune drying agent. In particular, THF, toluene, benzene and hexane were dried by refluxing over sodium and benzophenone and stored under nitrogen. Dichloromethane and isopropanol were dried over calcium hydride and distilled prior to use. Methanol, ethanol, n-hexane, and tetrahydrofuran (HPLC grade) were used without further purification. Cyclohexene oxide (CHO) was dried over CaH_2 and distilled under nitrogen. Phthalic anhydride was purified by dissolving it in toluene, filtering off impurities, recrystallizing and then subliming. All dry solvents and monomers were stored under nitrogen. Deuterated solvents for NMR experiments were stored at 20 °C over molecular sieves. NMR spectra were measured with 300/400/600 MHz Bruker AVANCE spectrometers at 20 °C. Chemical shifts δ are given in ppm relative to the residual solvent peak of the used deuterated solvent. Molecular masses (M_n and M_w) and their dispersities (M_w/M_n) were measured by GPC, using THF as the eluent (1.0

mL min^{-1}) and narrow polystyrene standards were used as the reference. MALDI-FT-ICR mass spectra were recorded using a Bruker solariX XR Fourier transform ion cyclotron resonance (FT-ICR) mass spectrometer (Bruker Daltonik GmbH, Bremen, Germany) equipped with a 7 T refrigerated actively shielded superconducting magnet (Bruker Biospin, Wissembourg, France). The samples were prepared at a concentration of 1.0 mg mL^{-1} in THF, while the matrix (DCTB) was mixed at a concentration of 10.0 mg ml^{-1}.

7.4.1 Synthesis of ligands

In a 25 mL two-neck flask, 0.600 mL of diethylamine was added to a suspension of 5-tert-butyl-2-hydroxybenzaldehyde (407 mg, 2.28 mmol) and formaldehyde (370 mg of 37% solution in H_2O, 4.56 mmol) in EtOH (3 mL). The reaction was heated under reflux for 24 h. The resulting product appeared as a yellow oil (Yield = 76%).

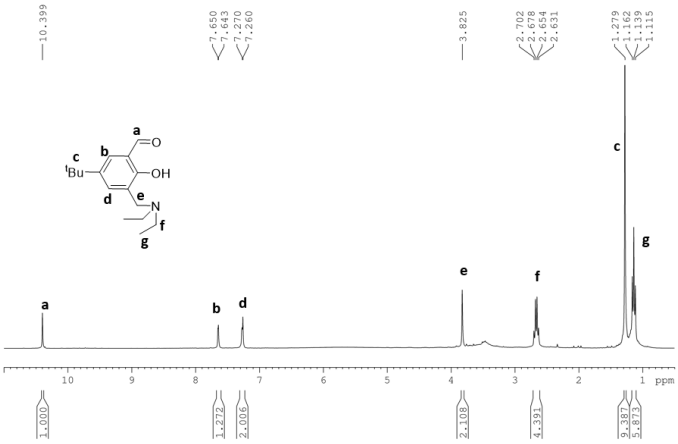

Figure 7.9 ^{1}H-NMR of 5-tert-butyl-2-hydroxy-3-(diethylamino-methyl) benzaldehyde ($CDCl_3$, 300 MHz, 25°C)

^{1}H-NMR (300 MHz, $CDCl_3$, 25 °C): δ (ppm) = 10.40 (1H, CHO), 7.65 (1H, d, CH-Ar), 7.27 (1H, d, CH-Ar), 3.83 (2H, s, CH_2), 2.66 (4H, m, CH_2), 1.28 (9H, s, $^{t-}$Bu), 1.40 (6H, m, CH_3).

In a 25 mL two-neck flask, 515 mg of dimethylamine (40% solution in H_2O, 4.56 mmol) was added to a suspension of 5-tert-butyl-2-hydroxybenzaldehyde (407 mg, 2.28 mmol) and formaldehyde (370 mg of 37% solution in H_2O, 4.56 mmol) in EtOH (3 mL). The reaction was heated under reflux for 24 h. The resulting product appeared as a yellow oil. (Yield = 76%)

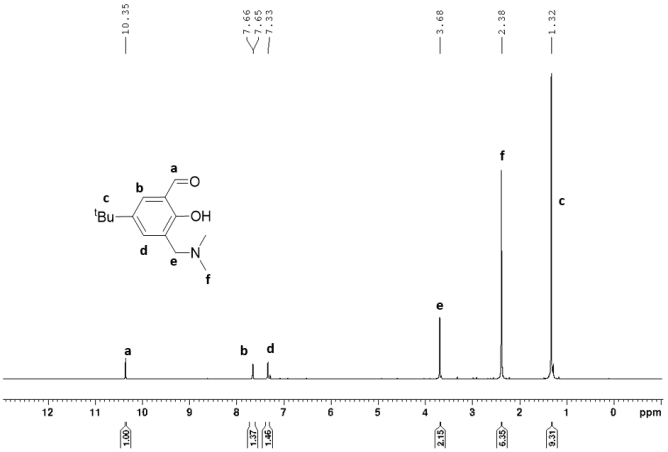

Figure 7.10 ^{1}H-NMR of 5-tert-butyl-2-hydroxy-3-(dimethylamino-methyl) benzaldehyde ($CDCl_3$, 300 MHz, 25°C)

^{1}H-NMR (300 MHz, $CDCl_3$, 25 °C): δ (ppm) = 10.35 (1H, CHO), 7.65-7.67 (1H, d, CH-Ar), 7.33 (1H, d, CH-Ar), 3.68 (2H, s, CH_2), 2.38 (6H, s, CH_3), 1.32 (9H, s, ^{t}Bu).

In a 12 mL vial, 495 mg (1.88 mmol) of 5-tert-butyl-2-hydroxy-3-(diethylaminoethyl)-benzaldehyde were added with 5 mL of EtOH and 108 mg (0.90 mmol) of 2,2-dimethyl-1,3-diaminopropane. The reaction was left under stirring for 24 h at room temperature. The resulting product after removal of the solvent by rotavapor, appeared as a yellow oil and was analysed by NMR in $CDCl_3$ (Yield = 81%).

^{1}H-NMR (300 MHz, $CDCl_3$, 25 °C): δ (ppm) = 13.80 (OH), 8.38 (1H, d, CH-N=), 7.51 (1H, d, CH-Ar), 7.20 (1H, d, CH-Ar), 3.63 (2H, s, CH_2), 3.48 (2H, s, CH_2), 2.54 (4, q, CH_2) 1.30 (9H, s, $^{t-}$Bu), 1.05 (9H, t, CH_3).

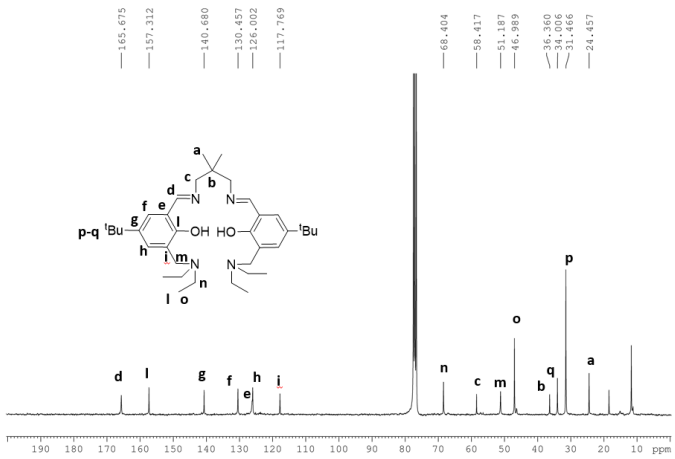

Figure 7.11 ^{13}C-NMR of L^1H_2 ligand (Solvent $CDCl_3$, 100MHz, 25°C).

^{13}C-NMR (100 MHz, $CDCl_3$, 25°C): δ (ppm) = 24.46 ((*C*H$_3$)$_2$-C-(*CH$_3$*)$_2$), 31.47 (C(*C*H$_3$)$_3$), 34.01 (*C*(CH$_3$)$_3$), 36.36 ((CH$_3$)$_2$-*C*-(C*H$_3$*)$_2$), 46.99 (*C*H$_3$-CH$_2$-N), 51.19 (*CH$_2$*-N(CH$_2$CH$_3$)$_2$), 58.42 (*CH$_2$*-N=CH), 68.40 (CH$_3$-*C*H$_2$-N), 117.77 (N-CH$_2$-*C*-Ar), 126.02 (CH-Ar), 126.55 (N=CH-*C*-Ar), 130.46 (CH-Ar), 140.68 (t-Bu-*C*-Ar), 157.31 (O-*C*-Ar), 165.68 (-CH=N-).

In a 12 mL vial, 442 mg (1.88 mmol) of 5-tert-butyl-2-hydroxy-3-(dimethylaminomethyl)-benzaldehyde were added with 5 mL of EtOH and 108 mg (0.90 mmol) of 2,2-dimethyl-1,3-diaminopropane. The reaction was left under stirring for 24 h at room temperature. The resulting product after removal of the solvent by rotavapor, appeared as a yellow oil and was analysed by NMR in $CDCl_3$ (Yield = 81%).

^{1}H-NMR (300 MHz, $CDCl_3$, 25 °C): δ (ppm) = 13.80 (OH), 7.89 (1H, d, CH-N=), 7.83 (1H, d, CH-Ar), 7.11 (1H, d, CH-Ar), 3.80 (2H, s, CH_2), 3.13 (2H, s, CH_2), 2.26 (6H, s, CH_3), 1.33 (9H, s, $^{t-}$Bu), 0.88 (3H, s, CH_3).

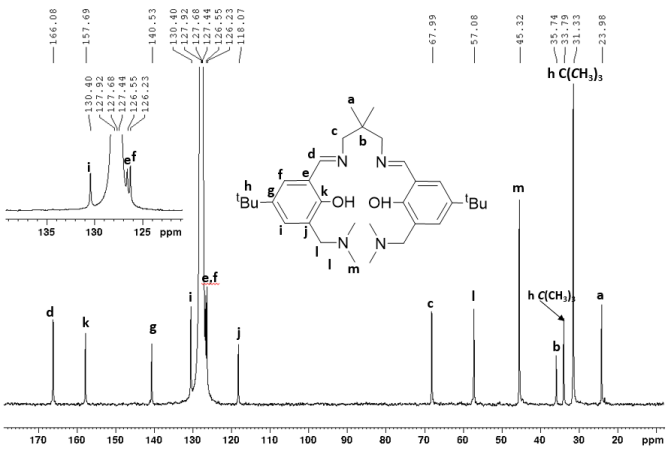

Figure 7.12. ^{13}C-NMR of L^2H_2 ligand (Solvent $CDCl_3$, 100MHz, 25°C).

^{13}C-NMR (400 MHz, $CDCl_3$, 25°C): δ (ppm) = 23.98 ((*C*H_3)$_2$-C-(*CH*$_3$)$_2$), 31.33 (C(*C*H_3)$_3$), 33.79 (*C*(CH$_3$)$_3$), 35.74 ((CH$_3$)$_2$-*C*-(C*H*$_3$)$_2$), 45.32 (CH$_3$-N), 57.08 (*CH*$_2$-N(CH$_3$)$_2$), 67.99 (*CH*$_2$-N=CH), 118.07 (N-CH$_2$-*C*-Ar), 126.23 (CH-Ar), 126.55 (N=CH-*C*-Ar), 130.40 (CH-Ar), 140.55 (^{t}Bu-*C*-Ar), 157.69 (O-*C*-Ar), 166.08 (-CH=N-).

7.4.2 Synthesis of complexes

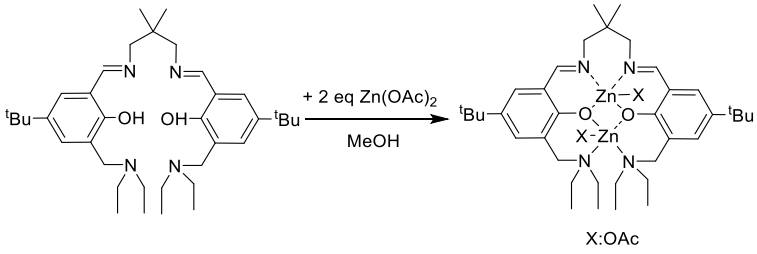

Scheme 7.3: Synthesis of di-Zinc complex **11**.

In two vials, 96.0 mg of L^1H_2 ligand (0.16 mmol) and 58.7 mg of Zn(OAc)$_2$ metal precursor (0.32 mmol) were weighed, dissolved in 3 mL of anhydrous methanol, and the precursor

solution was stirred until an opaque solution was obtained. At this point, the precursor solution was added to the stirring ligand solution. After 16 h, the complex was dried under reduced pressure. The pure product was obtained after washing with hexane followed by crystallization from THF/hexane at −40 °C and characterized by NMR spectroscopy (Yield = 67%).

^{1}H-NMR (400 MHz, CD_2Cl_2, 25 °C): δ (ppm) = 8.16 (2H, HC=N-), 7.28 (2H, s, CH-Ar), 7.16 (2H, s, CH-Ar), 4.18-3.39 (6H, m, *CH*$_2$-N=CH, *CH*$_2$-N-(C_2H_5)$_2$), 2.84-2.55 (10H, m, *CH*$_2$-N=CH, -*CH*$_2$-CH_3), 1.84 (6H, s, -OOC-*CH*$_3$), 1.28 (18H, s, CH_3 (^{t}Bu)), 1.25-0.86 (6H, s, -CH_2-*CH*$_3$; 6H, s, *(CH*$_3$*)*$_2$-C-CH_2-).

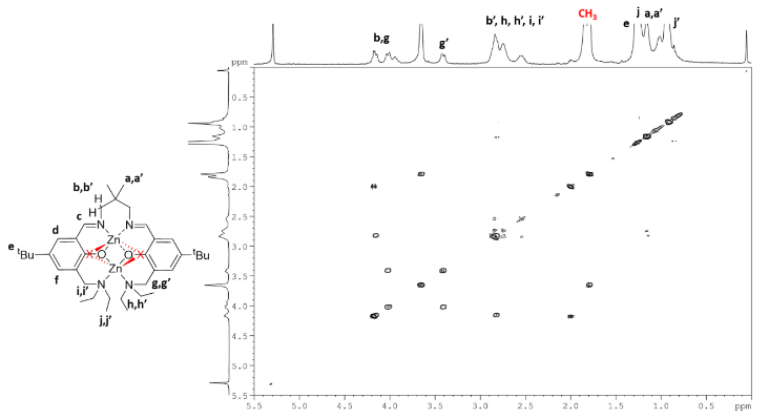

Figure 7.13. 2D-COSY NMR spectrum of complex **11** (Solvent CD_2Cl_2, 25°C, 400 MHz).

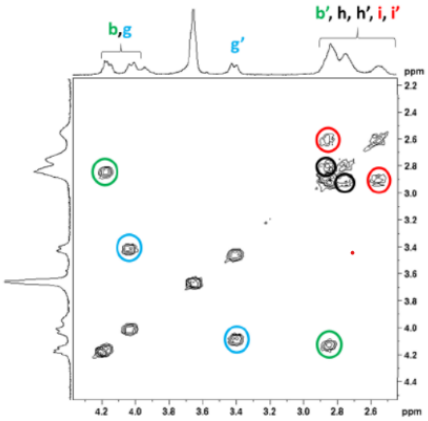

Figure 7.14. Enlargement 2D COSY spectrum of di-Zinc Complex **11**.

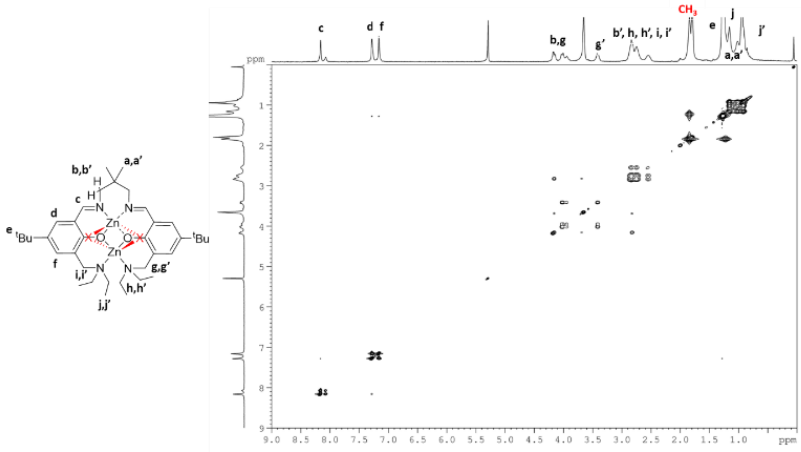

Figure 7.15. 2D-NOESY NMR spectrum of complex **11** (Solvent CD_2Cl_2, 25°C, 400 MHz).

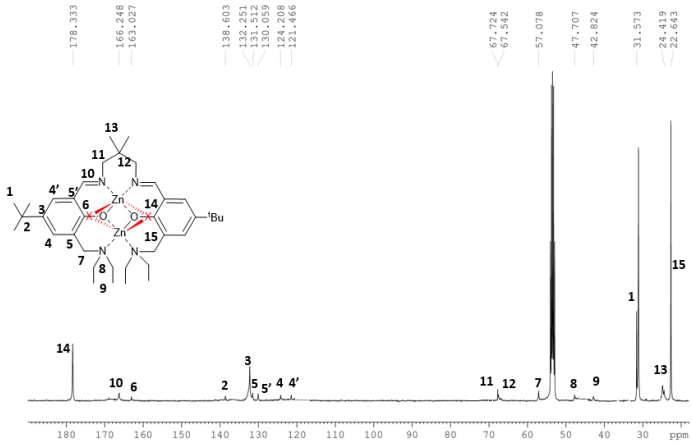

Figure 7.16. ^{13}C NMR spectrum of complex **11** (Solvent CD_2Cl_2, 25°C, 400 MHz).

^{1}H-NMR (400 MHz, CD_2Cl_2, 25 °C): δ (ppm) = 178.33 (CH_3-*C*OO^-), 166.25 (CH), 163.03 (Cq), 138.60 (*C*-^{t}Bu), 132.25 (Cq) 131.51 (Cq), 130.06 (Cq), 124.21 (CH), 121.47 (CH), 67.73 (CH_2-*C*-$(CH_3)_2$), 67.54 (*C*H_2-C-$(CH_3)_2$), 57.08 (*C*H_2-N-$(C_2H_5)_2$), 47.71 (N-(*C*H_2-$CH_3)_2$), 42.82 (N-(CH_2-*C*$H_3)_2$), 31.57 (^{t}Bu), 24.42 (CH_2-C-(*C*$H_3)_2$), 22.64 (*C*H_3-COO^-).

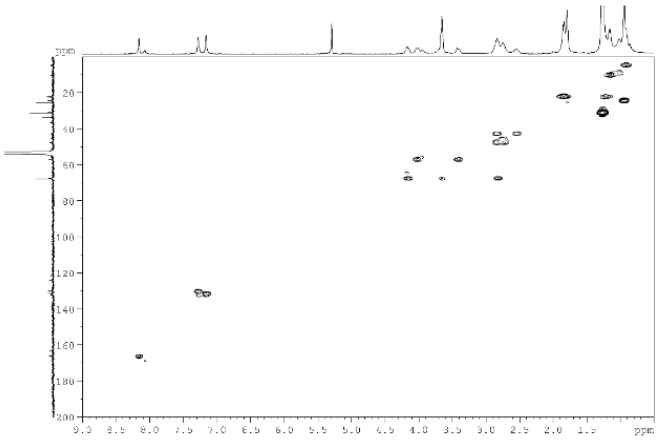

Figure 7.17. 2D-HSQC NMR spectrum of complex **11** (Solvent CD_2Cl_2, 25°C, 400 MHz).

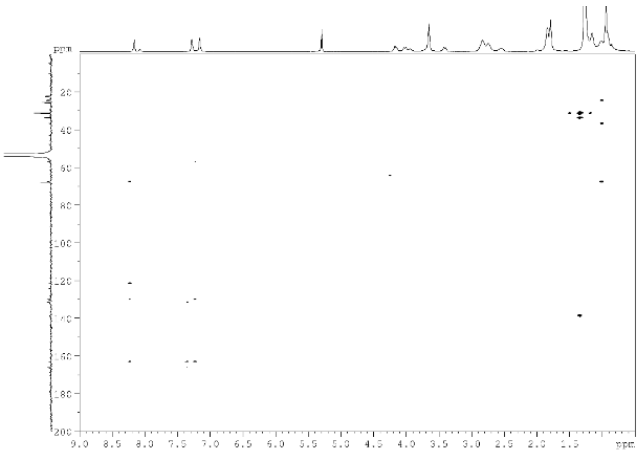

Figure 7.18. 2D-HMBC NMR spectrum of complex **11** (Solvent CD_2Cl_2, 25°C, 400 MHz).

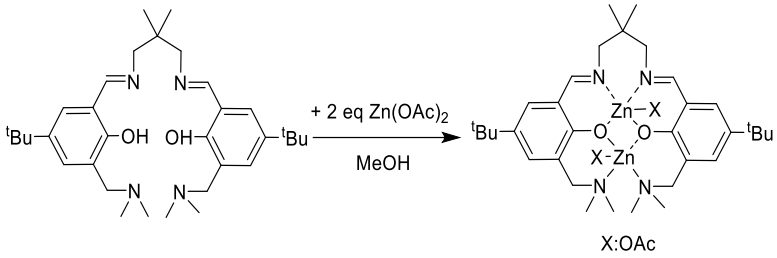

Scheme 7.4: Synthesis of di-Zinc complex **12**.

In two vials, 127.0 mg of L^2H_2 ligand (0.24 mmol) and 88.0 mg of $Zn(OAc)_2$ metal precursor (0.48 mmol) were weighed, dissolved in 13 mL of anhydrous methanol, and the precursor solution was stirred until an opaque solution was obtained. At this point, the precursor solution was added to the stirring ligand solution. After 16 h, the complex was dried under reduced pressure. The pure product was obtained after washing with hexane followed by crystallization from THF/hexane at −40 °C and characterized by NMR spectroscopy. (Yield = 53%)

^{1}H-NMR (400 MHz, CD_2Cl_2, 25 °C): δ (ppm) = 8.18 (2H, -HC=N-), 7.30 (2H, s, CH-Ar), 7.15 (2H, s, CH-Ar), 4.20-2.90 (8H, m, *CH_2*-N=CH, *CH_2*-N-$(CH_3)_2$), 2.51-2.20 (12H, s, -N-$(CH_3)_2$), 1.68 (6H, s, -OOC-CH_3), 1.29 (18H, s, CH_3 (^{t}Bu)), 0.99 (6H, s, CH_2-N-(*CH_3*)$_2$).

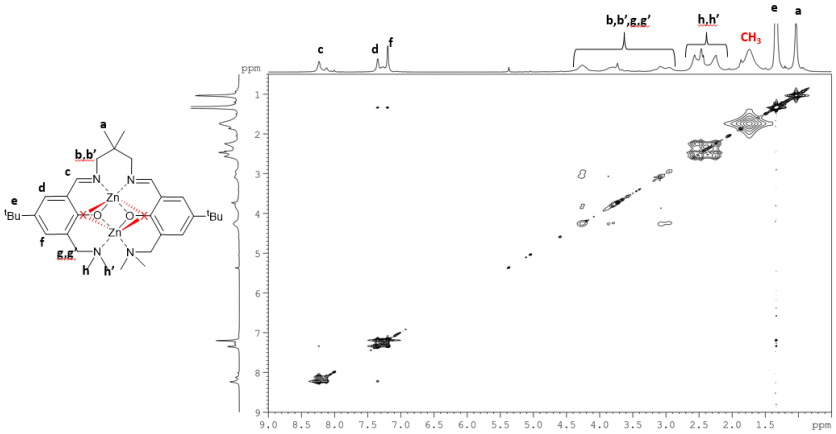

Figure 7.19. 2D-NOESY NMR spectrum of complex **12** (Solvent CD_2Cl_2, 25°C, 400 MHz).

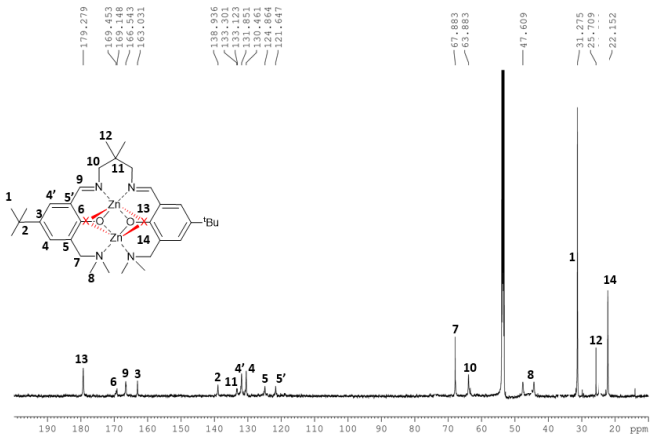

Figure 7.20. ^{13}C NMR spectrum of complex **12** (Solvent CD_2Cl_2, 25°C, 400 MHz).

^{13}C-NMR (100 MHz, CD_2Cl_2, 25 °C): δ (ppm) = 179.28 (CH_3COO^-) , 169.45 (Cq), 169.15, 166.54 (C=N), 163.03 (Cq), 138.94(C-^{t}Bu) ,133.30 (C-$(CH_3)_2$),133.12 (2 CH) ,131.85 (2 CH)

,130.46 (2 CH), 124.86 (Cq), 121.65 (Cq), 67.88 (*C*H_2-N-(CH_3)$_2$), 63.70 (*C*H_2-C-(CH_3)$_2$), 47.61 (-N-(*C*H_3)$_2$), 31.28 (^{t}Bu), 25.71 (-C-(*C*H_3)$_2$), 22.15 (*C*H_3COO^-)

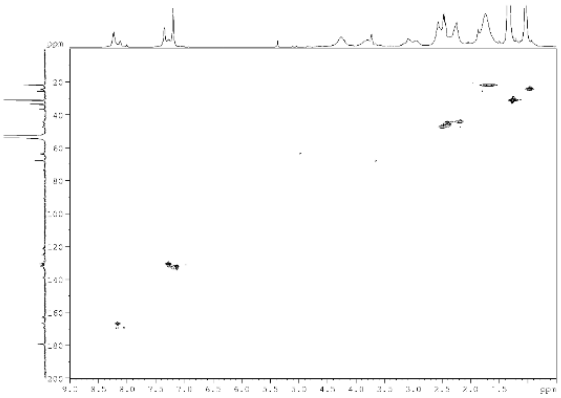

Figure 7.21. 2D-HSQC NMR spectrum of complex **12** (Solvent CD_2Cl_2, 25°C, 400 MHz).

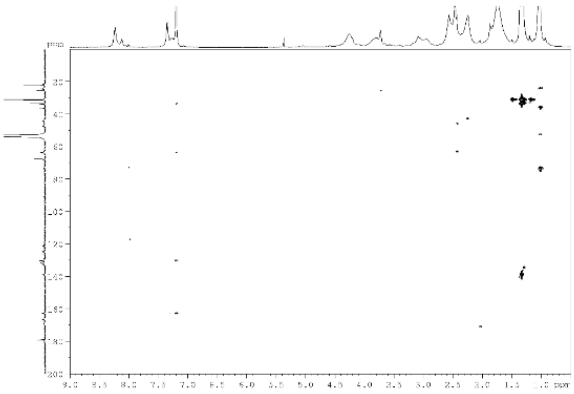

Figure 7.22. 2D-HMBC NMR spectrum of complex **12** (Solvent CD_2Cl_2, 25°C, 400 MHz).

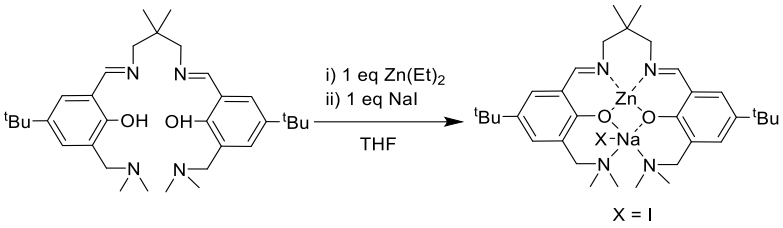

Scheme 7.5: Synthesis of Zinc-Sodium complex **13**.

In a vial, 40 mg of L^2H_2 ligand (74.5 µmol) were dissolved in 3 mL of THF. A 16 mg/3 mL solution of the metal precursor $ZnEt_2$ in anhydrous THF is prepared, 1.7 mL of which is taken and added to the ligand solution and stirred for 1 hour. After 1 hour, 2 mL of a 22.3 mg/4 mL NaI solution (pretreated overnight on sieves in anhydrous THF) was added to the mixture and stirred for approximately 30 minutes at room temperature. The solvent is then removed under reduced pressure, yielding a yellow powdery solid. The complex was analyzed by ^{1}H-NMR (Yield = 61%).

^{1}H-NMR (400 MHz, CD_2Cl_2, 25 °C): δ (ppm) 8.05 (2H, -HC=N-), 7.17 (2H, s, CH-Ar), 7.06 (2H, s, CH-Ar), 3.42 (4H, s, Ar-CH_2-N), 2.26-2.22 (4H, s, CH_2-N=CH; 12H, s, -N-$(CH_3)_2$), 1.28 (18H, s, CH_3 (^{t}Bu)), 1.00 (6H, s, $(CH_3)_2$-C-CH_2).

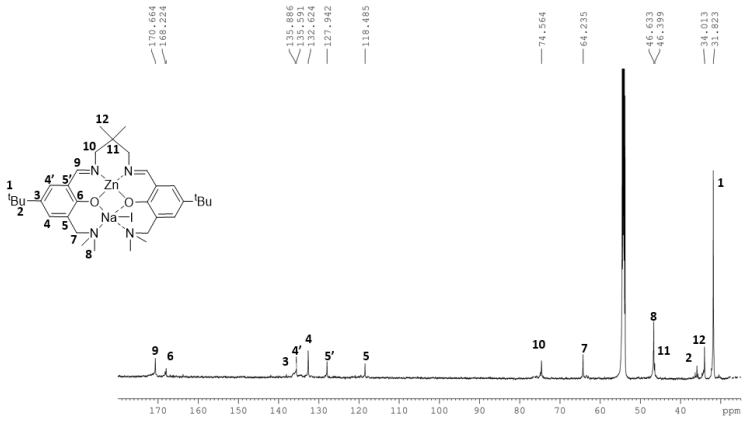

Figure 7.23. ^{13}C NMR spectrum of complex **13** (Solvent CD_2Cl_2, 25°C, 400 MHz).

^{13}C-NMR (100 MHz, CD_2Cl_2, 25 °C): δ (ppm) = 170.66 (C=N) , 168.22 (Cq), 135.88 (C-^{t}Bu), 135.59 (CH), 132.63 (CH) ,127.94 (Cq), 118.49 (Cq), 74.56 (*C*H_2-C-(CH_3)$_2$), 64.23 (*C*H_2-N-(CH_3)$_2$), 46.63 (-N-(*C*H_3)$_2$), 46.40 (-C-(*C*H_3)$_2$), 34.01 (-C-(*C*H_3)$_2$), 31.82 (^{t}Bu).

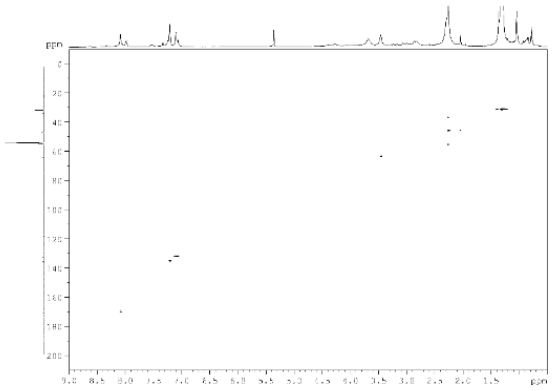

Figure 7.24 2D-HSQC NMR spectrum of complex **13** (Solvent CD_2Cl_2, 25°C, 400 MHz).

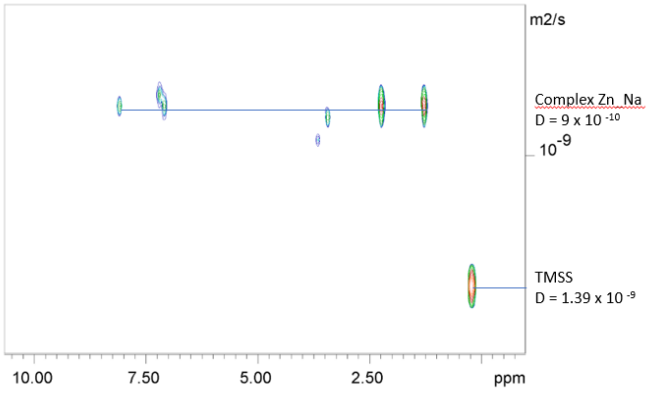

Figure 7.25. DOSY spectrum (CD_2Cl_2, 25°C, 600 MHz) of complex Zn_Na (D = 9 x 10^{-10} m^2 /s) in the presence of TMSS as standard (D = 1.4 10^{-9} m^2 /s). (Molecular weight of TMSS = 320.84 Da; estimated mass for complex **13** = 750 Da).

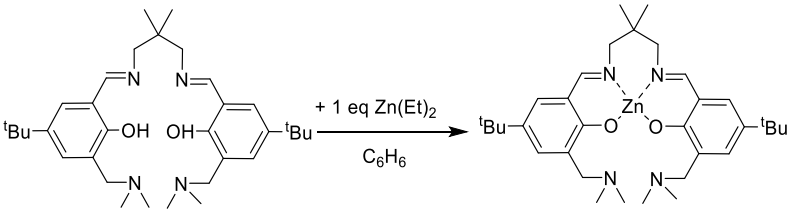

Scheme 7.6: Synthesis of Zinc complex **14**.

In one vial, 48.0 mg (89.0 µmol) of the ligand L^2H_2 was weighed and dissolved in 0.8 mL of anhydrous benzene. In another vial, 11 mg (1 eq) of the metal precursor $ZnEt_2$ was weighed and diluted in anhydrous benzene. The precursor solution was then added to the ligand solution. After a few minutes of stirring, the mixture was dried under reduced pressure until a yellow solid was obtained. The complex was then analyzed by NMR spectroscopy (Yield = 56%).

^{1}H-NMR (400 MHz, $CDCl_3$, 25 °C): δ (ppm) = 8.16-7.73 (2H, -HC=N-), 7.48-7.39 (2H, s, CH-Ar), 7.02-6.82 (2H, CH-Ar), 3.61-2.60 (8H, *CH*$_2$-N=CH, *CH*$_2$-N-$(CH_3)_2$), 2.31-2.01 (12H, s, N-(CH3)2), 1.27 (18H, s, ^{t}Bu),0.79- 0.71(6H, C-$(CH3)_2$).

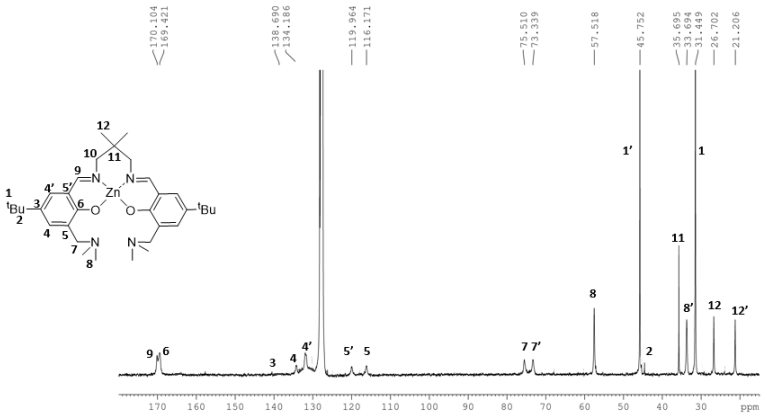

Figure 7.26. ^{13}C NMR spectrum of complex **14** (Solvent C_6D_6, 25°C, 400 MHz).

^{13}C-NMR (100 MHz, C_6D_6, 25 °C): δ (ppm) = 170.10 (C=N) , 169.42 (Cq), 138.69 (Cq), 134.19 (CH), 119.96 (Cq), 116.17 (Cq), 75.51-73.34 (*C*H_2-C-$(CH_3)_2$), 57.52 (CH_2-N-(*C*H_3)$_2$), 45.75 (-^{t}Bu), 35.70 (-*C*-$(CH_3)_2$), 33.70 (CH_2-N-(*C*H_3)$_2$), 31.45(-^{t}Bu), 26.70-21.21 (CH_2-C-(*C*H_3)$_2$).

7.4.3 Ring-Opening COPolymerization of Phthalic Anhydride and Cyclohexene Oxide

In a glovebox, the previously weighed monomer and the co-catalyst were transferred into a 10 mL Schlenk tube, equipped with a magnetic stirrer, and dissolved in 0.5 ml of toluene. In a 2 mL vial, the complex was weighed and dissolved in 0.5 mL solvent. Subsequently, the complex solution was transferred into the Schlenk tube: the latter was closed, taken out of the glovebox and immersed in a thermostated oil bath at a temperature of 110 °C. The polymerizations were stopped after the prescribed time

using dichloromethane. The solvent was removed under reduced pressure and the polymer was coagulated in methanol, filtered, dried in a vacuum oven and characterized by NMR spectroscopy and GPC analysis.

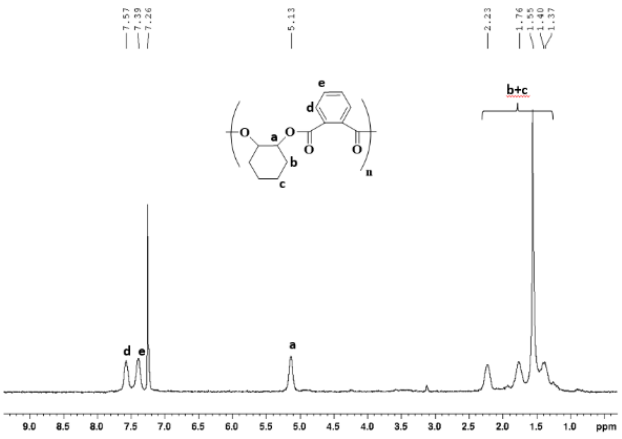

Figure 7.27. ^{1}H NMR spectrum (400 MHz, CDCl3, 25 °C) of P(CHO-PA).

7.5 References

(1) Yolsal, U.; Shaw, P. J.; Lowy, P. A.; Chambenahalli, R.; Garden, J. A. Exploiting Multimetallic Cooperativity in the Ring-Opening Polymerization of Cyclic Esters and Ethers. *ACS Catal.* **2024**, *14* (2), 1050–1074. https://doi.org/10.1021/acscatal.3c05103.

(2) Gruszka, W.; Garden, J. A. Advances in Heterometallic Ring-Opening (Co)Polymerisation Catalysis. *Nat. Commun.* **2021**, *12* (1), 3252. https://doi.org/10.1038/s41467-021-23192-y.

(3) Thevenon, A.; Garden, J. A.; White, A. J. P.; Williams, C. K. Dinuclear Zinc Salen Catalysts for the Ring Opening Copolymerization of Epoxides and Carbon Dioxide or Anhydrides. *Inorg. Chem.* **2015**, *54* (24), 11906–11915. https://doi.org/10.1021/acs.inorgchem.5b02233.

(4) Fennie, M. W.; DiMauro, E. F.; O'Brien, E. M.; Annamalai, V.; Kozlowski, M. C. Mechanism and Scope of Salen Bifunctional Catalysts in Asymmetric Aldehyde and α-Ketoester Alkylation. *Tetrahedron* **2005**, *61* (26), 6249–6265. https://doi.org/10.1016/j.tet.2005.03.117.

(5) Trott, G.; Garden, J. A.; Williams, C. K. Heterodinuclear Zinc and Magnesium Catalysts for Epoxide/CO_2 Ring Opening Copolymerizations. *Chem. Sci.* **2019**, *10* (17), 4618–4627. https://doi.org/10.1039/C9SC00385A.

Concluding Remarks

Plastic plays an important role in modern society: thanks to its low cost, light weight, and durability, it has found application in a variety of fields. However, its widespread use has led to the emergence of problems related to the use of non-renewable fossil fuels and its long-term persistence in the environment due to its non-biodegradability, with dramatic consequences for natural ecosystems. Various approaches have been adopted to curb this phenomenon, ranging from the chemical recycling of traditional plastics[1] to the introduction of new bio-based polymers.[2] In this context, aliphatic polycarbonates and polyesters represent the most promising materials, as they can be obtained from renewable resources and are characterized by good mechanical properties combined with complete biodegradability as well as offering the possibility of being chemically recycled. Currently, the industrial production of these materials requires toxic tin-based catalysts; therefore, the development of economical and non-toxic metal-based catalysts is crucial.[3] This doctoral project focused on the design of novel catalysts based on biocompatible metals, such as zinc and magnesium, capable of promoting both the synthesis and chemical degradation of these polymers. Specifically, catalysts supported by various categories of ancillary ligands, such as NHCs, tridentate phenoxy-amine and imine and multinucleating ligands (**Figure 8.1**), have been studied to evaluate how the choice of coordination environment can impact catalyst activity and selectivity.

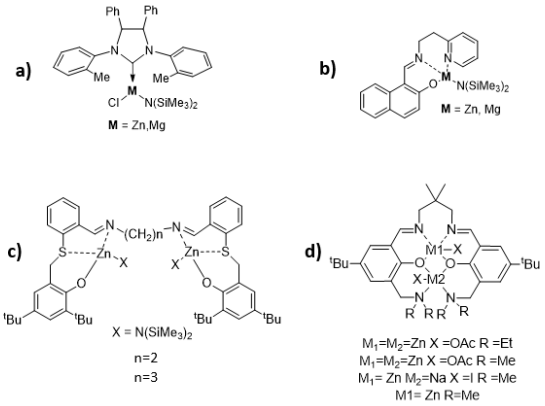

Figure 8.1 Complexes based on biocompatible metals, supported by a) N-heterocyclic carbens, b) phenoxy-imine-pyridine, c-d) Salen-like ligands, synthesized in this thesis.

In the first part, my project focused on the use of a zinc complex supported by an NHC ligand, with *syn*-phenyl groups on saturated backbone and N-tolyl substituents, in the synthesis of aliphatic polycarbonates. In combination with alcoholic initiators, these systems demonstrated moderate activity in the ROP of trimethylene carbonate (TMC) but excellent control, producing polymers with predictable molecular weights and narrow dispersities. The system maintained high performance even under industrially relevant conditions, achieving TOF values up to 760 h^{-1}. Subsequently, the versatility of the catalytic species was tested in the ROP of substituted cyclic carbonates, synthesized via sustainable procedures starting from CO_2 and 1,3-diols: in the case of the asymmetric 1-methyl-TMC monomer, it showed excellent regiocontrol, with regioselectivity values up to 0.92. Subsequent investigations confirmed a global second-order kinetic law (first-order with respect to both monomer and catalyst concentrations), while NMR studies supported a monomer-activated mechanism. Finally, the "living" nature of the system was successfully exploited in one-pot copolymerization reactions: the synthesis of complex architectures, such as block copolymers with polylactide (PLA) and polyethylene glycol (PEG), including telechelic systems, demonstrated the ability of this catalytic platform to optimize the properties and degradation behaviour of the final materials.

The study was then extended to the synthesis and characterization of analogous magnesium complexes, allowing for a direct comparison with zinc-based systems. A key aspect of this comparison concerned the structure of the ancillary ligand: NHC derivatives with *syn* and *anti* -phenyl groups on saturated backbone were used to evaluate how the ligand geometry influences the metal's reactivity. NMR spectroscopic analyses, corroborated by DFT calculations, highlighted an initial structural divergence: the higher positive charge density of magnesium stabilizes the interaction with the amine formed *in situ*, which remains within the coordination sphere, unlike the behaviour observed for zinc. Catalytic evaluation in the ROP of esters and cyclic carbonates confirmed that the ligand geometry, as well as the nature of the metal, determines reactivity: in detail, complexes supported by ligands with substituents in the *syn* configuration consistently showed greater activity than their *anti* isomers. Moreover, zinc complexes proved superior in the polymerization of L-lactide, glycolide, and methyltrimethylenecarbonate (MeTMC), while magnesium-based systems showed higher performance with ε-caprolactone, TMC, and dimethyltrimethylenecarbonate, revealing that the activity is strictly dependent on the substrate. These differences have been tentatively attributed to a combination of steric and electronic effects: future in-depth computational studies will be conducted to confirm the monomer-structure-activity relationship. From a mechanistic perspective, kinetic studies confirmed a first-order dependence on monomer concentration, supporting a dual activation hypothesis in which cooperation between the alcohol adduct and the *in situ* formed metal species plays a key role. Finally, the versatility of these catalysts was confirmed by their ability to effectively promote the alcoholysis of PLLA, demonstrating that both zinc and magnesium complexes, appropriately modulated, can actively contribute to chemical recycling strategies.

In the second phase of the study, the investigation focused on the development of zinc and magnesium complexes supported by tridentate naphthoxy-imino-pyridine ligands. Both systems proved to be efficient catalysts for the ring-opening polymerization (ROP) of cyclic esters and carbonates, providing excellent control over molecular weights and terminal group fidelity, as confirmed by GPC, NMR, and MALDI FT-ICR analyses. However,

a direct comparison between the two metals highlighted the superior performance of the zinc complex, particularly in the polymerization of lactide. Furthermore, the ROP kinetic profile of caprolactone revealed an induction period for the magnesium catalyst, attributed to the slower formation of the active species, absent in the zinc-mediated process. Taking advantage of the exceptional activity of the zinc complex, which ranks among the most efficient systems reported in the literature, random and diblock copolymers based on TMC were successfully synthesized. The formation of block and random architectures was unequivocally confirmed by NMR spectroscopy and thermal analysis, consistent with their microstructure. Finally, the same zinc complex was employed in microwave-assisted depolymerization, as an alternative heating source, for PTMC and its copolymers. A particularly interesting result was the selective depolymerization observed in the block copolymers, a phenomenon that opens new perspectives for the targeted recovery of monomers from complex materials.

The final phase of the project aimed to synthesize di- and trimetallic complexes using multinucleating ligands, designed to accommodate metal centers at an optimal distance and ensure intramolecular cooperativity. Initially, Salen-type aldimine-thioetherphenolate ligands were synthesized and used to synthesize bimetallic zinc complexes. They proved more active than their monometallic counterparts in the ROP of lactide and ε-caprolactone, and in the Ring-Opening COPolymerization of phthalic anhydride (PA) with cyclohexene oxide (CHO). Specifically, complexes with a propylene bridge (wider spacing) proved more active with bulky monomers such as lactide, while those with an ethylene bridge (narrower spacing) proved excellent with ε-caprolactone and in the ROCOP, suggesting that the intermetallic distance is affected by the steric hindrance of the monomer. Subsequently, the research extended to the design of new Salen ligands, functionalized with amino pendants *ortho* to phenol, to create a coordination pocket capable of hosting a second metal center. Initial synthetic attempts were then conducted to isolate zinc-based homo- and heterobimetallic complexes, with preliminary testing in the ROCOP of PA and CHO. The generated heterobimetallic systems ensured perfect selectivity toward the alternating polyester, suppressing ether formation and confirming the effectiveness of the synergy between different metals.

However, the monometallic species was found to be the most active, suggesting that the reduction of steric hindrance by the second metal center and the cooperation of the uncoordinated pendant arms (which act as internal bifunctional co-catalysts) may prevail over bimetallic cooperativity.

Finally, during my research abroad at the University of Edinburgh, in Dr. Jennifer Garden's research group, my work was focused on the synthesis of multinuclear heterometallic systems (Zn coupled to alkali metals, such as sodium and potassium) supported by pentadentate ProPhenol ligands (**Figure 8.2**). Applied for the first time to the polymerization of cyclic carbonates (TMC) and macrolactones (pentadecalactone, globalide), the heterometallic Zn_2/Na and Zn_2/K catalysts achieved complete conversions in a few seconds at room temperature, suggesting a strong cooperative synergy between the different metal centers.

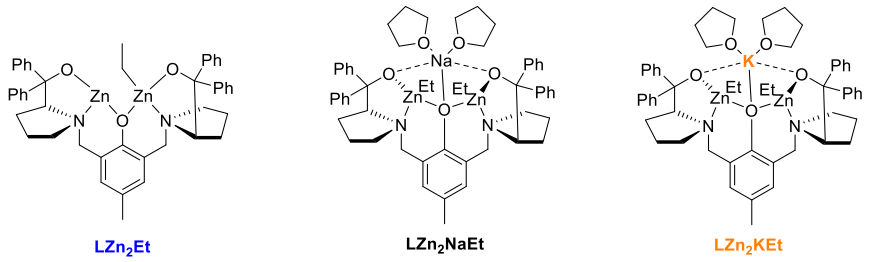

Figure 8.2 Homo and heterotrimetallic complexes supported by Prophenol ligand.

As general conclusion, this doctoral research focuses on the synthesis and chemical recycling of biobased polymers using novel complexes based on biocompatible metals. The study demonstrated how the polymerization process can be significantly influenced by the choice of the metal center and ancillary ligand, finely modulating their steric and electronic properties. Specifically, the study of NHC- and phenoxyiminopyridine-supported systems reveals how the geometry of the auxiliary ligand and the specific nature of the metal center determine catalytic performance, while the use of multidentate ligands ensures intermetallic cooperativity, which is strongly influenced by the distance between the metal centers. Furthermore, the development of

heterotrimetallic catalysts highlights the potential of synergy between different metals, ensuring a significant improvement in catalytic performance. Finally, the successful application of these platforms in microwave-assisted depolymerization and solvolysis validates their dual-use potential in closing the polymer lifecycle.

References

(1) Coates, G. W.; Getzler, Y. D. Y. L. Chemical Recycling to Monomer for an Ideal, Circular Polymer Economy. *Nat. Rev. Mater.* **2020**, *5* (7), 501–516. https://doi.org/10.1038/s41578-020-0190-4.

(2) Zhang, X.; Fevre, M.; Jones, G. O.; Waymouth, R. M. Catalysis as an Enabling Science for Sustainable Polymers. *Chem. Rev.* **2018**, *118* (2), 839–885. https://doi.org/10.1021/acs.chemrev.7b00329.

(3) Kaur, G.; Uisan, K.; Ong, K. L.; Ki Lin, C. S. Recent Trends in Green and Sustainable Chemistry & Waste Valorisation: Rethinking Plastics in a Circular Economy. *Curr. Opin. Green Sustain. Chem.* **2018**, *9*, 30–39. https://doi.org/10.1016/j.cogsc.2017.11.003.

Acknowledgments

The Interuniversity Consortium of Chemical Reactivity and Catalysis (CIRCC, Bari, Italy, Progetto Competitivo 2021 CMPT212338), the Italian Ministry of University and Research (MUR) through the PRIN PNRR 2022 project (CUP D53D23017170001) and the Università degli Studi di Salerno (FARB grant: ORSA231338) are acknowledged for funding.

Publications

- **Cooperative effects of Schiff base binuclear zinc complexes on the synthesis of aliphatic and semi-aromatic polyesters**

Santulli, F., Tufano, F., Cozzolino, M., D'Auria I., Strianese M, Mazzeo, M., Lamberti, M. *Dalton Trans.*, **2023,** 52(40), 14400–14408

- **CO_2-Based Polycarbonates through Ring-Opening Polymerization of Cyclic Carbonates Promoted by a NHC-Based Zinc Complex**.

Tufano F., Napolitano C., Mazzeo M., Grisi F., Lamberti M., *Biomacromolecules*, **2024**, 25(7), pp. 4523–4534

- **Versatile NHC-based biometal complexes for the synthesis and chemical recycling of aliphatic polyesters and polycarbonates**.

Tufano F., Santulli, F., Liguori C., Grisi F., Mazzeo M., Lamberti M., *Catal. Sci. Technol***., 2025**, 15, 822-835 .

- **Recyclable, Biobased Polycarbonates and Polyesters by Naphthoxy-Imine Zinc and Magnesium Complexes**

Tufano F., Galotto M.V., D'Elia A. Santulli F., Mazzeo M., Lamberti M., *Chemistry A European Journal*, **2025**, 31(35), e202501271

- **Fluorescent polyolefins by ring-opening metathesis polymerization of 3-susbstituted cyclooctenes**

Ciccone F., Tufano F., Pragliola S., Troiano R., Pierri G., Boccia A.C., Grisi F., *European Polymer Journal,* **2025**, 234, 114045

- **Polyethylenes and Polystyrenes with Carbazole Fluorescent Tags**

Tufano F., Grisi F., Costabile C., Mazzeo M., Venditto V., Boccia A. C, Fittipaldi R., Izzo L., Pragliola S., *Processes*, **2023**, 11(2), 515

- **N-Heterocyclic Carbene-Based Zinc Complexes: Same Precursors for Different Lactide Ring-Opening Polymerization Mechanisms.**

Tufano, F., Santulli, F., Grisi, F., Lamberti, M. *ChemCatChem,* **2022**, 14(20), e202200962

Scientific Contributions

- **Polymerisation and depolymerisation chemistry: the second century Faraday Discussion Oxford, 8-10 Settembre 2025**

Poster New Heteroleptic Zinc and Magnesium complexes for Synthesis and Chemical Recycling of Bioderived Polymer

Authors: Tufano Federica, Santulli Federica, Galotto Maria Vittoria, D'Elia Alfredo, Mazzeo Mina, Lamberti Marina

- **XI Workshop Gruppo Interdivisionale Green Chemistry – Chimica Sostenibile (Società Chimica Italiana – Gruppo interdivisionale Green Chemistry) Torino 24-25 Ottobre 2024**

Poster + Flash Presentation Sustainable Polymers obtained by Schiff Base-Based Zn and Mg Complexes

Authors: Tufano Federica, Santulli Federica, Galotto Maria Vittoria, D'Elia Alfredo, Vitiello Sabrina, Mazzeo Mina, Lamberti Marina

- **Convegno PLASTAMINATION – SIBS Società Italia di Biologia Sperimentale Salerno 23 Ottobre 2024**

Flash Presentation NHC-Zn Complexes for the synthesis and chemical upcycling of sustainable polyesters and polycarbonates

Authors: Tufano Federica, Santulli Federica, Grisi Fabia, Mazzeo Mina, Lamberti Marina

- **Suschem'24 Workshop on Sustainable Polymers and Circular Economy of Plastics Ischia 1-4 Settembre 2024**

Poster: NHC-Based Zinc Complexes for the synthesis and chemical upcycling of Polyesters and Polycarbonates

Authors: Tufano Federica, Napolitano Claudia, Liguori Concetta, Grisi Fabia, Mazzeo Mina, Lamberti Marina

- **XXIII International Symposium on Homogeneous Catalysis ISHC 2024 Trieste 21-26 Luglio 2024**

Poster Sustainable Polyesters and Polycarbonates through Ring-Opening Polymerization by NHC-based Biometals Complexes

Authors: Tufano Federica, Grisi Fabia, Mazzeo Mina, Lamberti Marina

- **6th EuchemS Conference on Green and Sustainable Chemistry Salerno 1-4 Settembre 2023**

Poster Bio-Based Polyesters and Polycarbonates by NHC-Zinc and Magnesium catalysts.

Authors: Tufano Federica, Mazzeo Mina, Grisi Fabia, Lamberti Marina

- **20th International Conference on Carbon Dioxide Utilization ICCDU XX Bari 25-29 Giugno 2023**

Poster Sustainable polycarbonates from CO_2 and Biobased Diols.

Authors: Tufano Federica, Mazzeo Mina, Grisi Fabia, Lamberti Marina

- **SCI Società Chimica Italiana Contributo dei Giovani Chimici in Campania Napoli 20 Giugno 2023**

Flash Presentation Aliphatic Polycarbonates from Ring-Opening Polymerization of Bio-Based Cyclic Carbonates

Authors: Tufano Federica, Mazzeo Mina, Grisi Fabia, Lamberti Marina

Teaching Activities

- **Course Name INORGANIC CHEMISTRY I**

  Lab Assistant

  Hourse 16 Academic Year 2023/2024

- **Course Name INORGANICAL CHEMISTRY II**

  Lab Assistant

  Hours 12 Academic Year 2023/2024

- **Course Name INORGANIC AND ORGANIC SYNTHESIS**

  Lab Assistant

  Hours 10 Academic Year 2023/2024

- **Course Name FUNDAMENTALS OF CHEMISTRY**

  Frontal Lesson

  Hours 10 Academic Year 2023/2024

- **Course Name INORGANICAL CHEMISTRY II**

  Lab Assistant

  Hours 14 Academic Year 2024/2025